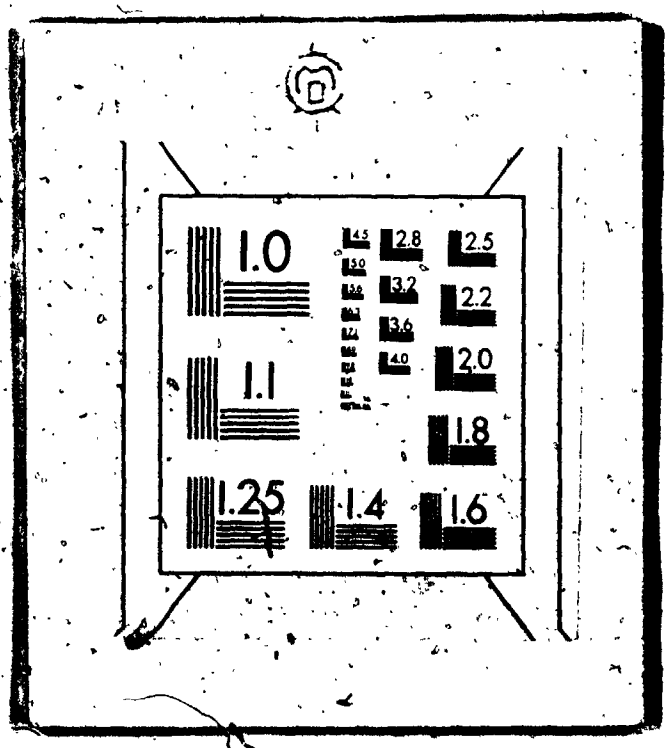
1.0
1.1
1.25
1.4
1.6
2.8
3.2
3.6
4.0
2.5
2.2
2.0
1.8

0-315-01674-4

National Library of Canada | Bibliothèque nationale du Canada | CANADIAN THESES ON MICROFICHE | THÈSES CANADIENNES SUR MICROFICHE

49531

NAME OF AUTHOR/*NOM DE L'AUTEUR* George C. Patterson

TITLE OF THESIS/*TITRE DE LA THÈSE* The Geology of the Kapkichi Lake Ultramafic-Mafic Bodies and Related Cu-Ni Mineralization Pickle Lake, Ontario

UNIVERSITY/*UNIVERSITÉ* Carleton University

DEGREE FOR WHICH THESIS WAS PRESENTED/*GRADE POUR LEQUEL CETTE THÈSE FUT PRÉSENTÉE* Ph.D.

YEAR THIS DEGREE CONFERRED/*ANNÉE D'OBTENTION DE CE DEGRÉ* 1980

NAME OF SUPERVISOR/*NOM DU DIRECTEUR DE THÈSE* D. Watkinson

Permission is hereby granted to the NATIONAL LIBRARY OF CANADA to microfilm this thesis and to lend or sell copies of the film.

The author reserves other publication rights, and neither the thesis nor extensive extracts from it may be printed or otherwise reproduced without the author's written permission.

L'autorisation est, par la présente, accordée à la BIBLIOTHÈQUE NATIONALE DU CANADA de microfilmer cette thèse et de prêter ou de vendre des exemplaires du film.

L'auteur se réserve les autres droits de publication; ni la thèse ni de longs extraits de celle-ci ne doivent être imprimés ou autrement reproduits sans l'autorisation écrite de l'auteur.

DATED/*DATÉ* December 10, 1979 SIGNED/*SIGNÉ* A C Patterson

PERMANENT ADDRESS/*RÉSIDENCE FIXÉ* 158 Brimorton Dr.
Toronto, Ontario
M1H 2C1

NL-91 (11-79)

National Library of Canada
Collections Development Branch

Canadian Theses on
Microfiche Service

Bibliothèque nationale du Canada
Direction du développement des collections

Service des thèses canadiennes
sur microfiche

NOTICE

The quality of this microfiche is heavily dependent upon the quality of the original thesis submitted for microfilming. Every effort has been made to ensure the highest quality of reproduction possible.

If pages are missing, contact the university which granted the degree.

Some pages may have indistinct print especially if the original pages were typed with a poor typewriter ribbon or if the university sent us a poor photocopy.

Previously copyrighted materials (journal articles, published tests, etc.) are not filmed.

Reproduction in full or in part of this film is governed by the Canadian Copyright Act, R.S.C. 1970, c. C-30. Please read the authorization forms which accompany this thesis.

THIS DISSERTATION
HAS BEEN MICROFILMED
EXACTLY AS RECEIVED

AVIS

La qualité de cette microfiche dépend grandement de la qualité de la thèse soumise au microfilmage. Nous avons tout fait pour assurer une qualité supérieure de reproduction.

S'il manque des pages, veuillez communiquer avec l'université qui a conféré le grade.

La qualité d'impression de certaines pages peut laisser à désirer, surtout si les pages originales ont été dactylographiées à l'aide d'un ruban usé ou si l'université nous a fait parvenir une photocopie de mauvaise qualité.

Les documents qui font déjà l'objet d'un droit d'auteur (articles de revue, examens publiés, etc.) ne sont pas microfilmés.

La reproduction, même partielle, de ce microfilm est soumise à la Loi canadienne sur le droit d'auteur, SRC 1970, c. C-30. Veuillez prendre connaissance des formules d'autorisation qui accompagnent cette thèse.

LA THÈSE A ÉTÉ
MICROFILMÉE TELLE QUE
NOUS L'AVONS REÇUE

Ottawa, Canada
K1A 0N4

The Geology of the Kapkichi Lake Ultramafic-Mafic Bodies and Related Cu-Ni Mineralization Pickle Lake, Ontario

by

© George Cameron Patterson, B.Sc., M.Sc.

A thesis submitted to the Faculty of Graduate Studies in partial fulfillment of the requirements for the degree of Doctor of Philosophy

Carleton University
Ottawa

January, 1980

The undersigned hereby recommend to the Faculty of Graduate Studies acceptance of this thesis, submitted by George Cameron Patterson, M.Sc., in partial fulfillment of the requirements for the degree of Doctor of Philosophy.

Chairman, Department of Geology

Supervisor

External Examiner

Abstract

The Kapkichi Lake ultramafic and mafic (um-m) rocks, including those of the Thierry Mine of Umex Corp. Ltd., located 450 kilometres N.W. of Thunder Bay occur in metabasalts of the Uchi Lake greenstone belt. The um-m rocks originally consisted of felsic to mafic gabbro with lesser amounts of peridotite; dunite and oxide layers now converted by middle amphibolite grade metamorphism to metagabbro, mafic metagabbro, olivine-tremolite-chlorite rock and talc-carbonate schist. Where these rocks have been sheared a blastomylonite (hornblende-chlorite-biotite schist) has developed.

The geological history is interpreted to have started with the extrusion of mafic volcanic rocks with minor felsic tuffs and sediments on a granitic terrain which was followed by the intrusion of a large granitic pluton (Pickle Lake Stock) and later u-um bodies with associated sulfides. This package of rocks was modified by four tectonic events. A tight isoclinal folding (D_1) producing a strong F_1 and lineation L_1, was folded by open folding D_2 with the axial plane $68^\circ/68^\circ N$ and weak folding D_3 which warped D_2 along an axial trace running north-south. A cataclastic event cut all D_1, D_2 and D_3 structures producing shears, faults, kink bands in amphibolite schist and, mylonite zone and associated blackwall alteration in the um-m rocks.

Whole rock chemistry shows the meta-volcanic rocks to have a high-iron tholeiite composition. The um-m rocks have some chemical characteristics in common with komatiiites but lack of textural evidence makes the komatiitic affinity difficult to prove. Plots of oxides contents versus distance in drill holes show distinct magmatic trends. Each of the um-m bodies, Thierry Mine, J+I and Kl:1 shows a distinct trend on normative olivine, plagioclase and hypersthene + augite plot. The bulk composition of the biotite-rich rocks of Kl:1 suggests that Al_2O_3, MgO and FeO were immobile while SiO_2, CaO, Na_2O and K_2O were mobile during the "blackwall" alteration process.

The regional metamorphism is mid-amphibolite grade at a temperature of approximately 600°C based on garnet-biotite, calcite-dolomite and magnetite-ilmenite geothermometer and a pressure of 7.0 kbar based on garnet-plagioclase and sphalerite-pyrite-pyrrhotite geobarometers. The assemblages observed in mafic volcanic, pelitic and calc-silicate rocks are consistent with mid-amphibolite grade metamorphism. The assemblages in the ultramafic rocks require the fluid phase to be CO_2-rich. The silicate and sulfide assemblages in the mylonite zone indicate that the last shearing event took place at greenschist facies conditions.

The whole rock chemistry of the mylonite zone in the Thierry Mine indicates that CaO, Na_2O and SiO_2 have been removed and K_2O, Cu and S have been added to the um-m rocks. The lack of plagioclase, the alteration of hornblende to actinolite, the coincidence of biotite and sulfide in the mylonite and the enrichment of epidote and carbonate in the amphibolitic wall rocks

suggest that the alteration of plagioclase and hornblende released sodium and calcium producing chlorite in the mylonite and epidote and plagioclase in the amphibolite. Potassium altering the chlorite to biotite was accompanied by a rise in pH possibly causing the precipitation of sulfide in the mylonite. The sulfur and metals were likely mobilized from the um-m body.

Five main ore types were recognized in the Thierry Mine; primary disseminated ore, breccia ore, chlorite-biotite schist ore (CBS), bornite ore and altered ore making up 1%, 40%, 56%, 2% and 1% respectively of the ore. The sulfide assemblages are po+py+pn, bio+py+pn, po+smy+pn in the breccia ore, (CBS ore) and primary disseminated ore; vio+mil, vio+vaes+py, vio+py in the altered ore; bn+Cu-Bi sulfosalts + carrollite in the bornite ore. Chalcopyrite in part altered to mackinawite is common to all sulfide assemblages. The sulfide types observed in the other Kapkichi um-m bodies are primary disseminated ore and metamorphosed disseminated ore with minor breccia and altered ores. The sulfides are interpreted to have been of primary magmatic origin modified by strong shearing which produced the CBS ore and breccia ore. The bornite ore was formed by the migration of more mobile elements (Cu,Ag,Pd and S) into amphibolite blocks included in the mylonite. Supergene alteration is evident in joints, faults and shear zones producing altered ore.

Precious metal minerals in the bornite and breccia ore are moncheite, merenskyite, kotulskite, stuetzite, native silver, acanthite and Ag_3BiTe_2. Pd and Ag tend to occur with chalcopyrite-

rich ore while Pt tends to occur with Ni-rich ore. Since Pd, Ag and Cu are relatively more mobile than Ni and Pt it suggests the former were concentrated during metamorphism.

The bulk composition of the sulfide ore at the Thierry Mine is unusual in comparison to other deposits in ultramafic to mafic hosts. The Cu-Ni ratio of the ore at Thierry Mine is 8:1 with a ratio of chalcopyrite to pyrrhotite of approximately 1:1. Models of emplacement of Cu-rich ore including fractionation of copper-rich magmatic sulfides, solidification of a sulfur deficient magma and late stage Cu-sulfide enrichment, mechanical separation by shear and stress induced diffusion were examined. The most feasible interpretation is that of mechanical separation by shear and stress induced diffusion.

Acknowledgements

The author, is indebted to D. Watkinson for having the patience and persistence to guide me through this project and to G. Skippen for taking the time to visit the Thierry Mine and provide critical review. I also wish to acknowledge the electron microprobe analyses of some of the sulfides done by P. Morton.

I wish to thank, T. Verbeek and R. Dehenne of UMEX Corp. Ltd for financial support and more importantly the freedom of access to the geological data at the Thierry Mine; to J. Lefebvre (UMEX research geologist) for providing precious metal data, X-ray data and, many long and helpful discussions; K. Kennedy and B. Zuckerkandel (Thierry Mine Staff) for help in mapping and producing the mine sections and C. Bowdidge (UMEX Research geologist) for providing the base map in the Kapkichi Lake Area.

Thanks are entended to R. Eckstrand (G.S.C.) for providing whole rock analyses, useful discussions and critical review. Lastly many thanks to my mother who typed this project.

TABLE OF CONTENTS

1.0	Introduction	1-11
1.1	Purpose	1-4
1.2	Previous Work	5
1.3	Mining History	6-8
1.4	Nomenclature	9-11
2.0	Geology of the Kapkichi Lake Area	12-50
2.1	Introduction	12
2.2	Regional Geology	12
2.3	Lithologic Units	14
2.3.1	Amphibolites	16
2.3.2	Metasedimentary Rocks	18
2.3.3	Ultramafic and Mafic Rocks	
	i) Thierry Mine um-m Rocks	19-20
	ii) G um-m Rocks	20
	iii) Kl:1 um-m Rocks	22-23
	iv) J+I um-m Rocks	24-29
2.3.4	Porphyritic Grandiorite and Felsic Dykes	30-33
2.4	General Geology of the Kapkichi Lake Area	34-48
2.5	Conclusions and Summary	49-50
3.0	The Chemical Characteristics of Rocks of the Kapkichi Lake Area	51-70
3.1	Introduction	51
3.2	Amphibolites	52-55
3.3	Ultramafic and Mafic Rocks	57-60
3.4	Magmatic Trends	61-65
3.5	Alteration of the Kl:1 um-m Rocks	66-69
3.6	Conclusions	70
4.0	Pressure and Temperature Conditions during Metamorphism	71-92
4.1	Introduction	71-72
4.2	Geothermometry and Geobarometry	73-76
4.3	Metamorphic Assemblages in the Kapkichi Lake Area	77-91
4.3.1	Mafic Rocks	77-80
4.3.2	Pelites	81
4.3.3	Calcsilicates	82-83
4.3.4	Ultramafic Rocks	84-90
4.3.5	Cataclastic Rocks	91
4.4	Conclusions	92

5.0	The Thierry Cu-Ni Mine and Associated Ultramafic and Mafic Rocks	93-121
	5.1 Introduction	93- 94
	5.2 Lithologies	95-102
	5.2.1 Metagabbro	95
	5.2.2 Mafic Metagabbro	96- 97
	5.2.3 Talc-Carbonate Schist	98
	5.2.4 Olivine-Tremolite-Chlorite Ultramafic Rock	98
	5.2.5 Hornblende-Chlorite-Biotite Schist	99-100
	5.2.6 Classification of Sulfide Mineralization	101-102
	5.3 General Geology and Structure of the Thierry Mine	103-114
	5.4 Chemical Alteration of Deformed Ultramafic Rocks	115-117
	5.5 Model for Alteration	118-120
	5.6 Summary and Conclusions	121
6.0	Sulfide Mineralogy at the Thierry Mine	122-166
	6.1 Introduction	122
	6.2 Classification of the Sulfide Assemblages in the Thierry Mine	123-124
	6.2.1 Breccia Ore	125-132
	6.2.2 Chlorite-Biotite Schist Ore	133-135
	6.2.3 Bornite Ore	136-137
	6.2.4 Primary Disseminated Sulfides	138-139
	6.2.5 Altered Ore	140-142
	i) Supergene Ore	140
	ii) Oxidized Breccia Ore	141-142
	6.3 Metamorphism of the Thierry Ore	143-144
	6.4 Alteration of the Thierry Sulfide Ores	145-149
	6.5 Low Temperature Assemblages and Equilbrium	150-152
	6.6 Stability of Low Temperature Assemblages in the Ni-Fe-S System	153-157
	6.7 Sulfide Mineralogy in the um-m Bodies	158
	6.7.1 J+I um-m Body	158-160
	6.7.2 G um-m Body	161-162
	6.7.3 K1:1 um-m Body	163
	6.8 Comparison of Sulfides from the Kapkichi Um-m Bodies and the Thierry Mine	164
	6.9 Conclusions	164-166

7.0	Platinum Group Metals, Silver and Gold in the Thierry Mine	167-177
	7.1 Introduction	167-168
	7.2 Mineralogy	169-170
	7.3 Distribution of Precious Metals in the Thierry Mine	170-175
	7.4 Conclusions	176-177
8.0	Summary, Conclusions and Discussion	178-192
	8.1 Geochemistry of the Ore at the Thierry Mine	178-186
	8.2 Summary and Conclusions	187-192
9.0	Plates	193-203
10.0	References	204-212
11.0	Appendices	213-331
	A. Petrography of Rocks from the Kapkichi Lake Area	216-243
	B. Modes of Polished Sections	244-257
	C. Electron Microprobe Analyses of Sulfides	258-275
	D. Electron Microprobe Analyses of Silicates and Oxides	276-288
	E. Whole Rock Chemistry	289-307
	F. Mine Sections	308-331

FIGURES

Fig. 1.1	Location of the Kapkichi Lake Area and the Thierry Mine	2
Fig. 1.2	Location of um-m Bodies and Sections in the Kapkichi Lake Area	7
Fig. 2.1	Geology of the Pickle Lake Area	13
Fig. 2.2	Diamond drill hole Locations, Outcrop Locations and summary of the Geophysical Data for the Kapkichi Lake Area	35
Fig. 2.3	Geology of the Kapkichi Lake Area	36
Fig. 2.4	Stereographic Plots of Hornblende Foliations and Lineations from Amphibolites in the Kapkichi Lake Area	37
Fig. 2.5	Oxide Weight Percent vs Depth in Drill Hole K61, J+I Mafic Intrusion	41
Fig. 2.6	Geological Interpretation of Section 46N	43
Fig. 2.7	Geological Interpretation of Section 76E	44
Fig. 2.8	Geological Interpretation of Section 0W	45
Fig. 2.9	Geological Interpretation of Section 0N	46
Fig. 2.10	Geological Interpretation of Section 180E	47
Fig. 2.11	Geological Interpretation of Section 160E	48
Fig. 3.1	Ni,Cr,TiO_2 vs MgO/(FeO+MgO) for Amphibolites from Kapkichi Lake Area	54
Fig. 3.2	Normative Olivine, Nephline, Quartz for Amphibolites from the Kapkichi Lake Area	56
Fig. 3.3	AFM Plot for Amphibolites from Kapkichi Lake Area	56
Fig. 3.4	AFM Diagram of Unaltered Mafic Rocks for Kapkichi Lake Area	59
Fig. 3.5	MgO,CaO,Al_2O_3 Diagram from Unaltered Mafic Rocks, Kapkichi Lake Area	59
Fig. 3.6	Wt% TiO_2 vs Wt% MgO Diagram from Mafic Rocks	60
Fig. 3.7	Wt% Al_2O_3 vs FeO/(FeO+MgO)	60
Fig. 3.8	Diagram of Normative Olivine, Plagioclase, Pigeonite for Unaltered K1:1 Samples	62
Fig. 3.9	Diagram of Normative Olivine, Plagioclase, Pigeonite for Unaltered Thierry and J+I Samples	62
Fig. 3.10	Minerals Present in the Various Rocks of the Layered Series and their Composition, Skaergaard Intrusion	64
Fig. 3.11	Minerals Present in the Various Rocks of the Layered Series and their Composition, Basistoppen Sheet	65
Fig. 3.12	Al_2O_3 vs Oxides for Mafic Rocks from K1:1 Body	67
Fig. 3.13	Normative Biotite vs Oxides for Altered Rocks from K1:1 Body	69

Fig. 4.1	Metamorphic Assemblages in Mafic Rocks	78
Fig. 4.2	ACF Diagrams for Rocks of Basaltic Compositions	79
Fig. 4.3	Isobaric (P_f=2kb) Phase Relations in the System $CaO-Al_2O_3-SiO_2-H_2O-CO_2$ to 800°C	83
Fig. 4.4	Equilibrium Conditions of Mineral Assemblages Stable at Isobaric Invariant Points C,D of Fig. 4.3	83
Fig. 4.5	Summary of Mineral Assemblages in Metamorphic Peridotitic Rocks	89
Fig. 4.6	Portion of the System $MgO-SiO_2-CO_2-H_2O$ Recalculated to 5 Kbars	89
Fig. 5.1	Location of Surface Drill Holes at the Thierry Mine	104
Fig. 5.2	Geological Interpretation of the 100 level of the Thierry Mine	105
Fig. 5.3	Composite of Sections through the Thierry Mine	106
Fig. 5.4	Variation of Chemical Composition along the 312 Level	107
Fig. 5.5	Cross Section through the 1600 Level Cross-Cut	110-111
Fig. 5.6	Section through 1600 Level Cross-Cut showing Amphibolite Schist-Granite Contact	112
Fig. 5.7	$CaO-Na_2O-K_2O$ Diagram for Rocks from the Thierry Mine	116
Fig. 5.8	Larsen Plot for Mafic Metagabbro, Metagabbro and Mylonitized Mafic Rocks from the Thierry Mine	117
Fig. 6.1	Reflectance Values for Low Ni-Fe Monosulfide	131
Fig. 6.2A	Schematic Interpretations of Low-temperature Relations in the System Fe-Ni-S	154
Fig. 6.2B	Low Temperature Relations in the System $K_2O-MgO-Al_2O_3-SiO_2$	154
Fig. 6.3	Portion of the System Ni-Fe-S	157
Fig. 7.1	Plot of Ag vs Ni Concentrations from Samples from Thierry Mine	174
Fig. 7.2	Plot of Ag vs Cu Values from Thierry Mine	174
Fig. 7.3	Ag/10-Pt-Pd Plot for Samples from Thierry Mine	175
Fig. 8.1	Relationship Between Cu/(Cu+Ni) Ratio in Sulfide Ores and the % MgO in the Host Rock	179
Fig. 8.2	The Relationship Between Pt/(Pt+Pd) and Cu/(Cu+Ni) Ratios in Sulfide Ores	179

Fig. 8.3 Average Copper and Nickel Content in Copper-Nickel Sulfide Ores Compared with the Composition of the Host Rock 181

Fig. 8.4 Schematic 1000°C Isothermal Diagram of the Cu-Fe-Ni-S System 181

Fig. 8.5 Projection of the Gu/Ni Ratio in the CBS Ores at the Thierry Mine 184

Fig. 8.6 Projection of the Cu/Ni Ratio in the Breccia Ores at the Thierry Mine 185

TABLES

Table 1.1	Nomenclature used by Geologists on the Thierry Mine Rocks	11
Table 2.1	Table of Formation of the Kapkichi Lake Area	15
Table 2.2	Characteristics of Amphibolites from the Kapkichi Lake Area	17
Table 2.3	Rocks from the Kl:1 Body	21
Table 2.4	Mafic Rocks from the J+I Body	25
Table 2.5	G Ultramafic Zone	26
Table 3.1	Trace Elements of Sediments and Tholeiites Compared to the Amphibolites from the Kapkichi Lake Area	53
Table 4.1	Temperature and Pressure of Metamorphism	74
Table 4.2	Assemblages in Ultramafic Rocks in the Kapkichi Lake Area	85
Table 5.1	Rocks of the Thierry Mine	94
Table 5.2	Electron Microprobe Analyses of Silicates from the Thierry Mine	97
Table 5.3	Alteration Reactions Associated with Mylonitization	119
Table 6.1	Average Analyses of Sulfides from Thierry Mine; Breccia Ore	126-127
Table 6.2	Powder X-ray Diffraction Pattern of Unnamed Fe,Ni Monosulfide	130
Table 6.3	Average Analyses of Sulfides from Thierry Mine Chlorite-Biotite Schist	134
Table 6.4	Average Analyses of Ore Sulfides from Thierry Mine, Bornite Ore	137
Table 6.5	Average Analyses of Sulfides from Thierry Mine; Disseminated Ore	139
Table 6.6	Average Analyses of Sulfides from Thierry Mine; Altered Breccia Ore	142
Table 6.7	Assemblages Observed in Supergene, Metamorphosed and Serpentinized Fe-Ni-S Ores	146
Table 6.8	Schematic Reactions Involving the Generation of Violarite	147
Table 6.9	Sulfide Assemblages in the J+I Body	159
Table 6.10	Sulfide Assemblages in G Body and Kl:1 Body	162
Table 7.1	Electron Microprobe Analyses of Precious Metal Minerals from Thierry Mine	168
Table 7.2	Precious Metal Analyses, Thierry Mine	171
Table 7.3	Metal Analyses of Composite Pulp and Mill Feed, Thierry Mine	172

1.0 Introduction

1.1 Purpose

The Kapkichi Lake area of northwestern Ontario, located 450 kilometres north-west of Thunder Bay (Fig. 1:1) contains several mineralized um-m bodies including the Thierry Cu-Ni Mine of Union Miniere Exploration and Mining Corporation Limited. Preliminary studies by Bowdidge (1970) and, Morton and Watkinson (1974) showed that the Thierry Mine has an unusually high Cu to Ni ratio (approximately 8:1) and that the sulfides show the effects of strong dynamic metamorphism and supergene alteration. Metallurgical tests carried out by Lakefield Research (1974) showed that the ore contained silver and platinum-group elements (PGE). However, Lakefield was unable to identify the minerals containing these metals. Morton and Watkinson (1974) found one mineral containing PGE but no silver-bearing minerals.

This thesis was carried out with the following objectives:

1) To produce a geologic interpretation of the Thierry Mine and the Kapkichi Lake area by compiling data from approximately three million feet of diamond drilling, regional geologic mapping (less than 1% outcrop) and underground and open pit mapping at the Thierry Mine

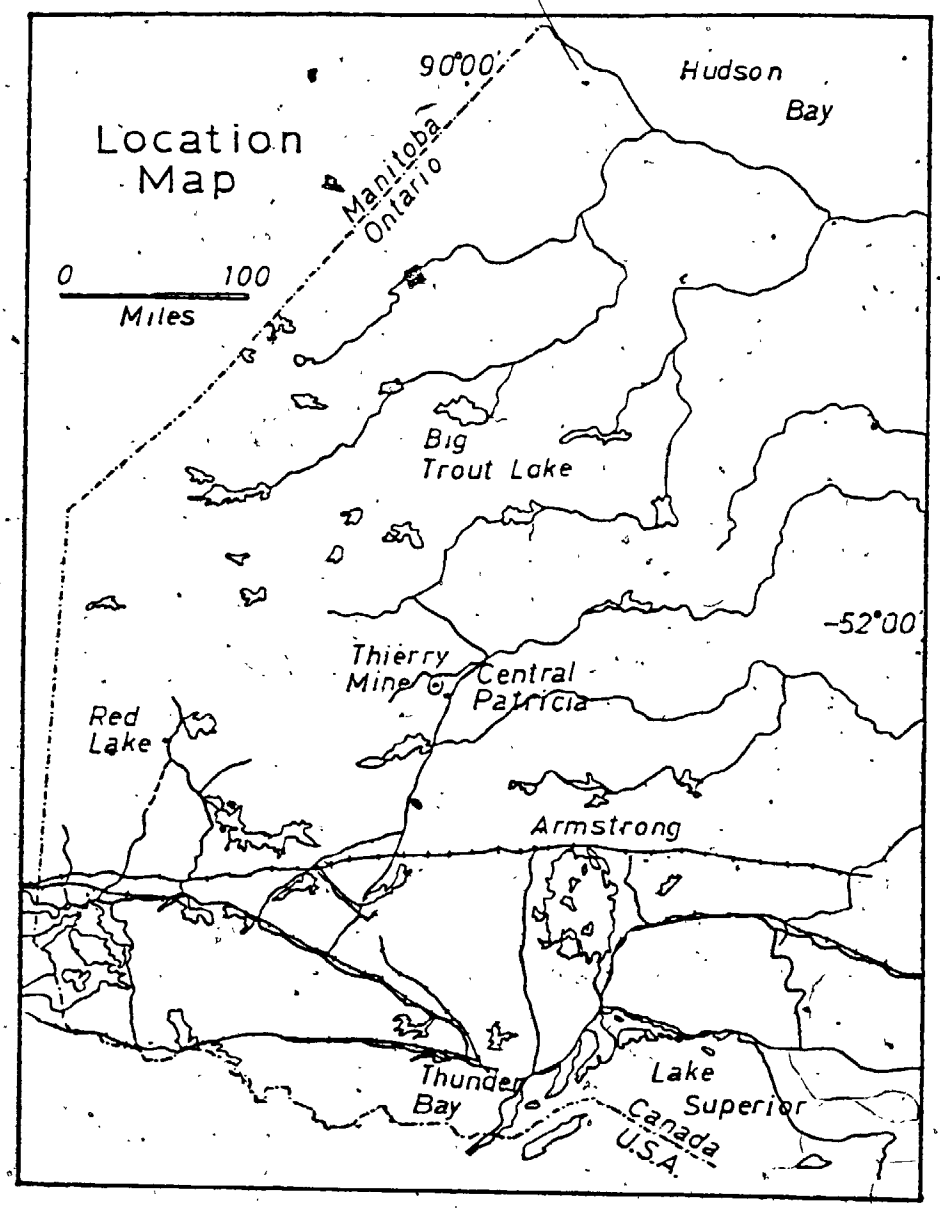

Fig. 1.1 Location of the Kapkichi Lake area and the Thierry Mine

2) To estimate the metamorphic conditions (temperature and pressure) in the Kapkichi Lake area.

3) To interpret the genesis of the sulfide mineral assemblages at the Thierry Mine.

4) To determine the minerals carrying PGE and Ag, and study their distribution in the Thierry Mine.

5) To explain the high Cu/(Cu+Ni) of sulfides associated with mafic and ultramafic rocks at the Thierry Mine.

The thesis has been written in three sections; Regional Geology, Chapters 2 to 4; The Thierry Mine and sulfide mineralogy, chapter 5 to 6; and PGE Mineralogy at the Thierry Mine, chapter 7.

The regional geology including a description of the rock units and general structural geology of the Kapkichi Lake area are discussed in chapter 2. The chemical analyses of the meta-volcanic rocks and the um-m rocks of Kl:1, J+I and the G bodies are presented and discussed in chapter 3. The chemical reactants involved in blackwall alteration in Kl:1 are determined and a model is presented to explain these effects.

The temperature and pressure of metamorphism are estimated using the calcite-dolomite, magnetite-ilmenite and garnet-biotite geothermometers, and plagioclase-garnet and pyrite-pyrrhotite-sphalerite geobarometers in chapter 4. The assemblages observed in the ultramafic rocks are compared to those observed in other lithologies.

In chapter 5 a detailed description of the Thierry Mine geology (lithologies, ore types and structural geology) is given. Based on whole rock chemistry and alteration effects observed in the sheared and mylonitized um-m rocks, a model is proposed to explain these effects.

The detailed chemistry and mineralogy of the sulfide ore present at the Thierry Mine is given in chapter 6. A model is suggested to explain the assemblages and mineralogy developed during the violaritization process. The topologies suggested for the low-temperature relations in the system Ni-Fe-S are compared to assemblages observed at the Thierry Mine. A brief description of the sulfide assemblages observed in K1:1, J+I and G um-m bodies are given and compared to those noted at the Thierry Mine.

In chapter 7 the PGE and Ag mineralogy and their distributions are described and compared to those of other Cu-Ni deposits. The variation of Cu:Ni ratio in the Thierry Mine ore, from chlorite-biotite schist ore and breccia ore is presented in chapter 8. The Cu/Ni ratio of the Thierry Mine ore is compared to other Cu-Ni deposits, and models involving segration of a copper-rich sulfide liquid, differentiation of nickel-rich liquid, stress induced diffusion, mechanical segration and chemical mobilization are evaluated to explain this ratio.

1:2 Previous Work

The first government survey in the region was carried out between 1903 and 1905 by McInnis (1912). He reported a seventeen mile-long belt of Keewatin rocks, 1 to 4 miles wide occurring along Kapkichegemaga (Kapkichi) Lake and River. Little attention was paid to the area until the summer of 1928 when gold was discovered at Pickle Crow and Central Patricia. A regional survey was carried out by Hurst (1930) in the summer of 1929 which covered an area from July Falls to Kawinogans Lake. He produced a more detailed map covering the area around the Pickle Crow gold deposit extending to the eastern end of Kapkichi Lake. The eastern end of the area was mapped by Thompson in 1938. The Central Patricia and Pickle Crow gold area has received considerable attention; much of the data were compiled by Ferguson (1966). The area was mapped by Sage and Breaks (1976) during the summer of 1972.

A preliminary petrological study was made by Bowdidge (1970). Morton and Watkinson (1974) carried out a study of the sulfide ore mineralogy. The geophysical interpretation of the Kapkichi Lake area was presented at the International Geological Congress in Montreal (Verbeek et al, 1972).

1:3 Mining History

The Kapkichi Lake um-m rocks have been actively explored for their Cu-Ni potential for the past 28 years. On the basis of mineralized float, Central Patricia Gold Mines Limited carried out a ground magnetic survey, trenching, diamond drilling (18 holes, totalling 4144 feet) from 1946-1950 and discovered the J+I um-m body (Fig. 1:2). Kapkichi Nickel Mines Limited obtained the property in 1956 and carried out a more complete ground magnetic and electromagnetic survey. They drilled 8 diamond drill holes (4609') discovering the G ultramafic body (Fig. 1:2).

In 1969, UMEX Corp. Ltd. (Union Miniere Exploration and Mining Corporation Limited) optioned 12 claims from Kapkichi Nickel Limited. UMEX carried out a detailed ground EM and Magnetometer survey. They drilled 60 holes outlining J+I, G and several other small um-m lenses. The geophysical survey was then extended to the north of Kapkichi Lake. An anomaly (K2:1) was discovered and drilling outlined a 12 million ton deposit containing 1.68% Cu, 0.18% Ni. The shaft was collared in 1973 and sunk to 1700'. In 1976 a decline was completed to the 600' level. In 1977 the mining operation of two small open pits was completed to the 200' level. The mill came into production in the summer of 1977. In 1970, an anomaly to the east of the mine (K1:1) was found. Approximately 100 drill holes outlined a deposit containing 73 million tons of ore grading 0.39%Cu and 0.11%Ni, to 600'.

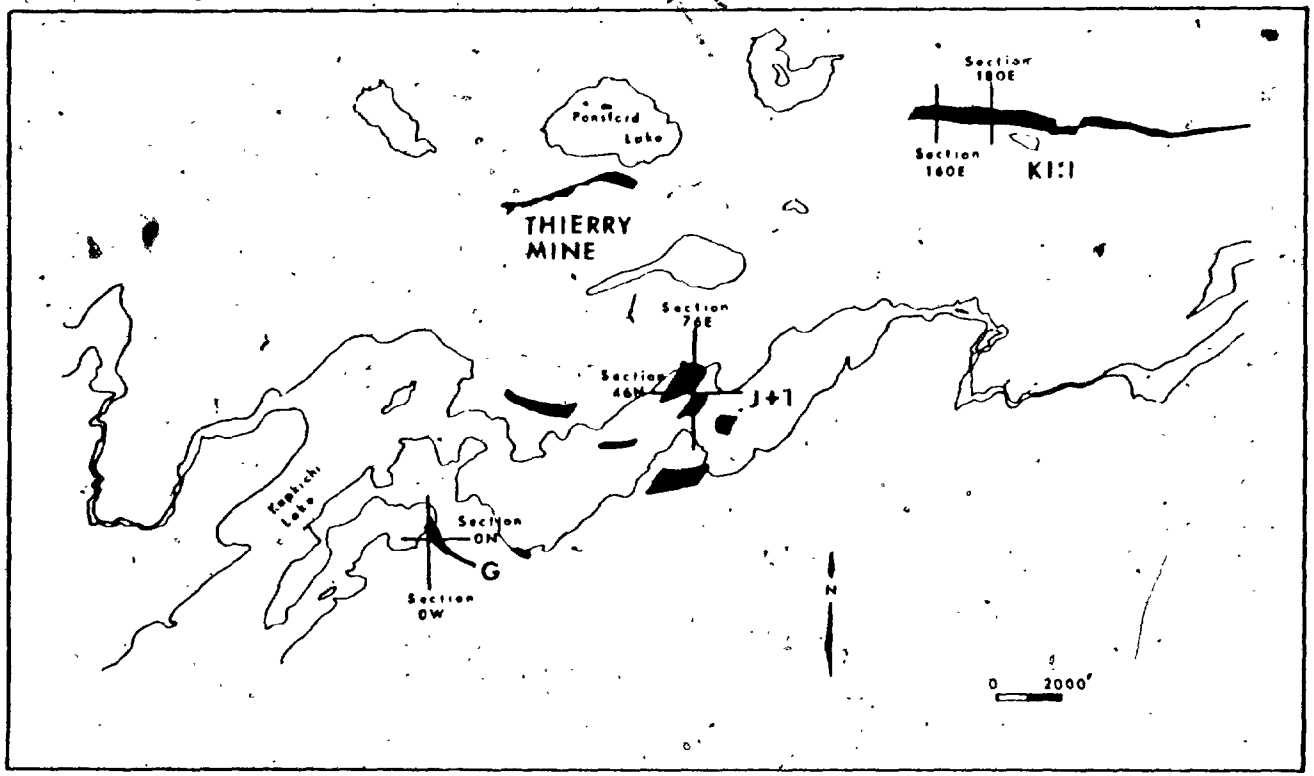

Fig. 1:2, Location of um-m bodies (black areas) and sections in the Kapkichi Lake area.

I became involved in the Kapkichi Lake area as a geophysical-geological assistant in 1971. In the summers of 1972-1974 this work was extended to regional mapping and geophysical studies centered on the Thierry Mine. In the summer of 1975 and 1976 I worked as mine geologist mapping in the open pit and underground and logging drill core (approximately 200,000 feet). In the summer of 1977, I was responsible for mine exploration and a drilling program on the K1:1 body.

1.4 Nomenclature

There are a number of problems concerning the classification of rocks from the Kapkichi Lake area.

1. There is some conflict in the use of the term ultramafic rock. The mineralogical definition of an ultramafic rock is; a rock having more than 90% mafic minerals. The rocks at the Kapkichi area have been converted to metamorphic assemblages. The calculation of the norms indicate they are gabbroic in composition containing 40 to 80% pyroxene and olivine; and 20 to 60% calcium plagioclase. This puts the rocks in the mafic class.

The term ultrabasic is based on the chemical composition. A rock containing less than 45% SiO_2 is considered to be ultrabasic. Examination of Appendix E shows that the normative gabbros are ultrabasic in composition (an average of 10 mafic gabbro contain 43.2% SiO_2 when calculated on an anhydrous basis).

Often these terms are used interchangably. For the purpose of this project, these rocks will be referred as ultramafic to mafic (um-m) rocks.

2. Mafic Metagabbro

This is the dominant um-m rock in the area, containing an average of 43.2% SiO_2 (the average of 10 whole rock analyses when calculated anhydrous) and normatively containing 40 to 80% mafic minerals. In thin section it contains 80 to 100% randomly oriented hornblende crystals (metamorphic in origin) and varying amounts of plagioclase, chlorite and biotite. The original rock varied from a gabbro to melano-gabbro. The term melano-metagabbro (or meta-melano-gabbro) was not used because of the range of composition and because the term is not common in the literature. The terms, hornblendite (refering to an igneous rock); amphibolite or epidiorite (contains a significant amount of plagioclase), hornblende ultramafic rock (implies an igneous origin for the hornblende) and hornfels (a rock that has suffered contact metamorphism) were thought to be ambiguous. Due to the lack of a clear rock category, the descriptive term mafic metagabbro will be used in this project.

3. Due to the number of geologists who worked at the Thierry Mine and the complexities in the amphibole-rich rock types, there are inconsistencies in the terminology used in the drill logs. Table 1.1 compares the rock names used in this project with those used by other workers at the Thierry Mine.

Table 1:1, Nomenclature Used by Geologists on the Thierry Mine Rocks

G. Patterson (This study)	M. Van Eyll	G. Mark	N. Bedwani	A. Gaudet	P. Kennedy	R. Overton
grandiorite	footwall granite	pink granite	granite	re[illegible]ite	granite	granitic rocks
granitic mylonite aplite	mylonitic granite micro-granite	mylonitic granite grey granite	crushed granite chert dyke	crushed granite silicified felsic rock	crushed granite fine grained grey granite	granite dyke felsite dyke micro-granite micro-diorite aplite
diorite	micro-diorite	diorite dyke	not logged	fine grained grey granite	fine grained grey granite	micro-diorite dark grey amphibolite
plagioclase-biotite schist	micro-granite	siliceous tuff	not logged	felsic biotite schist volcanics	diorite dyke	siliceous tuff
epidote-amphibolite schist	silicified schist	epidote-amphibolite	siliceous amphibolite	epidotized & granitized amphibolite	silicified & granitized amphibolite	meta-picrite
massive amphibolite	fine grained metagabbro	mafic tuff	amphibolite	metagabbro	intermediate volcanic	basic tuff amphibolite
mafic metagabbro	ultrabasic	ultrabasic pyroxenite	ultrabasic amphibolite altered peridotite	ultrabasic amphibolitized basic rock	ultrabasic	metadolerite metapyroxenite
talc-carbonate schist	ultrabasic schist	altered peridotite	ultrabasic chlorite schist	ultrabasic	ultrabasic	altered peridotite
hornblende-chlorite-biotite schist	chlorite-biotite schist	chlorite-biotite schist sheared ultrabasic	chlorite-biotite schist chloritic ultrabasic	chlorite-biotite schist silicified ultrabasic	chlorite-biotite schist	chlorite-biotite schist silicified tuff banded tuff

2. Geology of the Kapkichi Lake Area

2:1 Introduction

The Kapkichi Lake area (Fig. 1:1) is located within the Archean, Uchi Lake greenstone belt (Goodwin, 1976). The belt trends east-west from Lake Winnipeg to the Paleozoic cover west of James Bay and contains metamorphosed volcanic and sedimentary rocks of the Superior structural province of the Canadian Shield.

2:2 Regional Geology

The Uchi Lake greenstone belt (Pickle Lake subbelt, Fig. 2:1) consists of greenstones with minor felsic volcanics and metasedimentary rocks which have been intruded by granitic bodies; the Pickle Lake stock (south-east of the Thierry Mine), Ochig Lake stock (centered on Ochig Lake) and Hooker-Burkoski stock (south-west of Pickle Crow), and um-m intrusions; the Kapkichi Lake um-m bodies (Figl:2) and July Falls um-m body (west of Collishaw Lake). Foliations and fold axes tend to parallel the margins of the belt and contacts with large granitic stocks. The contact with gneissic terrain is characterized by lit par lit injection of granitic rocks. On large scale air photos there are several en echelon, NE trending lineaments along Trebell and Kiber Lake paralleling the edge of the belt. Many of the granitic dykes to the north of the Thierry mine show strong cataclastic textures.

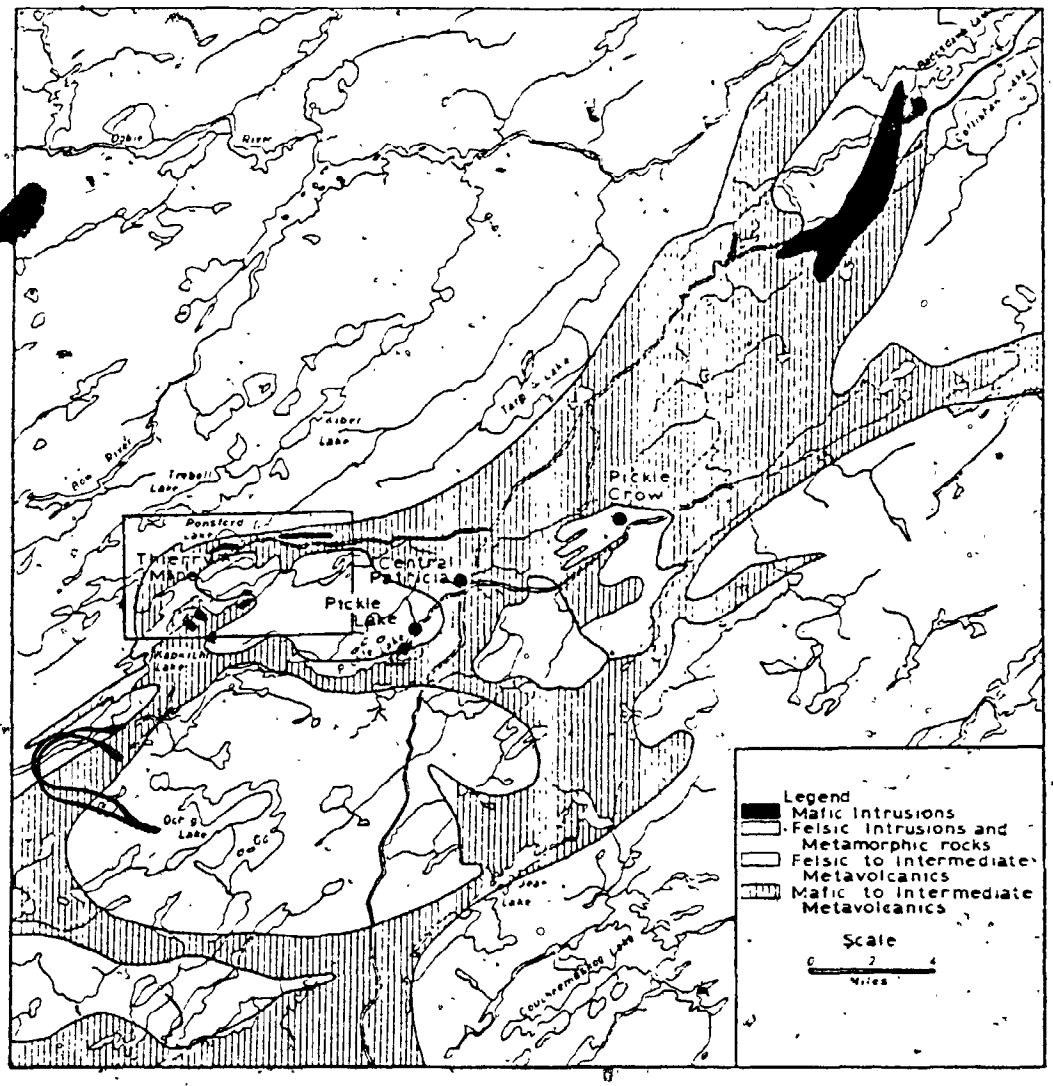

Fig. 2:1$_{pc}$ Geology of the Pickle Lake Area; after O.D.M. prelimary map, p809, Sage et al; 1973; rectangle outlines the Kapkichi Lake area.

2:3 Lithologic Units of the Kapkichi Lake Area

Metamorphosed intrusive, volcanic and sedimentary rocks make up 70%, 30% and 1% respectively of the rocks in the area. The intrusions are 90% granodiorite, 5% diorite and 5% metagabbro plus ultramafic rocks. The volcanic rocks are predominantly mafic with minor felsic tuffs and intercalated metasediments.

Table 2:1 Table of Formations of the Kapkichi Lake Area

Cenozoic

Recent:

peat, sand

Pleistocene:

sand, gravel, till

Precambrian

Late Veins:

quartz veins

Cataclastic Rocks:

hornblende-chlorite-biotite schist
granite breccia and granitic
mylonite

Dike Rocks:

diorite, granite, pegmatite

Ultramafic and Mafic Bodies

gabbro, peridotite, dunite

Felsic Plutonic Rocks:

porphyritic granodiorite to granite

Felsic to Intermediate Metavolcanics & Metasedimentary Rocks:

pelites, graphitic schist, calc-silicate gneiss,
tuff (biotite-plagioclase schist)

Mafic Metavolcanic Rocks:

amphibolite schist, epidote amphibolite
porphyroblastic amphibolite, carbonate-
epidote amphibolite, massive amphibolite

Felsic Intrusions and Metamorphic Rocks

2:3:1 Amphibolite

The mafic volcanic rocks in the map area have been converted to amphibolite and epidiorite by regional metamorphism. Very few primary igneous structures and textures are preserved. Only two outcrops of metavolcanic rocks show pillow-like structures. These pillows have been elongated or flattened parallel to the foliation. According to Sage et al (1973) the amphibolite in the map area is continuous with lower grade, pillowed mafic volcanic rocks in the Central Patricia area, 8 kilometres to the east.

Five varieties of amphibolite have been recognized; banded amphibolite schist, porphyroblastic amphibolite, massive amphibolite, epidote-amphibolite schist and epidote-carbonate schist, (Table 2:2). Detailed descriptions are given in Appendix A.

Biotite-Plagioclase Schist

Biotite-plagioclase schist is interpreted to have been tuff and occurs as conformable layers in the amphibolite from 8cm to 8 metres thick. In hand-specimen, the tuff is white, moderately well foliated, composed of 10 to 20% biotite and 80 to 90% quartz and plagioclase. The plagioclase (An_{20}) commonly occurs as indistinct fragments up to 2cm in length elongated parallel to the foliation. Accessory minerals are sphene, carbonate, pyrite with minor sphalerite, chalcopyrite and pyrrhotite.

Table 2:2, Characteristics of Amphibolites from the Kapkichi Lake Area

NAME	VOL. %	AVERAGE GRAIN SIZE	% HORNBLENDE	% PLAGIOCLASE	AN.	OTHER FEATURES
banded amphibolite schist	80	0.2mm	50-60	40-50	20-30	bands rich in plagioclase and hornblende
massive amphibolite	2	0.2mm	50-60	40-50	20-30	1-2% sphene
porphyroblastic amphibolite	2	0.5mm	50-60	40-50	20-30	hornblende as porphyroblasts up to 0.5mm
epidote-amphibolite schist	8	0.2mm	40-50	40-50	30-60	porphyroblasts of epidote, 10-20% epidote
epidote-carbonate-amphibolite schist	8	0.2mm	40-50	40-50	30-60	1-10% calcite-dolomite 10-20% epidote

2:3:2 Metasedimentary Rocks

The sediments occur in drill core as minor conformable layers associated with tuffaceous units (Fig. 1:2) to the east of the mine, in outcrop just south of K1:1 (L180E,100N) associated with amphibolite and on a small island 300 metres west of the G zone (120W,25S). Calc-silicate rocks are most common but minor pelitic and graphitic rocks also occur. Amphibolites of sedimentary origin occur south of K1:1. They are finely banded, highly variable in ratio of hornblende and plagioclase and intensely deformed. Detailed descriptions of the metasedimentary rocks are given in Appendix A.

2:3:3 Ultramafic and Mafic Rocks

i) The Thierry Mine um-m Rocks

The Thierry mine is located in ultramafic and metagabbroic blocks which have been sheared in a mylonitized zone. The um-m rocks are mafic metagabbro, talc-carbonate schist, olivine-tremolite-chlorite rock and metagabbro. Remnant igneous mineralogy of the metagabbro is plagioclase (An_{50}-An_{60}) and clinopyroxene with exsolved ilmenite. These alter to a mixture of hornblende and plagioclase. Clinopyroxene-rich gabbro alters to mafic metagabbro; plagioclase-rich gabbro alters to metagabbro. The talc-carbonate schist was originally dunite and the olivine-tremolite-chlorite rock, a peridotite. The metagabbro and mafic metagabbro are gradational into each other but the relationship of the talc-carbonate schist and the olivine-tremolite-chlorite rock to the mafic metagabbro and metagabbro is unknown. Shearing of these um-m rocks has produced hornblende-chlorite-biotite schist, a protoblastomylonite which is continuous throughout the length of the mine (2000 metres). The mylonite often includes large blocks of relatively undeformed amphibolite schist, mafic metagabbro, metagabbro and diorite. The petrology of the Thierry Mine ultramafic and associated rocks are more fully described in Chapter 5.

Sulfides occur as intercumulus material, breccia ore, chlorite-biotite schist ore, bornite ore, and altered ore making up 1%, 40%, 56%, 2% and 1% respectively of the ore. A detailed description of the sulfide mineralization is given in Chapter 6.

ii) G- Ultramafic and mafic Body

The um-m rocks from the G body are very similar to the partially altered um-m rocks from the J+I zone. The G Body rocks consist of 10% altered peridotite, 80% altered gabbro, minor altered dunite and 10% oxide-rich layer. The oxide layer occurs in the lower section of the fault block shown on section ON (Fig. 2:9), close to the southern contact with the granite.

The oxide layer consists of 70% polygonally recrystallized magnetite with exsolved ilmenite, 10% ilmenite, 10% olivine, 10% tremolite and antigorite. Minor minerals are Mg-Fe spinel, sulfides and graphite. The olivine is zoned from an iron-rich core (Fo_{60}) to magnesian rims (Fo_{68}). The olivine appears to be metamorphic in origin, polygonally recrystallized with included antigorite-tremolite masses. The Mg-Fe spinel contains up to 2.91% Zn (Appendix D, Table 8). The sulfides, described in chapter 6, occur as primary disseminated sulfides, metamorphosed disseminated sulfides and sulfides associated with the oxide layer.

Table 2:3, Mafic and Ultramafic Rocks from the K1:1 Body

ROCK	ORIGINAL ROCK	MINERALOGY	REMNANT MINERALOGY	PERCENTAGE OF THE K1:1 BODY
metagabbro	gabbro	50-80% hornblende 20-50% plagioclase (An_{20}-An_{30}) biotite, chlorite, sphene, apatite, ilmenite, magnetite	40% clinopyroxene with exsolved hypersthene and ilmenite 60% plagioclase (An_{50}) both as cumulus phases	25%
mafic metagabbro	mafic gabbro	80-100% hornblende 0-20% plagioclase (An_{20}-An_{30}) biotite, chlorite, cummingtonite	60% clinopyroxene with exsolved hypersthene and ilmenite 40% plagioclase (An_{50}) both as cumulus phases	25%
biotite-hornblende schist (blackwall alteration)	gabbro	20-80% biotite 10-70% chlorite 10-60% hornblende 10-50% tremolite sphene magnetite	as metagabbro or mafic metagabbro	50% near ultramafic-amphibolite contact, fault zones and dykes

iii) Kl:1 Ultramafic and Mafic Body

The Kl:1 um-m body, located 3 kilometres east of the Thierry Mine (Fig. 1:2) is lensoid with a fault-bounded northern contact and a southern contact that is conformable to the foliation in the amphibolite schist. All samples examined have metamorphic assemblages with only rare igneous remnant mineralogy. The mafic metagabbro and metagabbro formed from a gabbro containing clinopyroxene (with exsolved ilmenite) and plagioclase (An_{50}-An_{60}) as cumulus phases. Rare pods of peridotite and talc-carbonate schist are associated with mafic metagabbro. The um-m rocks occur near the core of the body and grade to biotite hornblende schist near the contact with amphibolites and faults. The biotitic rocks are interpreted to be metasomatic (blackwall alteration). Metagabbro occurs as dykes cutting the um-m body and as large lenses on the south side of the body. The mafic metagabbro, metagabbro and biotite hornblende schist make up 25%, 25% and 50% respectively of the um-m body. The sulfides occur as metamorphosed disseminated sulfides and more rarely as breccia ore (see Chapter 6 for full description).

Biotite-Chlorite Schist

Biotite-chlorite schist is interpreted as blackwall alteration. The alteration occurs in zones up to 50 metres wide adjacent to the contacts between amphibolite and ultramafic rocks and adjacent to fault zones and dykes (Fig. 2.10 and 2.11). Adjacent to dykes through several metres the ultramafic rock is converted to a schist containing 80% biotite (Plate 9F).

In handspecimen, the rock is medium-grained, well foliated with joints coated by dark green chlorite and often folded on a fine scale. In thin-section, the biotite-hornblende-schist is composed of 20 to 80% light brown, coarse laths of biotite, 10 to 70% light green chlorite as bladed crystals, 10 to 60% dark green hornblende oriented parallel to foliation and 10 to 50% colourless tremolite. In several specimens, hornblende is bent and fractured with chlorite-rich pressure shadows. Accessory minerals are sphene, magnetite as 5mm porphyroblasts and apatite. Epidote and carbonate occur as lenses and pods elongated parallel to foliation.

iv) J+I Ultramafic and Mafic Rocks

The ultramafic samples examined from the J+I bodies consist of metamorphic assemblages with only approximately 20% of the ultramafic rocks showing remnant igneous minerals. Both igneous and metamorphic olivine were observed, the latter occuring as coarse bladed crystals up to 3cm long (pseudo-spinifex) and as polygonal crystals with sharp triple junctions (Plate 3E). Both forms have overgrown antigorite and tremolite and have compositions of Fo_{85}-Fo_{90}. The igneous olivine occurs as brownish round cumulus crystals (Plate 3D) with a composition of Fo_{65}. The sulfide minerals, fully described in Chapter 6, occur as four main types; primary disseminated sulfides, metamorphosed disseminated sulfides, breccia ore and oxidized breccia ore.

Dunite

About 5% of the samples of the J+I bodies were dunites. They contain 20 to 70% remnant igneous olivine as round cumulus grains and iddingsite-talc-lizardite pseudomorphs after olivine, and 30 to 80% metamorphic products (chlorite anthophyllite and magnesite). The oxides and sulfides occur in an intercumulus position molded around olivine crystals.

Table 2:4, Rocks from the J+I Body

ROCK	MINERALOGY	ORIGINAL MINERALOGY	PERCENTAGE OF J+I ULTRAMAFIC BODY
dunite	20-70% olivine 0-70% serpentine 0-30% anthophyllite 0-5% magnesite 0-10% lizardite 0-10% talc, magnetite ilmenite, sulfides	olivine	5
peridotite	olivine, tremolite, anthophyllite serpentine, chlorite, dolomite magnesite, magnetite, ilmenite	50-80% olivine 20-50% clino- pyroxene with exsolved hypersthene	10
gabbro	clinopyroxene, plagioclase olivine, hornblende ilmenite, magnetite	50-70% clinopyroxene exsolved hypersthene 30-50% plagioclase as zoned cumulus crystals An_{50}-An_{60} minor olivine ilmenite magnetite	80
olivine gabbro	olivine plagioclase, tremolite ilmenite, magnetite	40-50% olivine 40-60% plagioclase An_{50}-An_{60}	5

Table 2:5, G Zone (10% peridotite, 80% altered gabbro)

ROCK	MINERALOGY	ORIGINAL MINERALOGY	PERCENTAGE OF G ULTRAMAFIC BODY
oxide layer	70% magnetite with exsolve ilmenite 10% ilmenite 10% olivine 5% tremolite 5% chlorite minor sulfides, graphite Mg-spinel	80% ilmenite-magnetite 10% olivine 10% clinopyroxene	10

Peridotite

Ten percent of the J + I Bodv is peridotite, mainly wehrlite, consisting of 50 to 80% olivine and 20 to 50% clinopyroxene with minor exsolved hypersthene. Orthopyroxene is the most readily altered of the primary phases which suggests that some of the more highly altered samples might have been lherzolites. Remnant orthopyroxene is intercumulus to olivine.

Secondary products are tremolite, anthophyllite, olivine, Mg-chlorite, dolomite and magnesite commonly as coronas related to the primary mineralogy. As many as six separate zones have developed between plagioclase and orthopyroxene:

a) Orthopyroxene remnants in part altered to lizardite and iddingsite

b) Tremolite, well crystallized to large patches with the same optical orientation,

c) Fibrous tremolite as radiating masses

d) Anthophyllite as randomly oriented crystals in a matrix of talc

e) Anthophyllite and Mg-chlorite

f) Mg-chlorite and Fe-chlorite

g) Coarse patches of light green chlorite, with dark green brunsvigite and fine opaques

Between olivine and clinopyroxene four zones occur consisting of

a) Olivine remnants, in part altered to lizardite and iddingsite

b) Tremolite, large patches surrounding the olivine remnants

c) Tremolite as randomly oriented bladed crystals and bladed Mg-chlorite

d) Coarse patches of dark green Fe-Chlorite and colourless bladed Mg-chlorite

These zones appear to be due to the incomplete diffusion of calcium to the margin of the magnesium-bearing phase and magnesium to the calcium-bearing phase during metamorphism.

Gabbro

Gabbro consists of 50 to 70% clinopyroxene with minor exsolved hypersthene and ilmenite and 30 to 50% zoned plagioclase with minor olivine and hypersthene. The plagioclase is An_{65} at the core and An_{50} at the rim, and many crystals show evidence of adcumulus growth. Olivine occurs only as poikilitic inclusions in the plagioclase.

A kelyphitic rim of hornblende occurs between clinopyroxene and plagioclase (Plate 1). In rocks with only minor amounts of original plagioclase, the rims have completely engulfed the plagioclase producing a rock composed of 100% hornblende.

Olivine gabbro consists of 40 to 50% olivine as rounded cumulus crystals up to 2mm in diameter, 20 to 30% plagioclase as zoned crystals (An_{50} to An_{65}) and 20 to 40% tremolite. The tremolite occurs as coronas similar to the hornblende in the clinopyroxene gabbro.

A complete gradation can be seen between the olivine gabbro and plagioclase peridotite but none is apparent between clinopyroxene gabbro and plagioclase peridotite.

Rhythmic layering

One sample showed rhythmic layering of dunite (20% olivine remnants and 80% serpentine) to mafic gabbro (20% clinopyroxene, 50% hornblende and 30% plagioclase) to gabbro (50% hornblende and 50% plagioclase) to dunite in a thin section. Contacts between individual layers are very sharp.

2:3:4 . Porphyritic Granodiorite

Porphyritic granodiorite (Pickle Lake Stock) occurs as a large intrusive body about 10 by 5km centred on Pickle Lake. The contact zone between the amphibolite and the Pickle Lake Stock is sharp to gradational and characterized by granitic dykes in amphibolite schist over one kilometre.

The porphyritic granodiorite is white, coarse-grained, massive to weakly foliated, composed of 30 to 40% euhedral, zoned, K-feldspar phenocrysts, 30 to 50% plagioclase (An_{10}-An_{15}) as small phenocrysts, 0 to 20% quartz, 10 to 15% green biotite and minor hornblende and perthite. Accessory minerals are sphene, apatite, zircon, pyrite and chalcopyrite. Alteration products are sericite, epidote and chlorite.

In the foliated samples mortar structure is evident; the margins of K-feldspar and plagioclase are bent and fractured and recrystallized to a fine-grained aggregate. A very strong joint set at right angles to the contact between the granodiorite and amphibolite is developed in the Thierry Mine. These joints are often filled with gypsum and thaumasite (Lefebvre, 1977).

Granitic Dykes

Granitic dykes are most common in the amphibolite in the contact zone with the Pickle Lake Stock. The dykes are from 10cm to 5 metres thick and have sharp contacts with the amphibolites. The dykes are fine-grained, grey to red, massive to weakly foliated, composed of 30-40% K-feldspar, 20-30% perthitic intergrowths of plagioclase and K-feldspar, 30-40% plagioclase, 10-20% quartz and minor biotite and hornblende. Accessory minerals are sphene, apatite and zircon. Alteration products are sericite and epidote.

Diorite Dykes

The diorite dykes are from 10cm to 2 metres thick with sharp contacts. The dykes cutting ultramafic rocks are dioritic while similar dykes in amphibolites are granitic in composition. The dykes are white, very fine-grained, massive to well foliated, composed of 40 to 50% plagioclase (polygonally recrystallized and zoned from An_{10} to An_{20}) 50% to 60% tremolite, minor biotite, accessory apatite, sphene and magnetite. The dykes cut the porphyritic granodiorite in the shaft at 1120' in the Thierry Mine. Many of the faults follow the diorite dykes, shearing the dyke into irregular blocks with mylonitic material between the blocks. Near the hornblende-chlorite-biotite schist in the Thierry Mine the plagioclase in the diorite dykes is altered to epidote along joint sets.

Pegmatites

Pegmatites are uncommon in the area. Several pegmatitic dykes occur on the 1600' level in the Thierry Mine. The pegmatites are massive, coarse-grained, red, composed of 75% plagioclase, 10% perthite, 10% quartz often at the core of the dykes and 5% hornblende and minor tourmaline.

Aplite Dykes

Aplite dykes are associated with ultramafic and metagabbro near the contact with chlorite-biotite schist. The dykes are 2cm to 30cm thick, white, massive, composed of 80 to 100% polygonally recrystallized plagioclase with oscillatory zoning (An_{20}-An_{30}) and 0 to 20% angular fragments of mafic metagabbro up to 2cm in diameter.

Quartz Veins

Quartz veins cut all rock types in the area but are most common in chlorite-biotite schist. The veins contain minor sulfides, hornblende, rock fragments and natrolite. The quartz is strained and polygonally recrystallized. Often the veins are in fault zones associated with diorite dykes.

Granitic Mylonite and Granite Breccia

Granitic mylonite occurs as narrow zones in faults cutting granites and amphibolites, and near the margin of the J & I um-m body. The mylonite is variable in composition and texture. It is commonly composed of 40 to 50% plagioclase as crystals with a mortar structure, 20-30% polygonally recrystallized and granulated quartz and 20-30% hornblende, mylonitized and concentrated into layers. In less deformed samples, brecciated fragments of granite occur in a matrix of mylonite.

2:4 General Geology of the Kapkichi Lake Area

The interpretation of the geology of the Kapkichi Lake area is largely based on drill hole data and geophysical information (Em250 broadside and magnetometer survey). Outcrops (less than 1% of map area) are small and confined to the edges of lakes. Fig. 2:2 shows drill hole locations, a summary of the geophysical data and outcrop location.

A detailed structural study was beyond the scope of this thesis since permission to carry out the structural interpretation was given to P. Cameron of The Pennsylvania State University. However some data were collected outside the limits of his area to help interpret the general geology of the area.

The belt consists of folded and metamorphosed mafic volcanic rocks, minor sediments, tuffs and um-m rocks with the Pickle Lake Stock, a porphyritic granodiorite, at the core of the folds (Fig. 2:3). The amphibolite schist has a strong foliation and lineation defined by prismatic hornblende crystals. Fig. 2:4B shows a S-pole diagram of 42 foliations in amphibolite. Measurements were made in areas unaffected by shears and faults to eliminate the possibility of rotation.

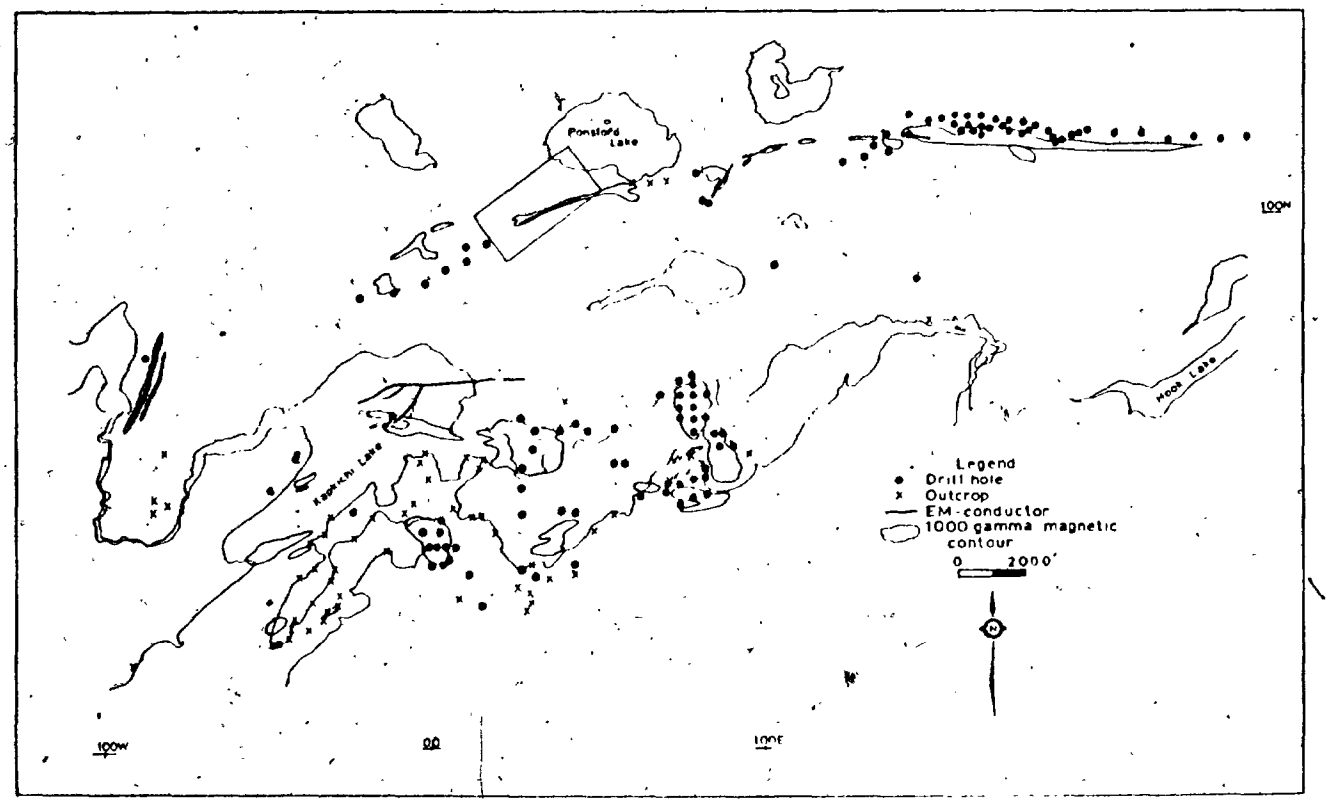

Fig. 2:2, Diamond drill hole locations, outcrop locations and summary of geophysical data for Kapkichi Lake area. Rectangle outlines the Thierry Mine area.

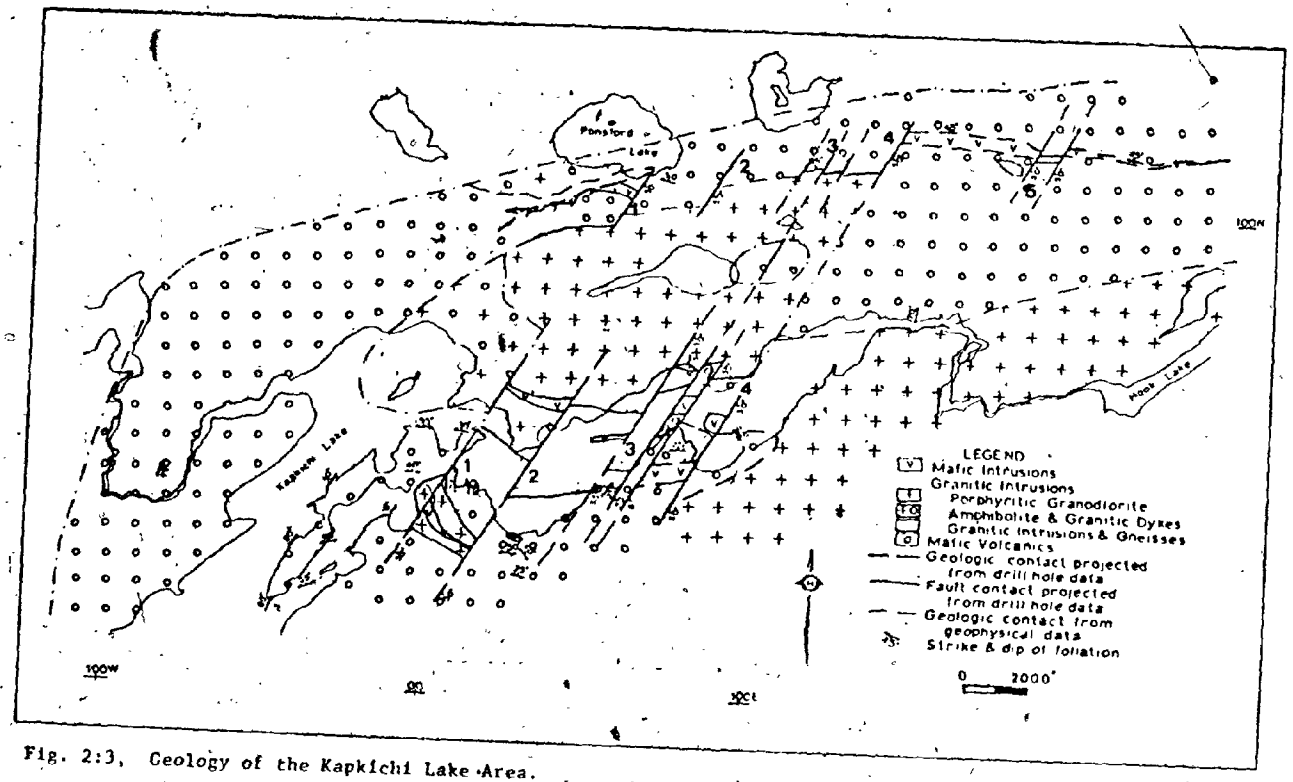

Fig. 2:3, Geology of the Kapkichi Lake Area.

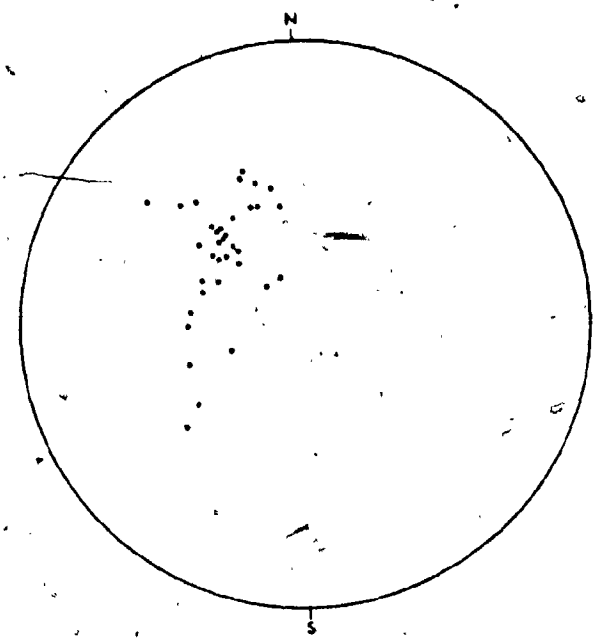

Fig. 2:4A, Sterographic Plot (Wulff net) of 35 hornblende lineations from amphibolites in the Kapkichi Lake area.

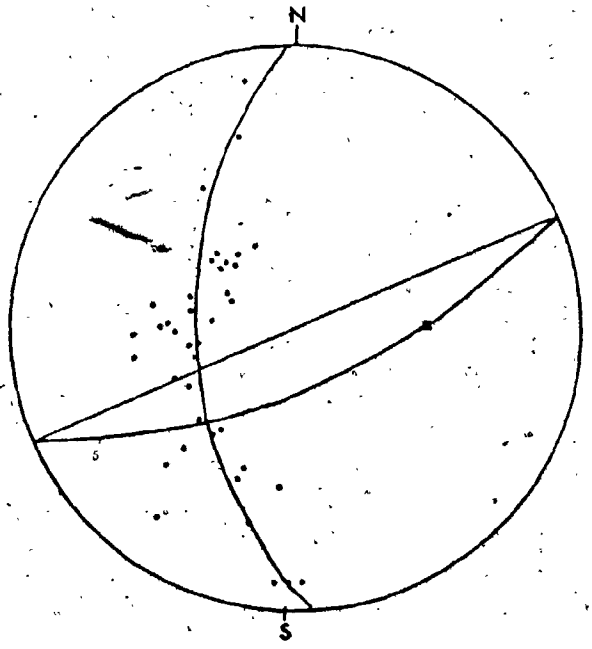

Fig. 2:4B, S-Pole sterographic plot of 42 foliations poles in the Kapkichi Lake area. Solid square is the pole to the axis of the second phase fold.

The foliations in the amphibolite schist plot along the great circle $2^{\circ}/52^{\circ}W$ with the axis at $92/38^{\circ}E$ (Fig: 2.4B). A fold-hinge trace at 68° is inferred from Fig. 2:3. This is parallel to the regional fold axis described by Ferguson (1967) in the Pickle Crow region ten kilometres to the east. This implies a dip on the axial plane of 68° to the north (Ragan, 1973). A stereogram of 35 hornblende lineations (Fig. 2:4A) shows that they may be described by a great circle $15^{\circ}/52^{\circ}W$. Based on limited observations in the porphyritic grandiorite, the foliations developed in it are parallel to those developed locally in the amphibolite schist. Minor folds developed in banding in the amphibolite schist are tight with their axial planes parallel to the foliation in the amphibolite schist and axial trace parallel to hornblende lineations.

These structures are interpreted to result from three phases of plastic deformation. A first phase of deformation produced tight isoclinal folds, minor folds, hornblende foliation and lineation, parallel to bedding. A second moderately tight folding event with an axial plane of $68^{\circ}/68N$ folded the pronounced foliation and lineation in the amphibolite schist from the first phase. The third phase is indicated by a broad bend in the second phase fold axis to the north. (Fig. 2:3).

Since no second phase minor structures were recognized it was not possible to determine the plunge and trend of the second phase folds. The third phase could be considered to be a continuation of the second phase. The main metamorphic event is associated with the first phase of deformation and development of hornblende foliation and lineation.

The fourth phase of deformation is dominantly cataclastic. Faults cuts all folds and rock units in the area. The main fault system runs at $30^{\circ}/50^{\circ}$E parallelling a major fault system developed in the mine area (Chapter 5). Evidence for the major faults (numbers refer to faults on Fig. 2:3) is as follows:

1. Faulting was recognized in the eastern end of the mine um-m rocks, a weak EM conductor (Fig. 2:2), a magnetic anomaly (Fig. 2:2) and the western side of the G um-m body. These maybe aligned and imply a major fault as shown in section OW (Fig. 2:9) and ON (Fig. 2:8). In the granites, a mylonite or granitic breccia is developed whereas in the um-m rocks a chloritic schist is developed.
2. Further to the east a second fault which contains a quartz-pyrite vein, cuts pyritic felsic tuffs. To the south the same fault cuts a ultramafic body to the north of Kapkichi Lake and the eastern end of the G um-m body.

3. A set of three closely spaced parallel faults are proposed to explain offsets in the electromagnetic expression of a pyritic tuff east of the Thierry Mine. A drill hole K168 (L86N, 110E) which intersects one of these faults ends in a mylonite. These faults also cut the J & I um-m bodies (Fig. 2:6 and Fig. 2:7), developing mylonitic zones. Fig. 2:5 shows whole rock chemical analyses from a drill hole, 200 feet west of section 76E. The data show a trend consistent with magmatic differtiation but at 550' the trend shows a discontinuity implying the presence of a fault.

4. A fourth fault cuts an electromagnetic conductor at the west end of K1:1 body and is shown in section 160E. (Fig. 2:11)

5. A fifth pair of faults offsets the K1:1 um-m body.

Other major faults in the area include the main shear in the Thierry Mine (Chapter 5). This may project as a major shear along the northern contact of the K1:1 um-m body. Section 160E (Fig. 2:11) shows that the shear cuts the faults at 30°/50E. To the west of the Thierry Mine, a drill hole penetrated a major fault zone which may be the western extension of the mine shear. Since the zone is not mineralized there is no geophysical expression and the shear cannot be traced beyond the mineralized um-m rocks.

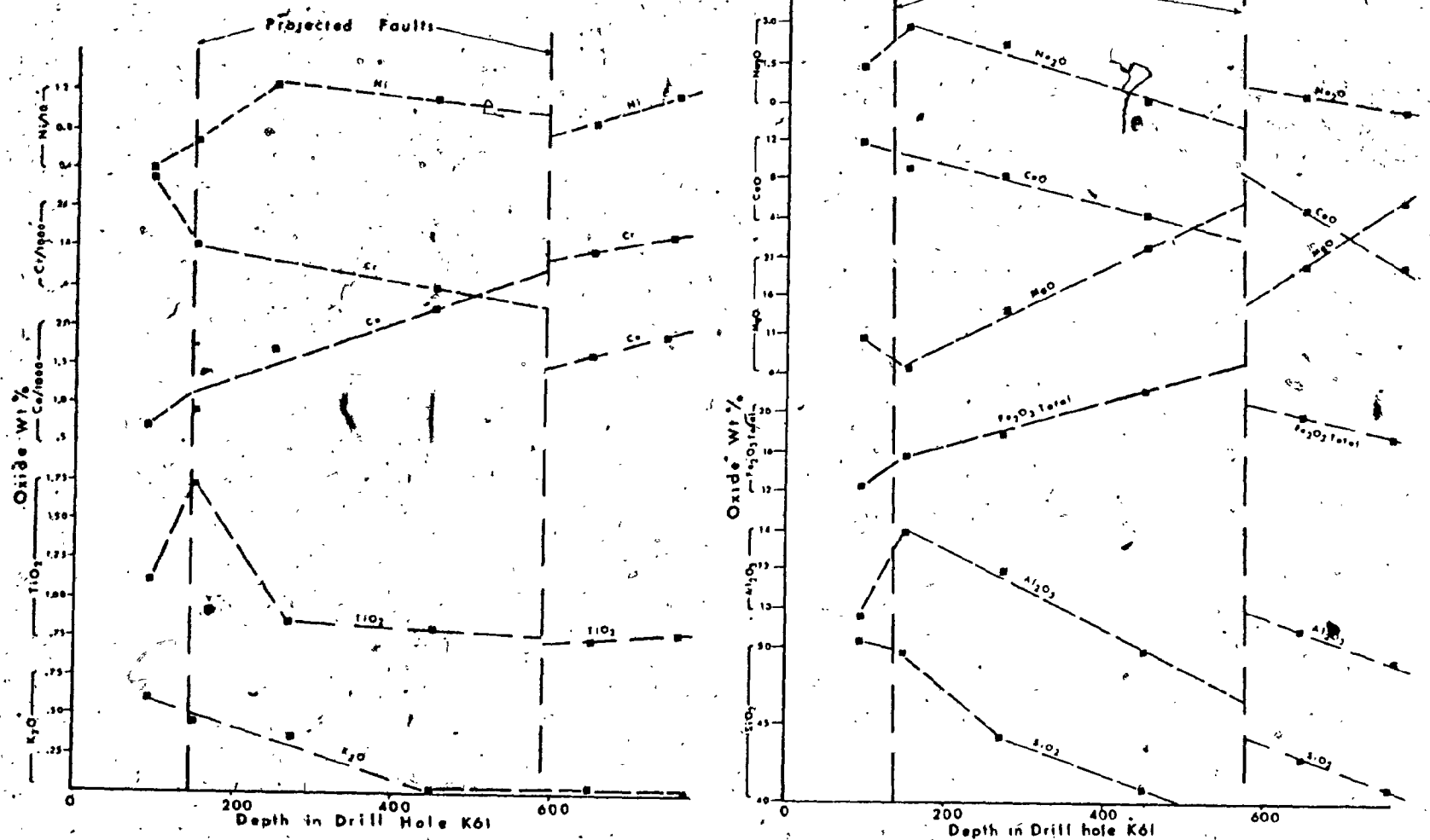

Fig. 2:5, Concentrations vs depth in drill hole K61, J+I ultramafic body, (Co, Cr, Ni, in ppm, TiO_2, K_2O, Na_2O, CaO, MgO, Fe_2O_3, Al_2O_3, SiO_2 in wt%)

The northern contact between granitic gneiss and amphibolite was only located by overburden drilling for the tailings pond of the Thierry Mine. The contact is gradational in that the number and size of granitic dykes increases to the north. The contact was drawn on the basis of results of airborne geophysics (450 gamma line).

The contact between the Pickle Lake stock and the amphibolites is very sharp where exposed in the Thierry Mine shaft. There are large blocks of amphibolite cut by quartz veins included in the Pickle Lake stock. To the south and west the contact is less distinct but the number of dykes and sills increases towards the stock. The G and J+I um-m bodies cut the stock (Fig. 2:6, 2:7, 2:8, 2:9) but are in general parallel to foliation in the amphibolite (Fig. 2:3). Minor chlorite- and biotite-rich (blackwall) alteration occurs near the contacts. The contact between the K1:1 mafic rocks and amphibolite is in general parallel to the foliation in the amphibolite. Extensive zones of blackwall alteration exist along fault contacts and contacts of amphibolites and dykes.

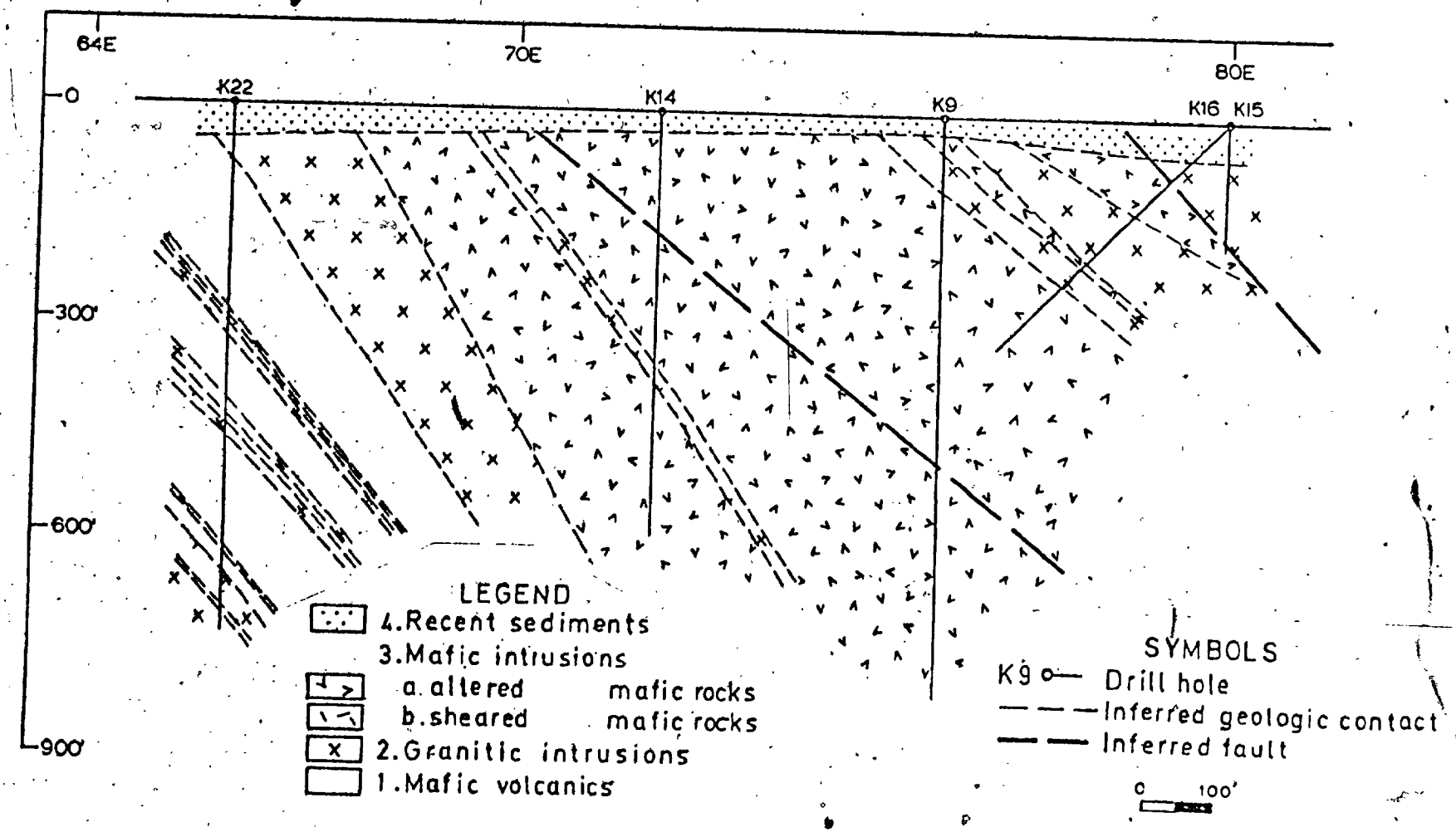

Fig. 2:6, Geological interpretation of Section 46N, J+I um-m Body Location on Fig. 1:2.

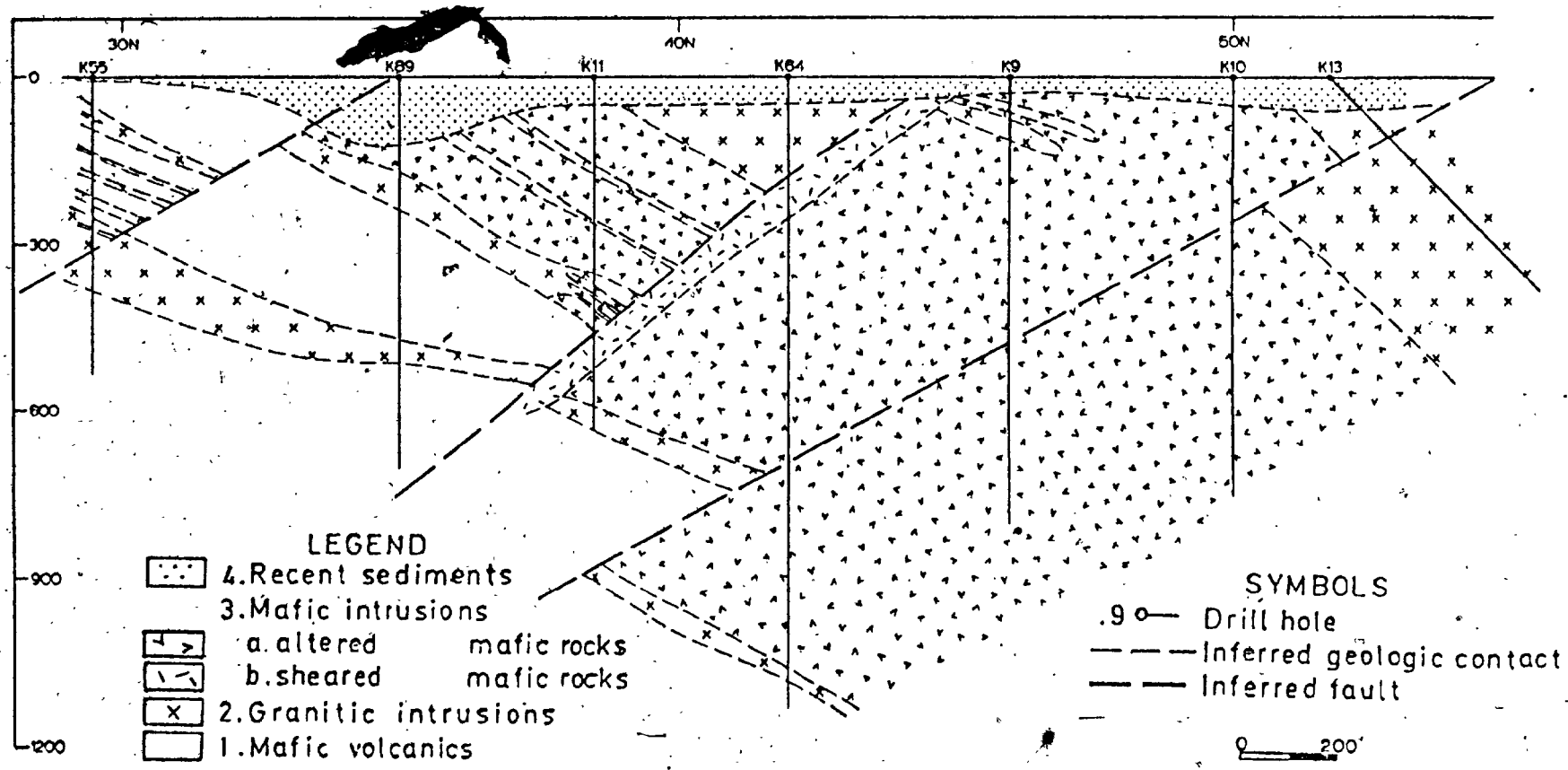

Fig. 2:7, Geological interpretation of Section 76E, J+I um-m Body, Location on Fig. 1:2.

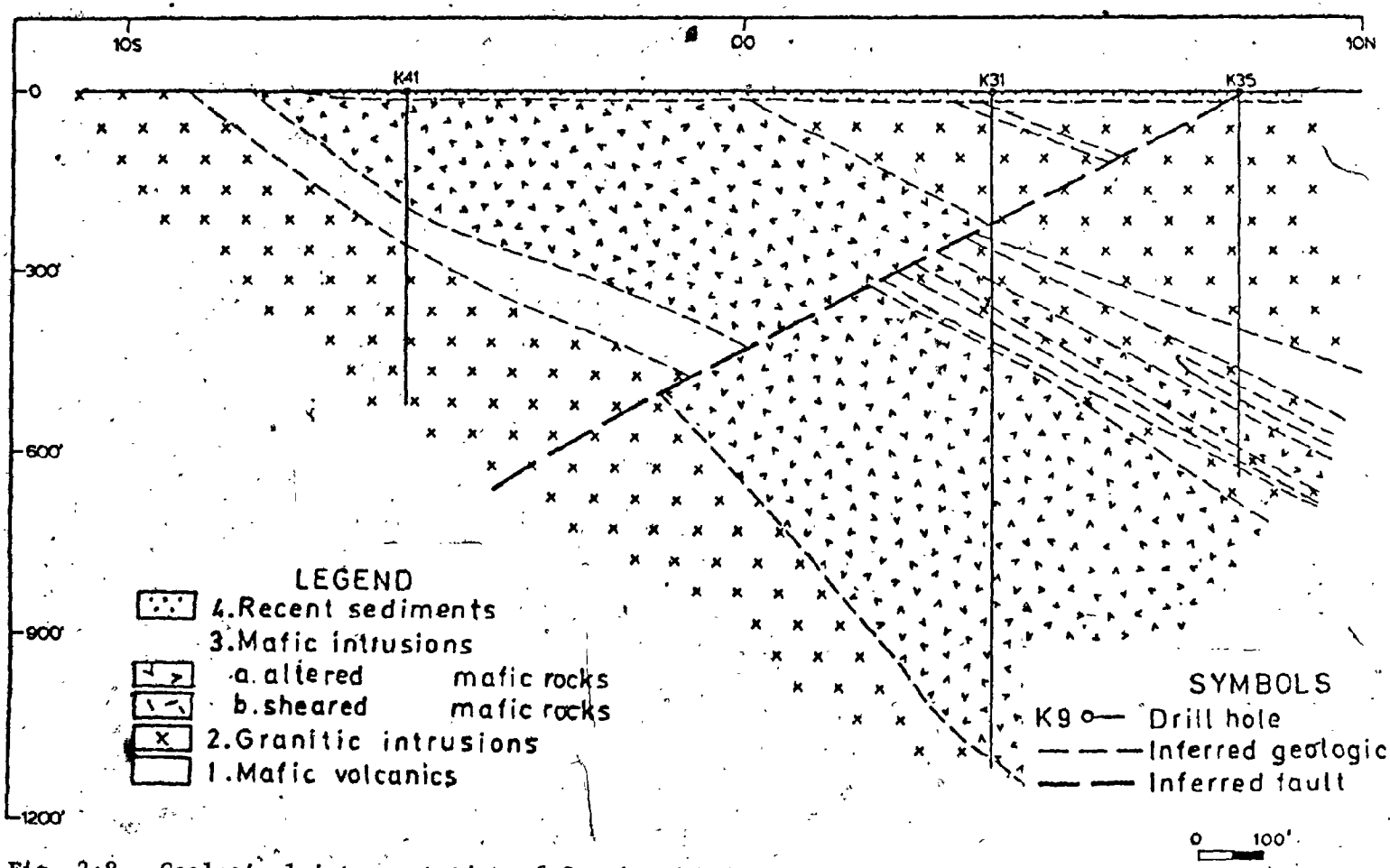

Fig. 2:8, Geological interpretation of Section OW, G um-m Body, Location on Fig. 1:2.

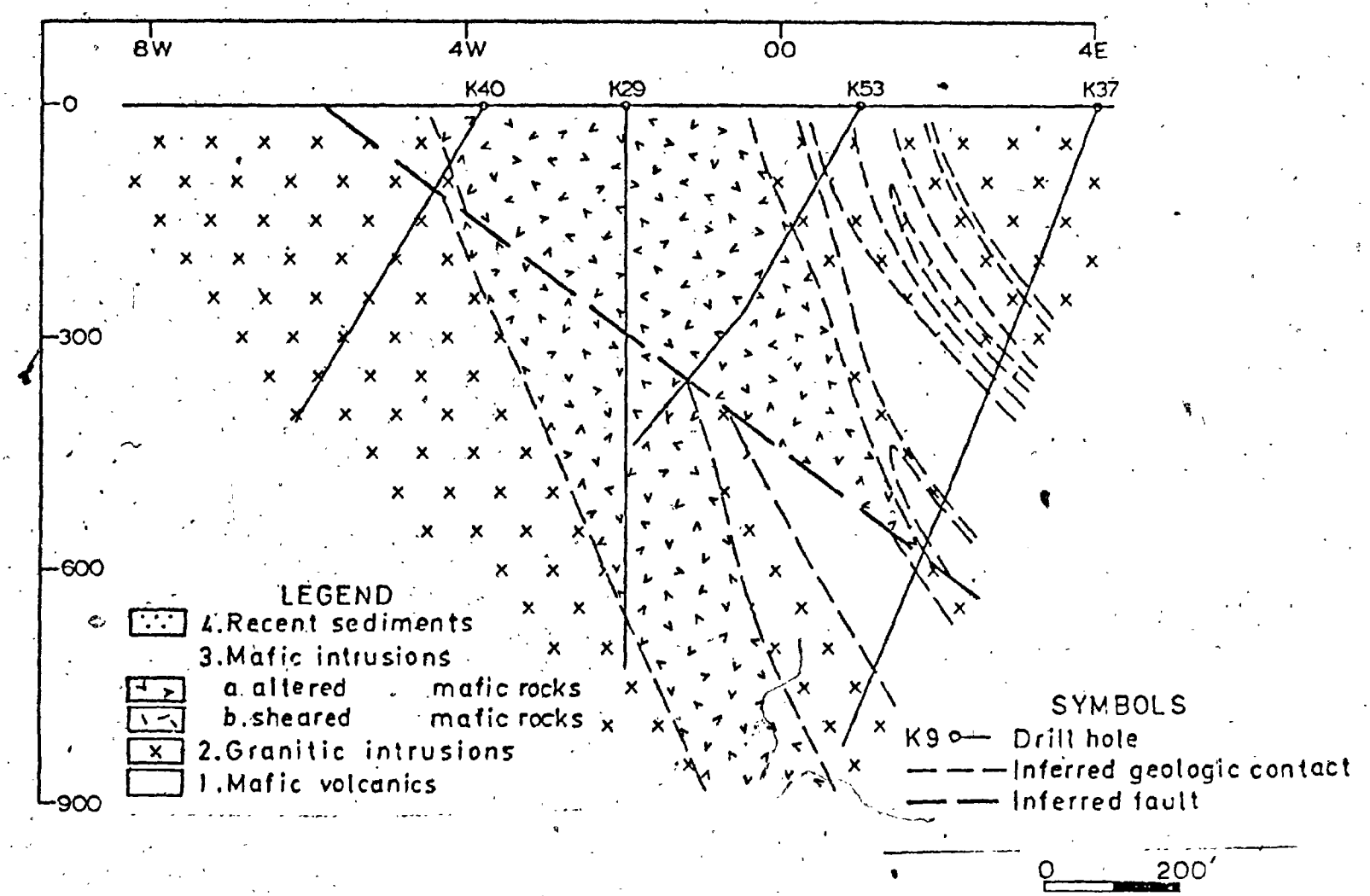

Fig. 2:9, Geological interpretation of Section ON,G-um-m Body, Location on Fig. 1:2.

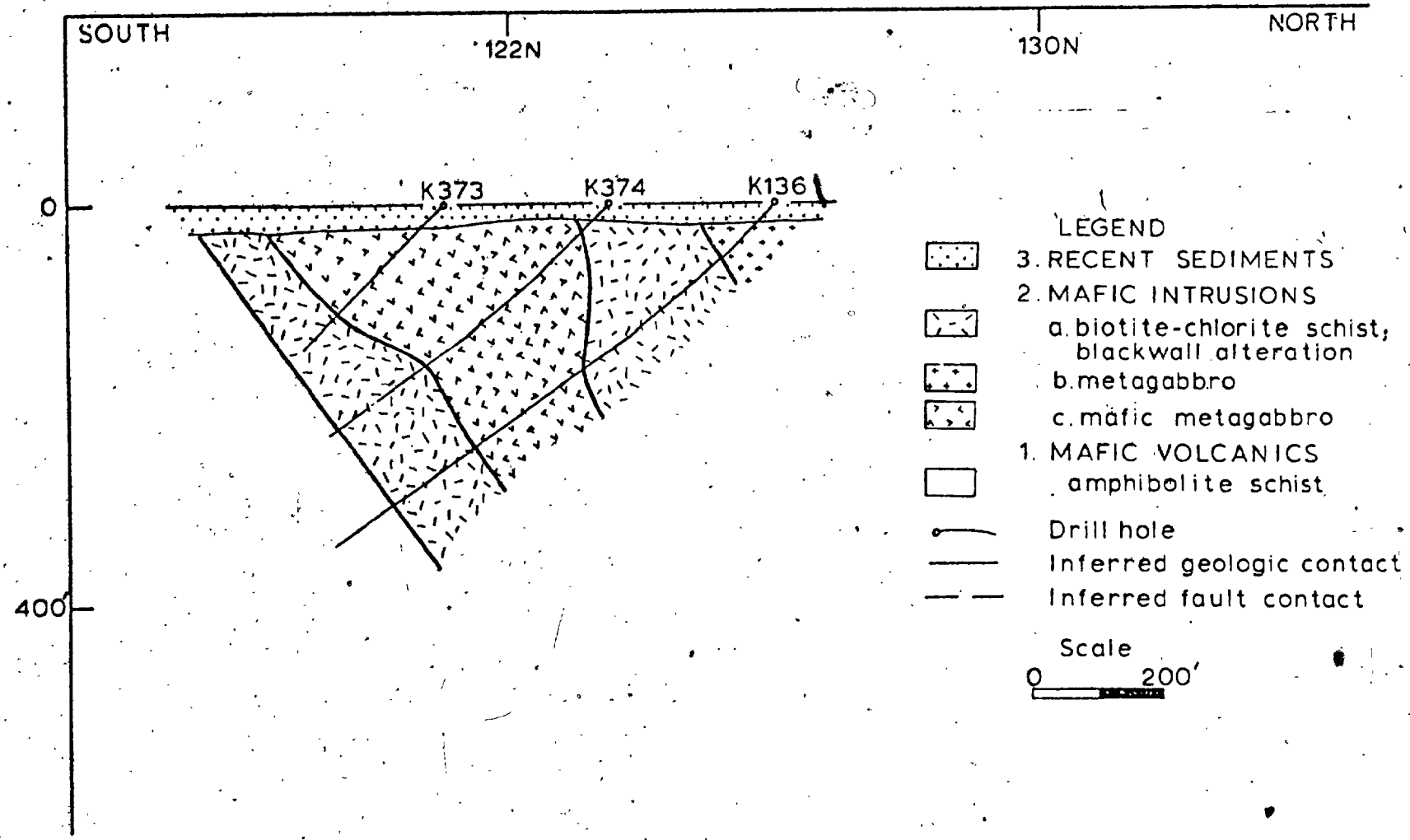

Fig. 2:10, Geological interpretation of Section 180E, K1:1 um-m Body, Location on Fig. 1:2.

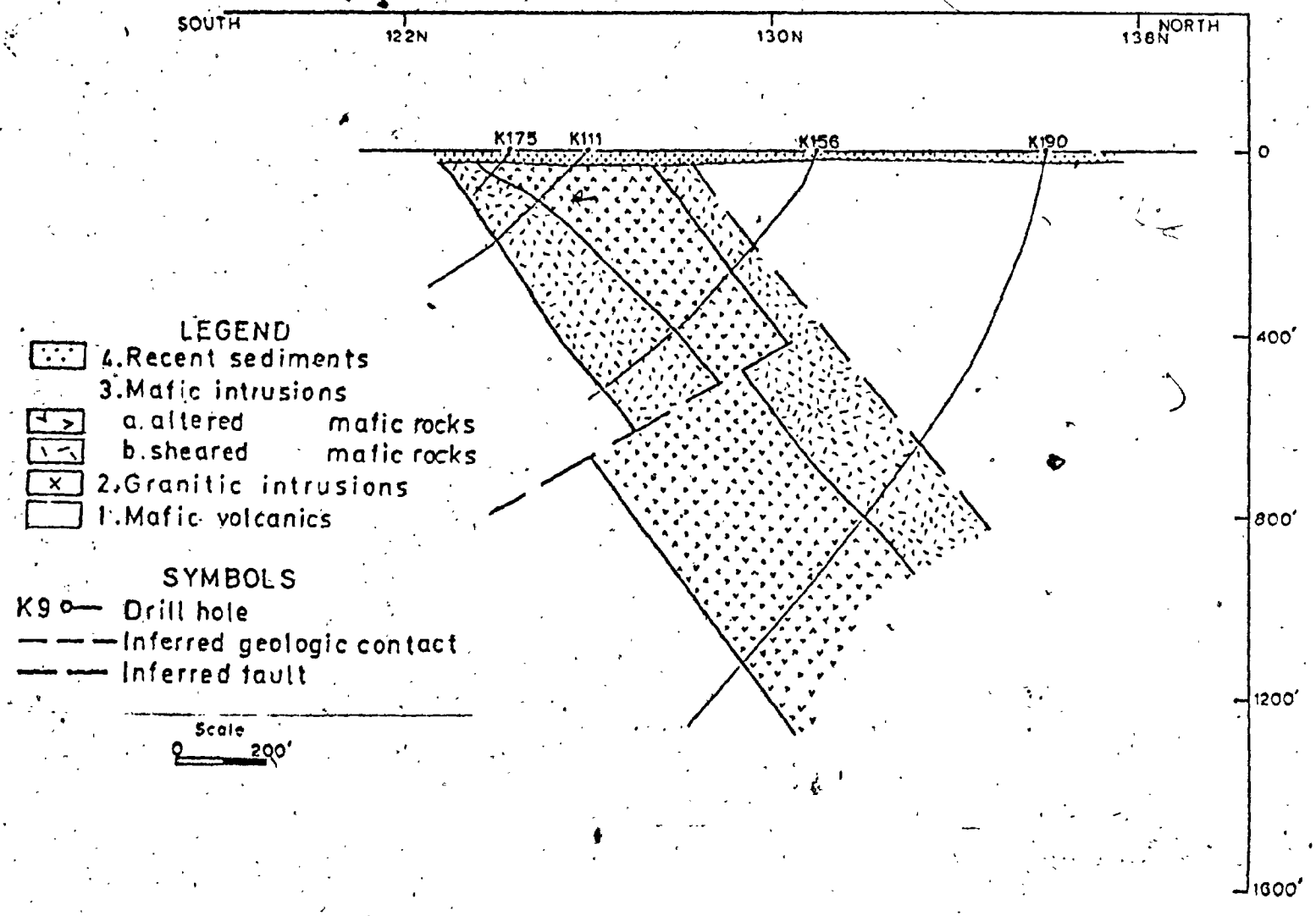

Fig. 2:11, Geological interpretation of Section 160E , KI: 1 um-m Body, Location on Fig. 1:2.

2.5 Conclusions and Summary of Geology of the Kapkichi Lake

Interpretation of drill hole and geophysical data together with observation from the few outcrops in the Kapkichi Lake area permit the following interpretation to be made of the geological history

1. The extrusion of mafic volcanic rocks with minor felsic tuffs and sediments on a granitic gneiss terrain was followed by the intrusion of a large granitic stock and later mafic and ultramafic bodies with associated sulfides.

2. The tectonic history of the Kapkichi Lake area involved four deformational events.

a) Isoclinal folding (D_1) produced a strong foliation F_1 which is parallel to tuff-amphibolite, and sediment-amphibolite contacts (Fo) and a lineation that is colinear with axial traces of minor folds.

b) Open folding (D_2) with axial plane $68^{\circ}/68^{\circ}N$ parallel to the folds in the Pickle Crow region, 10 kilometres to the east, folded the foliation F_1 and lineation L_1 observed in the granites and amphibolites.

c) A very weak fold warped the D_3 fold axis to the north.

d) A cataclastic event cut all the D_1, D_2 and D_3 structures producing shears, faults, kink bands in amphibolite schist and mylonitic zones and associated blackwall alteration in the ultramafic and mafic rocks.

3. The remnant mineralogy of the um-m bodies shows that olivine (Fo_{65}), plagioclase (An_{50}-An_{60}) and clinopyroxene with exsolved hypersthene were cumulus phases and hypersthene was an intercumulus phase. These have been metamorphosed to hornblende, plagioclase (An_{30}), olivine (Fo_{90}), anthophyllite, tremolite, carbonate, chlorite and biotite.

3.0, Chemical Characteristic of Rocks of the Kapkichi Lake Area

3.1, Introduction

Thin section examination of the Kapkichi Lake rocks shows that they consist of metamorphic assemblages. Some rock types in the Kapkichi Lake area, hornblende-chlorite-biotite schist and "blackwall" altered ultramafic rocks show that K_2O was mobile during alteration. Whole rock data for the hornblende-chlorite-biotite schist suggest that CaO and Na_2O were mobile whereas Al_2O_3, MgO, Fe_2O_3+FeO and TiO_2 were not mobilized during alteration (Chapter 5). The standard method of chemical classification of Irvine and Baragar (1971) is not directly applicable to the altered rocks since most of their diagrams are affected by the mobility of alkali elements. The Kapkichi rock samples have been divided into altered and unaltered groups on the basis of thin section examination (presence of biotite and cataclastic textures) and high K_2O contents in the whole rock chemical analyses. The location, rock type, modes and whole rock chemistry is given in Appendix E.

3.2, Amphibolites

Amphibolites from the Kapkichi Lake area are compared to tholeiites from the Sturgeon Lake belt and sediments from the English River gneiss belt in Table 3:1. Fig. 3:1 shows $MgO/MgO+FeO_t$ vs Cr_2O_3, TiO_2 and NiO for amphibolites. These show that the amphibolites are chemically consistent with trends shown by mafic volcanics (Hyndman, 1972).

Fig. 3:3, an AFM diagram, shows that the amphibolites plot in the tholeiitic or alkaline volcanic field. Fig. 3:2, a normative ne-ol-qtz plot shows that the amphibolites fall in the tholeiitic field (Irvine and Baragar, 1971). According to them, "The three kinds of tholeiitic basalt: olivine tholeiite, tholeiite, quartz tholeiite; cannot be distinguished chemically because a) many olivine basalts are quartz normative and b) the presence of small amounts of olivine in the norm is no guarantee that olivine is (or was) present modally". Since the amphibolites in the Kapkichi area contain olivine in the norm, they are classed as undersaturated tholeiites.

Table 3:1, Trace Elements of Sediments and Tholeiites compared to the Amphibolites from the Kapkichi Lake Area (Figures in ppm)

	Sediments		Tholeiites		Amphibolites	
	Average	Range	Average	Range	Average	Range
Ni	37	5-115	124	45-270	136	119-159
Cr	177	5-320	279	40-620	330	227-450
Cu	28	10-75	123	5-240	231	115-641
Rb	68	35-140	6.1		0.4	0.2-0.9
Zr	103	50-200	43	10-140	54	39-96
Ba	207	60-500	54	30-160	80	15-206
Rb/Sr		High		0.03-0.33	0.03	0.01-0.07
La/Ce		High		0.4	0.35	0.2 -0.48
Pb		10.		10	4.2	2-7

English River Gneiss Belt (Goodwin, 1976)	Sturgeon Lake Belt (Goodwin, 1976)	Amphibolites from Kapkichi Lake Area (Average of 10 Samples)

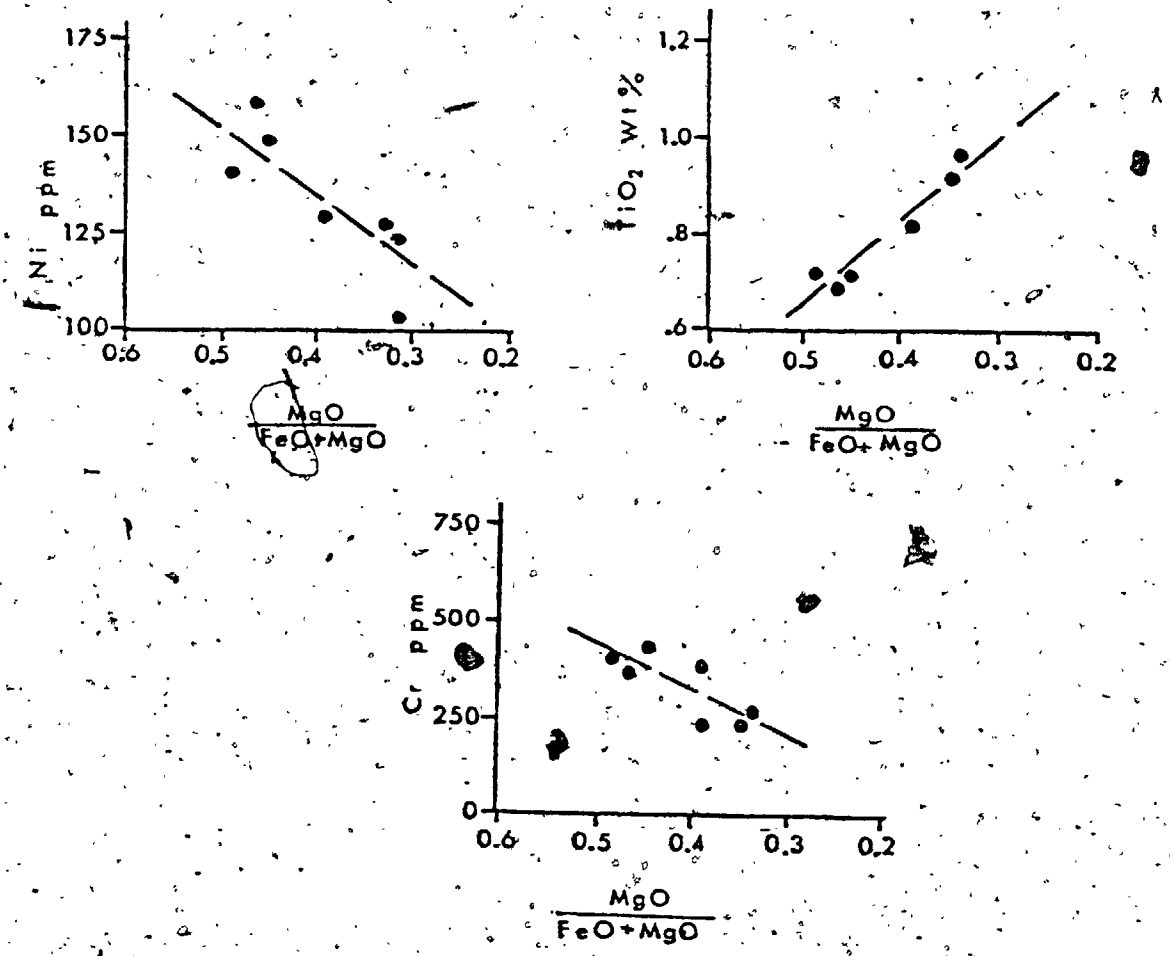

Fig. 3.1, Ni, Cr, TiO_2 vs MgO/(FeO+MgO) for amphibolites from Kapkichi Lake area.

Arndt et al (1977) stated that "the application of chemical criteria developed in Munro cannot provide a positive separation between all tholeiitic basalts and basaltic komatiites. Only in areas where the basalts are associated with ultramafic komatiites can chemical criteria be applied with confidence."

It is not possible to separate komatiitic rocks from tholeiites on the basis of chemical criteria alone. Due to the degree of metamorphism, alteration and deformation very few primary structures are preserved in the Kapkichi rocks. The problem of the possible komatiitic affinity of the amphibolites will be treated more fully in the section on the chemistry of the ultramafic rocks.

Comparison of the chemical composition of the meta-volcanic rocks from the Pickle Crow area (Wells et al, 1977) (10 kilometres east of the Kapkichi Lake area), shows them to be very similar to the amphibolite (Fig. 3:3 and 3:2). Wells et al class these volcanic rocks as high iron tholeiites.

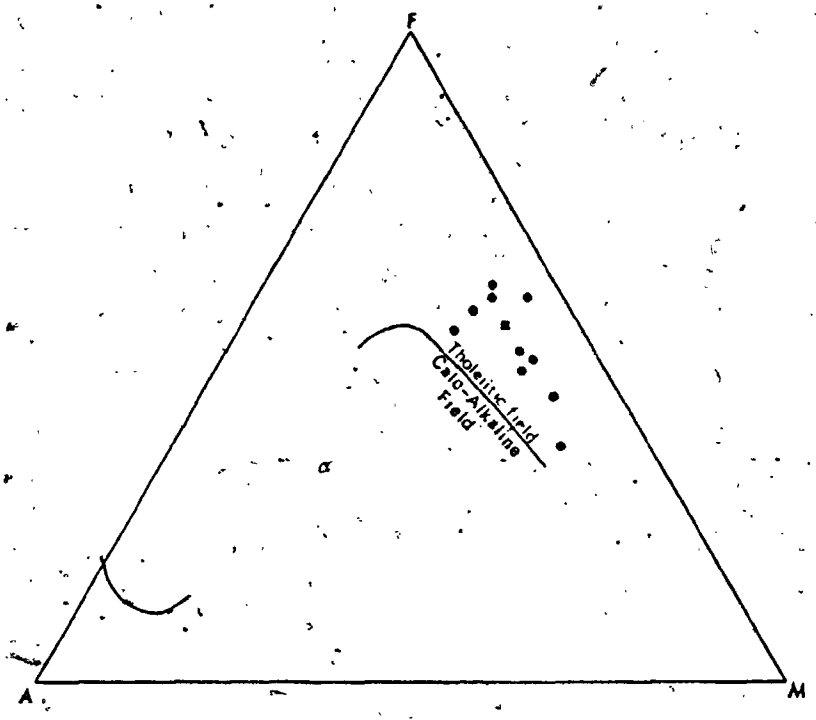

Fig. 3.3: AFM plot for amphibolites from Kapkichi Lake area. Solid circles, amphibolites, solid square average metavolcanic from Pickle Crow.

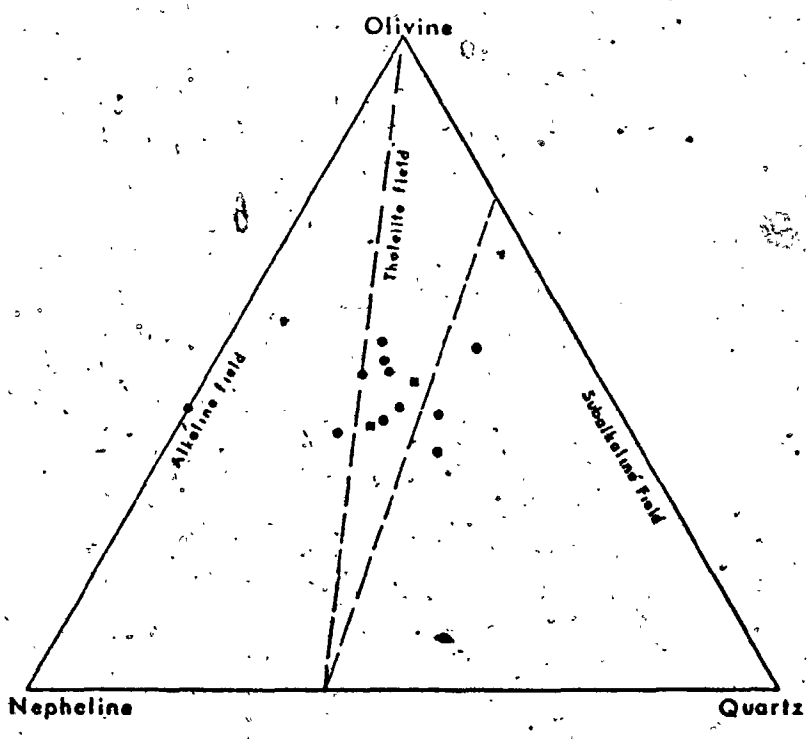

Fig. 3.2: Normative olivine, nepheline, quartz for amphibolites from the Kapkichi Lake area. Solid circles, amphibolites; solid squares, metavolcanics from Pickle Crow.

3:3, Ultramafic and Mafic Rocks

There is some dispute in the literature as to the chemical characteristics of komatiites. The original term komatiite was introduced by Viljoen and Viljoen (1969) for peridotitic and related mafic volcanic rocks that have features such as spinifex texture, pillows and polygonal jointing, which indicate an extrusive origin as mobile lava. Chemically, komatiites have low SiO_2, low FeO/(MgO+FeO) ratio, low alkali-element contents and high CaO/Al_2O_3 ratio compared to tholeiites. Brooks and Hart (1974) quantified the characteristics and redefined komatiites as rocks with MgO>9%, K_2O<0.5%, TiO_2<0.9 and CaO/Al_2O_3 ratios greater than 1. Using the features of the rocks in Munro Twp. Arndt (1977) defined a komatiitic series as follows:

> "It comprises noncumulate rocks ranging in composition from peridotite (30%MgO, 44%SiO_2) to basalt (8%MgO, 52%SiO_2) or andesite (12%MgO, 56%SiO_2) and cumulate rocks ranging from peridotite (30%MgO) to mafic gabbro (12%MgO). The compositions of the noncumulate rocks closely resemble the compositions of the silicate liquids from which they form. The series contains lavas that exhibit unusual textures and volcanic structures such as spinifex textures and polyhedral jointing. All members have low FeO*/(FeO*+MgO) ratios, low TiO_2 content and high MgO, NiO and Cr_2O_3 content and some but not all have high CaO/Al_2O_3 ratio"

The Kapkichi um-m rocks show some chemical similarities to komatiites. The plot of MgO, CaO, Al_2O_3 (Fig. 3:5) shows that they have high CaO/Al_2O_3 ratios (greater than 0.9). The diagram of TiO_2 vs MgO (Fig. 3:6) shows that the Kapkichi um-m rocks have TiO_2 contents similar to Munro Twp. komatiites. The FeO*/(FeO*+MgO) vs Al_2O_3 diagram (where FeO* is total iron calculated as FeO) Fig. 3:7, shows that the K1:1 um-m body analyses mostly fall in the same field as the Munro komatiites; the Thierry mine um-m rocks lie in both the komatiite and tholeiite fields and the J+I um-m rocks fall mainly in the tholeiite field. The samples that fall outside the komatiite field have low Al_2O_3 values with the FeO/(FeO+MgO) ratio remaining relatively constant. Arndt (1977) stated that some komatiites with low Al_2O_3 from South Africa fall in the tholeiitic field. These data suggest that the Kapkichi um-m rocks could be altered komatiites.

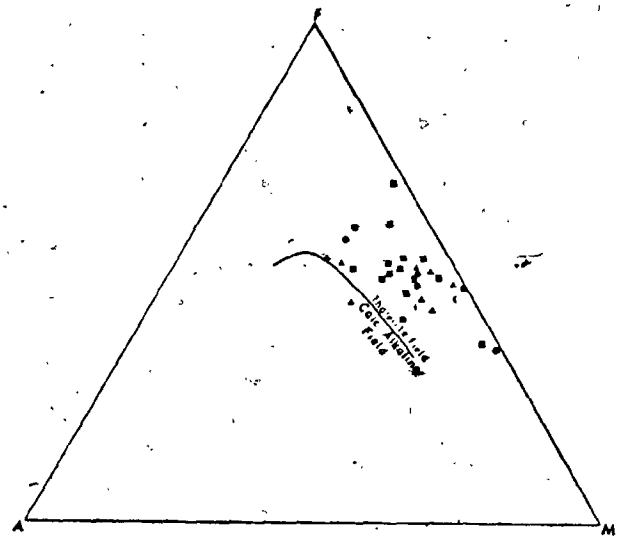

Fig. 3:4, AFM diagram of the chemistry from unaltered ultramafic rocks from Kapkichi Lake area. Solid circles, J+I body; solid squares, Thierry Mine body; solid triangles, K1:1 body. Solid line divides tholeiitic (above) and calc-alkaline field (below) Irvine and Baragar, 1971).

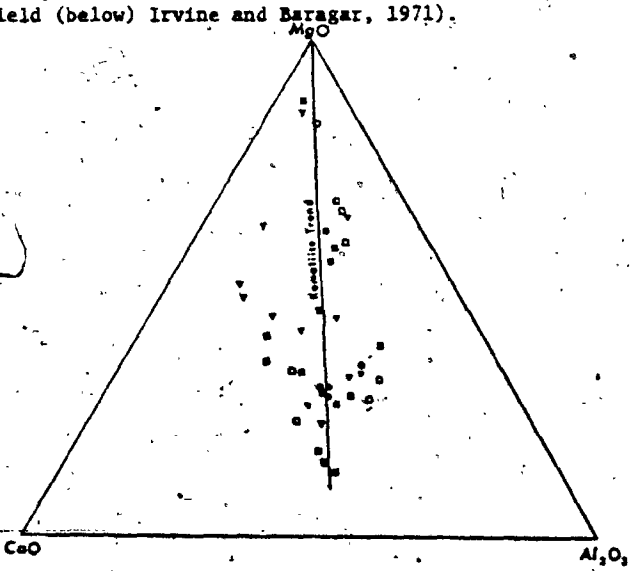

Fig. 3:5, MgO, CaO, Al_2O_3 diagram from unaltered ultramafic rocks, Kapkichi Lake area. Solid triangles, Thierry Mine; solid squares K1:1 body; open squares, J+I body; solid circles G body.

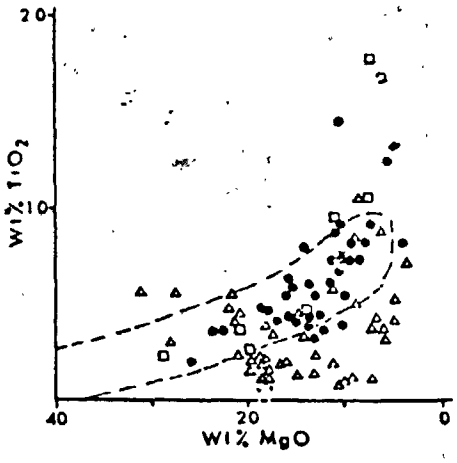

Fig. 3:6, Wt.% TiO_2 vs Wt.% MgO diagram from um-m rocks; solid circles, Thierry um-m body; open triangles, K1:1 body; open squares, J+I um-m body; dashed line outlines Munro twp. komatiites, Arndt (1975).

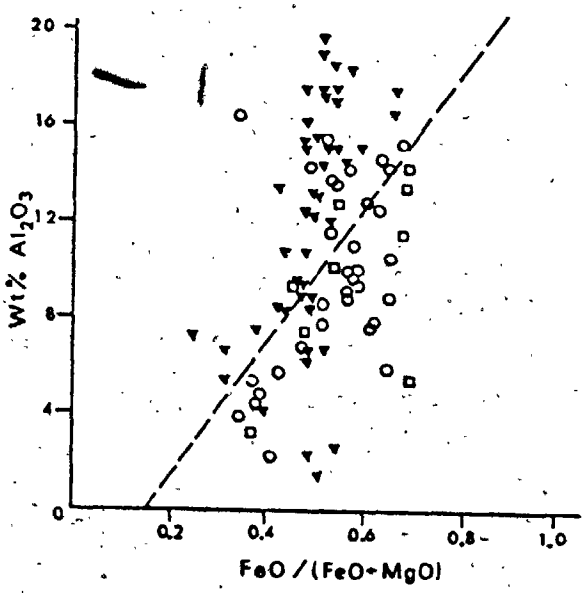

Fig. 3:7, wt% Al_2O_3 vs FeO/(FeO+MgO), solid triangles, K1:1 um-m body; open circles, Thierry mine um-m body, open squares J+I um-m body; the dashed line divides komatiites (above) and tholeiites (below) from Munro Twp. Arndt (1975)

3:4, Magmatic Trends in the Kapkichi Lake Ultramafic and Mafic Rocks

A north-south section through the J+I um-m body is shown in Section 76E (Fig. 2.7). Fig. 2:5 shows a plot of oxide vs depth in drill hole K61 (200wfeet offsection 76E, parallel to K64). Faults at 30°NE intersect the drill hole at 590' and 120'. The plot shows increasing amounts of MgO, Fe_2O_3 and decreasing CaO, Na_2O, K_2O, $Al_2O_3$and SiO_2 down the hole. The fault at 590' clearly disrupts the trend.

From thin section examination the remnant mineralogy is plagioclase An_{50}-An_{60}, olivine Fo_{85}, clinopyroxene and pigeonite (exsolved to hypersthene-clinopyroxene-ilmenite,) as cumulus phases. One sample contained hypersthene as an intercumulus phase to olivine. This suggests a plot of normative olivine, plagioclase and pigeonite (diopside + hypersthene) would most accurately model the magmatic process in these bodies. This plot shows that each of the um-m bodies has a distinct trend (Fig. 3.8 and Fig. 3.9).

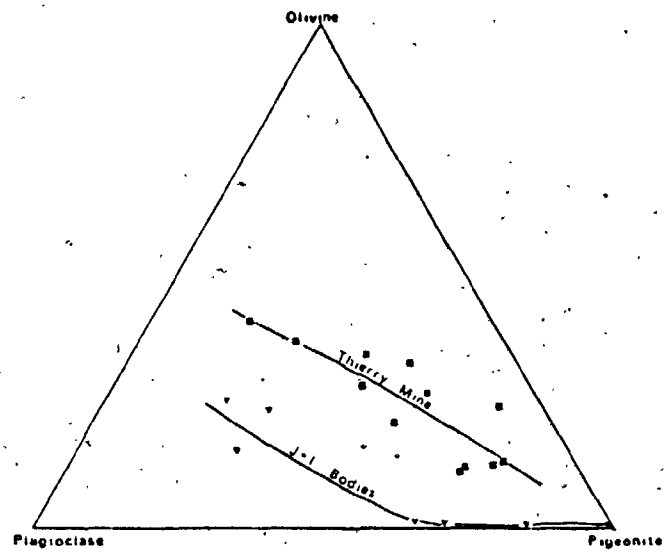

Fig. 3.9, Diagram of normative olivine, plagioclase, pigeonite for unaltered Thierry samples (solid squares) and J+I body (solid triangles).

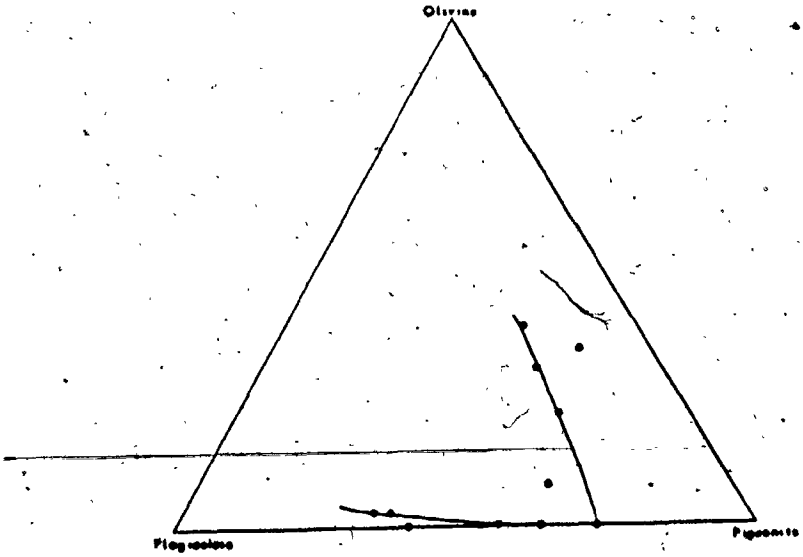

Fig. 3.8. Diagram of normative olivine, plagioclase, pigeonite for unaltered Kl:l samples; solid line implied trend.

Comparison of these implied trends to the trend in the Skaegaard intrusion (Wager and Brown, 1967) shows that the K1:1 trend is similar to those developed in the layered series of the Skaergaard intrusion. In both trends there is a break in olivine precipitation at a point where pigeonite ($CagMg_{52}Fe_{37}$) begins to precipitate (Fig. 3:10). This break is consistent with observed composition of olivine (Fo_{65}) and plagioclase (An_{55}) remnants in K1:1.

The J+I body shows a trend that is similar to that of the Blasistoppen sheet (near the Skaergaard intrusion) (Fig. 3:11). Two samples in this trend (G10, G8, Appendix E) have predominantly orthopyroxene in the norm suggesting that the initial rock was a bronzite-rich ultramafic rock. This rock changed to bronzite gabbro, to pigeonite gabbro and then to pyroxene ferrodiorite.

The Thierry Mine body has a trend that is consistent with the accumulation of olivine, pigeonite and plagioclase with a marked decrease in pigeonite and corresponding increase in olivine and plagioclase, (Fig. 3:9).

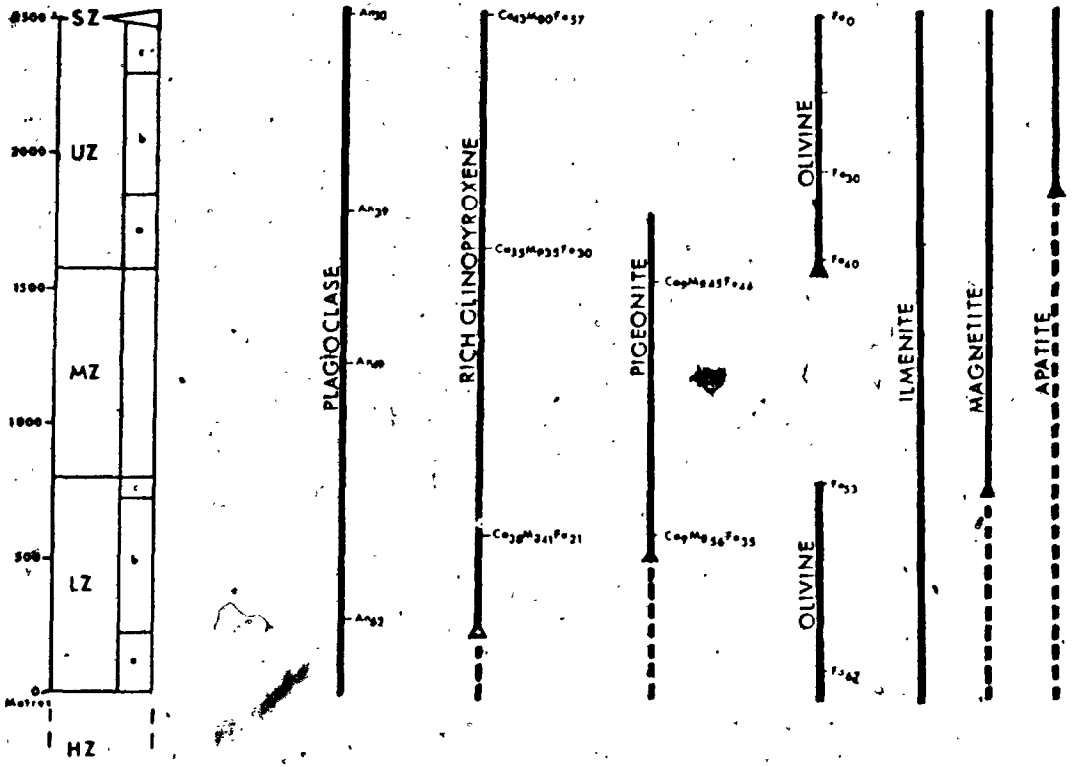

Fig. 3.10; Minerals present in the various rocks of the layered series, and their composition, Skaergaard intrusion, Greenland (after Wager and Brown (1967))

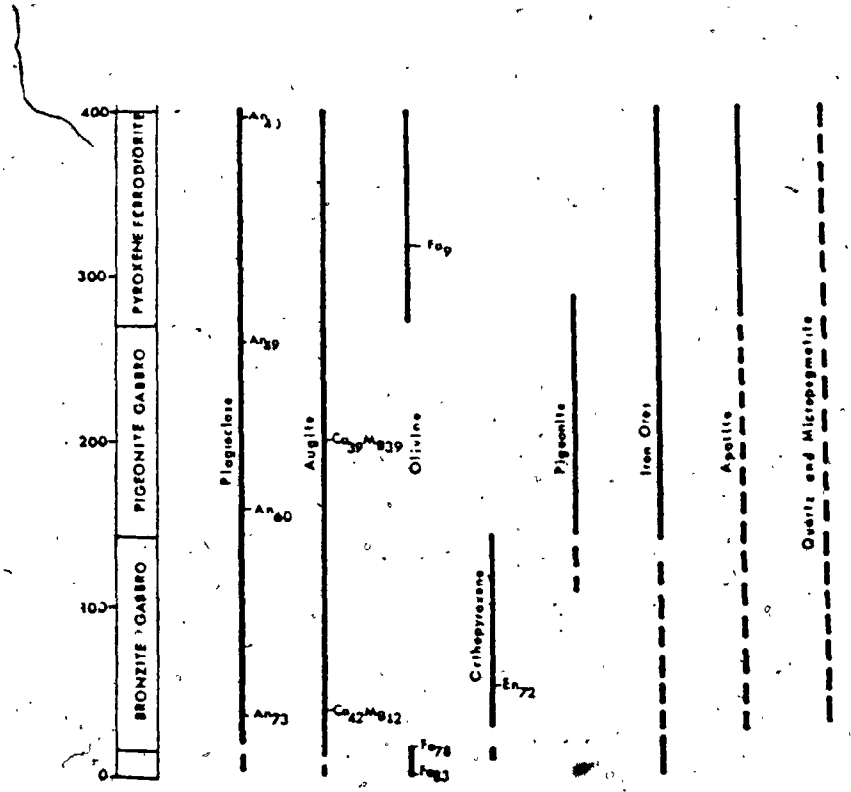

Fig.3.11, Minerals present in the various rocks of the layered series, and their composition, Basistopper sheet, Greenland. (after Wager and Brown (1967))

3:5, Alteration of the K1:1 Ultramafic and Mafic Body

The original mineralogy of the K1:1 um-m rocks was clinopyroxene with exsolved hypersthene and plagioclase An_{55}, now altered to hornblende and plagioclase An_{30} with chlorite-biotite-rich rocks occurring near the margins of the body, near faults and shears and dykes. Biotite was not observed in the fresh rocks and electron microprobe analyses show that the hornblende contains only minor amounts of potassium. It is assumed that potassium was added during alteration or metamorphism. The amount of potassium in a sample may be roughly proportional to the intensity of alteration and a plot of the contents of K_2O vs oxides may indicate which elements were mobile during alteration.

Plots of normative biotite against SiO_2, CaO, Na_2O (Fig. 3:13) show that with increasing amounts of biotite there is a corresponding depletion of these oxides. The trends of biotite versus SiO_2 and biotite versus Na_2O are opposite to those expected for magmatic trends, while the trend on the biotite versus CaO plot is parallel to a J+I magmatic trend (Fig. 2:5). This implies that SiO_2, CaO, Na_2O and K_2O were mobile during alteration. The plots of biotite against MgO, Al_2O_3 and FeO_{total} show a high degree of scatter implying that MgO, Al_2O_3 and FeO were not directly related to the alteration process.

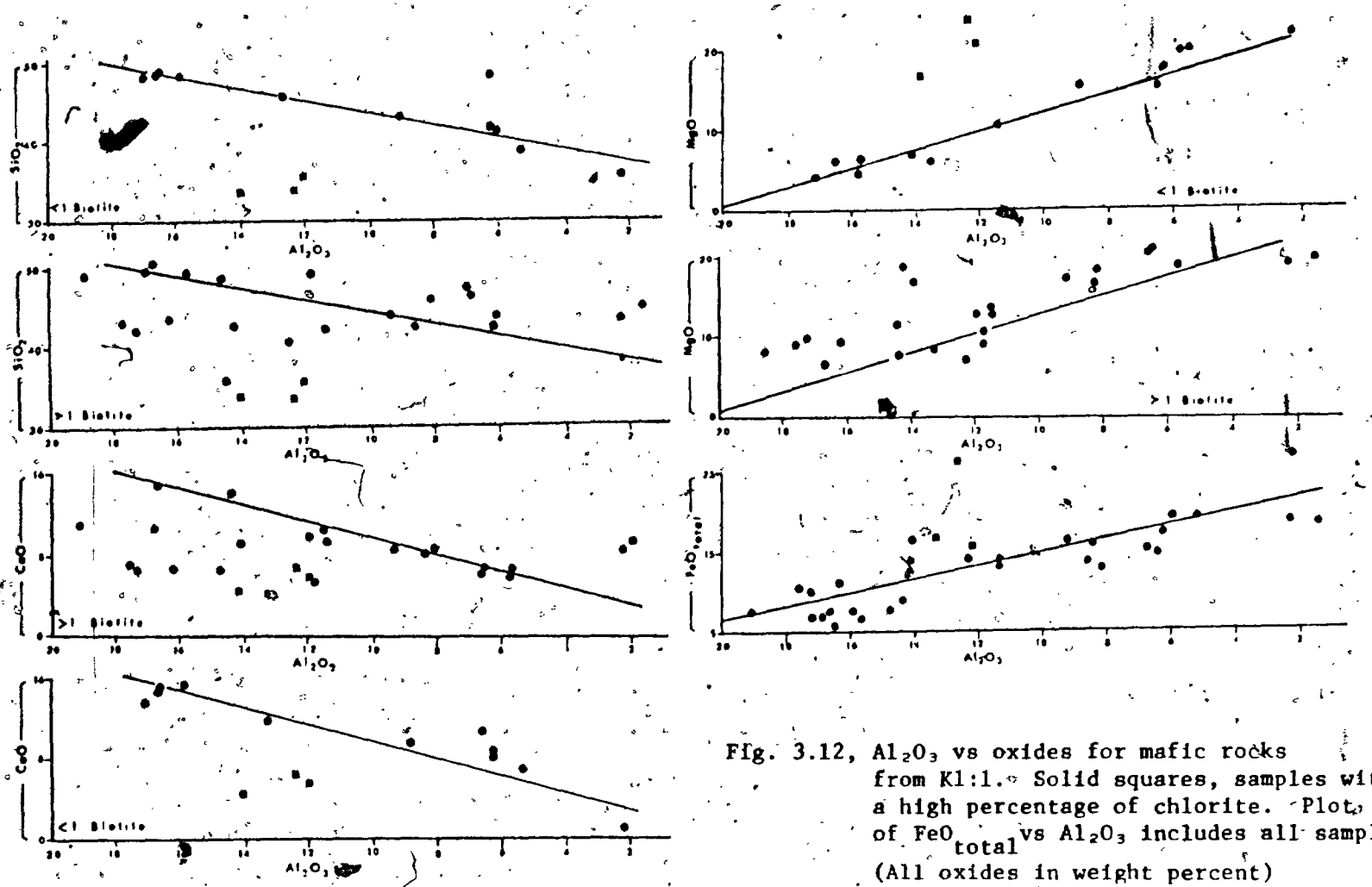

Fig. 3.12, Al_2O_3 vs oxides for mafic rocks from K1:1. Solid squares, samples with a high percentage of chlorite. Plot of FeO_{total} vs Al_2O_3 includes all samples. (All oxides in weight percent)

A plot of Al_2O_3 against SiO_2,CaO,MgO,FeO in samples with less than 1% normative biotite shows trends consistent with those of magmatic rocks (Fig. 3:13). Plots of Al_2O_3 against SiO_2 and CaO in rocks with more than 1% biotite show a strong deviation from this magmatic trend. Most of the scatter is below this trend, implying that the rock is depleted in SiO_2 and CaO. In summary, Al_2O_3, MgO, FeO were relatively immobile and SiO_2,CaO,Na_2O,K_2O were mobile during alteration. This is identical to the pattern of alteration on the hornblende-chlorite biotite schist in the Thierry Mine (Chapter 5).

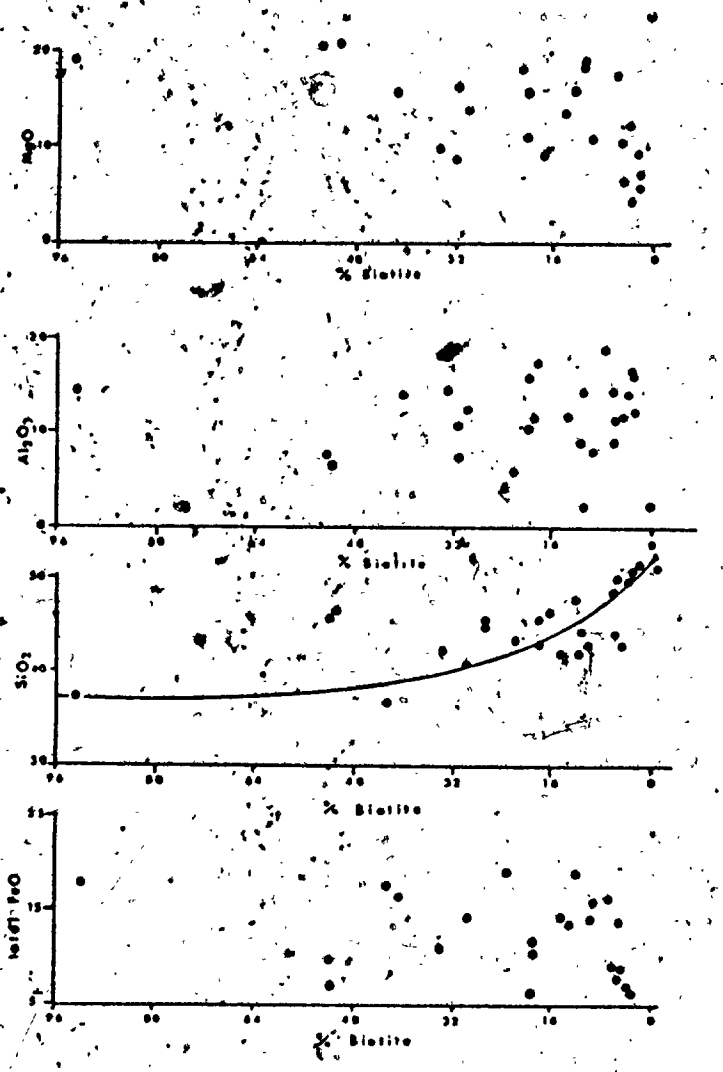

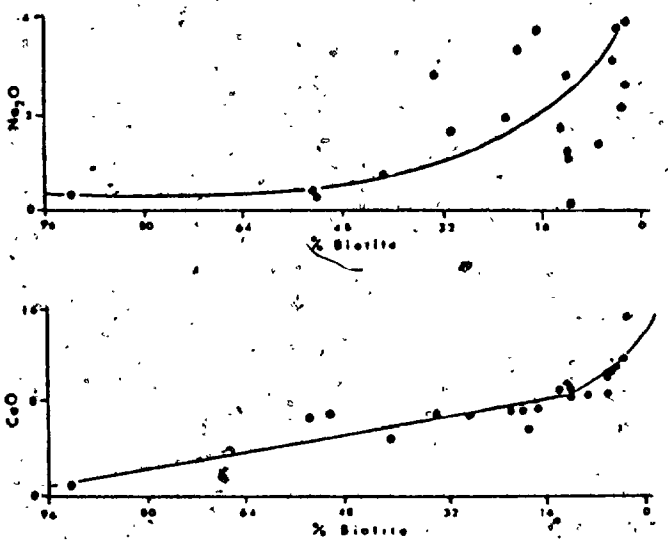

Fig. 3.13, % normative biotite vs oxides for altered ultramafic rocks from K1:1.

(Oxides in weight percent)

3:6, Conclusions and Summary of the Chemical Characteristic of Rocks of the Kapkichi Lake Area

1. The amphibolites from the Kapkichi Lake area have compositions similar to the tholeiitic basalts. In addition they have a composition similar to the high-iron tholeiites from Pickle Crow, ten kilometres to the east (Wells et al, 1977).

2. The um-m rocks have some chemical characteristics in common with komatiites; high CaO/Al_2O_3, low TiO_2 compared to MgO and a komatiitic trend on a $MgO-CaO-Al_2O_3$ diagram. However the lack of textural evidence such as spinifex texture makes the komatiite affinity difficult to prove. In addition the nature of the G and J+I um-m body contacts cutting granitic rocks suggest an intrusive origin. The nature of the contacts between the Thierry Mine and K1:1 um-m bodies and their associated amphibolites is obscured by shearing; these could be either intrusive or extrusive bodies.

3. Each of the um-m bodies, Thierry Mine, J+I and K1:1 shows a distinct trend on a normative olivine, plagioclase and hypersthene + augite plot.

4. The bulk composition of the biotite-rich rocks of K1:1 suggest that Al_2O_3, MgO and FeO were relatively immobile while SiO_2, CaO, Na_2O and K_2O were mobile during the "blackwall" alteration process.

4. Pressure and Temperature Conditions during Metamorphism

4:1, Introduction

Bowdidge (1970), Sage et al (1976) and Thurston and Breaks (1978) have shown that the metamorphic grade in the Kapkichi Lake area is mid-amphibolite facies. However assemblages observed by Ferguson (1966) in the Central Patricia area (8 kilometres east of the Thierry Mine) are consistent with lower greenschist facies conditions. Outcrops of metavolcanic rocks near the east end of Hook Lake and on the Crow River (Fig. 2:3) contain the same assemblages as those observed at the Thierry Mine. The volcanic rocks at the Central Patricia Gold Mine (2 kilometres east of the Hook Lake outcrops) contain sericite as well as relict volcanic textures such as pillows and amygdules. There is an abrupt change of metamorphic grade from the Kapkichi Lake area to the Central Patricia area (amphibolite to lower greenschist) over a distance of two kilometres. Lack of outcrop obscurs the details of this change.

The metamorphosed sediments and volcanics in the Kapkichi Lake area provide an opportunity to estimate the pressure and temperature of metamorphism by the assemblages generated and standard geothermometers and geobarometers (calcite-dolomite, magnetite-ilmenite, garnet-biotite, garnet-plagioclase and, sphalerite-pyrite-pyrrhotite). The determined metamorphic conditions are used to understand the assemblages generated in the ultramafic rocks using the model suggested by Tromsdorff and Evans (1971) for meta-ultramafic rocks of the contact aureole in the Bergell area in the Italian-Swiss Alps.

4:2, Geothermometry and Geobarometry

A brief summary of the methods used to estimate the temperature and pressure of metamorphism is given below. The results are given in Table 4:1. A detailed outline of the methods used for the garnet-biotite, calcite-dolomite and magnetite-ilmenite geothermometers; and the plagioclase-garnet and pyrrhotite-pyrite-sphalerite geobarometers are given in Appendix A.

The garnet-biotite geothermometry is based on the amount of iron in coexisting garnet and biotite. As the temperature increases the amount of iron in biotite increases. Dissassociation constants (K_D values) have been determined by Thompson (1976). A computer program (Leatherbarrow, 1977) was used to calculate temperatures based on these K_D values (Table 4.1). According to Leatherbarrow (1977) from comparison of temperatures determined from calcite-dolomite and garnet-biotite using different K_D values for metamorphosed sediments in the Shuswap area, B.C., the Thompson method gives the most consistent results. The Thompson K_D values give a temperature of $608^{\circ}C \pm 50^{\circ}C$ (average of 4 garnet-biotite pairs) for a pelite 1.5 kilometre east of the Thierry Mine in the Kapkichi Lake area.

Table 4.1 Temperature and Pressure of Metamorphism

Geothermometers

1. Thompson (1976)	Garnet-Biotite Geothermometer
Assemblage # 1	607°C
Assemblage # 2	612°C
Assemblage # 3	606°C
Assemblage # 4	604°C
Average	608°C ± 50°C
2. Ewert (1977)	Calcite-dolomite Geothermometer
Slide # 1	581°C
Slide # 2	590°C
Average	585.5°C ±50°C
3. Buddington and Lindsley (1964)	Magnetite-ilmenite Geothermometer
Average of 6	650 ± 100°C

Geobarometers

1. Ghent (1977) Garnet-Plagioclase Geobarometer

Method	Temperature	R & W	Helgeson
garnet-biotite	608°C	5.67 kbars	7.06 Kbars
calcite-dolomite	585°C	5.32 kbars	6.84 Kbars
magnetite-ilmenite	650°C	6.49 kbars	8.08 Kbars
assumed	600°C	5.5 kbars	7.0 K bars

2. Hutcheon (1977) Sphalerite-Pyrite-Pyrrhotite

chlorite-biotite schist	5.5 kbars
breccia ore	5.8 kbars
breccia ore	5.6 kbars

assumed temperature of 600°C

R & W - Robie and Walbaum (1968)

The calcite-dolomite geothermometer is based on the $MgCO_3$ content of calcite coexisting with dolomite. As the temperature increases the amount of $MgCO_3$ dissolved in calcite coexisting with dolomite, increases. Pressure has a minor effect; an equation developed by Ewert (1977) for 5 kbars was used to correct for this effect. The temperature determined with calcite-dolomite is $586^{\circ}C \pm 50^{\circ}C$ for a calc-silicate, 3 kilometers east of the Thierry Mine.

The magnetite-ilmenite geothermometer based on solid solutions between magnetite-ulvospinel and ilmenite hematite solid-solutions was difficult to use because the interpretation of textures between magnetite and ilmenite was not clear. However the estimated temperature of $650^{\circ}C \pm 100^{\circ}C$ is consistent with the garnet-biotite and calcite-dolomite geothermometer.

The garnet-plagioclase geobarometer is based on the breakdown of anorthite to grossular, sillimanite and quartz. By knowing the compositions of the minerals involved and the temperature, Ghent (1977) outlined a method for estimating the pressure. Assuming a temperature of $600^{\circ}C$, Robie & Walbaum's (1968) data give a pressure of 5.5 kbars whereas Helgeson's (1978) data give a pressure of 7.0 kbars.

The sphalerite geobarometer (Scott, 1973) is based on the increase in the iron content of sphalerite with increasing pressure when the sphalerite is in equilibrium with pyrite and pyrrhotite. Using Hutcheon's (1977) model, the sphalerite geobarometer gives a pressure of 5.5 kbars.

In summary, the geothermometers give a temperature of 600°C ±50 and the geobarometers a pressure of 7.0 kbars ±1 kbar.

4:3:1, Metamorphic Assemblages in the Kapkichi Lake Area

4:3:1, Mafic Rocks

The assemblages observed in the mafic volcanic rocks and metagabbros are

1. quartz + andesine + hornblende $\pm$ epidote
2. quartz + andesine + hornblende + diopside $\pm$ epidote
3. quartz + andesine + hornblende + almandine $\pm$ epidote

minor: biotite, tremolite, cummingtonite, sphene, carbonate

The predominant assemblage is 1. with assemblage 2. and 3. occurring only very rarely. The plagioclase is strongly polygonally recrystallized; the individual grains show oscillatory zoning from An_{20} to An_{35} (as determined optically). In rocks with a high percentage of epidote or sphene the plagioclase has an anorthite content from An_{60} to An_{80} reflecting a higher calcium content of the original rock or an alteration effect (see Chapter 5). The hornblende has a large component of pargasite and hastingsite (Appendix D, Table 4). In thin section the hornblende is strongly pleochroic. (dark green, green and yellow). Rare exsolution of tremolite and intergrowths with cummingtonite occur in hornblende.

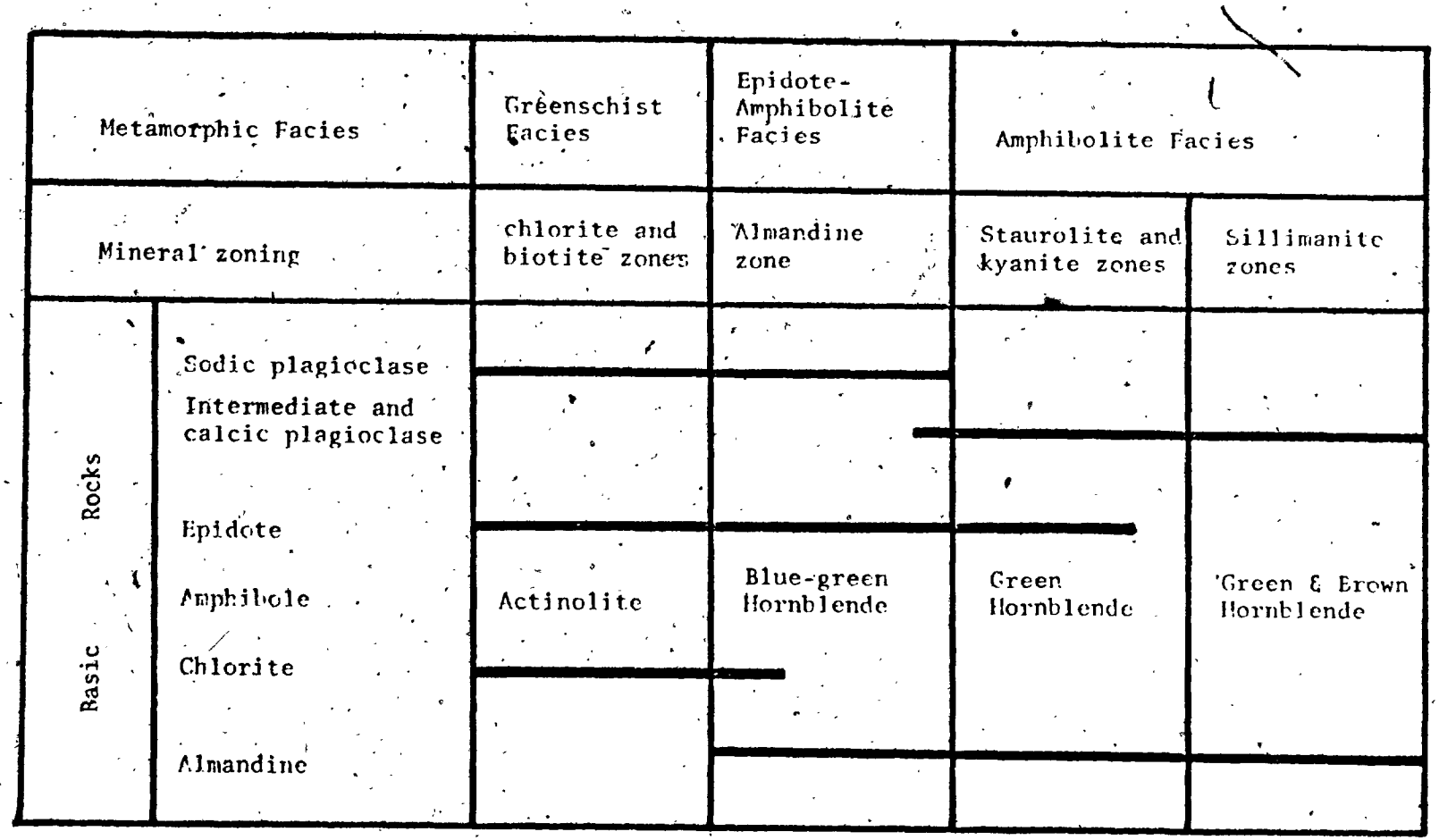

Fig.4.1, Metamorphic assemblages in basic rocks, kyanite-sillimanite type (Miyashiro(1973))

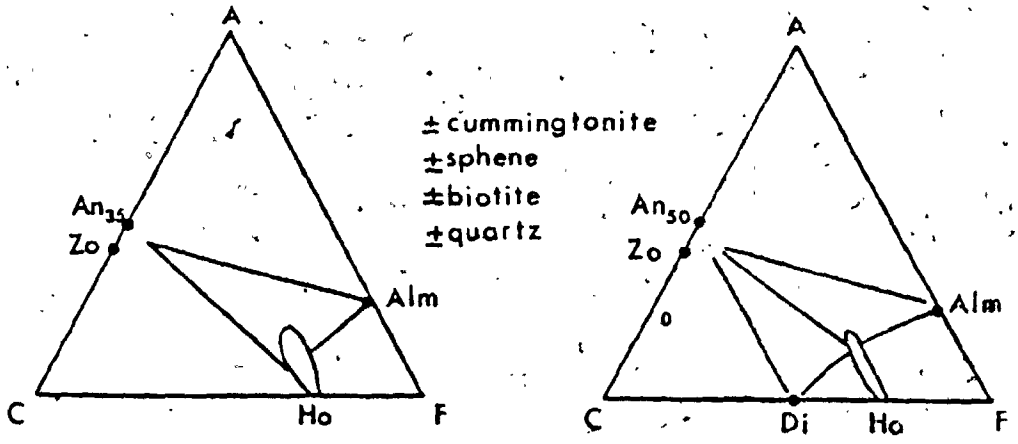

Fig. 4:2, ACF diagrams for rocks of basaltic composition. Left, andesine to oligoclase amphibolite, medium grade; right labradorite/bytownite amphibolite, high grade (after Winkler, 1976).

Miyashiro (1973) has shown that two main factors (other than temp) control the assemblages generated in mafic rocks; the pressure and the initial composition. The presence of epidote and almandine indicate that the rocks were metamorphosed at moderate pressure. (Kyanite-sillimanite type, Fig. 4:1). Fig. 4:2 illustrates the effect of composition on an ACF diagram. If the mafic volcanic contains more CaO, diopside is generated; if more FeO and Al_2O_3 are present garnet forms. Although the anorthite content of plagioclase is not an absolute measure of the metamorphic grade, statistically the higher the grade, the higher the anorthite content (Winkler, 1976). The average plagioclase composition of the Kapkichi Lake rocks is An_{30} (oligoclase amphibolite). The composition of the amphibole in mafic rock changes with increasing grade, the albite component of the plagioclase combining with the tremolite-actinolite component of the amphibole to produce a sodium aluminum rich amphibole with a much more intense pleochroism (Ernst, 1968). The hornblende in the Kapkichi Lake rocks is green to brownish green.

This suggests that the mafic volcanic rocks in the Kapkichi Lake area have been metamorphosed at a moderate pressure to mid-amphibolite grade. (oligoclase amphibolite, staurolite-kyanite type; see Fig. 4:1).

4:3:2, Pelites

The assemblages observed in the pelites are

quartz + plagioclase (An_{30}) + garnet + biotite $\pm$ sillimanite $\pm$ staurolite $\pm$ K-feldspar

This suggests that the metamorphic conditions correspond to almandine high grade, Winkler (1976). The presence of staurolite appears anomalous. Staurolite can break down by reactions involving muscovite and quartz such as

staurolite + muscovite + quartz = sillimanite + almandine + biotite + H_2O

staurolite + muscovite + quartz = sillimanite + biotite + H_2O

In the absence of muscovite, staurolite may persist to much higher temperatures; 700°C for Fe-rich staurolites, Winkler (1976).

staurolite + quartz = sillimanite + almandine + H_2O

If the position of the aluminium silicate triple point is taken as 600°C and 6 kilobars, (Richardson et al, 1969) the presence of sillimanite suggests a temperature of greater than 600°C.

The presence of a fluid phase would cause melting by reactions such as

albite + orthoclase + H_2O = liquid

At an inferred pressure of metamorphism (Chapter 4:1) of 5 to 7 kilobars, melting would take place at a temperature of about 620°, (Yoder, 1968) in pelites.

2

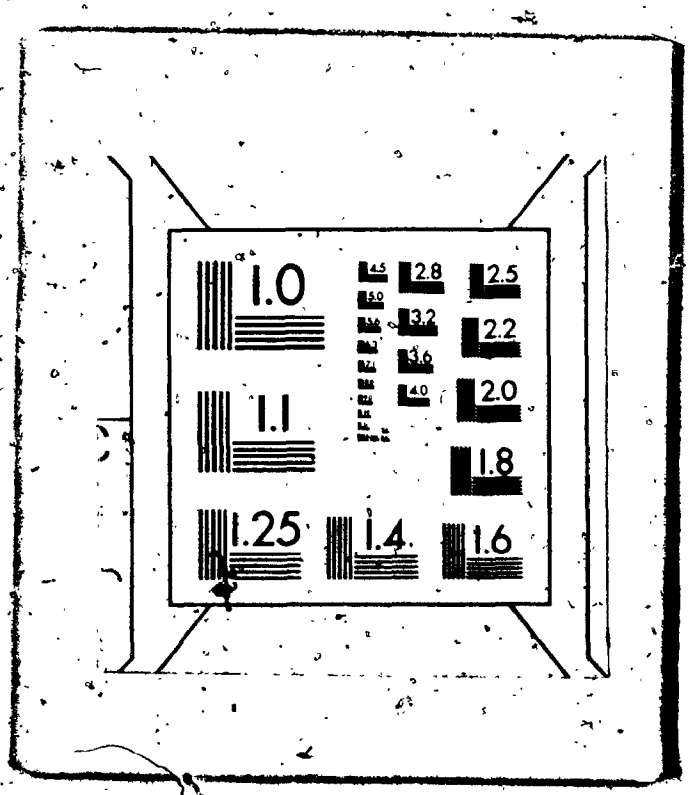

4:3:3, Calcsilicate Assemblages

The assemblages observed in the calcsilicates are

1. zoisite + tremolite + quartz + plagioclase+K-feldspar
2. zoisite + phlogopite + quartz + plagioclase+ calcite + K-feldspar
3. zoisite + phlogopite + quartz + plagioclase+ K-feldspar
4. zoisite + garnet + quartz + plagioclase+ calcite
5. zoisite + garnet + quartz + plagioclase+ K-feldspar + biotite + calcite
6. zoisite + garnet + quartz + plagioclase+ calcite + dolomite

Using a computer program by Moore (1976), the above assemblages were compared to assemblages in calcsilicate systems. This showed that assemblages 1. and 3. are univariant and assemblage 4. is invariant at constant pressures. The remaining assemblages 2. 5. and 6. are metastable.

An isobaric, T-X diagram for the system $CaO-Al_2O_3-SiO_2-H_2O-CO_2$ is shown in Fig. 4.3 with the invariant point C representing assemblage 4. The effect of pressure is shown in Fig. 4.4. At a temperature of 610°C (implied from the geothermometers) a pressure of 4.8 Kbars is indicated for end member compositions. No attempt was made to model the system more exactly because optically the epidotes are complexly zoned.

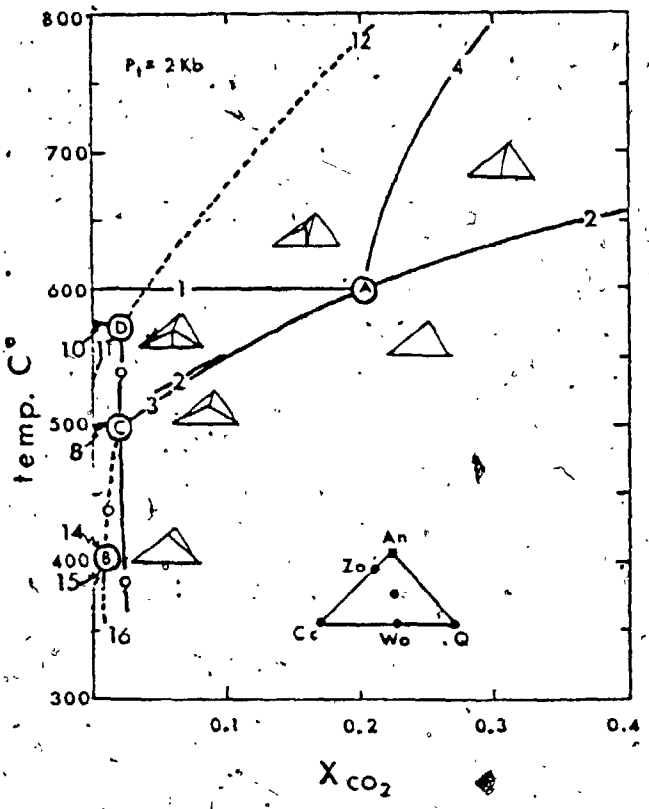

Fig. 4:3, Isobaric (P_f=2 kb) phase relations in the system $CaO-Al_2O_3-SiO_2-H_2O-CO_2$ to 800°C. Reactions involving margarite are excluded, (Storre and Nitsch, 1972).

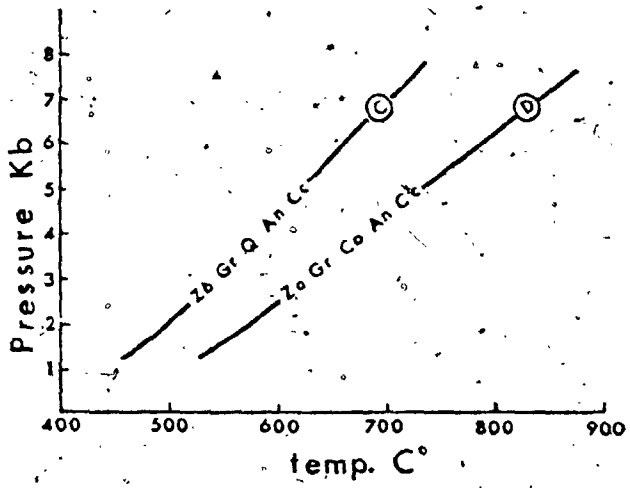

Fig. 4:4. Equilibrium conditions of mineral assemblages stable at isobaric invariant points C,D of fig. 4:6.

4:3:4, Ultramafic Rocks

In determining the metamorphic assemblages present, two problems concerning the genesis of the minerals exist. The first is the distinction between olivine from metamorphic processes and remnants of igneous olivine. In general the igneous olivine remnants occur as distinct round cumulus crystals often associated with clinopyroxene and plagioclase. The composition of the igneous olivine is Fo_{60}-Fo_{65}. The metamorphic olivine occurs in two textural forms; polygonal grains with sharp triple junctions and coarse lath-shaped grains with pseudospinifex texture. The composition of the metamorphic olivine is Fo_{85}-Fo_{90}. (Appendix D, Table 2.) Metamorphic olivine occurring in magnetite-ilmenite oxide layers is zoned with Fe-rich cores (Fo_{60}) and Mg-rich rims (Fo_{70}).

The second problem is the occurrence of talc as coarse lath-shaped crystals and fine-grained masses. The coarse lath-shaped crystals of talc are considered to be a prograde metamorphic mineral. The fine-grained masses are interpreted to be retrograde after tremolite and anthophyllite.

Only assemblages with mosaic textures and without chemical zoning were considered to be compatible. The assemblages observed are shown in Table 4:2.

Table 4:2, Assemblages in Ultramafic Rocks from the Kapkichi Lake Area

I. $MgO - Al_2O_3 - SiO_2 - H_2O$

Fo + Anth $\pm$ Chl

Fo + Anth $\pm$ Ta $\pm$ Chl

II. $MgO - CaO - Al_2O_3 - SiO_2 - H_2O$

Fo + Trem $\pm$ Chl

Fo + Ta $\pm$ Chl $\pm$ C c

Fo + Trem + Anth $\pm$ Chl

Trem + Ta $\pm$ Chl

III. $MgO - Al_2O_3 - SiO_2 - H_2O - CO_2$

Ta + Anth + Mag $\pm$ Chl

Fo + Anth + Mag $\pm$ Chl

Fo + Ta + Mag $\pm$ Chl

Anth + Mag $\pm$ Chl

IV. $CaO - MgO - Al_2O_3 - SiO_2 - H_2O - CO_2$

Fo + Trem + Mag $\pm$ Chl

Fo + Trem + Dol + Mag $\pm$ Chl

Ta + Trem + Mag + Dol $\pm$ Chl

Fo + Trem + Anth + Mag $\pm$ Chl

(Abbreviations in Appendix A)

Evans and Trommsdorff (1970) suggested reactions to explain the assemblages observed in the Bergell tonalite contact aureole in Switzerland (Fig. 4:5). Comparing their assemblages to those in the Kapkichi Lake ultramafic rocks the data suggest that metamorphism occurred at conditions near reaction 5 which defines the appearance of anthophyllite.

5 talc + 4 forsterite = 5 anthophyllite + $4H_2O$ (5)

and below reaction 6 which defines the first appearance of enstatite

anthophyllite + forsterite = 9 enstatite + H_2O (6)

Above 2 kbars pressure, $P_{total} = P_{H_2O}$, these reactions define a narrow anthophyllite stability field from 650 to 590°C. Using Raoult's law to model the substitution of iron for magnesium in the above phases, Evans and Tromsdorff (1970) showed that the effect of iron substitution is minor, moving reaction 5 and 6 to temperatures approximately 10°C lower.

The presence of calcium in the system produces tremolite by the equilibrium

antigorite + diopside = tremolite + forsterite + H_2O

The occurrence of anthophyllite with tremolite is likely a function of the bulk composition of the rock, as the rock is more magnesian, more anthophyllite will occur.

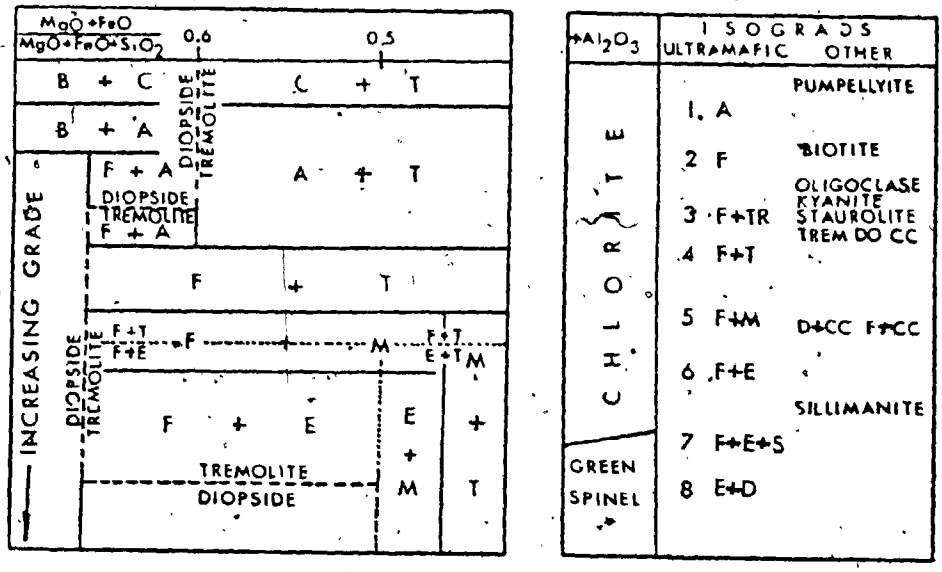

——— Phase boundaries for typical ultramafic compositions

····· Boundary for low Fe/Mg

– – – Boundary for coexisting Ca-Mg silicates

Fig. 4:5. Summary of mineral assemblages in metamorphic peridotitic rocks. Abbreviations: A. antigorite, B. brucite, C. Chrysotile, CC. calcite, D. diopside, DO dolomite, E. enstatite, F. olivine, M. magnesiocummingtonite/anthophyllite, S. spinel, T. talc, TR. tremolite. Numbers refer to reactions below.

1) Chrysotile/lizardite = antigorite
2) antigorite + brucite = olivine + $3H_2O$
3) 5antigorite + 2diopside = tremolite + 6olivine + $9H_2O$
4) 5antigorite = 6olivine + talc + $9H_2O$
5) 9talc + 4olivine = cummingtonite + $4H_2O$
6) cummingtonite + olivine = 9enstatite + H_2O
7) chlorite = olivine + 2enstatite + spinel + $4H_2O$
8) tremolite + olivine = 5enstatite + 2diopside + H_2O

(after Evans and Trommsdorff, 1970)

The presence of CO_2 in the fluid phase has a large effect on the temperature at which these reactions take place. At 2kb, $P_{total} = P_{H_2O}$, reaction 5 takes place at 675°C but at $X_{CO_2} = .80$ it takes place at 550°C.

Reactions in the system $MgO-Al_2O_3-SiO_2-H_2O-CO_2$ were recalculated to 5 kbars using the topology of Johannes (1969) (Fig. 4:6). The assemblage olivine + talc + magnesite suggests that the equilibrium is

4 forsterite + H_2O + $5CO_2$ = 5 magnesite

The above reaction is relatively independent of X_{CO_2}. This implies that the temperature was about 580°C to 610°C. The other assemblages indicate that the metamorphic conditions are close to the invarient point (talc, olivine, anthophyllite, magnesite). Evans and Trommsdorff (1974) suggested a number of topologies for the system $MgO-SiO_2-CO_2-H_2O$ to explain the occurrence of enstatite-talc at Val D'Efra, Lepontine Alps, (in Johannes' interpretation enstatite-talc are incompatible). The key reaction

anthophyllite = talc + enstatite

is not sufficiently accurately located to define which of Evans & Trommsdorff topologies is correct. The uncertainty in temperature is several hundreds of degrees C.

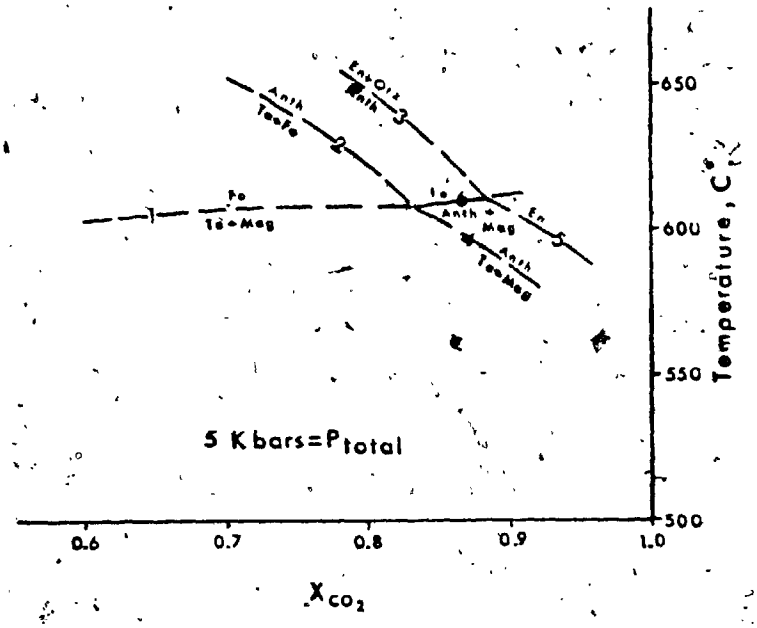

Fig.4.6, Section of the system $MgO-SiO_2-CO_2-H_2O$(Johannes(1969)) recalculated to 5Kbars using data from Evans and Trommsdorff(1974).

1. $4Fo+H_2O+CO_2 = Tc+5Mag$
2. $9Tc+4Fo = 5Anth+4H_2O$
3. $Anth = 7En+Qtz+H_2O$
4. $2Tc+Mag = Anth+H_2O+CO_2$
5. $Anth+Mag = 4En+H_2O+CO_2$
6. $Anth+9Mag = 8Fo+H_2O+9CO_2$

abbreviations: Fo:olivine, Tc:talc, Anth:anthophyllite, En:enstatite, Mag:magnesite

Furthermore, the position of this reaction is greatly affected by composition of these phases; iron-magnesium exchange causes a variation of $\pm 200^{\circ}C$. Since enstatite is not present in the Kapkichi ultramafic rocks, Johannes' interpretation of the system $MgO-SiO_2-H_2O-CO_2$ (1969) is consistent with observed assemblages.

The addition of calcium to the above system permits tremolite and dolomite to occur as additional phases. The occurrence of Al_2O_3 as an additional component has little effect on the topology of the system $MgO-SiO_2-H_2O-CO_2$ because the only additional phase is chlorite (Mg spinel only occurs at higher grades). The substitution of aluminium for silicon in antigorite and tremolite is minor.

4:3:5, Cataclastic Rocks

The stable assemblage in the hornblende-chlorite-biotite schist is actinolite + biotite + chlorite $\pm$ plagioclase $\pm$ quartz. Hornblende commonly occurs with a rim of colourless actinolite. The chlorite is intensely pleochroic and very fine-grained, compared to the weakly coloured to colourless chlorite in the ultramafic rocks. The plagioclase is An_{17}. Comparing this to Myashiro's (1961) data, this assemblage is consistent with greenschist facies metamorphism.

The textures of the deformed sulfides indicate that pyrrhotite and pentlandite were separate minerals during deformation forming distinct pods and lenses containing only one mineral. Above 400°C pyrrhotite and pentlandite exist as the monosulfide solid solution (Craig, 1973) thus 400°C is a maximum temperature for the cataclastic event.

4:4, Conclusions

1. The temperature of metamorphism (based on geothermometers) is a) $608^{\circ}C \pm 50$ (garnet-biotite, Thompson 1976)

   b) $590^{\circ}C \pm 50$ (calcite-dolomite, Ewert 1977)

   c) $650^{\circ}C \pm 100$ magnetite-ilmenite (Buddington and Lindsley 1964)

2. The pressure of metamorphism based on

   a) Garnet-plagioclase (Ghent, 1977) at a temperature of $600^{\circ}C$ is 5.67 kbar using Robie & Walbaum (1968) or 6.84 kbar using Helgeson et al (1978) data

   b) Sphalerite-pyrite-pyrrhotite (Hutcheon, 1977; Scott, 1973) gives a pressure of 5.6 kbar.

3. The assemblages observed in mafic volcanic rocks, pelites and calc-silicates are consistent with mid-amphibolite facies metamorphism. The assemblages observed in the ultramafic rocks are consistent if the fluid phase is CO_2 rich.

4. The grade of metamorphism during the cataclastic event was greenschist facies (below a temperature of $400^{\circ}C$).

5:0, The Thierry Cu-Ni Mine and Associated Ultramafic Rocks

5:1, Introduction

The purpose of this section is to describe the lithologies, sulfide ore types and detailed structural geology of the Thierry Mine. The whole rock chemistry for the um-m rocks and sheared equivalents is presented and a model for the alteration associated with shearing is discussed.

The Thierry Mine whose workings consist of two open pits (Appendix F), a shaft to 1700' level and a decline to 700' level, is owned by Union Miniere Exploration and Mining. The mine occurs in um-m rocks (Table 5.1) and their sheared equivalents on the north edge of the Pickle Lake greenstone belt between the Pickle Lake Stock and a granitic gneiss terrain (Fig. 2:3). The greenstone belt is only 800 metres wide in the mine area. The amphibolites, host to the um-m rocks, are chemically high-iron tholeiites similar in composition to metavolcanic rocks of the Pickle Crow area (Chapter 4). The ultramafic and mafic rocks consist of 75% mafic metagabbro, 20% metagabbro and 5% talc-carbonate schist with minor olivine-tremolite-chlorite rock. The um-m rocks are highly deformed along shear zones and faults resulting in the development of a protoblastomylonite. This unit, host to two-thirds of the ore (Kennedy, 1978) is referred to as the CBS shear (chlorite-biotite schist shear).

Table 5.1. Mafic and Ultramafic Rocks of the Thierry Mine

ROCK	ORIGINAL ROCK	MINERALOGY	ORIGINAL MINERALOGY	COMMENTS
metagabbro	gabbro	50-80% hornblende 80-50% plagioclase An_{20} An_{30} biotite, chlorite, sphene apatite, ilmenite, magnetite	50% clinopyroxene with exsolved hypersthene and ilmenite 60% plagioclase An_{50} both as cumulus phases	20% of mine as large lens in amphibolite and ultramafic dykes; hornblende has kelyphitic rims
mafic metagabbro	mafic gabbro	80-100% hornblende 0-20% plagioclase An_{20}-An_{30} biotite, chlorite cummingtonite	60% clinopyroxene with exsolved hypersthene and ilmenite 40% plagioclase An_{50} both as cumulus phases	70% of mine intrusion, grades to metagabbro; hornblende has kelyphitic rims
talc-carbonate schist	dunite	80% talc, 20% carbonate olivine, lizardite chlorite	olivine Fo_{85} as a cumulus phase	10% of mine intrusion
olivine tremolite-chlorite rock	peridotite	30% olivine Fo_{90} 30% chlorite 30% tremolite 10% magnetite pseudo-spinifex texture	olivine & pyroxene	rare in mine
hornblende-chlorite-biotite schist	mylonitized mafic metagabbro	40-60% hornblende cummingtonite, quartz plagioclase fragments 40-60% biotite and chlorite matrix- 20-10% sulfides	fragments of largely mafic metagabbro amphibolite, diorite quartz veins	in large shear zone from 1 to 30 metres wide

5;2, Mafic and Ultramafic Rocks in the Thierry Mine

5:2:1, Metagabbro

Metagabbro occurs in three associations; as large lens-shaped bodies in amphibolite schist (section 115E, 110E, 95E), as large masses gradational to mafic metagabbro (section 98E, 101E, 103E) and as narrow dykes from 5cm to 3 metres wide in mafic metagabbro often near the contact between hornblende-chlorite-biotite schist and mafic metagabbro (section 101E). The metagabbro associated with amphibolite schist is commonly well foliated and gradational to amphibolite schist. Metagabbro occurring in dykes is much coarser-grained, with hornblende crystals up to 3cm as compared to 0.5 cm in other types of metagabbro. In hand-specimen the metagabbro is green, massive to well foliated, medium-to coarse-grained, composed of 50 to 90% dark green hornblende as patches of randomly oriented crystals (0.5 to 3cm) and 10 to 50% fine-grained white plagioclase.

5:2:2, Mafic Metagabbro

The mafic metagabbro occur as blocks up to 100 metres to 30 metres in the largest dimension. In handspecimen, the mafic metagabbro is dark green, medium-grained, massive to weakly foliated and composed of nearly 100% hornblende of metamorphic origin (Plate 1F). In thin section, the mafic metagabbro is made up of a mosaic of hornblende. Large crystals of hornblende with dusty inclusions of opaque minerals are rimmed by finer-grained hornblende crystals. The hornblende commonly shows fine exsolution of tremolite producing a herringbone texture. Several specimens have remnant clinopyroxene (Table 5:2) with kelyphitic rims of hornblende against plagioclase (An_{60}). Accessory minerals are sphene, magnetite and ilmenite; alteration products are chlorite, sericite, epidote and carbonate.

Table 5:2, Electron Microprobe Analyses of Silicates from Thierry Mine. (n.a. not analysed, n.d. not detected, tr. trace)

Weight Percent

	1	2	3	4	5	6
K_2O	n.a.	0.11	0.17	0.16	n.a.	n.a.
Na_2O	n.a.	0.66	2.06	1.88	n.a.	n.a.
CaO	24.4	13.7	11.8	12.0	n.a.	tr
MgO	13.6	13.3	11.5	11.8	31.4	48.6
FeO	7.47	14.9	16.0	15.9	30.9	10.7
TiO_2	tr	0.38	0.53	0.55	n.a.	n.a.
MnO	0.17	0.18	0.25	0.21	n.d.	0.64
NiO	tr	0.26	0.13	0.14	n.d.	tr
Al_2O_3	0.84	6.94	12.2	12.4	n.d.	n.d.
SiO_2	52.5	47.5	42.7	42.3	37.4	39.7
Total	98.98	97.93	97.34	97.34	99.7	99.6

Atomic Proportions

K	--	0.02	0.03	0.03		
Na	--	0.20	0.62	0.57		
Ca	3.99	2.27	1.98	2.02		tr
Mg	3.09	3.05	2.67	2.75	7.61	10.8
Fe	0.92	1.92	2.11	2.08	4.22	1.33
Ti	--	0.04	0.06	0.06		
Mn	0.02	0.02	0.03	0.03		0.07
Ni	--	0.03	0.02	0.02		tr
Al	0.15	1.26	2.28	2.28		
Si	7.85	7.31	6.66	6.63	6.08	5.91

1. Clinopyroxene in mafic metagabbro 4-013, Average of 6
2. Hornblende after clinopyroxene in mafic metagabbro average of 4, 4-013,
3. Hornblende in mafic metagabbro, 600 cross-cut, Average of 7
4. Hornblende in mafic metagabbro, 1600 cross-cut, Average of 5
5. Olivine remnants; 4-016, Average of 7, (Fo_{64}) in altered dunite
6. Metamorphic olivine, 1600 level, Average of 10, (Fo_{89}) in olivine-tremolite-chlorite

5:2:3, Talc-Carbonate Schist

Talc-carbonate schist, interpreted to have originally been dunite, makes up 5% of the ultramafic rocks. It occurs as blocks in the east pit associated with chlorite-biotite schist. In handspecimen, it is grey, fine-grained, massive to well foliated, strongly magnetic with a soapy feel. In thin section, massive samples have serpentine-talc pseudomorphs after olivine (Plate 3D). Rare samples contain olivine remnants, (Fo_{65}) (Table 5:2) in a talc-carbonate matrix. The carbonate is a mixture of dolomite and magnesite as shown by X-ray diffraction (Lefebvre, 1977).

5:2:4, Olivine-Tremolite-Chlorite Rock

The olivine-tremolite-chlorite rock, originally a peridotite, is rare in the mine area. It was observed in one drill hole on 1600' level, section 101E. In handspecimen the rock is grey, massive and composed of 30% dark blades of olivine up to 3cm long in a fine-grained matrix. In thin section the matrix is composed of fine laths of tremolite and coarse, bladed antigorite overgrown by lath-shaped olivine crystals, indicating a metamorphic origin for the olivine. The olivine is Fo_{89} (Table 5:2) and is commonly altered to lizardite and magnetite.

5:2:5, Hornblende-Chlorite-Biotite Schist

The hornblende-chlorite-biotite schist is a protoblastomylonite. It occurs in a shear-zone that pinches and swells (up to 100 metres in thickness), often including fragments of relatively undeformed mafic metagabbro (Plate 2E) metagabbro, minor amphibolite schist, diorite and quartz vein. The unit is highly variable in character. In handspecimen, it is dark grey, well foliated and fine-grained, is heavily jointed with the joint surfaces coated with dark chlorite and smeared with sulfides. The protoblastomylonite is commonly banded with white felsic bands, epidote layers and quartz veins from 1mm to 5cm thick. These show complex folding often on a fine-scale (Plate 2F) producing complex interference patterns. Several samples are brecciated, with angular fragments of mylonitized material in a very fine-grained matrix of chlorite and sulfides (Plate 4D).

In thin section, the protoblastomylonite is made up of 40 to 60% fragments, predominantly hornblende with minor cummingtonite, quartz plagioclase and rock fragments, in a fine-grained matrix of sulfide, biotite and chlorite. The fragments have a random optical orientation and are rounded, bent, fractured and stretched parallel to the foliation with the matrix flowing around them leaving pressure shadows (Plate 2C, 2D, 2E).

Banding is due to variations in the relative proportions of chlorite and biotite in the matrix and the relative percentage of fragments. Many samples have quartz-rich layers parallel to the foliation. Some of the quartzose layers are mylonitized; individual quartz grains are polygonally recrystallized and strained in a matrix of very fine-grained quartz. Many of the fragments of hornblende are zoned from dark green hornblende at the core to colourless tremolite on the rims (Plate 2D).

There is a complete gradation between the protoblastomylonite and mafic metagabbro. The amphiboles in the mafic metagabbro are deformed, bent and fractured with biotite and chlorite between the fragments. As the amount of deformation increases the amount of biotite and chlorite increases, the size of the amphibole fragments decreases and the banding increases in intensity.

Accessory minerals are fluorite, barite, sphene, epidote, carbonate and sulfides. There is a positive qualitative relationship between the amount of biotite and sulfide in a layer (Plate 4B, 4F). Most sulfides occur as disseminations deformed parallel to foliation and in pressure shadows. Some sulfides occur in fractures which cut foliation.

5:2:6, Classification of Sulfides in the Mine

Five sulfide types can be recognized; breccia ore, chlorite-biotite schist ore, bornite ore, primary disseminated sulfide and oxidized ore, making up 40%, 56%, 2%, 1% and 1% respectively of the sulfides in the Thierry Mine.

a) The breccia ore composed of 20 to 50% sulfides consists of rounded to angular fragments of gangue in a matrix of chalcopyrite, pyrrhotite, pyrite and pentlandite partly altered to violarite.

b) The chlorite-biotite schist ore contains 5 to 20% sulfide as stringers of chalcopyrite, pyrrhotite, pentlandite and pyrite smeared out along cleavages paralleling the foliation. Texturally the breccia ore is gradational into chlorite-biotite schist ore. The fragments gradually become elongated and flattened parallel to foliation.

c) The bornite ore contains 1 to 5% sulfides as stringers and disseminations of chalcopyrite and bornite in carbonate veins associated with blocks of amphibolite schist in the main shear zone.

d) Primary disseminated sulfides occur as composite blebs of chalcopyrite, with exsolution of bornite or cubanite, plus pyrrhotite and pentlandite between olivine remnants or its metamorphic equivalents.

e) Oxidized ore is composed of two types;

i) Altered breccia ore consisting of spongy masses of millerite, polydymite, vaesite, pyrite, bornite and chalcopyrite surrounding fragments of gangue and,

ii) A narrow zone of supergene ore occurring near surface on joints and fault surfaces; hematite, malachite, native copper, chalcocite, pyrite and chalcopyrite are the prominent minerals.

Three minor sulfide types developed locally but are quantitatively insignificant. Stringers usually rich in chalcopyrite occur in joints and faults in amphibolite schist, disseminations of chalcopyrite, pyrrhotite and minor pentlandite (usually less than 1% sulfide) occurring in metagabbro, and remobilized ore as pods in diorite dykes where the dykes intersect the ultramafic rocks. The pods consist of chalcopyrite and cobaltian pyrite forming a matrix to K-feldspar crystals. The sulfide mineralogy is discussed in detail in Chapter 6. Precious metal minerals commonly occurring in breccia and bornite ore are described in Chapter 7.

5:3. General Geology and Structure of the Thierry Mine

All the um-m rocks in the Thierry Mine are hosted in amphibolite schist. The amphibolite schist merges into granitic gneiss to the north and is cut by Pickle Lake Stock (Fig. 5:6), a porphyritic granodiorite, to the south (Fig. 2:3).

The ultramafic rocks occur as blocks along a zone of mylonitized (C.B.S.) and sheared um-m rocks which are traceable for over 2000 metres in the mine area (Fig. 5:2 and Appendix F). In several of the larger blocks of um-m rock, a complete gradation from metagabbro to mafic metagabbro over a hundred metres is apparent. The metagabbro occurs predominately on the footwall with the mafic metagabbro on the hanging wall as illustrated in Section 101E (Fig. 5:3).

Whole rock analyses along the 312 cross-cut; section 101E, are shown in Fig. 5:4; shows the chemistry of the mafic meta-gabbro to meta-gabbro. The relationship of the talc-carbonate schist and the olivine-tremolite-chlorite rock to the mafic metagabbro is unclear. Both the talc-carbonate schist and the olivine-tremolite-chlorite rock are highly sheared and localized along faults.

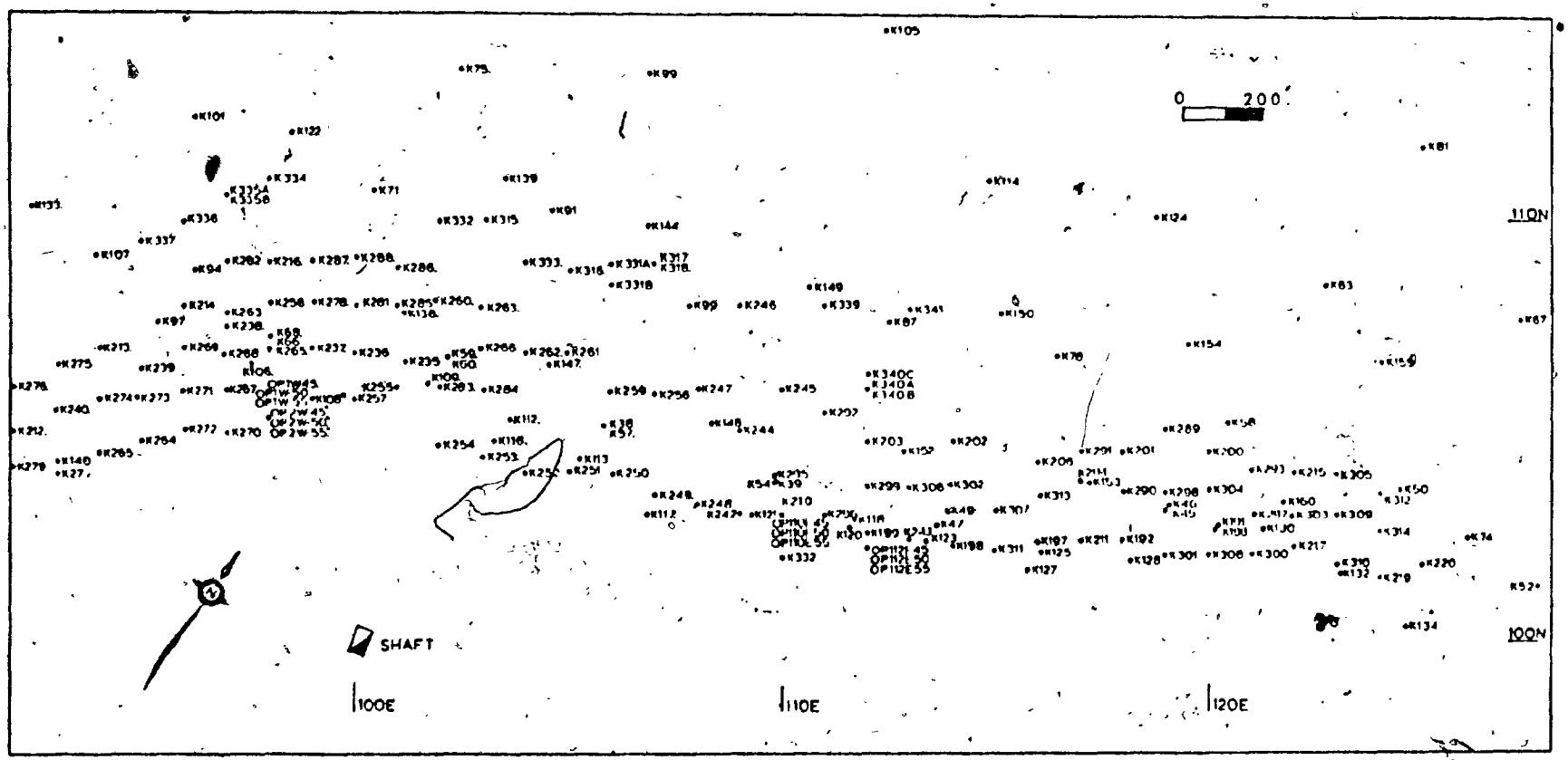

Fig. 5:1, Location of surface drill holes at the Thierry Mine.

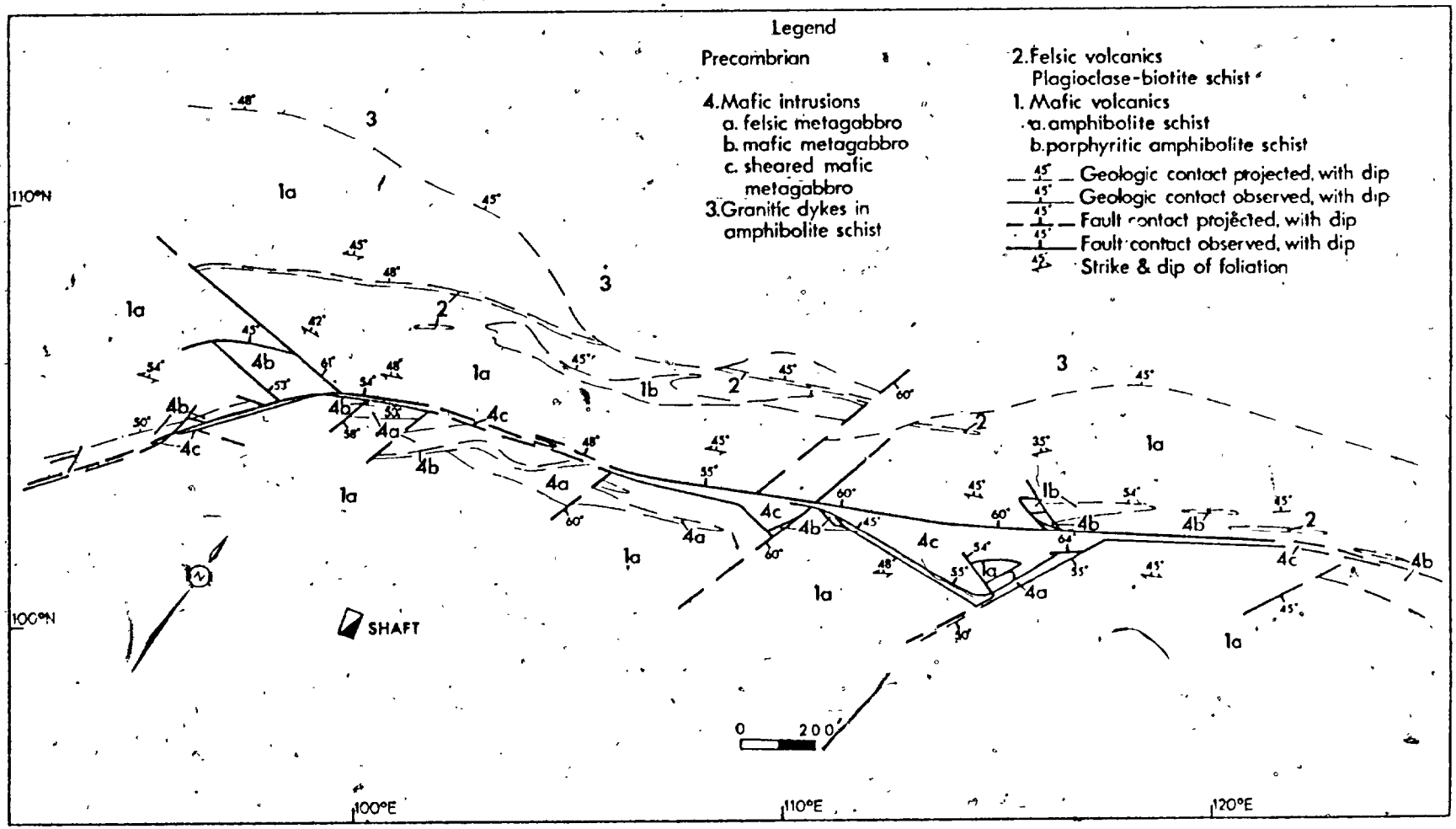

Fig. 5.2. Geological Interpretation of the 100' Level of the Thierry Mine.

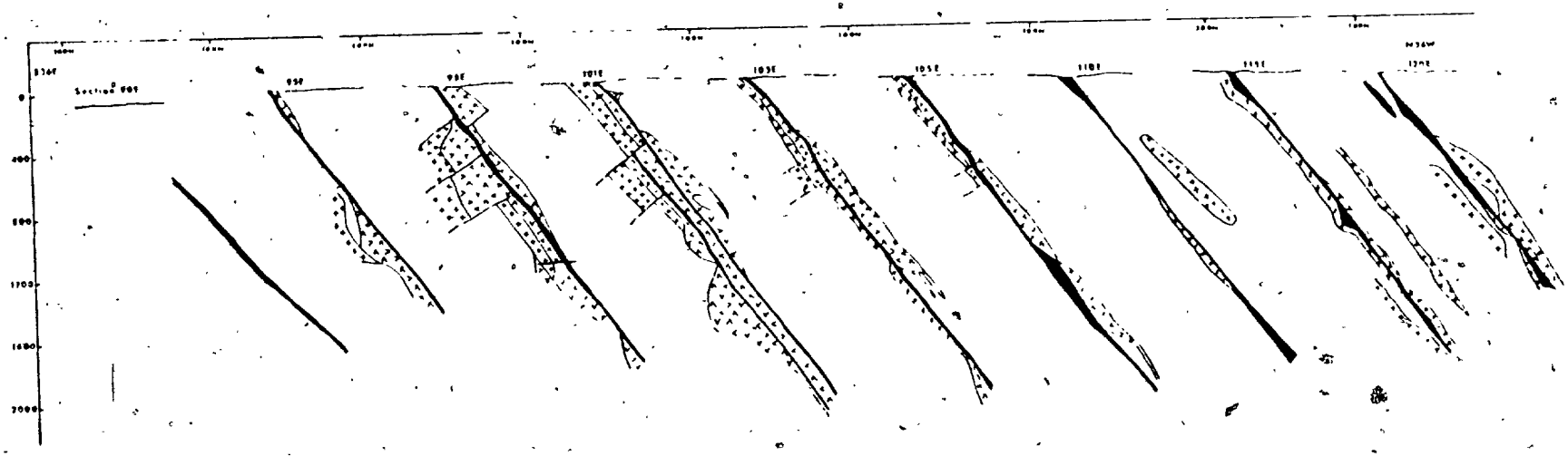

Fig[illegible]mposite of sections through the Thierry Mine; black, hornblende-chlorite-biotite schist; V's, Um-m Rock ; X's metagabbro; white amphibolite schist.

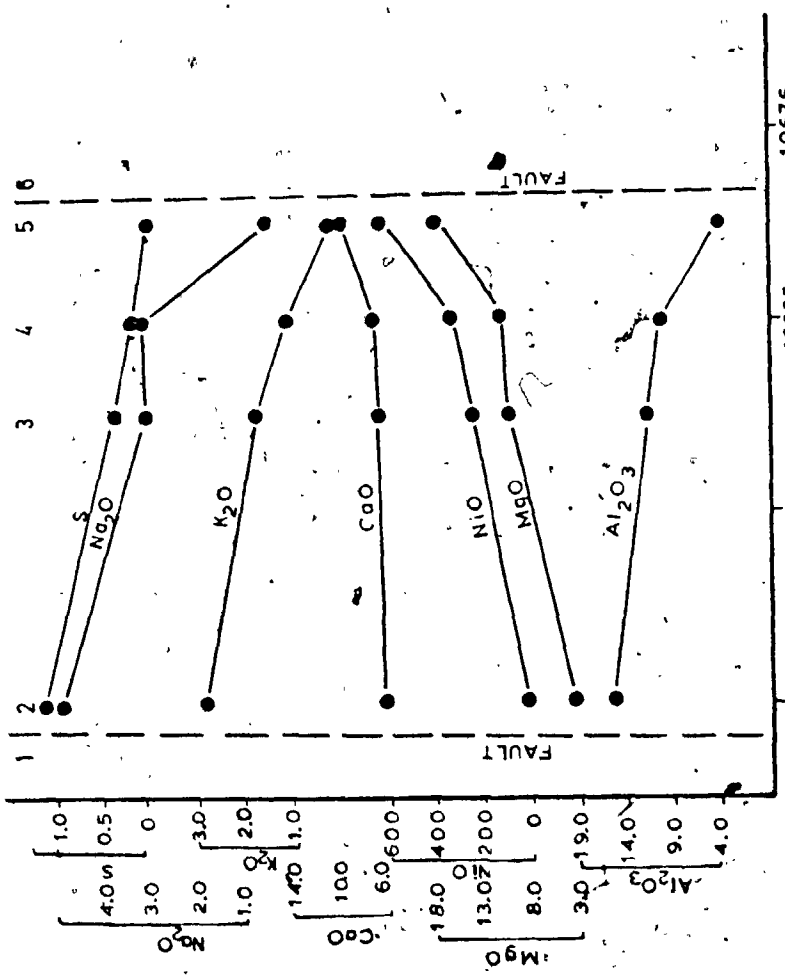

Fig. 5:4, Variation in chemical composition of Al_2O_3, MgO, NiO, CaO, K_2O, Na_2O and S along the 312 level drift.

The zone of sheared and mylonitized um-m rock is thickest (50metres) in the east, section 115E, where it has included large blocks of amphibolite schist containing bornite ore. The mylonite is one or two metres thick between the east and west pits (section 105E) then expands to 5 metres from section 103E to section 95E. The percentage of matrix to fragments and the thickness of the mylonite zone is greatest when the zone cuts um-m rocks. When the shear zone cuts amphibolites (section 90E, 120E), the mylonitized zone consists of amphibolite blocks often highly altered to chlorite and epidote with narrow bands of mylonite between the fragments. Where both the footwall and hanging-wall rocks are amphibolite the mylonite is barren or only weakly mineralized. There is a strong positive relationship between the amount of biotite and the amount of sulfides in the mylonite. (Kennedy, Personal Communication).

There are shears subparallel to the main zone of sheared and mylonitized ultramafic. The strongest of these is shown on section 101E starting at the 500' level and traceable to below the 1600' level as a zone of sheared ultramafic from 1 to 3 metres thick. In section 103E and 98E, the shear is in ultramafic rock but in section 95E and 105E it disappears in amphibolite schist.

The internal structure of the mylonite is very complex. Quartz veins, layers rich in epidote, chlorite or biotite define complex folds of several generations producing interference patterns. Some of the folds are related to dragging against the wall rocks and others to faults within the mylonitized zone. Fig. 5:5 shows a map of a cross-cut through the 1600 level (Section 101E). The contact between the mylonite (sheared ultramafic rock) and the amphibolite schist is very sharp with the amphibolite schist showing only minor deformation. The contact between the mylonite and ultramafic rock is less distinct with the ultramafic rock becoming less deformed and sheared to the south. The amount of breccia ore is highest at the contact between the mylonite and ultramafic rocks and decreases away from the fault. Within the mylonite there are distinct fault-bounded zones or blocks of mylonitized rock. These internal faults do not cross the main shear contacts, are commonly curved and filled with a blue-grey fault gouge. Parallel to the main shear there is often a zone that has been extensively altered. Amphibolite contains bands rich in epidote and carbonate whereas the ultramafic rock contains epidote and chlorite. Several diorite dykes exposed in the east pit near the main shear have epidote alteration developed along joint systems.

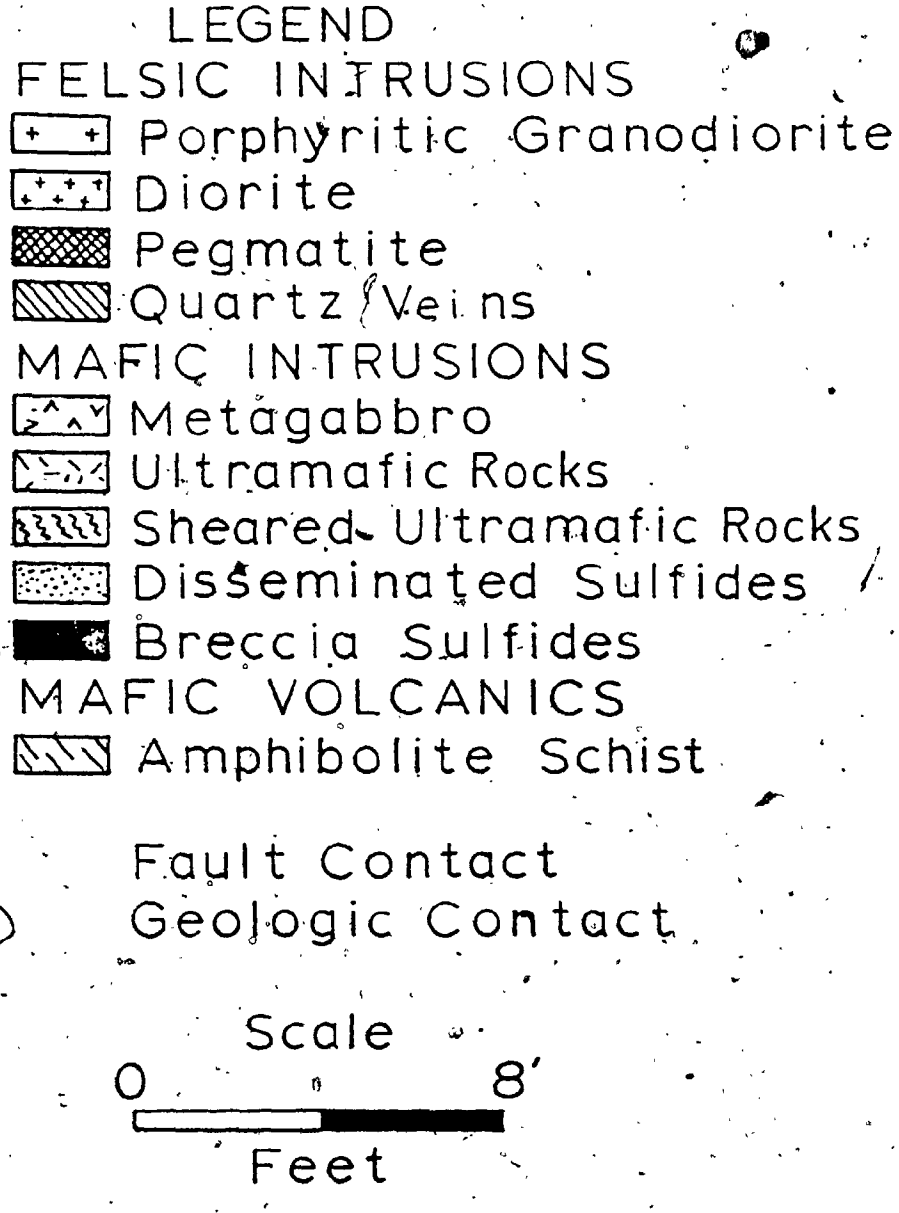

Legend for Fig. 5.5 and Fig. 5.6

Fig.5.5 , Cross section through the 1600 level cross cut, east and west walls folded flat.

Fig.5.6, Section through 1600 level cross cut showing amphibolite schist - granite contact east and west walls folded flat.

1600' LEVEL CROSS-CUT

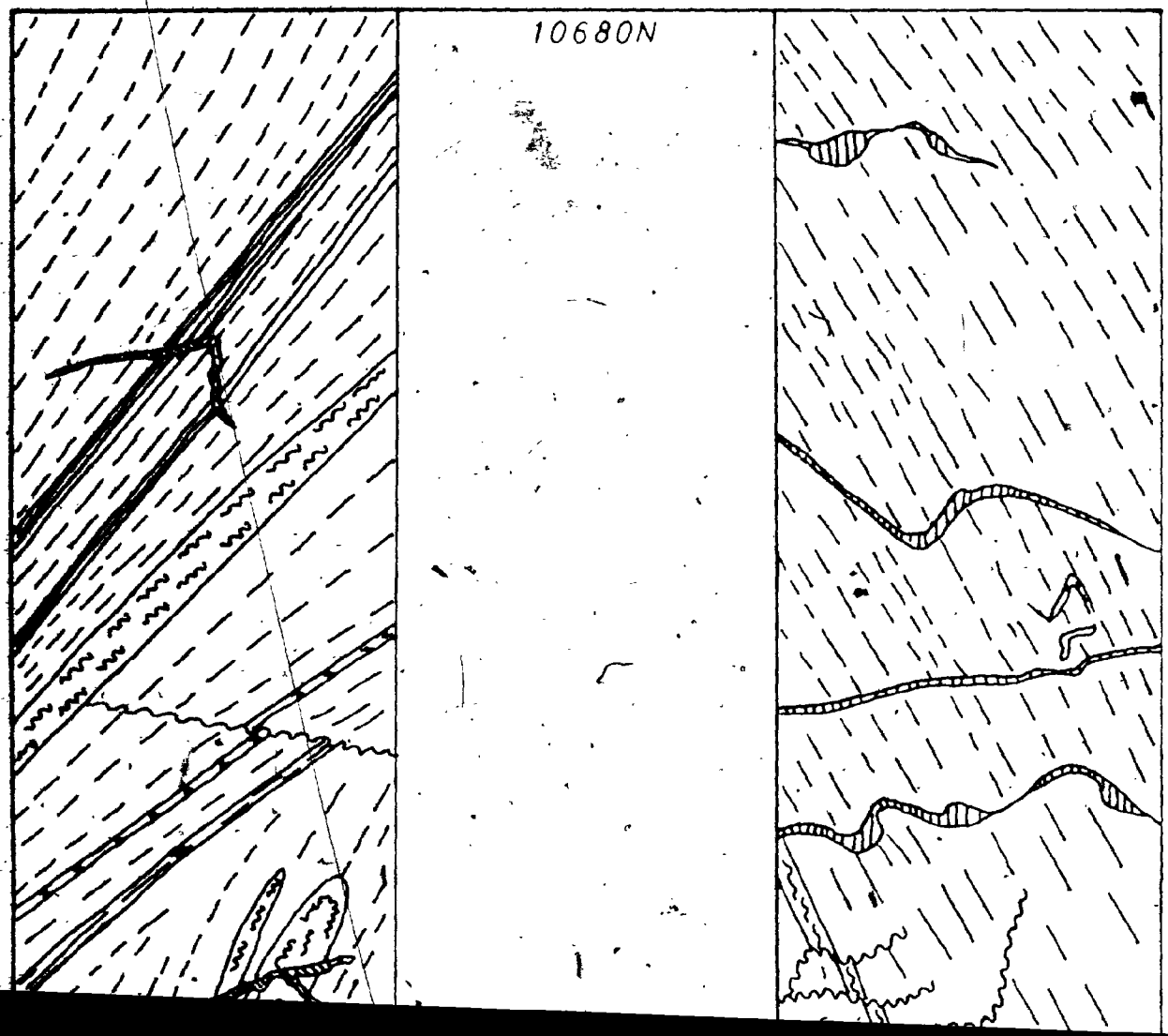

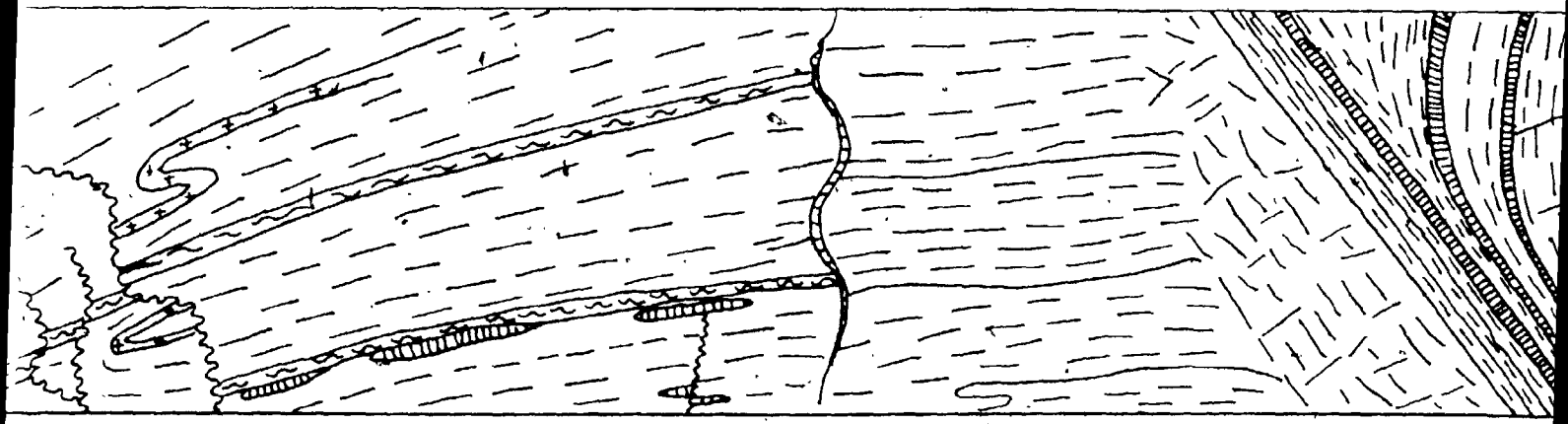

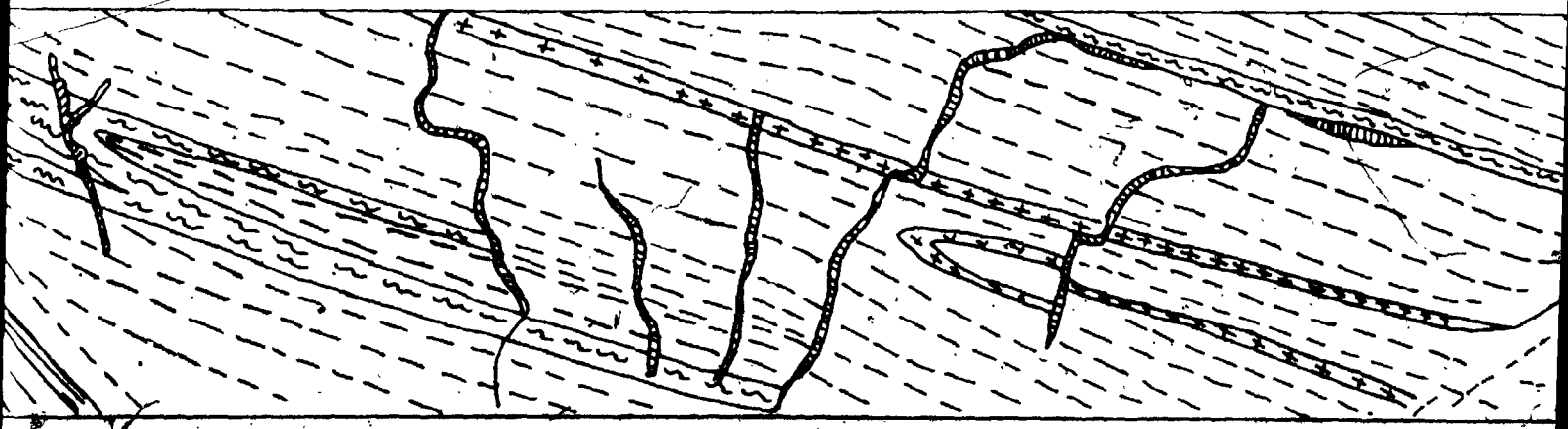

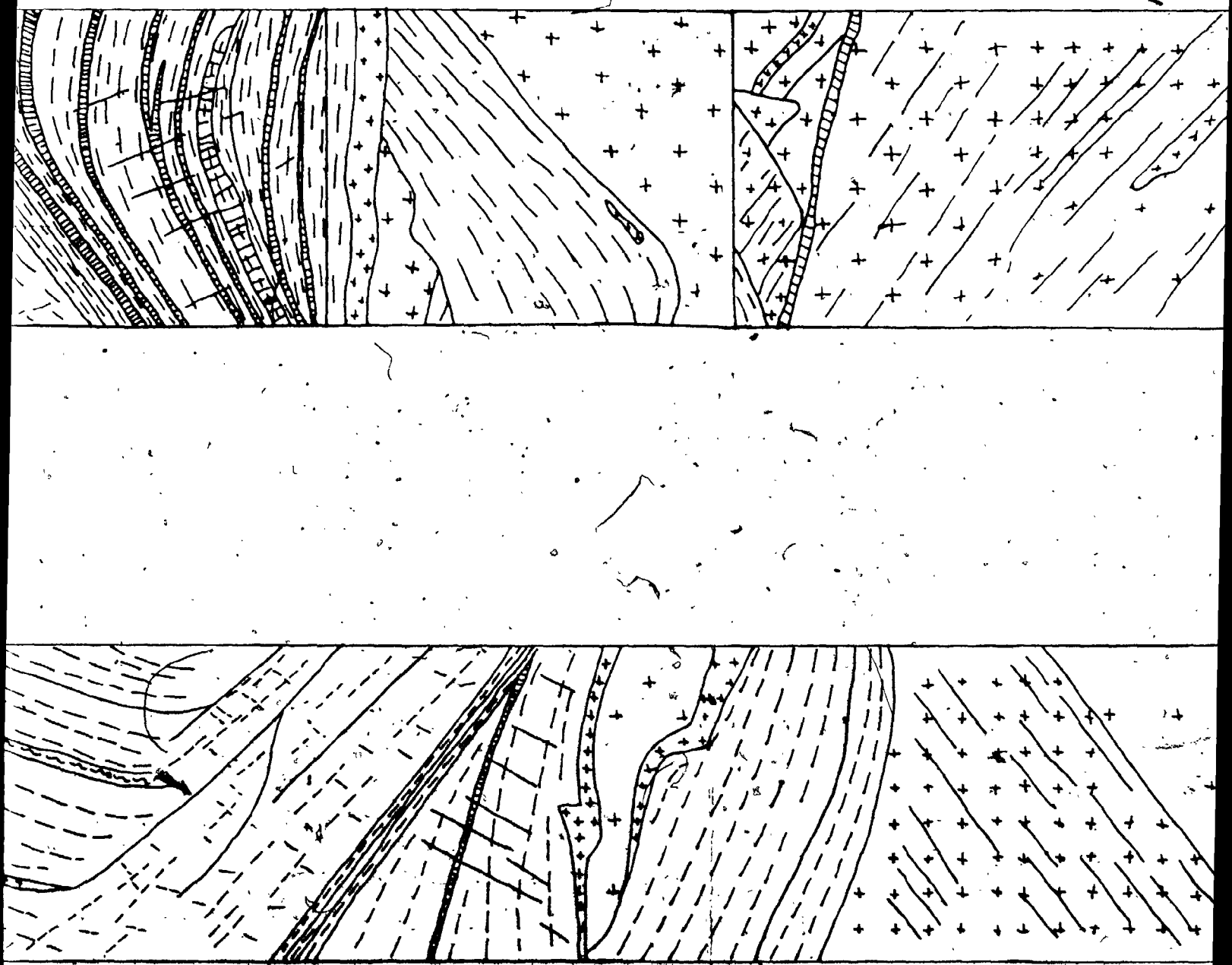

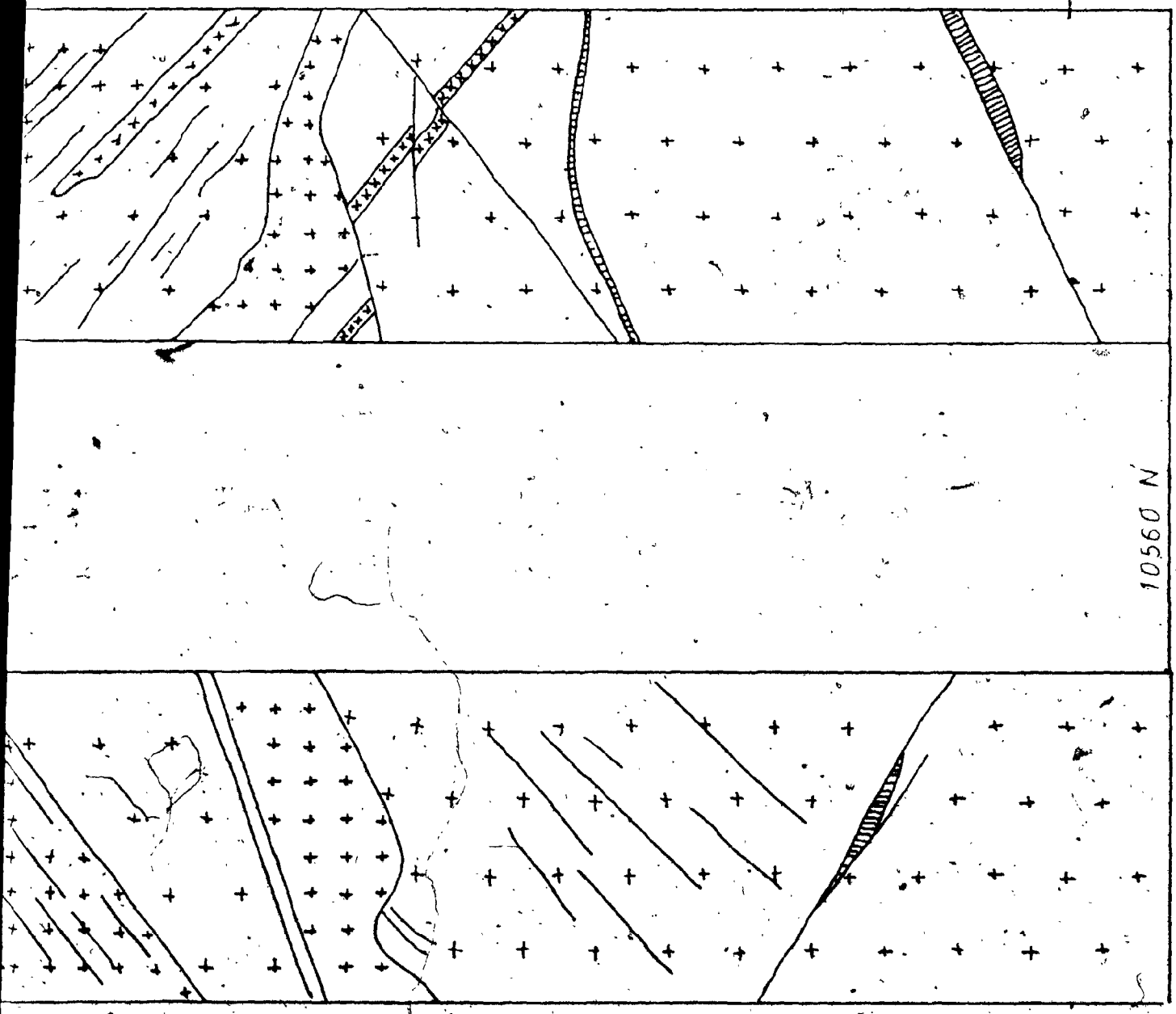
10560 N

1600' LEVEL CROSS-CUT

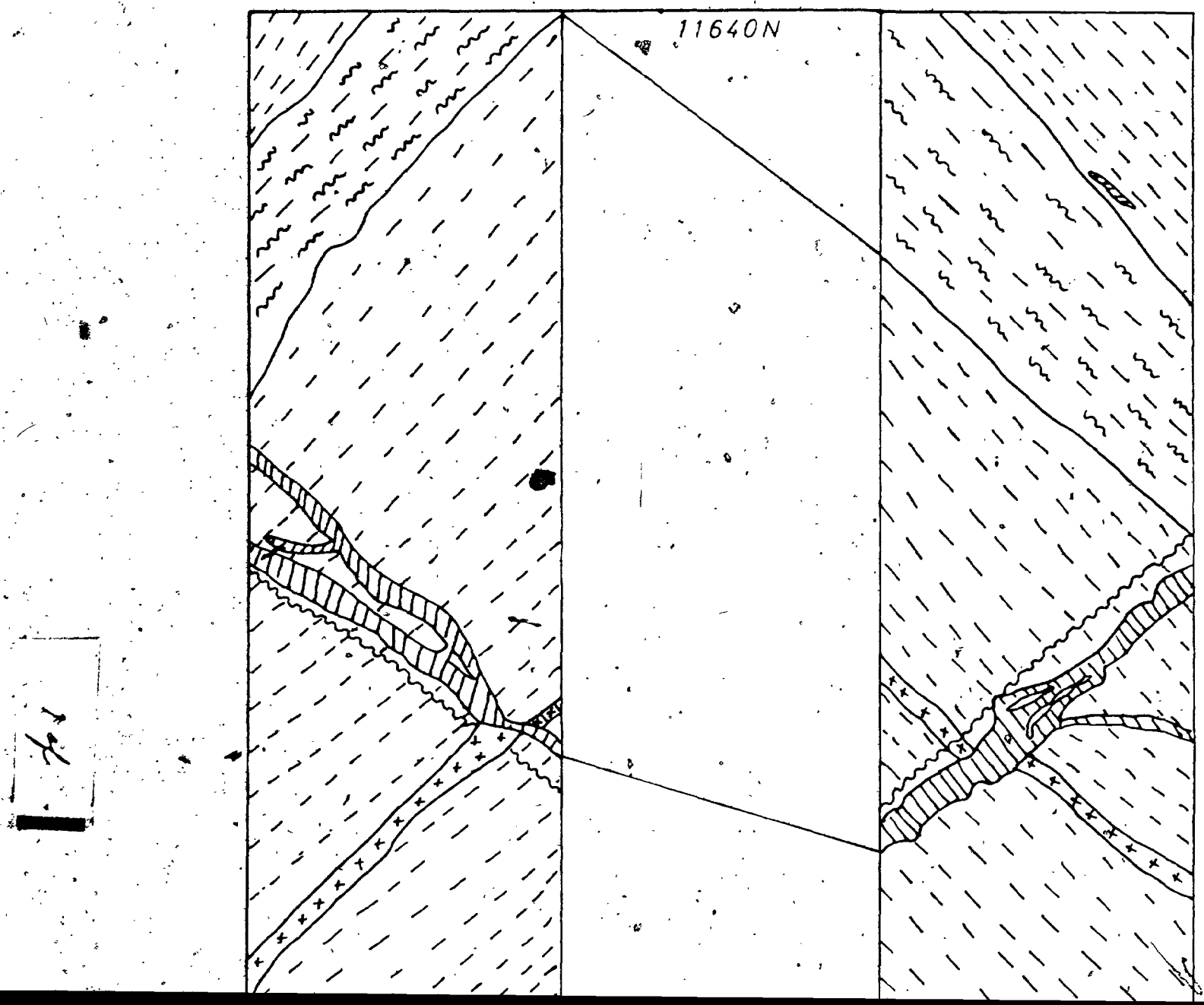

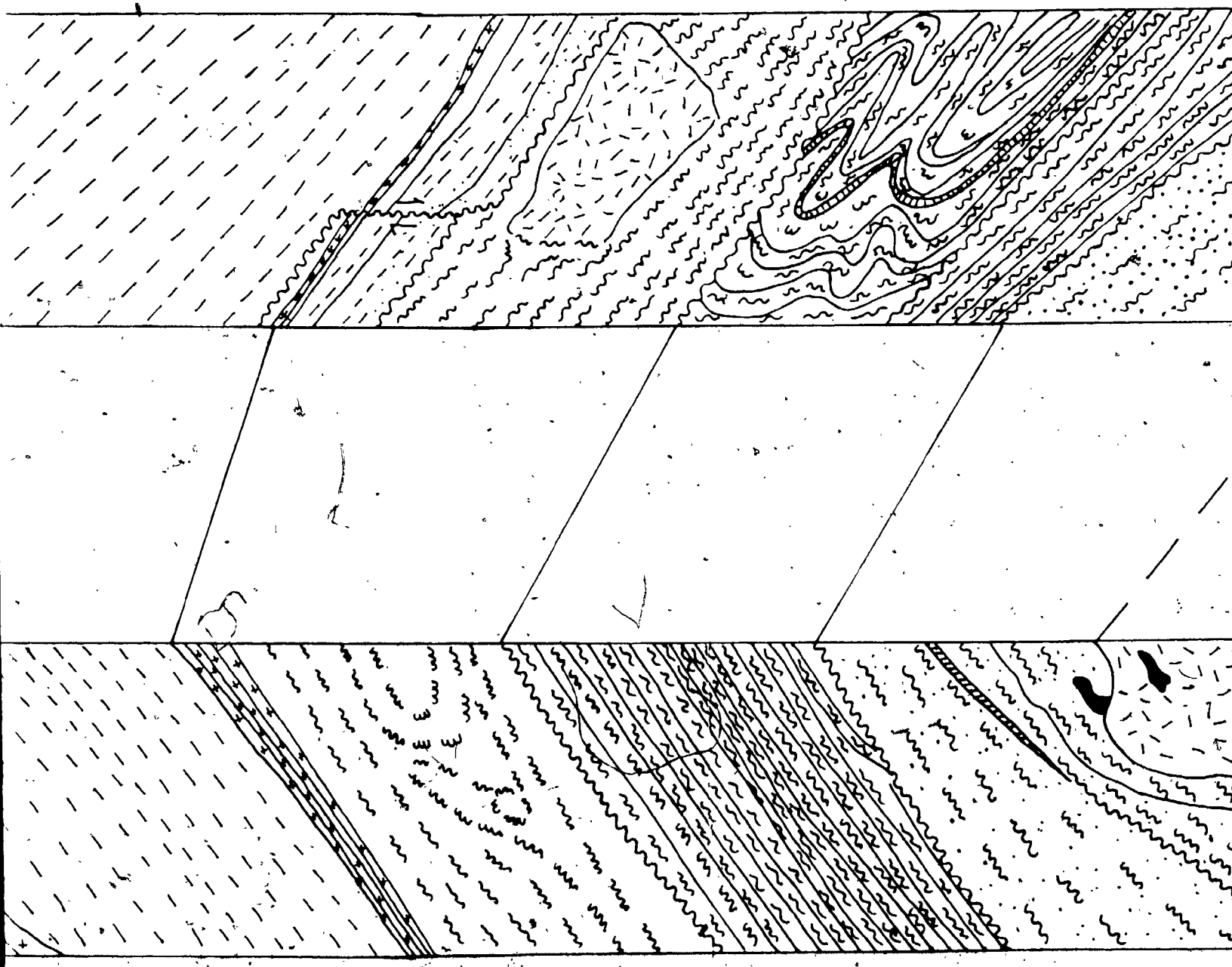

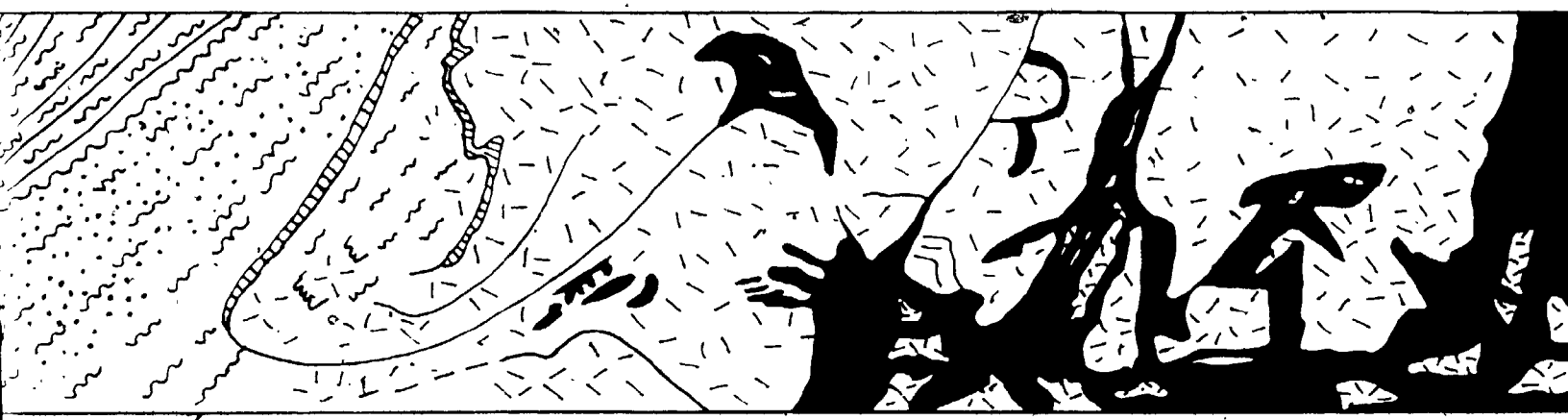

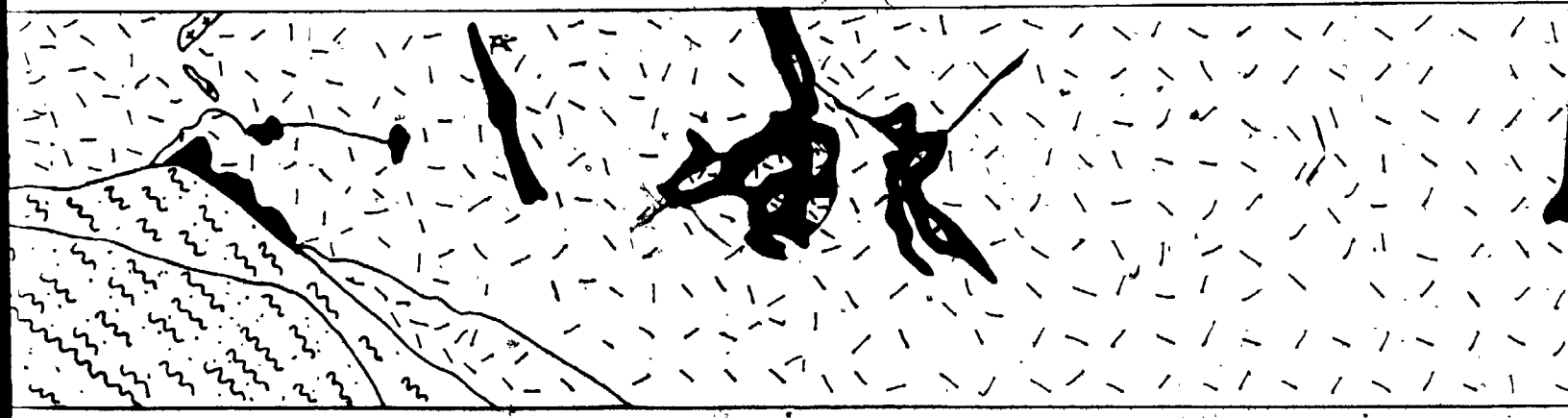

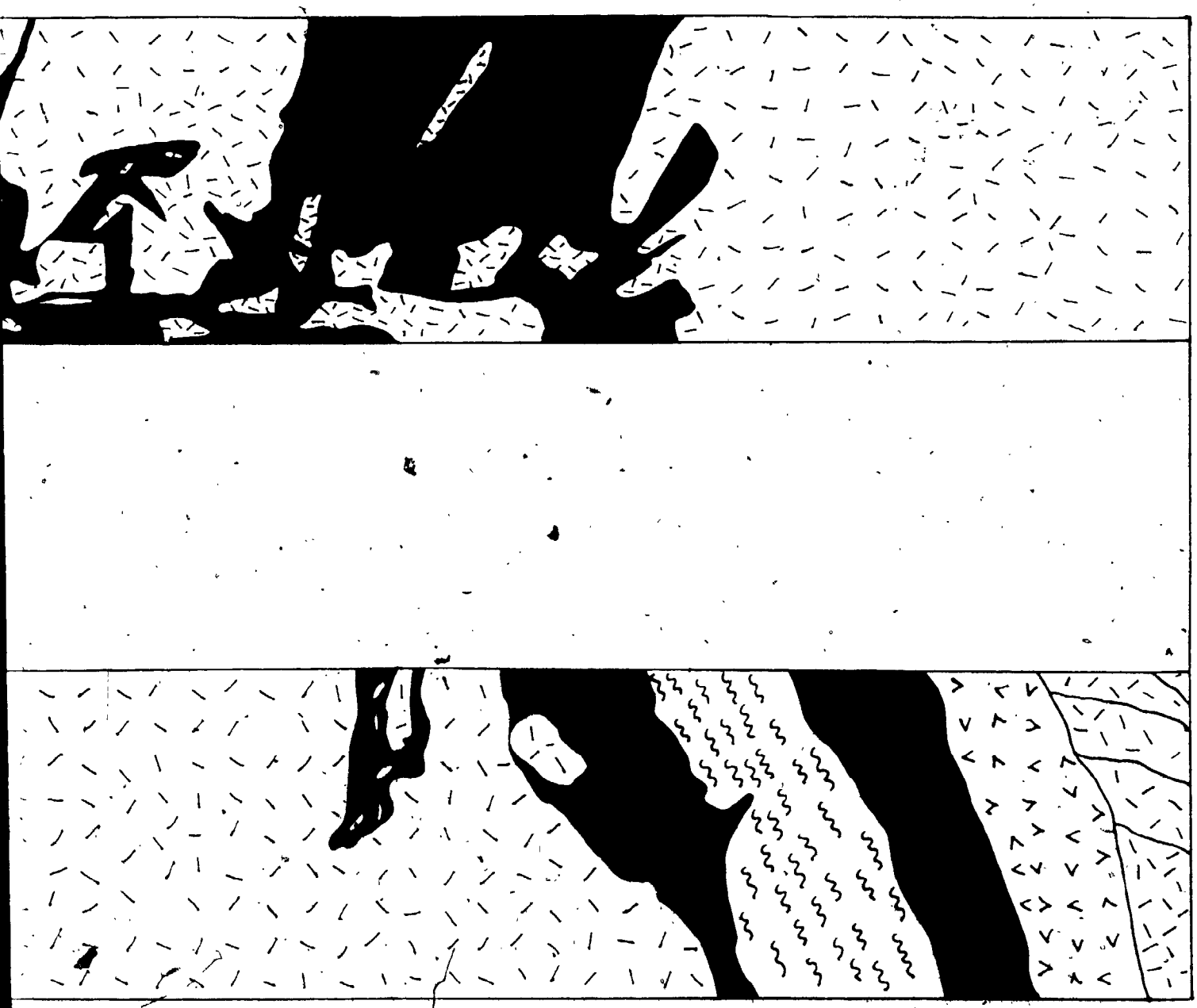

11520N

There are two other major fault systems which cut all other units including the Pickle Lake Stock in the mine area in addition to the main C.B.S. shear. These fault systems are conjugate; that is, symmetrical about the main shear with their line of intersection in the plane of the main shear. In general the faults striking at $90^{\circ}/45^{\circ}N$ are cut by faults striking at $25^{\circ}/55^{\circ}E$ which are in turn cut by the mylonite shear $60^{\circ}/50^{\circ}N$. There are several exceptions where the mylonite shear is cut by faults running at $25^{\circ}/55^{\circ}E$ causing offsets of up to 20 metres of the mylonitized zone. These are interpreted as late movement renewed on old shears. The pattern of splays associated with these faults (Kennedy, 1978) and the offsets in the stratigraphy imply reverse movements with offsets of one to 90 metres. Many of the conjugate faults are localized in diorite dykes. (section 101E, 105N, 600 level) and often the fragments are coated with gypsum and thousmanite. Where the faults cut the um-m rocks, hornblende chlorite-biotite schist is developed. Many of the undulations in the ultramafic (section 103E, 98E, 95E) are probably due to these conjugate faults. However where these faults cut the amphibolite schist, only a narrow chlorite-coated surface is developed. These are very similar to joint planes which makes their mapping difficult.

Much of the breccia ore is concentrated where the conjugate fault cuts the um-m rocks. In the west pit 96E-109E, all of the breccia ore is on the hanging wall side of the main shear. The central portion of the um-m body is barren with breccia ore concentrated along its margin. This pattern is repeated underground to below 1600 level where the breccia ore is concentrated to the north side of the main shears; with minor exceptions this is true throughout the deposit.

5:4, Chemical Alteration of Deformed Ultramafic and Mafic Rocks

From the 312 level drift (section 101E), samples were analysed in a block of um-m rock which showed only minor deformation and continuous gradation from metagabbro to mafic metagabbro. Al_2O_3, MgO, NiO, CaO, K_2O, Na_2O and sulfur show a continuous trend with distance along the drift (Fig. 5:4) consistent with a magmatic trend. A plot of Na_2O - CaO-K_2O (Fig. 5:7) shows that the sheared um-m rocks and chlorite-biotite schist are enriched in Na_2O and K_2O (or depleted in CaO) relative to the um-m rocks and amphibolites.

Fig. 5:8 shows a plot of the Larsen factor vs oxides weight percent. The line of the diagrams join points on the magmatic trend shown on the 312 level cross-cut. Al_2O_3, Cr_2O_3, MgO fall on this magmatic trend. There is enrichment of K_2O and depletion in CaO, SiO_2 and Na_2O in the same set of samples relative to this curve. Thin section examination of these samples indicate they contain cataclastic textures (chlorite-biotite schist and sheared um-m rocks). Fe_2O_3, FeO or total iron for the 312 drift samples do not fall on a magmatic trend. The Larsen factor vs Fe (not shown) shows a large scatter. Examination of the whole rock analyses (Appendix E) shows there is enrichment of CO_2, S, Cu, Ba and Zn in the deformed rocks.

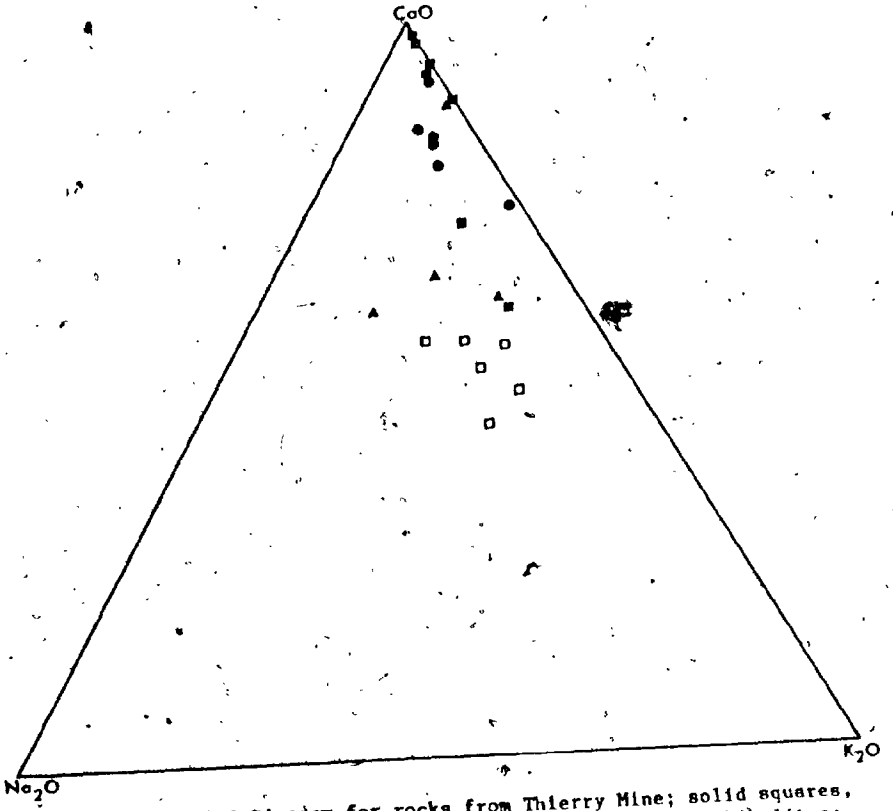

Fig. 5:7, CaO-Na_2O-K_2O Diagram for rocks from Thierry Mine; solid squares, mafic metagabbro; triangles, metagabbro; circles, amphibolites; open squares, hornblende chlorite-biotite schist and sheared ultramafic rocks.

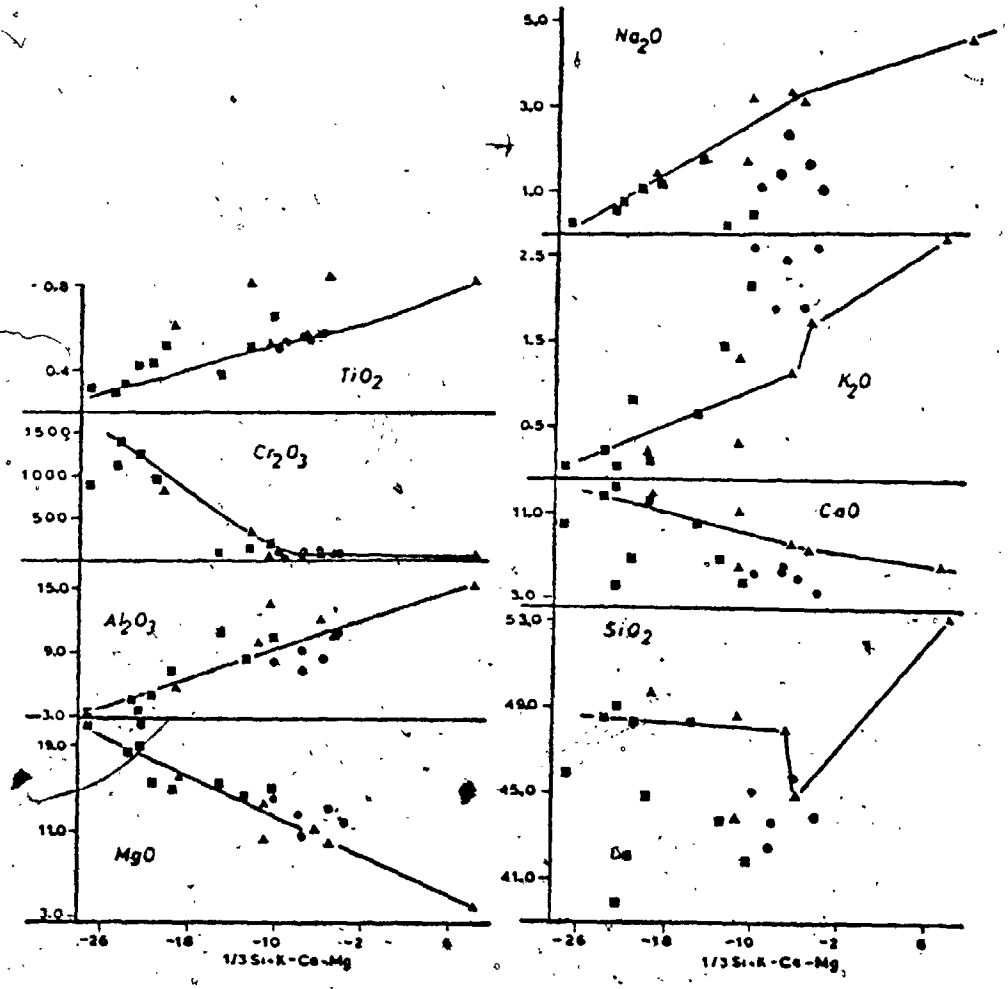

Fig. 5:8, Larsen plot for mafic metagabbro (solid squares) metagabbros (solid triangles) chlorite-biotite schist (solid circles) from the Thierry Mine. Line joins samples from trend observed on 312 level drift, Fig. 5:4.

5:5, Model for Alteration

The whole-rock analyses of altered um-m rocks show that Mg,Fe,Al were relatively immobile whereas K,Ca,Si and Na were mobile. The following model is suggested based on the observed textures and whole rock chemistry to explain the alteration. Reactions are listed in Table 5:3.

1. The hornblende fragments in the mylonitized mafic metagabbro commonly have rims of tremolite. These rims are interpreted to have had Na,K,Fe and Al removed from the original hornblende leaving tremolite by reaction 4.

2. The original rock, mafic metagabbro and metagabbro both carry plagioclase. Plagioclase is rare in the mylonite and is altered to chlorite and epidote. This suggests that the plagioclase may have been converted to chlorite (reaction 1 a and 1 b and epidote reaction 3).

3. The chloritic matrix could be converted to biotite (reaction 2) by the addition of K from the breakdown of hornblende (reaction 4) and/or the addition of K from outside the system.

4. The silicon and sodium released in the generation of chlorite with the wall rocks (predominantly amphibolite schist, composed of andesine and hornblende) to produce albite-rich plagioclase and clinozoisite.

Table.5.3., Alteration Reactions Associated with Mylonitization

1. Chlorite Generation

a. $2NaAlSi_3O_8 + 4(Mg,Fe)^{2+} + 2(Fe,Al)^{3+} + 10H_2O =$

Andesine

$(Mg,Fe)_4^{2+}\ (Fe,Al)_2^{3+}\ Si_2O_{10}\ (OH)_8 + 4SiO_2 + 2Na^+ + 12H^+$

Chlorite

b. $(Na,K)_{0-1}Ca_2(Mg,Fe,Al,Fe)_5(Al,Si)_8O_{22}(OH,F)_2 + CaAl_2Si_2O_8$

Hornblende Anorthite

$+2H^+ = (Mg,Fe)_4(Fe,Al)_2Si_2O_{10}(OH)_8 + SiO_2 + H_2O + Ca^{+2},Na,K)$

Chlorite

c. $(Na,K)_{0-1}Ca_2(Mg,Fe,Al,Fe)_5(Al,Si)_8O_{22}(OH,F)_2 + CaAl_2Si_2O_8$

Hornblende Anorthite

$= (Mg,Fe)_4^{2+}(Fe,Al)_2Si_2O_{10}(OH)_8 + Ca_2(Mg,Fe)_5Si_8O_{22}(OH,F)_2^+$

Chlorite Actinolite

$Na^+ + K^+$

2. Biotite Generation

$Al(Mg,Fe)_3AlSi_3O_{10}(OH)_8 + (Mg,Fe)^{2+} + 2K^+ + 3Si^{4+} + 11/2O_2 =$

Chlorite

$2K(Mg,Fe)_3AlSi_3O_{10}(OH)_2 + 4OH^-$

Biotite

3. Epidote Generation

$2NaCaAl_3Si_3O_{16} + 2SiO_2 + Ca + H_2O =$

Andesine

$Ca_2Al_3Si_3O_{12}(OH) + (Na,Ca)\ (Al,Si)_3O_8 + H^+$

Clinozoisite Albite

4. Hornblende Alteration

$(Na,K)_{0-1}Ca_2(Mg,Fe,Al,Fe)_5\ (Al,Si)_8(OH,F)_2 + H^+ =$

Hornblende

$Ca_2(Mg,Fe)_5\ (Al,Si)_8\ (OH,F)_2 + (Na,K,Al) + H_2O$

Actinolite

Phase relations for the system K_2O, MgO, Al_2O_3, SiO_2 at 500°C and 1 kbar are shown in Fig. 6.2B (Richter and Hemley, 1959). Using this to model reaction (2), it is apparent that a change from the chlorite to phlogopite field involves a drop in H^+ concentration, other conditions remaining constant. Since the solubility of copper sulfides is pH dependent and more copper is soluble in acidic than in basic solutions (Barnes, 1972), a rise in pH could cause copper to be deposited. It has been observed that the amount of biotite in the matrix of the mylonite is proportional to the amount of sulfide (Kennedy, 1978). This suggests that the formation of biotite also triggered the deposition of copper sulfides. The most likely source of the sulfur and metals would be the um-m body itself.

Comparing the elements mobile during alteration based on whole rock data to those suggested in the above model, Na,Ca,Si are removed from the sheared ultramafic rocks to produce epidote and plagioclase in the amphibolite, and K is added to the mylonite zone producing biotite. Mg,Fe and Al are immobile. This pattern of alteration was also observed in shear zones in amphibolite at Yellowknife, N.W.T. by Kerrick et al (1976).

5:6, Summary and Conclusions

The Thierry Mine occurs in ultramafic and metagabbroic blocks sheared and deformed into hornblende-chlorite-biotite schist, a mylonite. The original rock was predominantly gabbro with minor peridotite and dunite emplaced in high-iron tholeiites. These were folded and metamorphosed to mid-amphibolite-facies conditions, (600°C and 5.5. kbars). The mineralogy and texture of the sulfides in the mylonitized zone indicate that latest shearing took place at a temperature below 400°C.

The whole rock chemistry indicates that Ca,Na,Si have been removed and K,Cu and S have been added to the mylonitized zone. The lack of plagioclase, the alteration of hornblende to actinolite, the coincidence of biotite and sulfide in the mylonite and the enrichment of epidote and carbonate in the amphibolite wall rocks suggest that the alteration of plagioclase and hornblende produced chlorite in the mylonite, releasing sodium and calcium generating epidote and plagioclase in the amphibolites. Potassium also released from hornblende break down altered the chlorite to biotite; this was accompanied by a rise in pH possibly causing the precipitation of sulfide in the mylonite. The sulfur and metals were likely mobilized from the um-m body.

6. Sulfide Mineralogy at the Thierry Mine

6.1 Introduction

Preliminary studies on the sulfide mineralogy by Bowdidge (1970) and Morton and Watkinson (1974) have shown that the Thierry Mine ores are chalcopyrite-rich and have suffered violaritization. The purpose of this study is to describe the sulfide mineralogy in the ores from the Thierry Mine to establish the relative importance of magmatic, metamorphic and metasomatic features and to clarify some problems concerning low-temperature alteration of sulfides in Cu-Ni ores.

6:2, Classification of Sulfide Assemblages in the Thierry Mine

There are five main sulfide types in the Thierry Mine; primary disseminated sulfides, breccia ore, chlorite-biotite schist ore, bornite ore and altered ore making up 1%, 40%, 56%, 2%, 1% respectively of the sulfide mineralization at the Thierry Mine. Breccia ore is composed of 20 to 50% sulfides and 50 to 80% rounded to angular fragments of gangue. The most common sulfides are chalcopyrite 60%, pyrrhotite 30%, pyrite 5% and pentlandite, commonly altered to violarite 5%. Chlorite-biotite schist ore contains 5 to 20% sulfide. The sulfides consist of stringers of chalcopyrite, pyrrhotite, pentlandite and pyrite smeared out along cleavages paralleling the foliation. Texturally the breccia ore is gradational into chlorite-biotite schist ore. The fragments gradually become elongated and flattened parallel to foliation with the sulfides along foliation planes (Plate #9). Bornite ore contains 1 to 5% sulfides as stringers and disseminations of chalcopyrite and bornite in carbonate veins associated with blocks of amphibolite schist in the main shear zone. Primary disseminated sulfides occur as intercumulus blebs (up to 3% by volume) between remnant olivine grains or their metamorphosed equivalents.

The sulfides consist of chalcopyrite, with exsolved bornite or cubanite, and pyrrhotite with exsolution of pentlandite. Oxidized sulfides form from altered breccia ore and consist of a spongy mass of millerite, polydymite, vaesite, pyrite, bornite and chalcopyrite surrounding fragments of gangue. They also occur as supergene sulfides near the surface on joint and fault surfaces. The minerals are hematite, malachite, native copper, chalcocite, pyrite and chalcopyrite. Three other minor sulfide types develop locally but are quantitatively insignificant.

i) Stringers usually rich in chalcopyrite occur in joints and faults associated with the footwall and hangingwall amphibolite.

ii) Disseminations usually less than 1% by volume in metagabbro of chalcopyrite, pyrrhotite and minor pentlandite.

iii) Remobilized ore as pods up to 1 metre in diameter in diorite dykes where the dykes intersect the um-m rocks. The pods consist of chalcopyrite and Co-pyrite forming a matrix to K-feldspar crystals.

6:2:1, Sulfide and Oxide Mineralogy of the Thierry Ore

a) Breccia Ore

The breccia ore consists of angular to subrounded, chlorite-coated fragments of gangue, predominately mafic metagabbro, with minor amphibolite schist and chlorite-biotite schist, in a matrix of sulfides. The fragments vary in diameter from two metres to 2mm. The sulfides consist of chalcopyrite, monoclinic pyrrhotite, pentlandite, violarite after pentlandite, lamellar violarite after pyrrhotite, smythite, cobalt-rich pyrite, nickel-rich pyrite, resorbed pyrite, low nickel-iron monosulfide, sphalerite, Pd-Pt-Ag minerals and galena. Compositions of some of these sulfides are given in Table 6:1. Chalcopyrite, the most abundant sulfide mineral occurs as large grains up to 2cm in diameter enclosing all other sulfide minerals. Small wormlike inclusions of mackinawite containing 0.42%Ni and 2.75%Cu are found throughout the chalcopyrite. Minor chalcopyrite is present as very fine emulsions in sphalerite.

Monoclinic pyrrhotite is the next most abundant mineral. It is commonly polygonallly recrystallized with sharp 120° triple junctions and rare deformation twins. Pyrrhotite forms rims up to 3cm wide around fragments of gangue. The fragments often contain hematite with magnetite on the contact between sulfide and silicate (Plate 9A).

Table 6.1, Average Analyses of Sulfides from Thierry Mine Breccia Ore

	NO. OF	WEIGHT PERCENT AND ATOMIC RATIO							
	GRAINS	S	Fe	Co	Ni	Cu	Zn	TOTAL	FORMULA
chalcopyrite	9	34.8	30.3	tr	n.d.	34.2	n.d.	99.3	$CuFeS_2$
		1.09	0.54	-	-	0.54	-		
m. pyrrhotite	27	40.5	57.6	0.18	0.96	n.d.	n.d.	99.24	$M_{6.93}S_8$
		1.26	1.03	0.003	0.016	-	-		
pyrite (Resorbed)	6	52.9	43.3	0.15	2.88	n.d.	n.d.	99.63	$M_{1.01}S_2$
		1.65	0.782	0.003	0.049	-	-		
pyrite (Co-rich)	4	53.7	44.1	2.62	tr	n.d.	n.d.	100.42	$M_{0.99}S_2$
		1.677	0.790	0.044	-	-	-		
pyrite (Ni-rich)	11	52.4	43.8	0.25	2.67	n.d.	n.d.	99.12	$M_{1.02}S_2$
		1.636	0.784	0.004	0.045	-	-		
smythite	4	40.7	56.6	0.16	1.66	n.d.	n.d.	99.16	$M_{9.03}S_{11}$
		1.27	1.01	0.003	0.03	-	-		
pentlandite	6	33.6	26.4	3.20	36.4	0.17	tr	99.62	$M_{8.8}S_9$
		1.05	0.47	0.054	0.62	0.003			
violarite (in Pn)	7	41.7	25.9	2.39	27.7	-	-	97.69	$M_{3.01}S_4$
		1.30	0.464	0.041	0.472				
violarite (in Po)	9	40.8	28.0	1.55	27.3	n.a.	n.a.	97.65	$M_{3.12}S_4$
		1.27	0.501	0.026	0.465				

Breccia Ore (Continued)									
sphalerite	5	32.2	6.22	0.12	0.15	1.05	59.9	99.05	$M_{1.03}S$
(in Po)		1.0	0.11	0.002	0.002	0.017	0.92		
sphalerite	1	32.6	7.71	n.a.	n.a.	n.a.	59.9	100.65	$M_{1.03}S$
(Py+Po)		1.02	0.138	-	-	-	0.916		

In sulfide-rich sections pyrrhotite occurs as discontinuous bands or streaks in massive chalcopyrite. In rare pyrrhotite-rich sections hexagonal and monoclinic pyrrhotite are present in a complex intergrowth. The structural formula of monoclinic pyrrhotites from an average of eleven analyses is $M_{6.97}S_8$ with a nickel content of 0.52% and cobalt content of 0.18%.

Pentlandite (5-10% of the sulfide minerals) occurs at grain boundaries of polygonally recrystallized pyrrhotite as flames and pods implying that pentlandite and pyrrhotite exsolved from a single phase (Plate 8A). The freshest pentlandite occurs in flames from 10 to 20 microns in width at the edges of pyrrhotite within chalcopyrite. Violarite is present in most pentlandite grains ranging from small rare flecks to complete pseudomorphs after pentlandite (Plate 8C). Violarite develops as lamellae along cleavages with pentlandite remnants at the cores (Plate 8F). Where the pentlandite is completely replaced by violarite, blocky octahedral cleavage or shrinkage fractures after the cleavages in pentlandite are apparent. Pyrite and marcasite develop along the shrinkage fractures (Plate 8F). Pentlandite contains an average of 3.2 weight % cobalt with an average atomic Fe/Ni ratio of 0.76. Violarite after pentlandite contains up to 4.2% cobalt with an average of 2.39% Co.

Fine lamellar violarite occurs along fractures and grain boundaries as a replacement of monoclinic pyrrhotite (Plate 8D). This violarite has a distinctly lower cobalt content of 1.40% and a high iron content. Smythite is associated with violarite alteration in pyrrhotite (Plate 8B), and contains an average of 1.66% nickel compared to 0.52% nickel in the associated pyrrhotite.

In some samples a low nickel-iron monosulfide occurs with the same d-spacing as that reported by Desborough and Czamanske (1973) (Table 6:2). It has physical properties very similar to monoclinic pyrrhotite and cannot be readily distinguished in handspecimen or under the reflecting microscope. The reflectance values (Fig. 6:1) are inconclusive, overlapping those of smythite. The low nickel-iron monosulfide, containing 1.23%Ni is associated with nickel-rich pyrite. The structural formula of the low nickel-iron monosulfide is $M_{8.8}S_{11}$ compared to M_9S_{11} reported by Desborough and Czamanske (1973).

The breccia ore contains three varieties of pyrite; white euhedral, cobalt-rich pyrite (Plate 6A) (average of 3.06% cobalt) makes up to 2 to 3% of the sulfides. Resorbed, yellowish white pyrite containing only minor nickel and cobalt occurs in chalcopyrite (Plate 6B). Nickel-rich pyrite occurs in cracks along grain boundaries in pentlandite (Plate 8F) associated with marcasite (Plate 6C).

Table 6:2, Powder X-Ray Diffraction Pattern of Unnamed Fe, Ni Monosulfide

1		2		
d	I	d		I
		3.34	(vio)	10
2.99	100	2.99		90
2.81	80	2.85		70
		2.74	(vio)	50
2.56	70	2.56		70
2.47	30	2.46		40
2.25	20	n.d.		
2.21	20	n.d.		
2.15	30	2.14		30
2.01	30	2.03		30
1.98	80	1.99		70
1.92	20	1.92		10
1.73	80	1.73		100
		1.67	(vio)	40
1.56	20	1.57		20
1.50	30	n.d.		

1. compiled from Table 3, Desborough and Czamanske (1973) eliminating lines due to other minerals

2. $(Fe,Ni)_{8.8}S_{11}$ + violarite from the Thierry Mine taken using Cu radiation and Ni filter

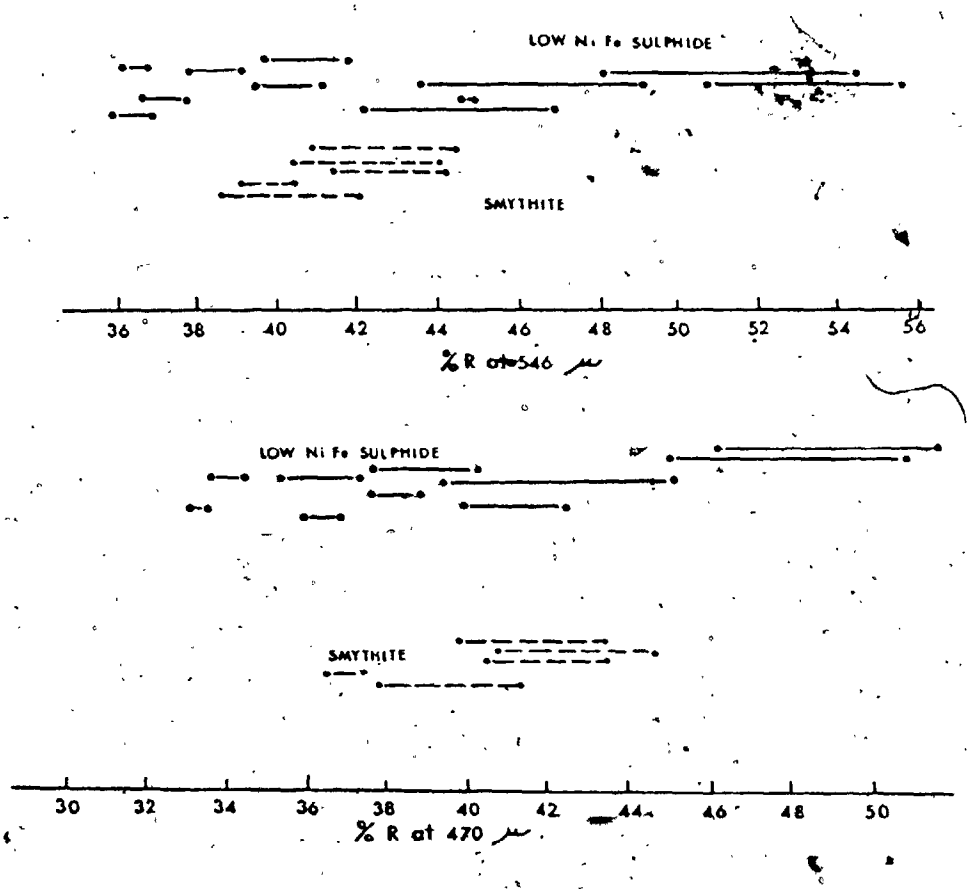

Fig. 6.1, Reflectance values for low Ni-Fe monosulfide compared to smythite, in sample of breccia ore from Thierry Mine.

Magnetite occurs as discrete grains with sharp grain boundaries within chalcopyrite, pyrrhotite and gangue. Several specimens show a symplectic intergrowth with chalcopyrite. Most of the magnetite occurs as porphyroblastic crystals up to 2cm in diameter (Plate 5C). These have a similar texture to snowball garnets (Spry, 1969).

Minor minerals that occur in the breccia ore are galena, moncheite-merenskyite, kotulskite, stuetzite, an unnamed Ag-Bi-telluride and valleriite. The Pd-Pt-Ag minerals are more fully described in Chapter 7.

6:2:2, Chlorite-Biotite Schist Ore

The sulfide mineralogy of the chlorite-biotite schist ore is very similar to that of the breccia ore. The sulfides occur molded around silicate fragments, penetrating rock fragments and crystal fragments, in pressure shadows and in stringers elongated parallel to the foliation. The sulfides tend to occur in biotite-rich layers in the chlorite-biotite schist. Ductile sulfides such as chalcopyrite and pyrrhotite tend to occur in fine veinlets and in pressure shadows to silicate fragments (Plate 4) whereas more competent sulfides such as cobalt-rich pyrite occur as euhedral grains. Magnetite occurs as euhedral porphyroblasts in sulfides and as broken and shattered fragments scattered through the matrix of the chlorite-biotite schist (Plate 5E & 5F).

Chalcopyrite shows deformation twins. Monoclinic pyrrhotite is polygonally recrystallized with deformation twins. Pentlandite with associated violarite alteration occurs as isolated grains and as exsolution blebs along grain boundaries in pyrrhotite. A nickel-rich pyrite (averaging 1.97% nickel) occurs as narrow crosscutting veins in pentlandite. The pentlandite contains an average of 26.6%Fe, 34.3%Ni (an atomic ratio of Fe/Ni of 0.75) and 0.94% Co. The associated violarite has 1.44% cobalt. Smythite and lamellar violarite occur in fractures in pyrrhotite. Rebsorbed pyrite occurs in chalcopyrite.

Table 6.3, Average Analyses of Sulfides from Thierry Mine Chlorite-Biotite Schist Ore

	NO. OF GRAINS	WEIGHT PERCENT AND ATOMIC RATIO S	Fe	Co	Ni	Cu	Zn	TOTAL	FORMULA
chalcopyrite	5	34.6	29.6	tr	n.a.	34.2	n.a.	98.4	$CuFeS_2$
		1.08	0.53	-	-	0.54	-		
m. pyrrhotite	15	40.4	58.7	0.12	0.75	-	-	99.97	$M_{6.76}S_8$
		1.26	1.05	0.002	0.013				
pyrite (Ni-rich)	3	53.5	45.5	0.14	1.97	-	-	101.11	$M_{1.01}S_2$
		1.68	0.914	0.002	0.034	-	-		
pyrite (Co-rich)	7	53.7	45.5	2.71	tr	-	-	100.91	$M_{1.02}S_2$
		1.68	0.814	0.046	-				
pentlandite	3	36.9	26.6	0.44	34.3	-	-	98.24	$M_{8.4}S_9$
		1.15	0.476	0.007	0.584				
violarite (in Pn)	5	39.9	27.2	1.44	27.2	-	-	95.74	$M_{3.12}S_4$
		1.246	0.487	0.024	0.497				
Sphalerite (Po+Py)	2	31.6	7.56	-	-	tr	60.4	99.56	$M_{1.05}S$
		0.99	0.13				0.92		

Minor amounts of sphalerite occur with emulsion textures in chalcopyrite. Associated with the sulfides are fluorite, quartz, barite seams up to 6cm thick and thausmanite ($CaSiO_3$:$CaCO_3$:$CaSO_4$15H_2O).

6:2:3, Bornite Ore

The bornite ore occurs in carbonate-feldspar veins and as disseminations in amphibolite schist. The schist occurs as large blocks in the mylonitized um-m rocks. The main sulfide minerals are chalcopyrite and bornite typically intergrown (Plate 7C & 7D) with associated copper-bismuth sulfosalts (wittichenite, Cu_3BiS_3 and emplectite $CuBiS_2$). Typically the sulfosalts show exsolution textures with bornite (Plate 7D). Linnaeite (carrollite) containing an average of 40% Ni and 10.3% Cu occurs as small inclusions in bornite with millerite. Native silver with acanthite and stuetzite occur as small grains (0.1mm) near the margins of chalcopyrite-bornite blebs. A grain of merenskyite was found associated with minor millerite and linnaeite (Plate 7C).

Table 6.4, Average Analyses of Sulfides from Thierry Mine, Bornite Ore

	NO OF ANALYSES	WEIGHT PERCENT AND ATOMIC RATIO S	Bi	Fe	Co	Ni	Cu	TOTAL	FORMULA
millerite	4	34.7 1.08	n.a.	1.44 0.026	5.40 0.092	58.3 0.99	1.69 0.027	101.51	$M_{1.03}S$
carrollite	3	38.5 1.02	n.a.	0.99 0.018	33.6 0.57	11.3 0.19	10.9 0.17	98.42	$M_{2.95}S_4$
bornite	2	25.2 0.79	n.a. -	14.1 0.25	n.d. -	n.d. -	60.8 0.96	100.1	$Cu_{4.86}Fe_{1.27}S_4$
chalcopyrite	2	35.3 1.10	n.a. -	30.7 0.53	n.d. -	n.d. -	33.6 0.55	99.6	$CuFeS_2$
wittichenite	1	19.2 0.60	43.2 0.21	n.d. -	n.a. -	n.a. -	38.4 0.60	100.8	$Cu_{2.9}BiS_{2.9}$
emplectite	1	19.2 0.60	61.0 0.29	n.d. -	n.a. -	n.a. -	19.4 0.31	99.6	$CuBiS_2$

6:2:4, Primary Disseminated Sulfides

Primary disseminated sulfides are rare in the Thierry Mine. The sulfides (chalcopyrite, pyrrhotite, pentlandite, bornite and cubanite) are intergrown with magnetite between olivine remnants (Plate 7F). Cubanite occurs as distinct lamellae in chalcopyrite (Plate 7E). In some samples chalcopyrite is intergrown with bornite (Plate 7B). Cobalt-rich pentlandite (9.13%Co) is exsolved with pyrrhotite as flames and pods. In one sample an emulsion texture occurs between pentlandite and chalcopyrite. The pentlandite is partly altered to mackinawite. The mackinawite contains 5.95%Ni and 1.82% cobalt.

Table 6.5, Average Analyses of Sulfides from Thierry Mine, Disseminated Ore

	NO OF GRAINS	WEIGHT PERCENT AND ATOMIC RATIO S	Fe	Co	Ni	Cu	TOTAL	FORMULA
chalcopyrite	2	34.6 1.081	30.6 0.534	-	-	33.9 0.548	99.1	$Cu_{0.99}Fe_{1.01}S_2$
bornite	3	26.9 0.840	14.8 0.265	tr -	- -	58.1 0.914	99.94	$Cu_{4.35}Fe_{1.26}S_4$
cubanite	3	35.4 1.105	40.1 0.719	- -	- -	24.8 0.391	100.3	$Cu_{1.0}Fe_{1.95}S_3$
pyrrhotite	3	36.6 1.143	62.6 1.12	- -	- -	- -	99.2	$M_{7.84}S_8$
pentlandite	3	32.6 1.019	27.5 0.492	9.13 0.155	29.8 0.507	1.55 0.024	100.21	$M_{9.2}S_8$

6:2:5, Altered Ore

i) Supergene Ore

A minor zone of supergene alteration is developed along fractures, faults and joints within the upper one metre of the ore body. This zone consists of malachite, native copper, chalcocite, pyrite, marcasite, chalcopyrite and hematite. The native copper occurs as dendritic coatings with hematite and malachite on joint surfaces. Chalcocite occurs as rims on chalcopyrite grains with spongy masses of pyrite and marcasite. Much of the pyrite contains a trellis-work of hematite alteration.

ii) Altered Breccia Ore

Associated with the supergene alteration is more penetrative alteration in the breccia ore near surface and in major faults. Three distinct assemblages developed. The first consists of vaesite, polydymite, pyrite, chalcopyrite and bornite. Vaesite occurs as distinct yellow-grey masses with weak anisotropism associated with white cobalt-rich pyrite (1.20%Co) and cobalt-nickel free pyrite intergrown with silicates. Polydymite has a composition of 10.3% Cu, 40% Ni and 7.34% Fe. It shows a strong development of octahedral shrinkage fractures implying that it is a product of pentlandite alteration. Bornite develops as rims on chalcopyrite and along shrinkage fractures in polydymite.

The second assemblage consists of millerite, polydymite, and chalcopyrite. Polydymite is very cobalt-rich containing an average of 12.8%Co. Millerite occurs as fine laths in chalcopyrite.

The third and most common assemblage consists of a deep violet, porous violarite with strongly developed octahedral shrinkage cracks (Plate 6E) and pyrite often intergrown with silicates and partly altered to hematite (Plate 6F). All gradations from a violarite-pyrite assemblage to the "fresh" pyrrhotite-pentlandite assemblage are present.

Table 6.6, Average Analyses of Sulfides from Thierry Mine, Altered Breccia Ore

	NO OF GRAINS	WEIGHT PERCENT AND ATOMIC RATIO							
		S	Fe	Co	Ni	Cu	Zn	TOTAL	FORMULA
millerite	3	35.0 1.09	0.24 0.018	0.69 0.012	60.6 1.03	0.24 0.004	n.d. -	97.52	$M_{1.04}S$
polydymite (Co)	4	41.8 1.305	8.24 0.148	12.8 0.217	34.4 0.586	tr -	n.d. -	97.24	$M_{2.91}S_4$
polydymite (Cu)	3	38.6 1.205	7.34 0.131	0.91 0.015	40.0 0.681	10.3 0.162	n.d.	97.15	$M_{3.28}S_4$
vaesite	2	51.2 1.588	0.16 0.003	0.52 0.009	48.4 0.824	n.d. -	n.d.	100.28	$M_{1.05}S_2$
pyrite (Co)	4	54.0 1.686	44.7 0.80	1.20 0.02	n.d. -	n.d. -	n.d. -	99.9	$M_{0.97}S_2$
bornite	2	26.2 0.916	6.40 0.114	n.d. -	n.d. -	64.8 1.02	n.d. -	97.4	$Cu_5Fe_{5.6}S_8$
chalcopyrite	2	34.3 1.09	29.6 0.54	n.d. -	n.d. -	36.0 0.576	n.d.	99.9	$Cu_{1.06}FeS_2$

6:3, Metamorphism of the Thierry Ore

The ores at the Thierry Mine have textures which show they have been modified by metamorphism. The breccia ore has strongly polygonally recrystallized pyrrhotite with pentlandite exsolved along the margins of the grains implying that the ore had been heated above 400°C to form monosulfide solid solution presumably during metamorphism (Craig and Kullerud, 1969). The chlorite-biotite schist, a mylonitized version of the breccia ore, commonly contains stringers of pyrrhotite, pentlandite and chalcopyrite, isolated grains of pentlandite and chalcopyrite-pyrrhotite in pressure shadows behind pyrite suggesting that dynamic metamorphism affected ore in which chalcopyrite, pyrite, pyrrhotite and pentlandite were separate phases. This occurred below 400°C, the lower temperature limit of monosulfide solid solution. The breccia ore has a highly variable Fe/Ni ratio (Kennedy, 1978) implying that deformation of the sulfides took place at temperatures when pyrrhotite and pentlandite were separate phases. There are fragments of the chlorite-biotite schist in the breccia ore which show strong deformation textures. Many of the magnetite porphyroblasts show a texture which suggest they have been rolled. Deformation twins in chalcopyrite and pyrrhotite are common.

The above textures suggest that the sulfides at Thierry have recorded two metamorphic events, one which homogenized the ore to monosulfide solid solution allowing pentlandite to exsolve along polygonally recrystallized pyrrhotite grain boundaries, and the second; a dynamic metamorphism, at a temperature below 400°C when pyrrhotite and pentlandite were separate phases. The inclusions of highly deformed chlorite-biotite schist suggest that the breccia ore may be the product of metamorphism of an original massive ore. Barrett et al (1977) suggested that most deposits in the Yilgarn Block, Australia which contain breccia and massive sulfides are the result of dynamic metamorphism of disseminated ores. All deposits in Yilgarn Block, Australia which contain massive breccia ore have been metamorphosed amphibolite grade or higher.

Chalcopyrite has moved into fracture systems in both the footwall and hangingwall rock, a feature common in dynamically metamorphosed ore deposits (Ross and Hopkin, 1975). The occurrence of bornite-rich ores associated with relatively undeformed blocks of amphibolite schist in the chlorite-biotite schist imply the movement of metals during metamorphism. The bornite commonly shows an exsolution texture with chalcopyrite. Brett (1964) stated that at temperatures above 350°C intermediate solid solutions of bornite-chalcopyrite exist.

6:4, Alteration of the Thierry Sulfide Ores

The near-surface Thierry ore shows many similarities to the sulfide ores in Australia which have undergone supergene alteration. The assemblages observed at Thierry and Kambalda, Australia are shown in Table 6:7. Nickel et al (1974) suggested reactions that involve the release of iron and nickel in solution. The nickel released from the violaritization of pentandite (reaction 1, Table 6:8) combines with smythite (reaction 2) to form an iron-rich violarite (reaction 3). Evidence for these reactions can be seen in the partially altered breccia ores. Flecks and lamellae of violarite form in pentlandite along cleavage and fractures. Smythite forms flames invading pyrrhotite with lamellar violarite forming along grain boundaries. Nickel et al (1974) suggested that smythite represents an intermediate alteration stage between pentlandite and violarite. Smythite has a composition similar to the iron end-member of the violarite series Fe_3S_4. Erd et al (1957) suggested that the crystal structure of smythite is related to the NiAs-type structure, thus smythite may develop readily from pyrrhotite with only minor reorganization of the pyrrhotite structure. Smythite can accommodate extra nickel atoms in a vacant NiAs layer hence its higher nickel content.

Table 6:7, Assemblages observed in Supergene, Metamorphosed and Serpentinized Fe-Ni-S Ores

I Kambalda Supergene Profiles, summarized from Watmuff (1974), Nickel et al (1974) and Keele and Nickel (1974)

Primary Ores:	Co-pyrite + monoclinic pyrrhotite + pentlanite
Transition Ores:	pentlandite altering to violarite pyrrhotite altering to smythite and violarite pyrrhotite altering to pyrite and marcasite
Supergene Ores	pyrite and violarite
Oxide Zones	hydrated ferric oxides, gaspeite, nickeloan- magnesite, bornite, digenite, covellite, pyrite.

II Assemblages interpreted as metamorphosed supergene minerals, summarized from Groves et al (1974) and Keele and Nickel (1974) at Kambalda; and Graterol and Naldrett (1971) at Marbridge, Quebec.

millerite + pyrite + violarite
vaesite + pyrite + violarite
millerite + pyrite + pentlandite

III Assemblage from serpentinized ores, summarized from Eckstrand (1975), Dumont serpentinite and Chamberlain (1967), Muskox intrusion, N.W.T.

awaruite $\pm$ heazlewoodite

heazlewoodite $\pm$ pentlandite

pentlandite $\pm$ heazlewoodite $\pm$ millerite

Table 6:8, Schematic Reactions Involving the Generation of Violarite

1. $Fe_4Ni_5S_8$ = $Fe_2Ni_4S_8$ + Ni^{+2} + $2Fe^{+2}$ + 5e
   Pentlandite — Violarite I

2. $(Fe,Ni)_7S_8$ = $(Fe,Ni)_9S_{11}$ + Fe^{+2} + $(Fe,Ni)_8S_{11}$ + Fe^{+2}
   Pyrrhotite — Low Ni Fe Monosulfide — Smythite

3. $(Fe,Ni)_8S_{11}$ + Ni^{+2} = $Fe_3Ni_3S_8$
   Smythite — Lamellar Violarite

4. $(Fe,Ni,Co)_3S_4$ = Fe^{+2} + $2(Fe,Ni)S_2$ + $(Ni,Fe,Co)_3S_4$
   Violarite I — Ni Pyrite — Violarite III

5. $(Ni,Fe,Co)_3S_4$ = Fe^{+2} + $(Ni,Fe)S_2$ + $(Fe,Co)S_2$ + $(Ni,Co,Fe)_3S_4$
   Violarite III — Vaesite — Co Pyrite + Violarite IV

6. $(Fe,Ni,Cu)_3S_4$ = Fe^{+2} + NiS + $(Ni,Cu,Fe)_3S_4$
   Violarite II — Millerite — Violarite V

Taylor and Williams (1972) stated that smythite and greigite are not polymorphic and conversion from a NiAs-type structure to thiospinel structure involves considerable reorganization. As smythite is not stable above 75°C (Craig and Scott, 1974) and the generation of smythite is related to violaritization, it implies that violarite formation took place at low temperature related to percolating meteoric waters. The low nickel-iron monsulfide may be an intermediate stage between smythite and monoclinic pyrrhotite. Misra and Fleet (1974) stated that the compositional field of smythite overlaps that of the low nickel-iron monosulfide and suggested that it is a type of smythite.

If this type of process were to continue, some of the nickel and iron may be further released from violarite after pentlandite producing nickel-rich pyrite and nickel-rich violarite (reaction 4). A further breakdown of this violarite would produce vaesite, a cobalt-rich pyrite and a nickel-cobalt rich violarite (reaction 5). The breakdown of lamellar violarite would produce millerite and a nickel-copper violarite. It is possible that the copper-rich violarite may break down further. Vokes (1967) reported bornite replacing polydymite along fractures. One specimen of oxidized breccia ore contained bornite forming along shrinkage fractures in violarite.

Much of the pyrite associated with the nickel-rich violarite and millerite is altered to hematite. Many of the faults and joints contain magnetite seams up to 3cm thick. These suggest that much of the iron removed during the formation of violarite has been converted to oxides.

The group of minerals smythite, pyrrhotite, pentlandite and violarite occurs throughout the deposit (as deep as 500m). This group is typical of the transition zone of the Australian deposits occurring to a depth of only 100 metres. At the Thierry Mine the presence of many faults and shear systems has allowed access of fluid to much deeper levels than would normally be expected. According to Nickel (1957), violarite can form on fresh pentlandite in drill core in as short a time as two months.

6:5, Low Temperature Assemblages and Equilibrium

In dealing with low-temperature assemblages in the nickel-iron-sulfur system there are problems in determining what equilibrium assemblages exist in natural rocks. Hyndman (1972) lists criteria that imply equilibrium has been achieved in metamorphic rocks.

1. Coexisting minerals show no textural indication of disequilibrium such as rims on grains or relict cores. Without exception violarite at the Thierry Mine occurs armouring pentlandite from a contact with pyrrhotite or smythite. This is similar to the descriptions of violarite from Kambalda (Groves et al (1974)); Whistle and Discovery sites, Sudbury (Arnold and Malik (1974)); Fort Lick, Virginia (Craig and Higgins, 1975) and various other localities (Misra and Fleet, 1974, Nickel et al, 1974). This implies that the assemblage pyrrhotite (or smythite), violarite and pentlandite are not compatible and it is questionable to imply equilibrium among these phases.

2. Minerals having the same composition and structure form at the same grade from rocks of the same bulk composition.

In the samples of breccia ore there are four types of pyrite, generated at different times during the formation and modification of the ores. From textural and chemical evidence, the Ni-rich pyrite is part of the violaritization process forming along shrinkage fractures in violarite. The Co-rich pyrite appears to be a higher temperature mineral. The initial partitioning of cobalt between pyrite and residual monosulfide is strongly in favour of pyrite (Ewer and Hudson, 1972). After the formation of pentlandite and pyrrhotite, the amount of cobalt and nickel available to pyrite would be low at low temperature the pyrite generated would contain minor nickel and cobalt. This suggests that the resorbed pyrite is a lower temperature mineral than the high-Co-pyrite.

This means that any sample containing more than one of these pyrites is incompatible and equilibrium cannot be assumed. A similar argument can be applied to the two forms of violarite present in some section. The lamellar violarite after pyrrhotite and violarite after pentlandite are compositionally distinct. If both forms are present in the section the assemblage should be considered metastable.

In applying experimental work on sulfides to natural systems, it is often assumed that the sulfides act as a closed system with respect to the silicates. This is clearly not true during the serpentinization process. Iron and nickel released from silicates may react with sulfides which have been affected by serpentinization such as Dumont, Quebec (Eckstrand, 1975) and Muskox (Chamberlain, 1967). The assemblages typically contain minerals such as native copper, nickel-iron alloys and heazlewoodite which are sulfur-poor and metal-rich. Serpentinization tends to increase the Ni:Fe ratio of sulfide bulk composition.

During the oxidation process, iron and to a much lesser extent nickel is lost from the sulfide bulk as oxides. This moves the composition away from the iron corner of the Ni-Fe-S triangle. In some cases the removal of iron so increases the cobalt content of the system particularly in violarite and pyrite, that one must consider the minerals in Ni-Fe-Co-S space. Considering these problems, the only assemblages that are clearly compatible at the Thierry Mine are

millerite + violarite
monoclinic pyrrhotite + pentlandite + pyrite
monoclinic pyrrhotite + pentlandite
violarite + pyrite
violarite + vaesite + pyrite

and possibly (since violarite is replacing pentlandite)

pyrite + pentlandite + violarite

6:6, Stability of Low Temperature Assemblages in the Ni-Fe-S System

Pyrite-pentlandite (Fig. 6:2) is thought to be a stable low-temperature assemblage (Graterol and Naldrett, 1971; Misra and Fleet, 1974). The coexistance of violarite and pyrrhotite with or without smythite must be metastable. The problem with applying experimental work is the experimental work was done in the system Fe-Ni-S while the natural system is Fe-Ni-S-O. The stability of pyrite vs pyrrhotite with magnetite is controlled by the amount of oxygen in the system. Oxidation of the original pyrrhotite-pyrite-pentlandite assemblage has permitted the bulk composition of the sulfide assemblage to migrate from the iron corner of the Fe-Ni-S system such that pyrite-pentlandite-violarite and violarite-pyrite stability field are reached.

The assemblage millerite-pyrite-magnetite-violarite reported at Black Swan (Groves et al, 1974) and Marbridge (Graterol and Naldrett, 1971) can be explained by the metamorphism of a supergene altered pyrite-violarite assemblage. Kullerud (1969) has shown that thiospinels in general break down on metamorphism to a NiAs-type and a pyrite-type structure

$Fe_3S_4 = 2Fe_{(1-x)}S + FeS_2$ at 100°C

$Ni_3S_4 = 2NiS + NiS_2$ at 340°C

$Co_3S_4 = 2CoS + CoS_2$ at 600°C

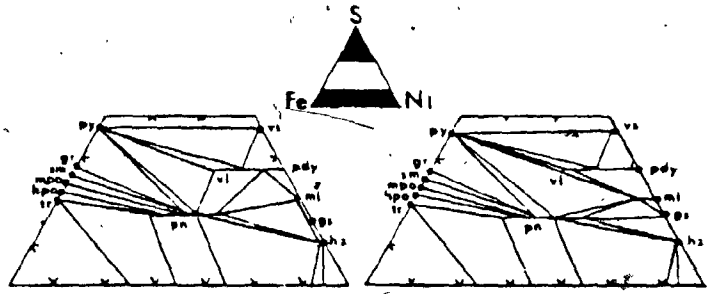

Fig.6.2, Schematic interpretations of low-temperature relations in the system Fe-Ni-S. (after Craig(1974))

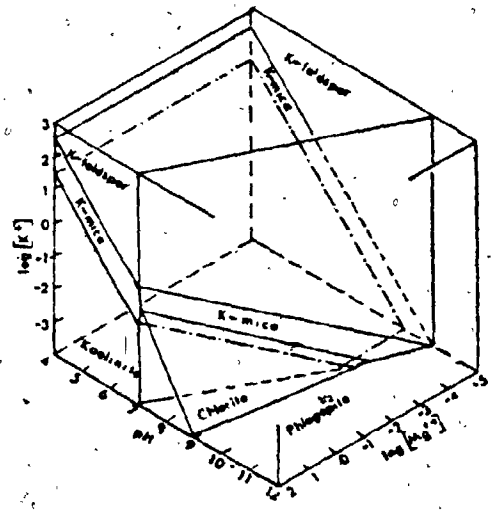

Fig.6.2B, Low Temperature relations in system K_2O- MgO-Al_2O_3-SiO_2 at 1000 bars total pressure in the presence of quartz, after Richter and Hemley (1959)

The Co-rich violarite reported from Black Swan and Marbridge is texturally very different from the violarite formed by supergene alteration. They are unpitted, have a high reflectance and take a good polish, (Groves et al, 1974). Misra and Fleet (1974) have shown that violarite forms a solid solution from the nickel to cobalt members and naturally occurring iron-rich violarite usually contains only minor cobalt. Consider the metamorphism of a violarite

$$(Fe,Ni,Co)_3S_4 = FeS_2 + 2NiS + (Ni,Co,Fe)_3S_4$$

The violarite is now a cobalt-rich phase and is in effect removed from the Fe-Ni-S system. Millerite and pyrite could remain stable to lower temperatures. This pair appears to resist the violaritization process, although P. Morton (1978) has reported the generation of Fe-Ni rich violarites at Shebandowan.

Millerite could be generated by supergene processes directly by moving the bulk composition of the system into the millerite stability field. Examples of this were reported at Black Swan by Groves et al (1974) associated with supergene violarite.

The secondary mineral assemblages from Thierry Mine are plotted in Fig. 6:3. Cobalt has been apportioned between Fe and Ni in violarite (Misra and Fleet (1974)). The amount of cobalt in violarite formed from pentlandite is markedly higher than that formed from pyrrhotite. The iron content is also related to the initial phase. Violarite after pentlandite contains 25.9% and violarite after pyrrhotite contains 28%Fe. This has been noted in the Ni-Fe ores at Kambalda, Australia (Ewers and Hudson 1972). On this basis the low temperature assemblages suggested by Misra and Fleet (1974) explain the compatible assemblage at the Thierry Mine.

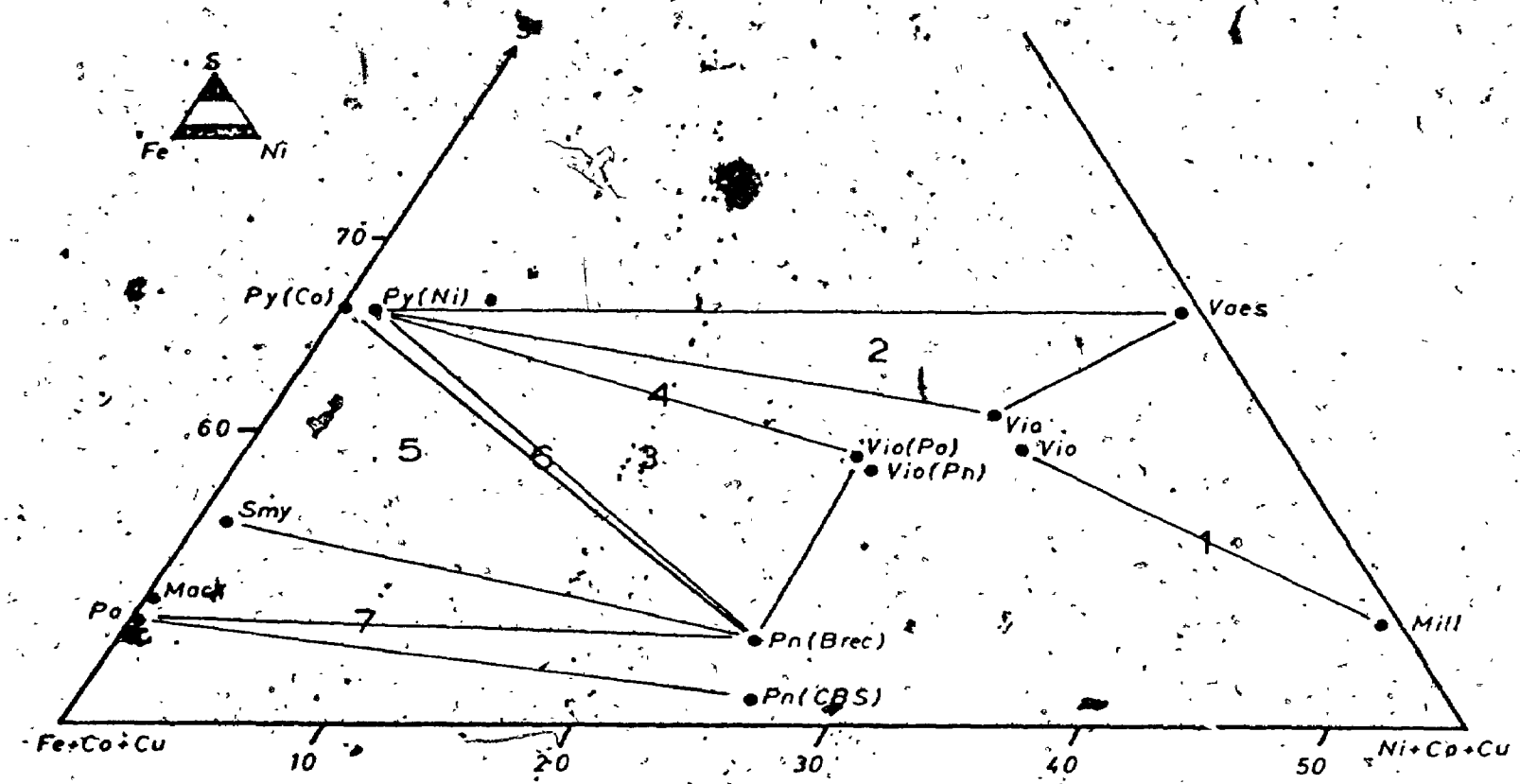

Fig. 6:3, Portion of the system Ni-Fe-S with mineral assemblages present at the Thierry Mine plotted from electron-microprobe data. Co-Cu are equally divided between Ni and Fe sites.

6:7, Sulfide Mineralogy in the Ultramafic and Mafic Bodies of the Kapkichi Lake Area

6:7:1 J+I Ultramafic and Mafic Body

There are four types of sulfide occurrences in the J+I ultramafic body; primary disseminated sulfides, metamorphosed disseminated sulfides, breccia sulfides and oxidized sulfides (Table 6:9).

1. Primary disseminated sulfides occur between olivine crystals or serpentine-talc pseudomorphs after olivine. In some specimens the amount of sulfide becomes high enough (greater than 5%) to form a net texture. The predominant sulfide assemblage is chalcopyrite (50%), pyrrhotite (30%) with exsolved pentlandite (20%) intergrown with magnetite and ilmenite. The pentlandite is generally very fresh with only minor alteration to violarite and mackinawite. Rare lamellae of cubanite up to 0.2mm thick occur in chalcopyrite. Pyrite occurs as rare partially resorbed masses in pyrrhotite.

One specimen with the assemblage chalcopyrite with exsolved bornite, pyrite and magnetite occurs in a very olivine-rich ultramafic rock.

Table 6:9, Sulfide Assemblages in the J+I um-m Body
(Symbols Appendix B Table 1)

1. Primary disseminated sulfides
   cpy + po.pn. +mag
   cpy.cub. +po.pn. +mag
   cpy.bn. +py +mag
   altered assemblage
   cpy (mack) +po(py).pn(vio).

2. Metamorphosed disseminated sulfides
   cpy +po.pn. +mag ± sph.cpy.
   cpy.cub. +po.pn. +mag
   altered assemblage
   cpy(mack) +po(py).pn(vio).
   cpy +py +vio
   cpy +py(hem) +vio

3. Breccia ore
   cpy +po.pn +mag
   altered assemblage
   cpy(mac) +po(py).pn(vio). +mag

4. Oxidized ore
   cpy(mack) +po(py).pn(vio).
   cpy +py +vio
   cpy +py(hem) +vio

2. Metamorphosed disseminated sulfides

Sulfides occur as wedge-shaped disseminated aggregates up to 2mm across between silicate minerals tremolite, anthophyllite, chlorite and olivine. Some sulfides occur as fine dissemination in cleavages of silicate minerals. The mineralogy and assemblages are identical to the primary disseminated sulfide (Table 6:9). Several specimens contain sphalerite in emulsion texture with chalcopyrite. The above textures are interpreted to have resulted from recrystallization and slight remobilization of primary sulfide during metamorphism.

3. Breccia sulfides

The breccia sulfides occur as narrow zones of sulfide with angular fragments of um-m host rock. One sulfide intersection grades from breccia to net-textured and disseminated sulfides over a distance of one metre. The sulfide assemblages are identical to those in the primary disseminated sulfide except that the proportions are pyrrhotite 50%, pentlandite 25% and chalcopyrite 25%.

4. Oxidized sulfides

Minor zones of oxidized sulfide occur near faults and at the top of the ultramafic body. The development of violarite after pentlandite and pyrite after pyrrhotite is pronounced, and similar to that observed at the Thierry Mine. Hematite develops as a complex trellis work in pyrite.

6:7:2, G Zone Ultramafic and Mafic Body

There are three types of sulfide association in the G zone um-m body; primary disseminated sulfide; metamorphosed disseminated sulfide and oxide-layer sulfides (Table 6:10). The primary and metamorphic disseminated sulfides are identical to those in the J+I ultramafic body. Sulfides occur in an oxide layer consisting of ilmenomagnetite, ilmenite and gahnite (Plate 5A, 5B). Chalcopyrite and bornite are intergrown and associated with pyrite and bornite are intergrown and associated with cobalt-rich pentlandite (Plate 7B). Pentlandite shows a complex emulsion texture with chalcopyrite. Mackinawite commonly occurs as an alteration of the pentlandite. All sulfides are intergrown with radiating masses of graphite.

Table 6:10 Sulfide Assemblages in G Um-m and K1:1 Um-m Body (Symbols in Appendis B, Table 1)

G Um-m Body

1. Primary disseminated sulfide & metamorphosed disseminated sulfides
   - cpy +po.pn.+mag
   - cpy.cub. +po.pn. +mag

   altered
   - cpy(mac) +po.pn(vio). +mag
   - cpy+py +vio +mag

2. Oxide layer sulfides
   - cpy +po.pn. +mag
   - cpy.bn. +pn +graphite +mag

K1:1 Um-m Body

1. Metamorphosed disseminated sulfides
   - cpy +po.pn. +mag
   - cpy. +po.pn. +py +mag

2. Breccia Ore
   - po.pn. +cpy +mag ± pyrite

6:7:3, K1:1 Ultramafic and Mafic Body

There are three types of sulfide associations in the K1:1 um-m body; metamorphic dissemination, dissemination in biotite-schist and breccia sulfide making up 40%, 50% and 10% respectively of the sulfides.

Metamorphic disseminations occur as wedge-shaped masses up to 2mm across in metagabbro and mafic metagabbro. The main assemblage is chalcopyrite and pyrite. The sulfides associated with the biotite schist occur as stringers and lenses elongated parallel to the foliation. The breccia sulfides are composed predominantly of pyrrhotite and pentlandite forming a matrix around angular fragments of um-m rocks. Chalcopyrite occurs as veins in the ultramafic rock fragments and near the margins of the fragments. Minor violarite alteration occurs in the pentlandite.

6:8, Comparison of Sulfides from the Kapkichi Lake Mafic and Ultramafic Bodies, and the Thierry Mine

The Kapkichi Lake um-m rocks contain sulfides which have been metamorphosed without major shearing. There appears to be only local remobilization of the sulfides during the growth of metamorphic silicates. Only in the Kl:1 um-m body are the sulfides deformed. On the other hand the Thierry Mine sulfides have recorded two periods of metamorphism, one regional amphibolite grade metamorphism and a second strong dynamic metamorphism which has strongly remobilized the ore. The sulfides in the Kapkichi um-m rocks show only minor supergene-type alteration (violaritization and oxidation of sulfides) near major faults and surface. The Thierry Mine sulfides show extensive supergene alteration which resulted from oxidation by access of ground water along numerous faults.

6:9, Conclusions

1. The primary sulfide assemblages observed as intercumulus sulfides in altered dunites are;

chalcopyrite + pyrrhotite + pyrite + pentlandite
chalcopyrite + pyrrhotite + pentlandite

2. The Thierry deposit has suffered supergene alteration by the removal of iron through oxidation of primary sulfide assemblages. The apparently compatible assemblages observed are:

pyrite + violarite + magnetite
millerite + violarite + magnetite
pyrite + violarite + vaesite + magnetite

and the probably incompatible assemblage.

pyrrhotite + smythite + pentlandite + violarite + magnetite

The iron removed from the sulfides formed magnetite and minor hematite. The supergene process effectively moved the bulk composition of the sulfides in the Fe-Ni-S system away from the iron corner producing nickel-and-sulfur-rich sulfide compositions.

3. The compatible assemblages observed at the Thierry Mine are best explained by Misra and Fleet's (1974), interpretation of the Fe-Ni-S system at low temperature (Fig. 6:3).

The alternate interpretation suggested by Naldrett and Graterol (1971) may be explained by the metamorphism of violarite-bearing assemblages producing the assemblages millerite-pyrite-Co-rich-violarite similar to those observed at Black Swan and the Marbridge deposit. The Co-rich-violarite generated during metamorphism is prevented from reequilibrating with pyrite and millerite by the presence of cobalt.

4. The sulfides at the Thierry Mine have been modified by two periods of metamorphism. The first, amphibolite grade regional metamorphism, recrystallized the sulfides to polygonal masses with pentlandite exsolved around the margins of pyrrhotite polygonal crystals. The second, a cataclastic event at greenschist grade, mylonitized the breccia ore producing isolated bands of pyrrhotite, chalcopyrite and pentlandite with sulfides commonly occupying pressure shadows behind amphibolite fragments. The bornite ore, occurring in amphibolite schist often included as large blocks in the mylonite zone, is likely due to the mobilization of metals during the cataclastic event.

5. Comparison of the sulfides occurring in the other Kapkichi um-m bodies shows they have been metamorphosed without major shearing. In addition only minor supergene-type alteration is present near major faults and shears.

7:0, Platinum-Group Elements, Silver and Gold at the Thierry Mine

7:1, Introduction

Two distinct associations of precious metals minerals have been found in the Thierry Mine.

1. In the breccia ore, the precious metal minerals; merenskyite, moncheite, stuetzite and Ag_3BiTe_3 occur with chalcopyrite, pyrrhotite, pentlandite, pyrite and violarite.

2. In the bornite ore, the precious-metal minerals, native silver, acanthite, stuetzite and merenskyite are associated with chalcopyrite, bornite and copper bismuth sulfosalts.

The electron microprobe analyses of the precious metal minerals are listed in Table 7.1.

Table 7.1, Electron Microprobe Analyses of Precious Metal Minerals from Thierry Mine

	NO OF ANALYSES	WEIGHT PERCENT AND ATOMIC RATIO S	Te	Bi	Ag	Au	Pd	Pt	Ni	Fe	TOTAL
moncheite	11	n.d.	55.4	7.38	n.d.	n.d.	11.6	22.8	0.93	0.22	98.33
$M_{1.08}(Te,Bi)_2$		-	0.43	0.035	-	-	0.109	0.117	0.016	0.002	
merenskyite[1]	2	n.a.	60.1	8.01	2.12	n.d.	26.0	3.80	n.d.	n.d.	100.03
$M_{1.12}(Te,Bi)_2$		-	0.47	0.038	0.02	-	0.249	0.019	-	-	
merenskyite[2]	1	n.a.	61.1	6.38	9.53	n.d.	16.9	3.52	n.d.	n.d.	97.48
$M_{1.02}(Te,Bi)_2$		-	0.48	0.031	0.088	-	0.155	0.018	-	-	
kotulskite	1	n.a.	53.5	1.80	n.d.	n.d.	44.3	2.31	n.d.	n.d.	101.9
$M_{0.99}(Te,Bi)$		-	0.42	0.009	-	-	0.41	0.012	-	-	
stuetzite[3]	5	n.a.	39.7	tr	56.8	1.54	0.75	0.38	n.d.	n.d.	99.17
$M_{3.29}Te_3$		-	0.31	-	0.53	0.008	0.007	0.002	-	-	
unknown	2	n.a.	33.0	25.7	40.1	n.a.	n.d.	n.d.	0.57	n.d.	99.37
Ag_3BiTe_2		-	0.26	0.13	0.37	-	-	-	0.01	-	
acanthite[4]	1	13.4	n.d.	tr	8.70	n.d.	n.a.	n.a.	n.a.	n.a.	100.7
$Ag_{1.99}S$		0.42	-	-	0.81	-	-	-	-		
native silver	1	n.d.	n.d.	n.d.	97.8	2.1	n.a.	n.a.	n.a.	n.a.	99.1
(Ag,Au)		-	-	-	0.91	0.11	-	-	-	-	

1. exsolved with kotulskite
2. exsolved with stuetzite
3. high std. dev.
4. 0.30% Cu

7:2, Mineralogy

Moncheite occurs as grains up to 0.5mm in diameter. In air, it is grey-white against chalcopyrite and strongly anisotropic (brown to yellow brown). All observed grains contain stuetzite as very fine lamellae and blebs along grain boundaries (Plate 10). The grains of moncheite are included in chalcopyrite and pentlandite. The chemical formula on the basis of eleven analyses is $Pt_{0.54}$ $Pd_{0.51}$ $(Te,Bi)_{2.0}$.

Merenskyite (Plate 10E) is white against chalcopyrite in air and strongly anisotropic (brown to green brown). Many of the grains contain stuetzite similar to merenskyite and Ag tellurides described by Cabri and Pickwick (1976) from the Stillwater complex. The high silver values in Thierry merenskyite (up to 9.53%) may be due to fine lamellae of silver tellurides. The grains are commonly lensoid and associated with pentlandite and pyrrhotite. The chemical formula is $Pd_{1.06}Pt_{.04}Ag_{.02}(Te,Bi)_2$ based on 3 microprobe analyses.

Kotulskite occurs as lamellae from 10 to 100um wide in merenskyite. The kotulskite is creamy white, anisotropic (grey to dark grey in air), and contains only minor platinum and bismuth.

Stuetzite appears grey in contact with calcopyrite and weakly antisotropic (brown to yellow in air). Stuetzite occurs as lamellae in merenskyite and moncheite in breccia ore and as discrete grains with native silver in bornite ore. The chemical formula is $M_{5.29}Te_3$ based on 5 electron microprobe analyses and it contains up to 4.12%Au. This is more metal-rich than those reported by Cabri et al (1977), possibly due to standards used in the electron microprobe analyses of the Thierry ores.

Ag_3BiTe_2 occurs in one sample as intergrowths with stuetzite and merenskyite in breccia ore. It is dark grey and anistropic from grey to orange brown in air. (Plate 10D)

Native silver is associated with acanthite and stuetzite in bornite ore as irregular grains up to 0.2mm in diameter. The silver contains 2.1%Au. Acanthite occurs as rims on the native silver.

7.3, Distribution of Precious Metals in the Thierry Mine

Analyses for precious metals were made by X-ray Assay Labs on a wide variety of ore types (Table 7:2). The composite analyses on the mill feed are shown in Table 7:3. These were made by analyzing the crushed ore collected from the crushed ore feed at one hour intervals over a one-month period. In addition several of the samples (Table 7:3) were passed through heavy liquids and a magnetic separator to produce purified chalcopyrite, pyrrhotite-pentlandite and magnetite fractions (Lefebvre, 1977). The purity of each fraction was checked by x-ray diffraction.

3

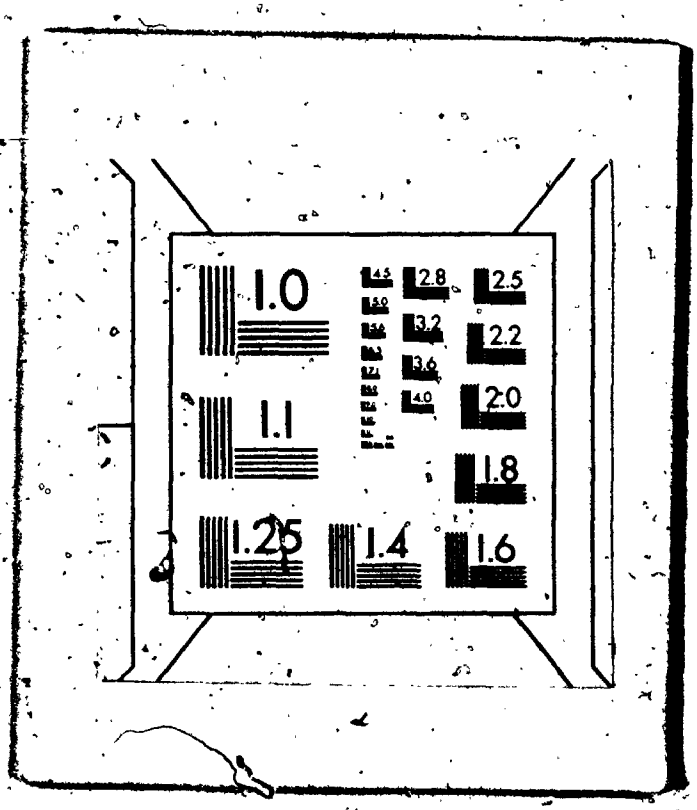

Table 7.2. Precious Metal Analyses ,Thierry Mine

	Cu%	Ni%	Au oz/ton	Ag oz/ton	Pt oz/ton	Pd oz/ton
1	0.48	2.97		0.24	0.030	0.070
2	1.70	0.58	0.030	0.36	0.010	0:070
3	0.51	4.04		0.20	0.040	0.030
4	0.45	0.13		0.20	0.030	0.010
5	19.40	0.05	0.020	3.37	0.005	0.005
6	2.70	0.39	0.010	0.20	0.008	0.012
7	6.16	0.65	0.014	1.32	0.064	0.120
8	3.96	0.10	0.017	0.22	0.012	0.018
9	0.02	4.20	0.250	0.10	0.298	0.327
10	2.40	0.48	0.020	0.36	0.15	0.045
11	5.01	0.29	0.008	0.34	0.005	0.009

	12	13	14	15	16	17
Fe%	57.20	30.50	31.67	71.10	56.50	32.78
Cu%	0.56	33.53	33.10	0.20	0.41	32.86
Ni%	1.44	0.08	0.11	0.07	1.28	0.46
S %	34.70	34.50	35.26	0.24	28.59	33.88
Total	93.90	98.61	100.14	71.61	86.78	99.98

Mineralogy Composition Based on Average Composition

Cpy	1.13	97.15	95.8	0.58	0.77	95.22
Po	81.76	1.13	4.03	—	68.3	0.33
Pn	2.44	0.20	0.23	0.20	2.25	1.29
Mt	1.44	0.49	0.29	99.48	22.70	4.89

Precious Metals Oz/ton

Pt	0.013	0.020	0.006	0.005	0.036	0.003
Pd	0.096	0.038	0.112	tr	0.059	0.006
Au	0.005	tr	0.008	tr	0.006	0.019
Ag	0.330	3.860	3.83	tr	tr	4.432

1. Breccia ore in ultramafic rocks, 600-102E-15°NW depth 320'
2. Chalcopyrite rich veins in amphibolite 400 level section 101E
3. Breccia ore, 600-102E-55° depth 297'
4. Breccia ore, 600-102E-55 depth 376'
5. Chalcopyrite rich vein with epidote-feldspar, 1200 level drift 116 z south wall
6. Sulfides in silicified amphibolite, 1200 level 117E
7. Breccia ore, 600 level 10950N
8. Breccia ore, 600 level 10885N
9. Pyrrhotite rich breccia ore, open pit bench 85
10. Chlorite-biotite schist, open pit bench 60
11. Breccia ore, open pit bench 85, amphbolite fragments in chalcopyrite pyrrhotite matrix
12. Pyrrhotite fraction of breccia ore, west open pit, 1st bench
13. Chalcopyrite fraction of breccia ore, west open pit, 1st bench
14. Breccia ore (12 +13) west open pit, 1st bench, cpy rich
15. Magnetite veins in ultramafic, 500 level hanging wall drift
16. Pyrrhotite rich [illegible]ccia, west pit, bench 85
17. Chalcopyrite in [illegible]dote vein in massive amphibolite, east pit, lower bench

Table 7:3, Metal Analyses of Composite Pulp and Mill Feed, Thierry Mine

	Au oz/ton	Ag oz/ton	Pt oz/ton	Pd oz/ton	Cu%	Ni%
Oct/76	0.005	0.19	0.007	0.017	1.02	0.125
Nov/76	0.0042	0.198	0.005	0.013	1.10	0.134
Jan/77	0.0052	0.24	0.005	0.016	1.28	0.155
Feb/77	0.0042	0.203	0.005	0.016	1.17	0.150
Mar/77	0.0062	0.191	0.004	0.013	1.11	0.136
April/77	0.0040	0.194	0.006	0.016	1.05	0.152
May/77	0.0040	0.211	0.005	0.014	1.30	0.188
June/77	0.0045	0.226	0.005	0.014	1.31	0.171
July/77	0.0035	0.200	0.005	0.013	1.23	0.185
Sept/77	0.0050	0.310	0.006	0.021	1.48	0.139
Average	0.0046	0.216	0.005	0.015	1.21	0.154

The strongest positive correlation of metals is between silver and copper (Fig. 7:2). The least-square line has a correlation coefficient of 0.82 (note that the very high silver values were not included in this calculation because it would produce a "two-point" line). There is a corresponding negative correlation between silver and nickel (Fig. 7:1) at values greater than 0.5%Ni. The weak trend on Fig. 7:3 is also a reflection of this. The points plotting near the silver apex are copper-rich whereas those plotting near the Pt-Pd base are nickel-rich.

There is no significant correlation between Cu and Pd or Ni and Pt. There is a weak tendency for the Pd/Pt ratio to increase in the copper-rich ores relative to nickel-rich ore (Fig. 7:3).

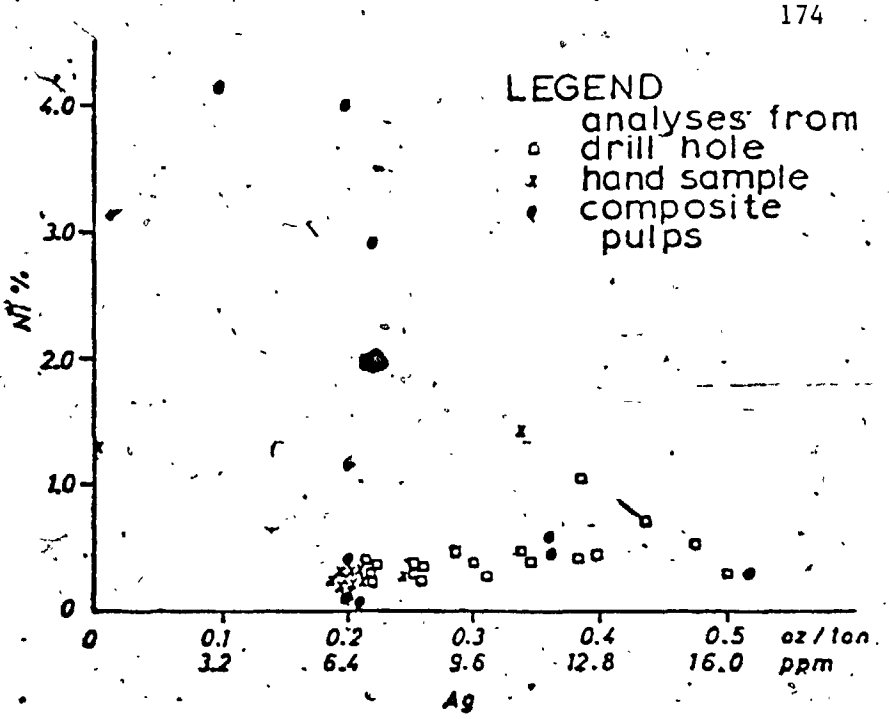

Fig. 7.1, Plot of Ag vs Ni concentrations from samples in Table 7.2 from Thierry Mine

Fig. 7.2, Plot of Ag vs Cu values from samples in Table 7.2 from Thierry Mine.

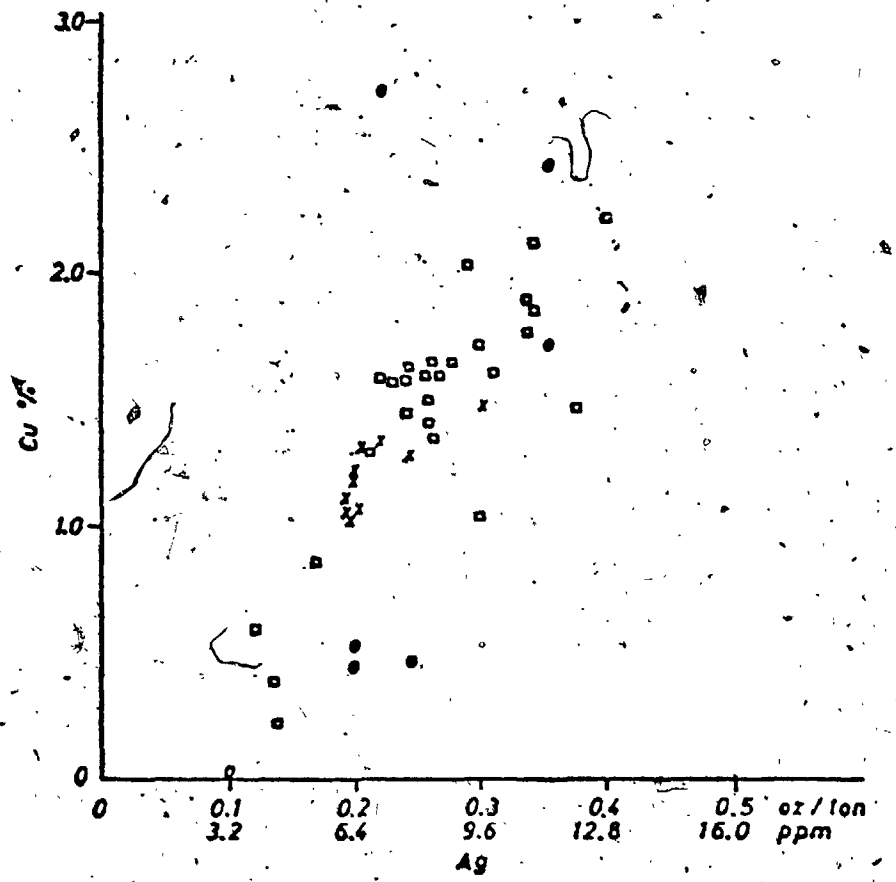

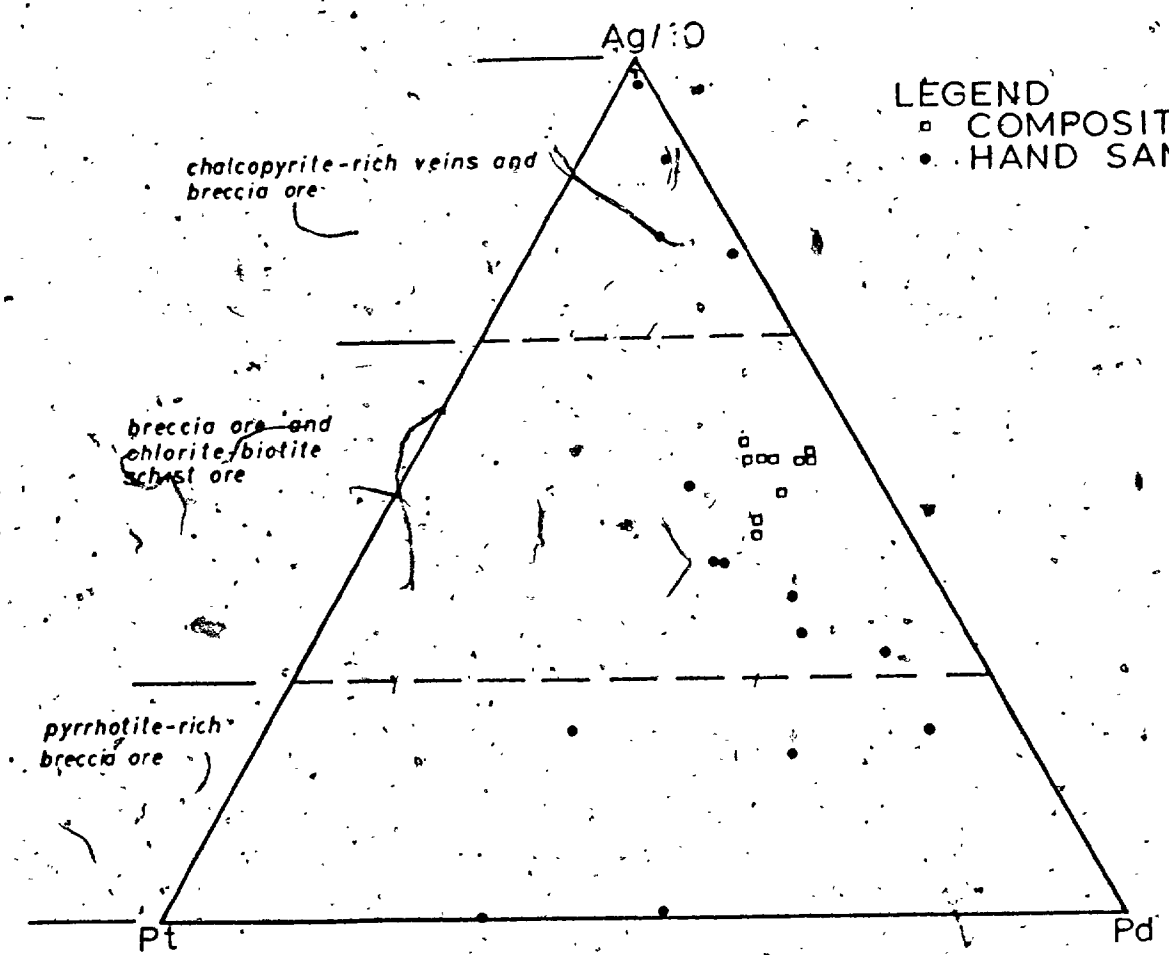

Fig. 7:3, Ag/10-Pt-Pd plot for samples from Thierry Mine.

7.4, Conclusions

The precious metal minerals observed at the Thierry Mine are primarily bismuth tellurides. According to Kingston (1966) tellurium tends to form distinct minerals when present even in low concentrations due to its very different atomic size and electronegativity compared to sulfur. Pshenichnii (1961) has shown that tellurium and bismuth tend to be concentrated in the later stages of sulfide liquid crystallization. Skinner et al (1976) state that PGE would be enriched in an immiscible sulfide liquid relative to silicate liquid and that pyrrhotite crystallization would cause Pt-Pd to be enriched in the remaining sulfide liquid which is usually copper-rich. This implies that from a theoretical point of view chalcopyrite and Pd tellurides would occur together.

From field evidence at Noril'sk and Sudbury, Cousins and Vermaak (1976) showed a general tendency for progressive enrichment of Pd relative to Pt with the amount of chalcopyrite in sulfide ore. This is confirmed by Keays and Crocket (1970) who found Pd and Au were enriched in magmatic chalcopyrite at Sudbury.

In hydrothermal systems Ag,Te,Cu and Pd tend to be more mobile than Au,Ni and Pt. Mihalik et al (1974) found high Ag,Te and Pd/Pt ratios in hydrothermal deposits at Messina, S.A. Similarly McCallum et al (1976) have shown at the New Rambler deposit, Wyoming that Pd is greatly enriched in the sheared and hydrothermal ores.

At Thierry the high mobility of Pd is compatible with the high Pd/Pt ratio in the bornite ore (which is interpreted to have been mobilized into amphibolite schist during the cataclastic metamorphism) and in chalcopyrite-rich ores in fissures in footwall and hangingwall amphibolite schist. The tendency for Pd to occur in chalcopyrite-rich breccia ore may be a metamorphic effect or the tendency of Pd enrichment late in the paragenetic sequence.

8:0, Discussion, Summary, Conclusions

8:1, Geochemistry of the Ore at the Thierry Mine

Wilson and Anderson (1959), and Naldrett and Cabri (1976) have noted that the Cu to Cu+Ni ratio for magmatic deposits associated with ultramafic rocks varies as a function of the MgO content of the initial magma. This is due to the difference between the partition coefficient between a magma precipitating olivine and a magma precipitating clinopyroxene or the generation of a magma through different degrees of partial melting. A magma with high MgO content contains a large amount of nickel and produces olivine-rich cumulates whereas a low magnesian magma contains lesser nickel relative to copper and produces pyroxene-rich cumulates. The Cu/(Cu+Ni) ratio in the Thierry Mine ore is 0.9 and the average MgO content of the mafic rocks is 15% (Chapter 3) as shown in Fig. 8:1. The diagram of Pt/(Pt+Pd) vs Cu/(Cu+Ni) (Fig.8:2) is also shown with the average, unusual composition of the Thierry Mine ore. The tenor of the sulfide ore at the Thierry Mine is also unusual in that the chalcopyrite to pyrrhotite ratio is approximately 1:1. Stanton (1972) stated that the normal ratio is 1:8, for ores associated with rocks of this type.

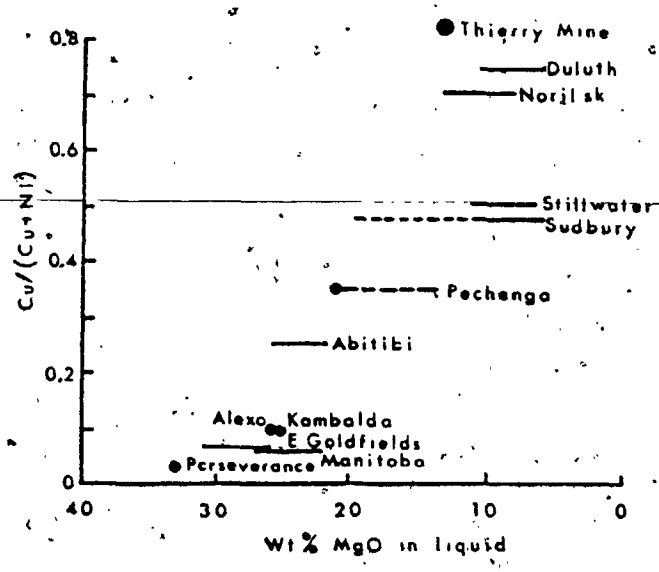

Fig. 8:1, Relationship between Cu/(Cu+Ni) ratio in sulfide ores and the % MgO in the host rock. (after Naldrett and Cabri, 1976)

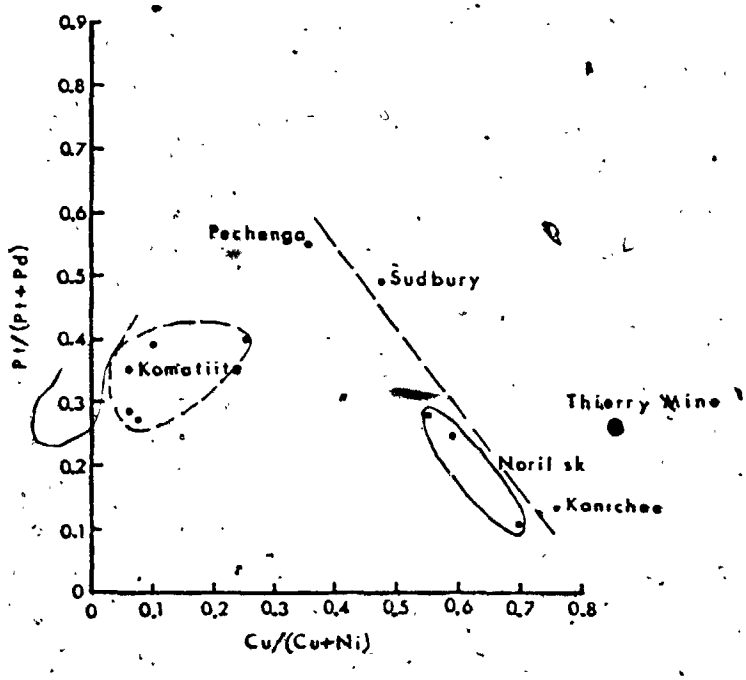

Fig. 8:2, The relationship between Pt/(Pt+Pd) and Cu(Cu+Ni) ratios in sulfide ores (after Naldrett and Cabri, 1976)

There are several methods by which a basic magma may become enriched in chalcopyrite relative to pyrrhotite and pentlandite. Craig and Kullerud (1963) studied the system Fe-Ni-Cu-S at 1000°C (Fig. 8:4) and showed that a copper-rich liquid coexists with monosulfide solid solution. This might be a reasonable explanation for Thierry ore if the sulfide liquid could segregate from MSS and the silicate magma. However, the precipitation of olivine, pyroxene and plagioclase would probably lock in any immiscible sulfide droplets making it difficult for such a copper-rich liquid to separate from the other solid sulfides and silicates. If the sulfide magma formed a massive unit, it is unlikely that a copper-rich liquid could migrate because the density contrast between the liquid and the pyrrhotite-pentlandite would be small. A similar argument could be made for generation of Cu-rich liquids in a system containing oxygen where the iron oxides and iron-nickel sulfide would solidify leaving a copper-rich liquid.

Bowdidge (1970) suggested that the copper-rich sulfides at Thierry Mine were generated from the solidification of a magma that was sulfur deficient. The nickel and iron would have been concentrated in olivine and pyroxene structures enriching the remaining magma in copper. When the magma became sulfur-saturated, sulfide liquid enriched in copper would precipitate from a magma depleted in nickel and iron.

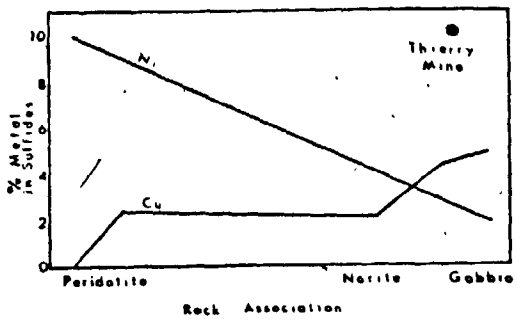

Fig. 8:3, Average copper and nickel content in copper-nickel sulfide ores compared with the composition of the host rock. (after Wilson and Anderson (1959)

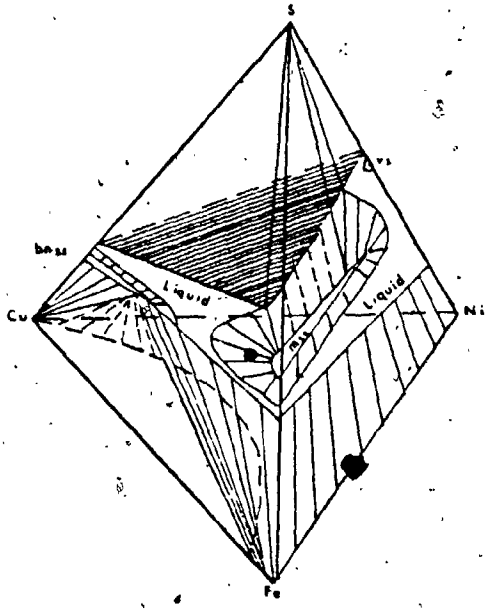

Fig. 8:4, Schematic 1000°C isothermal diagram of the Cu-Fe-Ni-S system in the presence of vapour. The solid circle represents the average composition of the Thierry sulfide ores. (after Craig and Kullerud, (1969)

However in the Stillwater complex (Wager & Brown, 1968) copper-rich sulfides did not precipitate until 90% of the body was crystallized.

Examination of the ratio of barren um-m rock to ore-bearing um-m rocks at the Thierry Mine shows that virtually all the um-m rock contains sulfide. In the initial stages of exploration, UMEX analyzed all um-m rocks by an acid leach method, which determined only the amount of nickel and copper as sulfides. An integration of the sulfide nickel and copper over the whole um-m body yelded a ratio of copper to nickel of 3:1 (Bowdidge, 1970). This ratio is similar to that observed in the other Kapkichi Lake ultramafic bodies. However even this ratio is unusually high for magmatic sulfides genetically related to um-m rocks (Fig. 8:1).

The main contrast between the Thierry Mine ultramafic rocks and the other Kapkichi ultramafic rocks is the amount of shearing and mylonitization. Barrett et al (1977) suggested that most economic concentrations of iron-nickel sulfides were due to dynamic metamorphism. They stated

> "Although Fe-Ni sulfides occur in all metamorphic domains, particularly in the dunitic intrusions, only disseminated deposits have been discovered in greenschist metamorphic domains. The matrix and massive sulfides that now represent economic or subeconomic concentrations of nickel in both volcanic-type and dikelike hosts are confined to amphibolite facies domains. Most deposits occur in mid- to -high-amphibolite facies domains of dominantly dynamic style"

On a local scale within the Thierry Mine it is common to have copper-rich sulfides concentrated in minor faults and shears. Experimentally determined relative strengths of pyrrhotite and chalcopyrite (Kelly and Clark, 1975) suggested that mechanical separation of chalcopyrite and pyrrhotite is not a major process and that stress induced diffusion is more important. In order to explore such possible mechanisms Fig. 8:5 and Fig. 8:6 were constructed by projecting drill hole data and ore grades onto a vertical plane parallel to the strike of the ore zones. The Cu/Ni variation within the breccia ore shows no distinct pattern. However the Cu/Ni ratio varies from low values in the east to high values in the west in the mylonite (C.B.S.) ore. This could be caused by the migration of copper to the west under a stress field. The occurrence of mylonitized um-m rocks, folded rock fragments and wall rocks in the breccia suggest it is remobilized massive ore or generated from primary disseminated ore. The highly variable Fe/Ni ratio in the breccia ore tends to support this. Sections of the breccia ore are rich in pyrrhotite and pentlandite (Kennedy, 1978), producing strong variation in the Fe/Ni ratio. This implies that deformation took place below a temperature of 400°C when pyrrhotite and pentlandite existed as separate minerals, rather than monosulfide solid solution.

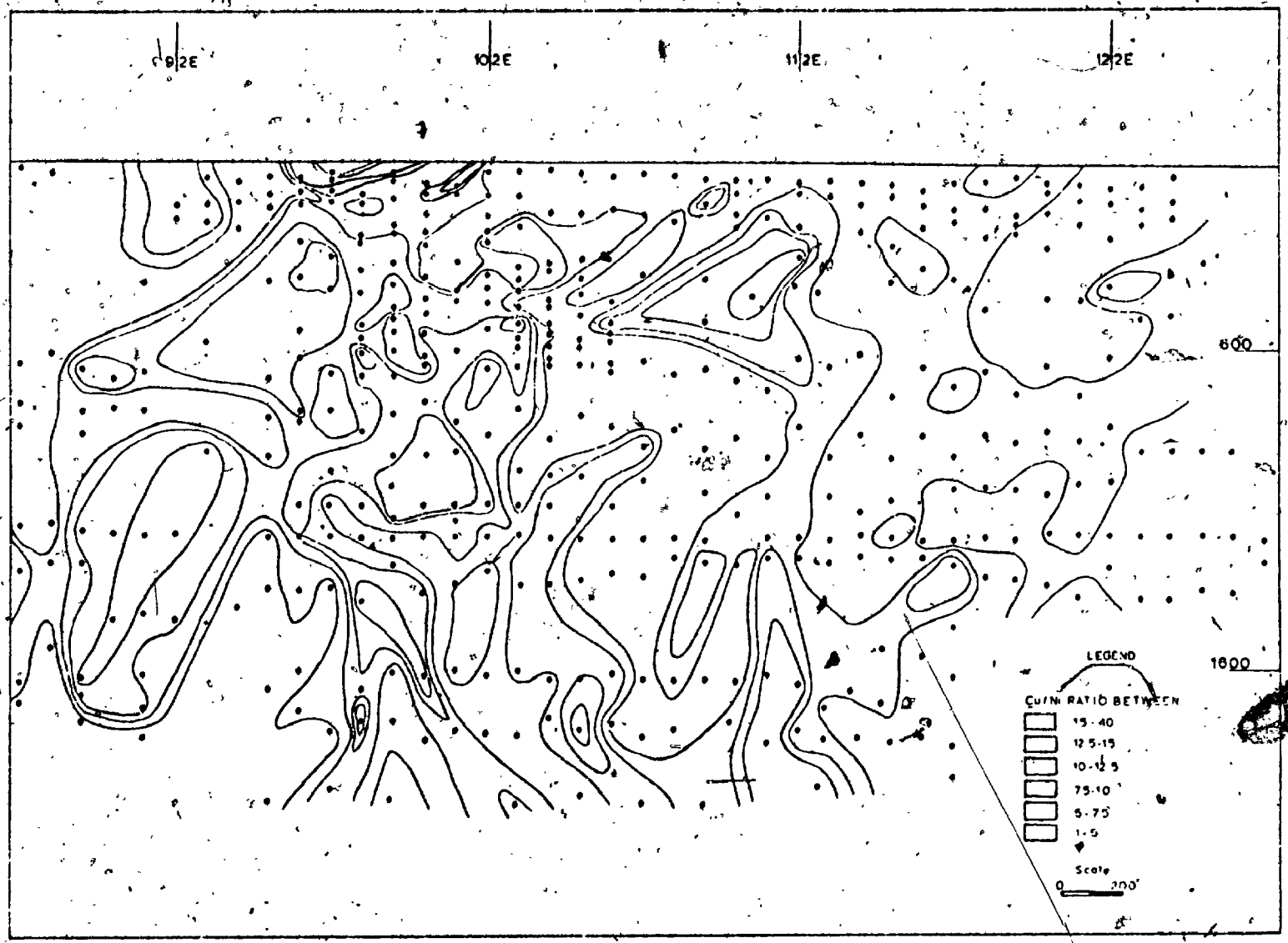

Fig. 8.5. Projection of Cu/Ni ratios in the mylonite ore.

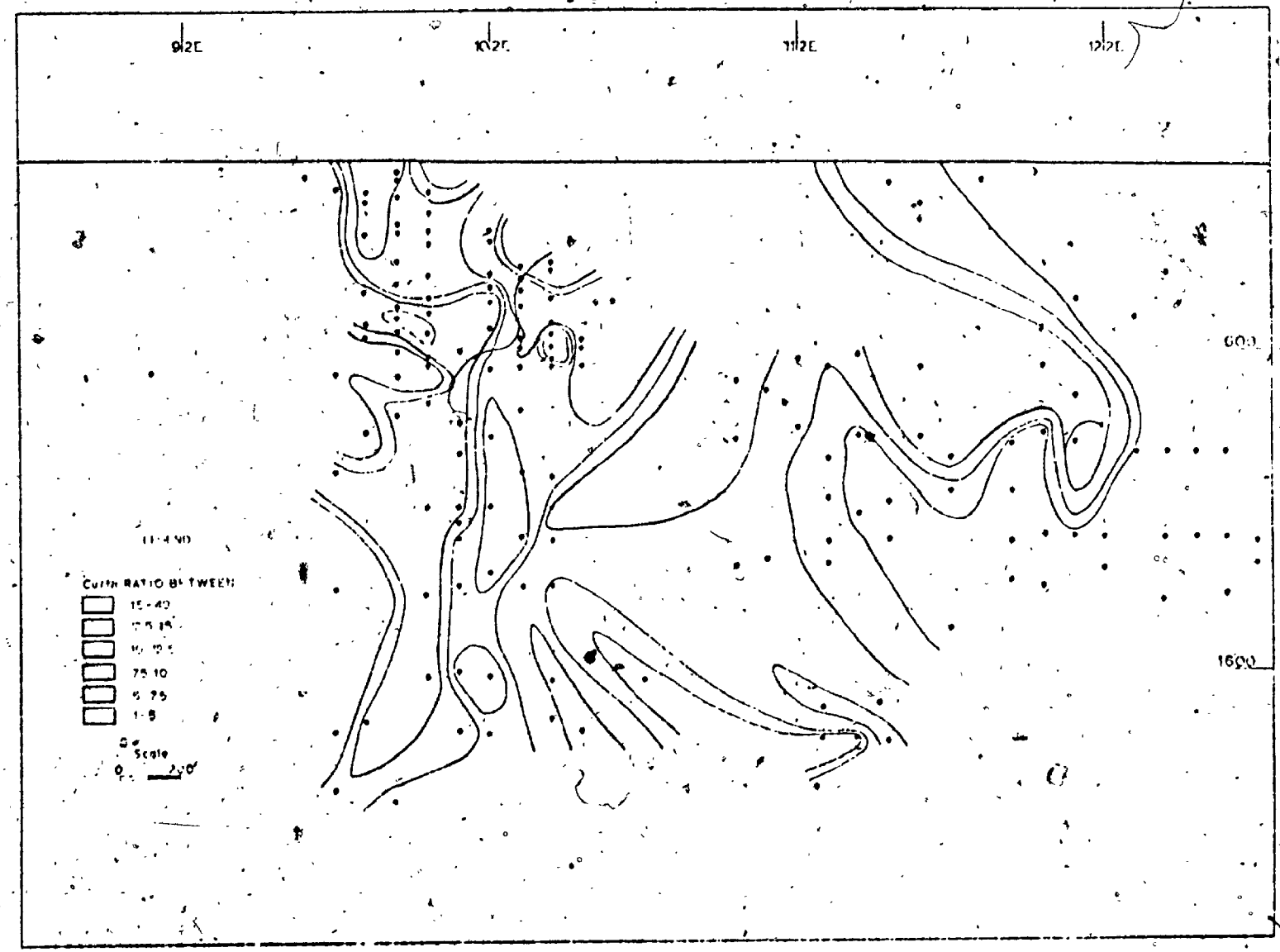

Fig. 8.6. Projection of Cu/Ni ratios in the Breccia ore

The presence of a chemical alteration pattern (Chapter 5) in the mylonitized zone suggests that copper could have been selectively moved into the shear zone leaving nickel, a less mobile element (Patterson, 1974) in the original ultramafic rock. However the lack of solubility data on nickel sulfides makes a detailed assesssment of this model impossible. It seems likely that the pattern of alteration observed in the silicates and sulfides at the Thierry Mine was produced under the influence of stress-induced diffusion.

8:2 Summary and Conclusions

The Kapkichi Lake area is located within the Uchi Lake greenstone belt in the Superior structural province of the Canadian Shield, 400 kilometres N.W. of Thunder Bay, Ontario. The extrusion of mafic volcanic rocks (high-iron tholeiites) with minor felsic tuffs and metasediments on a granitic gneiss terrain was followed by the intrusion of large granitic stocks and later ultramafic bodies with associated Cu-Ni sulfides. Four main tectonic events were recognized: 1. a period of isoclinal folding with associated amphibolite-grade metamorphism produced a strong foliation and lineation in the amphibolite schist and Pickle Lake Stock; 2. deformation generating folds with an axial plane at $68^{\circ}E/68^{\circ}N$ affected all first-phase structures: 3. a broad open folding event warped the second phase fold axis to the north; and 4. a dominatly cataclastic phase at greenschist facies metamorphism produced shear zones, faults, kink bands and mylonitized zones. Metasomatic effects in the mylonitized zones and at contacts between the um-m rocks and amphibolite schist took place during that last event.

The whole rock chemistry and remnant mineralogy of the um-m bodies show that the original um-m rocks consisted of olivine (Fo_{65}), plagioclase (An_{50}-An_{60}), clinopyroxene with exsolved hypersthene as cumulus minerals and hypersthene and sulfides as intercumulus material. These have been altered and metamorphosed to hornblende, plagioclase (An_{20}-An_{30}), olivine, anthophyllite, tremolite, carbonate, chlorite and biotite.

The temperature of metamorphism based on garnet-biotite, calcite-dolomite, and magnetite-ilmenite geothermometers was 600°C ± 50°C. The pressure of metamorphism based on garnet-plagioclase and sphalerite-pyrite-pyrrhotite equilbria was 5.6-6.8 kilobars. The assemblages observed in the mafic volcanic rocks, pelites and calc-silicates are consistent with the above conditions. The assemblages observed in the ultramafic rocks are consistent only if the fluid phase was CO_2-rich. The grade of metamorphism in the cataclastic rocks based on the silicate and sulfide assemblages is greenschist facies below 400°C.

Five main ore types were recognized at the Thierry Mine. These are primary disseminated ore, breccia ore, chlorite-biotite schist ore, bornite ore and altered ore making up 1%, 40%, 56%, 2% and 1% respectively of the total. The primary sulfide assemblages in addition to chalcopyrite were

pyrrhotite + pyrite + pentlandite and
pyrrhotite + pentlandite

These were altered in near surface zones by the removal of iron during surface-related oxidation to produce the following apparently compatible assemblages.

pyrite + violarite + magnetite
pyrite + vaesite + violarite + magnetite
millerite + violarite + magnetite

and the probably incompatible assemblage

pyrrhotite + smythite + pentlandite
+ violarite + magnetite

The iron removed from the sulfide produced magnetite. These supergene processes increased the relative Ni and S content of the sulfide assemblages.

The compatible assemblages observed at the Thierry Mine are best explained by the interpretation of Misra and Fleet (1974) of low-temperature phase relations in the Fe-Ni-S system.

Precious-metal minerals in the bornite and breccia ore are moncheite, merenskyite, kotulskite, stuetzite, native silver, acanthite and Ag_3BiTe_2. There is a correlation of copper with silver and palladium in the Thierry ore. Tellurides may have been concentrated with chalcopyrite late in magmatic crystallization or more likely the copper, silver and palladium minerals were more mobile than iron and nickel sulfides under metamorphic conditions.

Comparison of the sulfide mineralization at the Thierry Mine with that in the Kapkichi Lake area show that the sulfides in the Kapkichi Lake um-m rocks have suffered only local mobilization; they occur predominantly as primary intercumulus blebs of sulfide blebs modified by recrystallization of silicates during metamorphism. Supergene effects in the Kapkichi Lake sulfides are minor compared to those at the Thierry Mine.

The whole-rock chemistry from the ultramafic rocks in the Thierry Mine indicate that Ca,Na,Si have been removed and K,Cu have been added to the mylonitized zone in a metasomatic event. The lack of plagioclase, the alteration of hornblende to actinolite, the correlation of biotite and sulfide in the mylonite, and the enrichment of epidote and carbonate in the amphibolite wall rocks suggest that the alteration of plagioclase and hornblende produced chlorite in mylonite, with the released sodium and calcium altering the plagioclase in the amphibolites to epidote and albite.

Chlorite plus released potassium generated biotite producing a rise in pH of the metasomatic solutions causing copper to precipitate as sulfides. The genesis of the sulfides is interpreted as the formation of primary intercumulus sulfide formed as an immiscible melt in a magma of gabbroic composition. The sulfides were subjected to regional metamorphism which caused their polygonal recrystallization and modification by the growth of metamorphic minerals. A strong cataclastic event caused the mobilization of Cu relative to Ni in the um-m body depositing it as chalcopyrite in the mylonite zone. The stress-induced diffusion produced the observed metasomatic effects. Further cataclastic events and diffusion produced the breccia ore and bornite ore. The concentration of these minerals formed the ore zones at Thierry. Due to the heavy faulting and shearing, percolating ground water allowed supergene alteration to take place, producing assemblages of violarite, pyrite and magnetite.

The implication for exploration in the Kapkichi Lake area is that the most likely ore-bearing um-m rocks are those that are the most intensely sheared and faulted with the possibility of ore associated with these faults. In the mine area Fault #1, (Fig. 2:3) to the west of the Thierry Mine terminates the mineralization. It is suggested that this fault should be drilled.

Examination of the literature of Canadian Cu-Ni deposits indicates that most economic deposits have suffered a metamorphic event under dynamic stress at greenschist or higher grades. This suggests that stress may have played a role in concentrating the sulfides to economic grades.

9.0 Plates

1. Metamorphic textures of gabbroic rocks
2. Deformation textures
3. Metamorphic textures
4. Distribution of sulfides in blastomylonite
5. Textures of oxide minerals
6. Textures in pyritic rocks
7. Sulfide textures
8. Textures in violarite-bearing ores
9. Breccia and chlorite-biotite schist ores
10. Platinum-group minerals from the Thierry Mine

Plate 1, Metamorphic Textures of Gabbroic Rocks

a) Clinopyroxene with exsolution of ilmenite-magnetite marginally altered to hornblende, 101 , 1cm=0.01mm

b) Cumulus clinopyroxene and plagioclase (An_{60}) partially altered to hornblende along the margin of the clinopyroxene crystal, 101 , 1cm=0.08mm

c) Radiating masses of hornblende replacing clinopyroxene with remnant plagioclase (An_{60}), 342 , 1cm=0.08mm

d) Remnant plagioclase (An_{60}) partly altered to sericite in a matrix of recrystallized hornblende and plagioclase (An_{30}), Th11 , 1cm=0.08mm

e) Polygonal hornblende and plagioclase which shows strong oscillatory zoning (An_{20}-An_{30}), Th17 , 1cm=0.08mm

f) Mafic metagabbro consisting of 100% amphibole, dominatly dark green hornblende often rimmed by colourless actinolite, 1cm=0.04mm, Th47

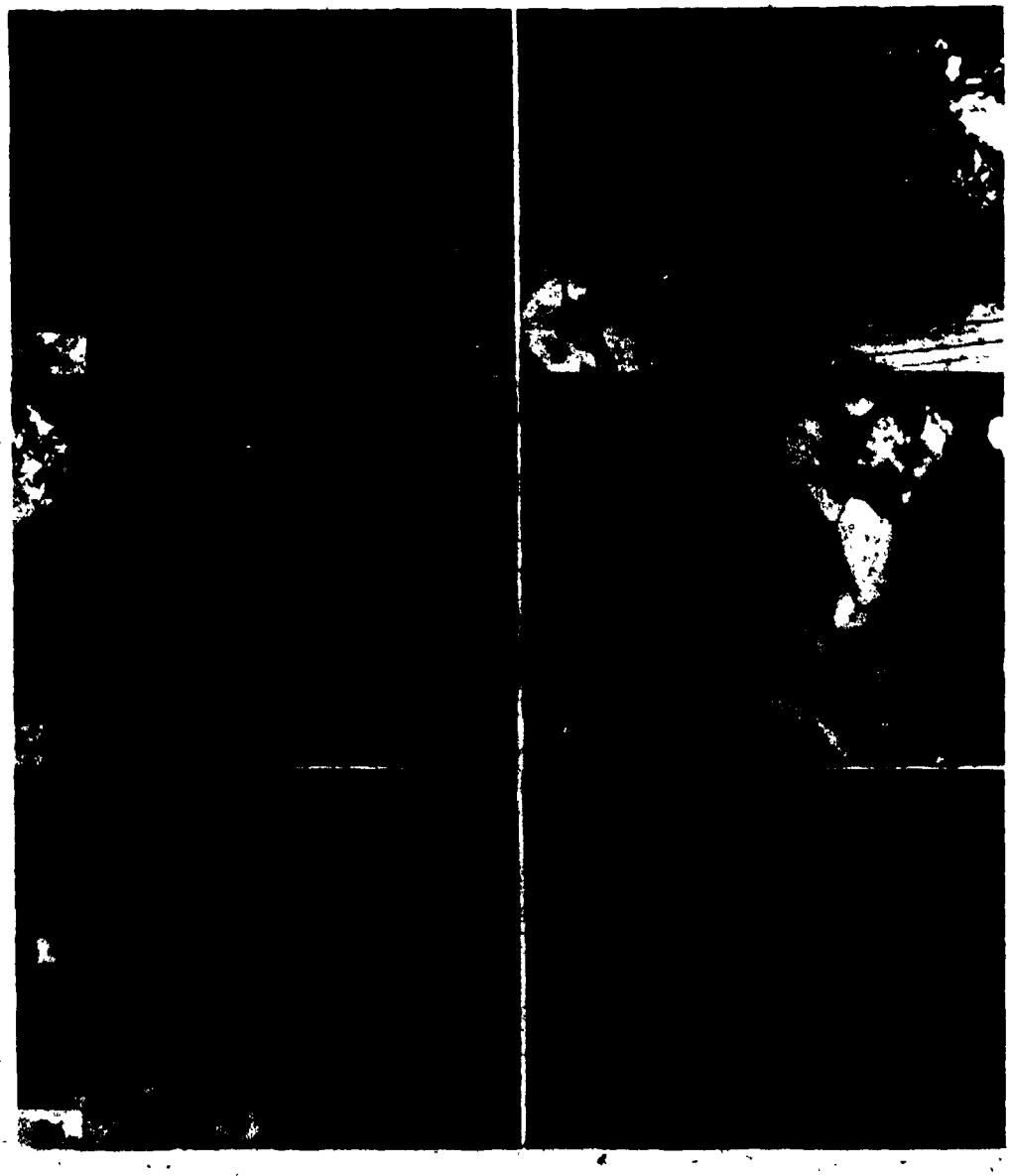

Plate 2, Deformation Textures

a) Kink bands in biotite from biotite-hornblende schist (black wall altered ultramafic rock) 1cm=0.04cm, K328-569

b) Deformation twins in iron-rich chlorite from chlorite-biotite schist (black-wall altered ultramafic rock) 1cm=0.04cm, 346

c) Hornblende chlorite-biotite schist or blastomylonite showing fragments of hornblende in matrix of chlorite and biotite, 1cm=0.04cm, Th-46

d) Fragment of hornblende with actinolitic margins in hornblende-chlorite-biotite schist, 1cm=0.01cm, 371

e) A deformed fragment of mafic metagabbro in hornblende-chlorite-biotite schist, 1cm=0.04mm, Th56

f) Hornblende-chlorite-biotite schist with quartz-and mafic-rich folded bands, 1cm=0.08mm, Th9

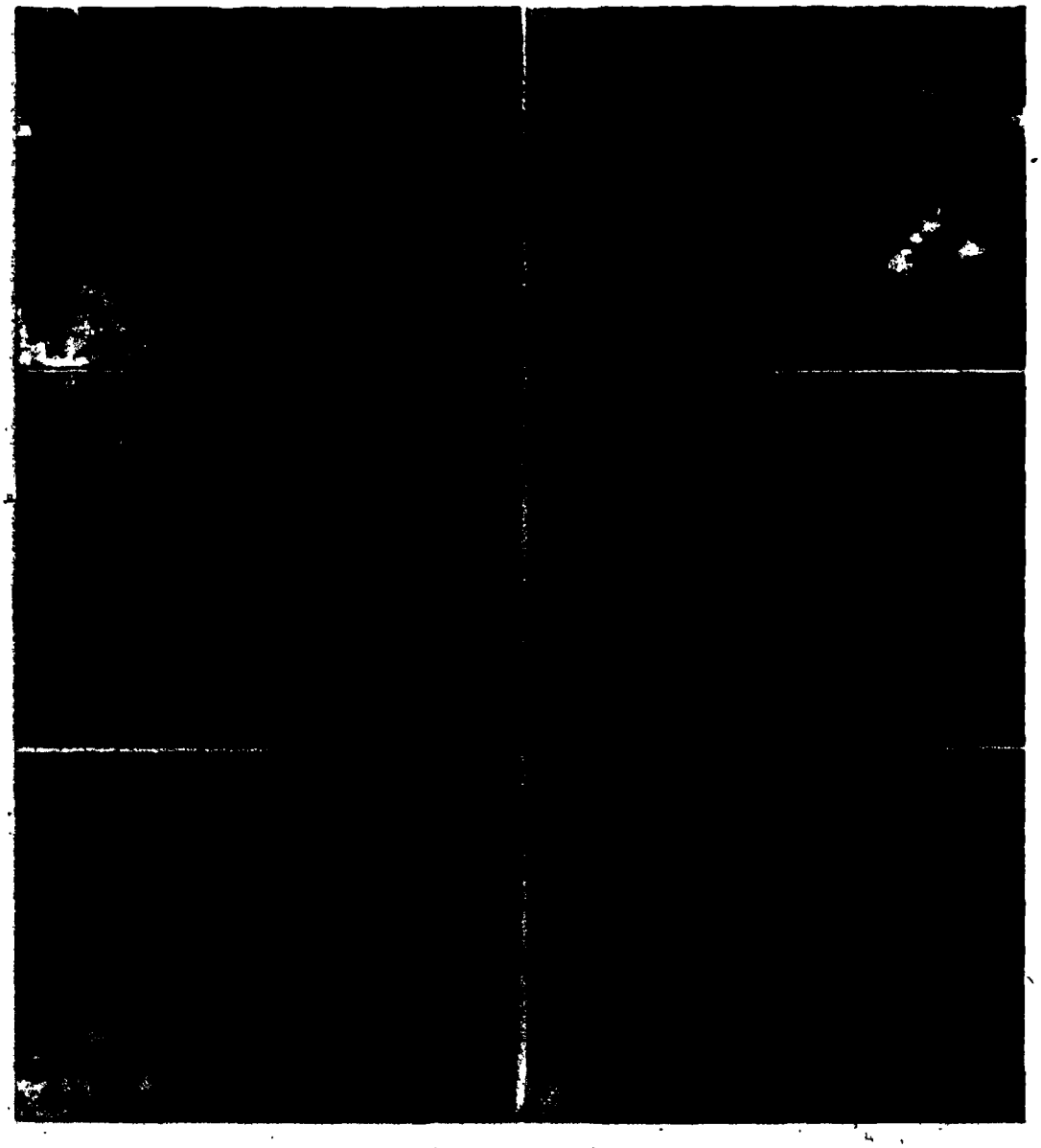

Plate 3, Metamorphic Textures; all photographed areas are 1 cm=0.08mm

a) Metamorphosed pelite consisting of garnet + biotite + sillimanite + staurolite + plagioclase (An_{29}) + quartz, PE

b) Metamorphosed calc-silicate metasediment containing Ca-garnet (left side of photo) with calcite-dolomite (light grey) and tremolite, CAL-SIL

c) Banded amphibolitic schist with fine-grained well foliated layer containing hornblende + plagioclase (An_{30}) and coarse grained hornblende layers. 376

d) Altered dunite showing talc-carbonate-magnetite pseudomorphs after olivine. Th-26

e) Metamorphic olivine with inclusions of Mg chlorite and tremolite in altered peridotite. Th73

f) Polygonally recrystallized metamorphic olivine with minor tremolite in altered peridotite. 62

A
B

Plate 4. Distribution of Sulfides in Blastomylonite

a) Chalcopyrite and pyrrhotite in fractures which cut but do not disrupt the foliation in the blastomylonite, 1cm=0.-8mm, Th23

b) Banded blastomylonite containing layers rich in biotite and opaques, and chlorite, 1cm=0.04mm, Th28

c) Banded blastomylonite with folded sulfide-rich layers and sulfide-filled fractures cutting foliation, 1cm=0.08mm, Th9

d) Fragments of brecciated blastomylonite in a sulfide-rich matrix, 1cm=0.08mm, 363

e) A sulfide-filled pressure shadow adjacent to a fragment of mafic metagabbro in a blastomylonite, 1cm=0.04mm, 369

f) A banded blastomylonite with layers rich in quartz, hornblende, biotite and opaques, 1cm=0.01mm, Th-46

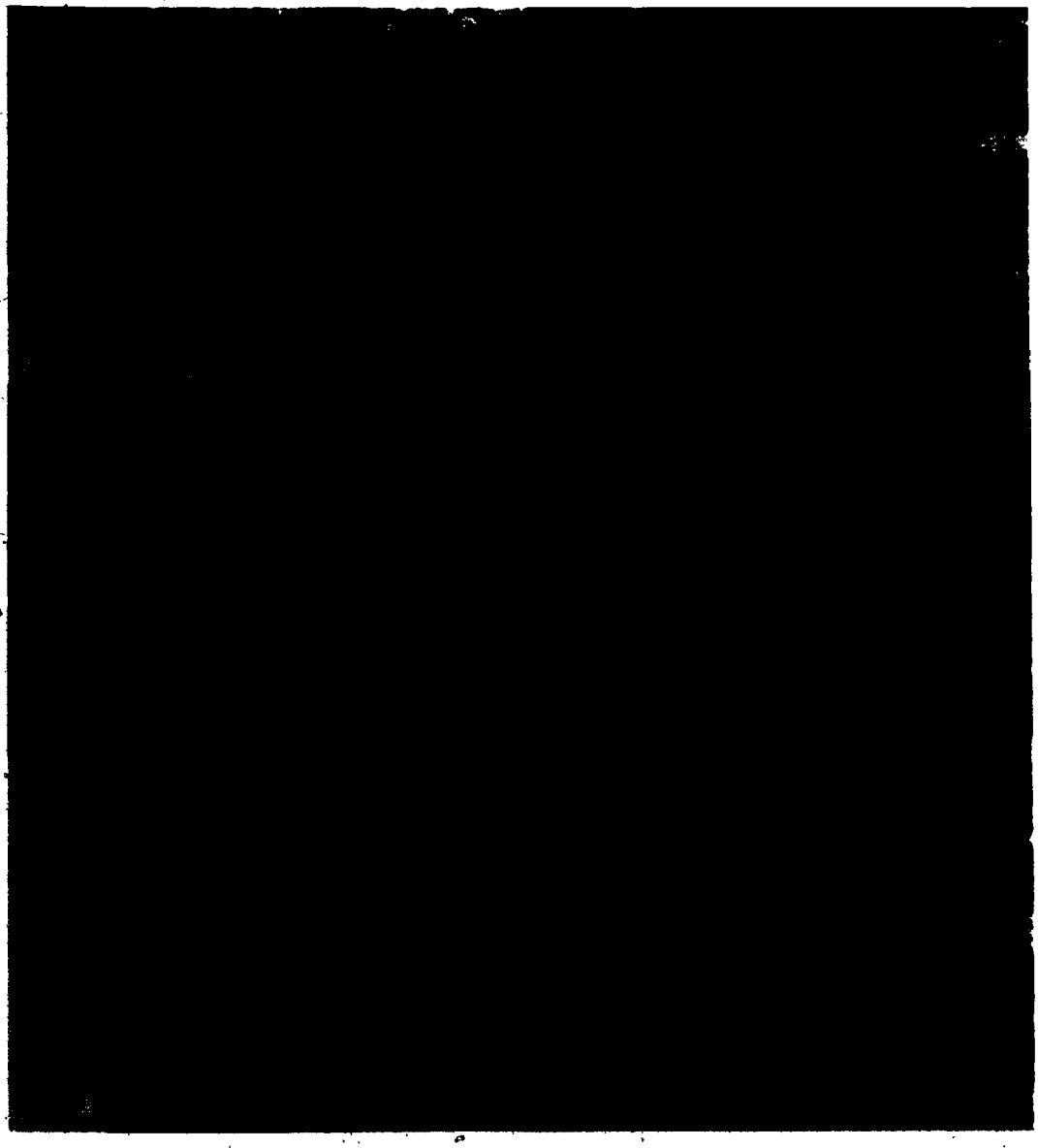

Plate 5. Textures of Oxide Minerals. All photographs of an area 0.32cm

a) Mg-spinel with ilmenite in oxide layer of the G ultramafic-mafic body, K31-1005

b) Ilmenite grains and exsolution lamellae in magnetite from oxide layer in the G ultramafic body, K31-1005

c) Magnetite porphyroblast with zonally arranged inclusions associated with chalcopyrite and pyrite in blastomylonite, 4-035-71

d) Magnetite porphyroblasts with a spiral arrangement of inclusion in breccia ore, 4-032-153

e) Deformed magnetite porphyroblast in blastomylonite with chalcopyrite, 260/99/132

f) A highly deformed and brecciated magnetite porphyroblast in blastomylonite, K71 424

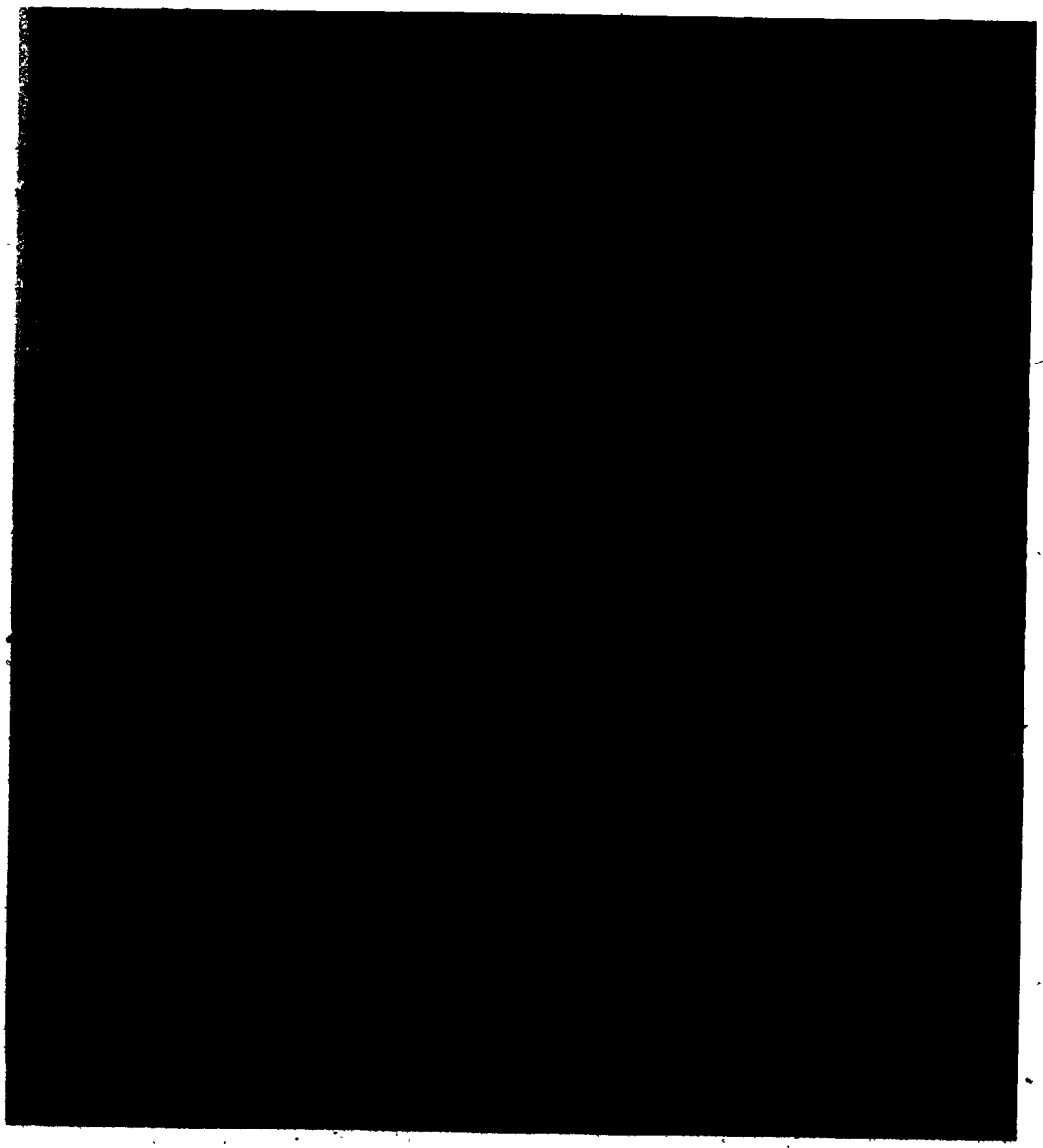

Plate 6, Textures in Pyritic Rocks

a) Cobalt-rich pyrite euhedra in chalcopyrite, from breccia ore, 1cm=0.08mm, K68 632

b) Resorbed pyrite in chalcopyrite from breccia ore, 1cm=0.08mm, 600-1E-HOR-93

c) Resorbed pyrite altered to marcasite in chalcopyrite, 1cm=0.08mm, K50 315

d) Pyrite intergrown with chlorite, 1cm=0.08mm, K68 290

e) Dendritic pyrite after pyrrhotite with spongy violarite in altered breccia ore, 1cm=0.04mm, 600-1E-HOR-65

f) Pyrite partly altered to hematite in breccia ore, 1cm=0.04mm, K71 424

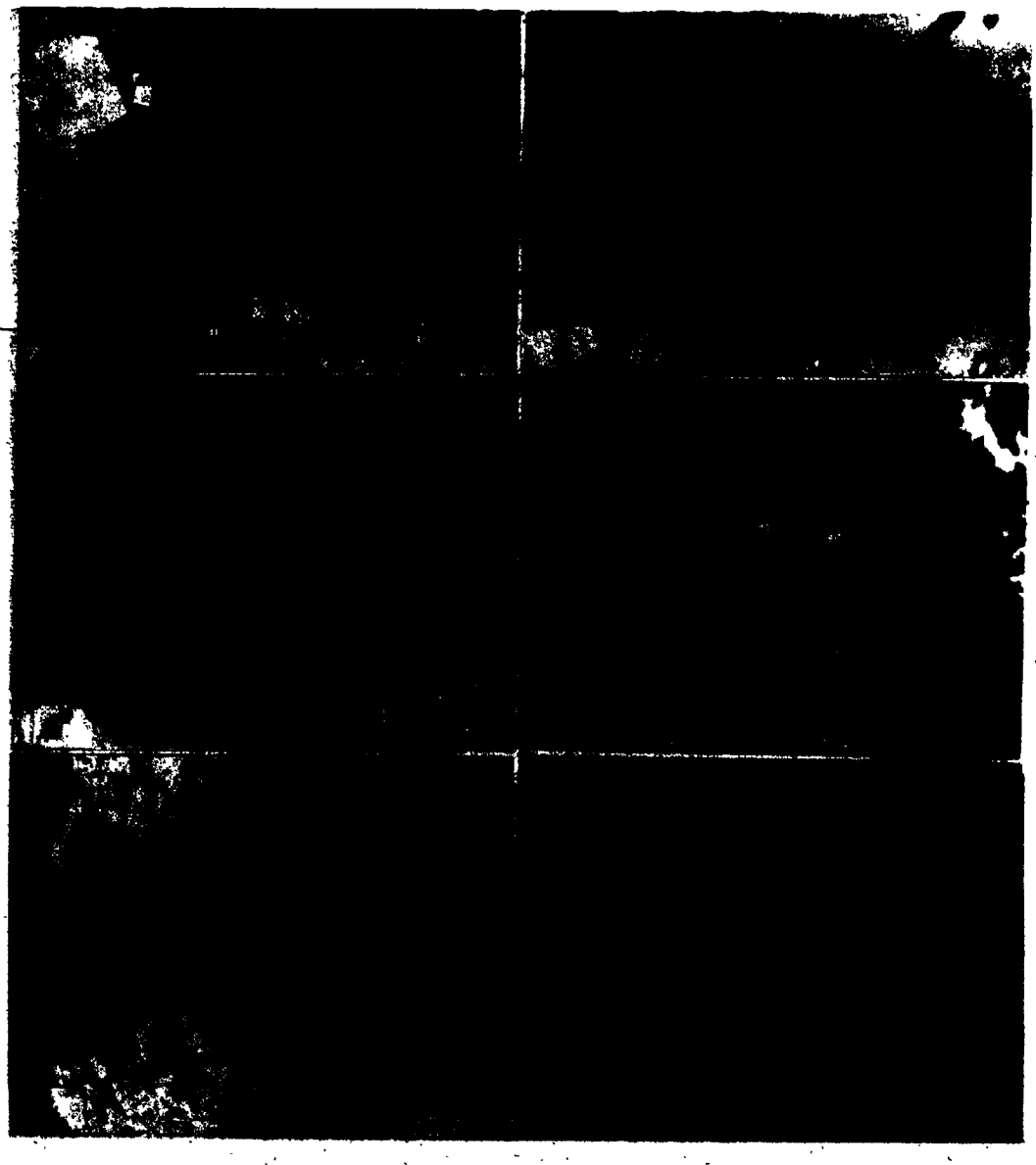

Plate 7, Sulfide Textures

a) Pentlandite (light grey) exsolved from pyrrhotite (dark grey) with low-nickel iron monosulfide (intermediate grey) in breccia ore, 1cm=0.04mm, Th2

b) Chalcopyrite and exsolved bornite with cobalt-rich pentlandite from oxide layer in the G ultramafic-mafic 1cm=0.01mm, K31-1005

c) Bornite exsolved from chalcopyrite in bornite ore 1cm=0.01mm, Th5

d) Wittichenite Cu_3BiS_3 and emplectite $CuBiS_2$ with bornite and chalcopyrite in bornite ore, 1cm=0.01mm , Bn West

e) Cubanite lamellae in chalcopyrite from primary disseminated ore, 1cm=0.01mm, K9-382

f) Intercumulus material composed of pyrrhotite with minor pentlandite and magnetite in an altered dunite (primary disseminated ore), 1cm=0.08mm, K9-208

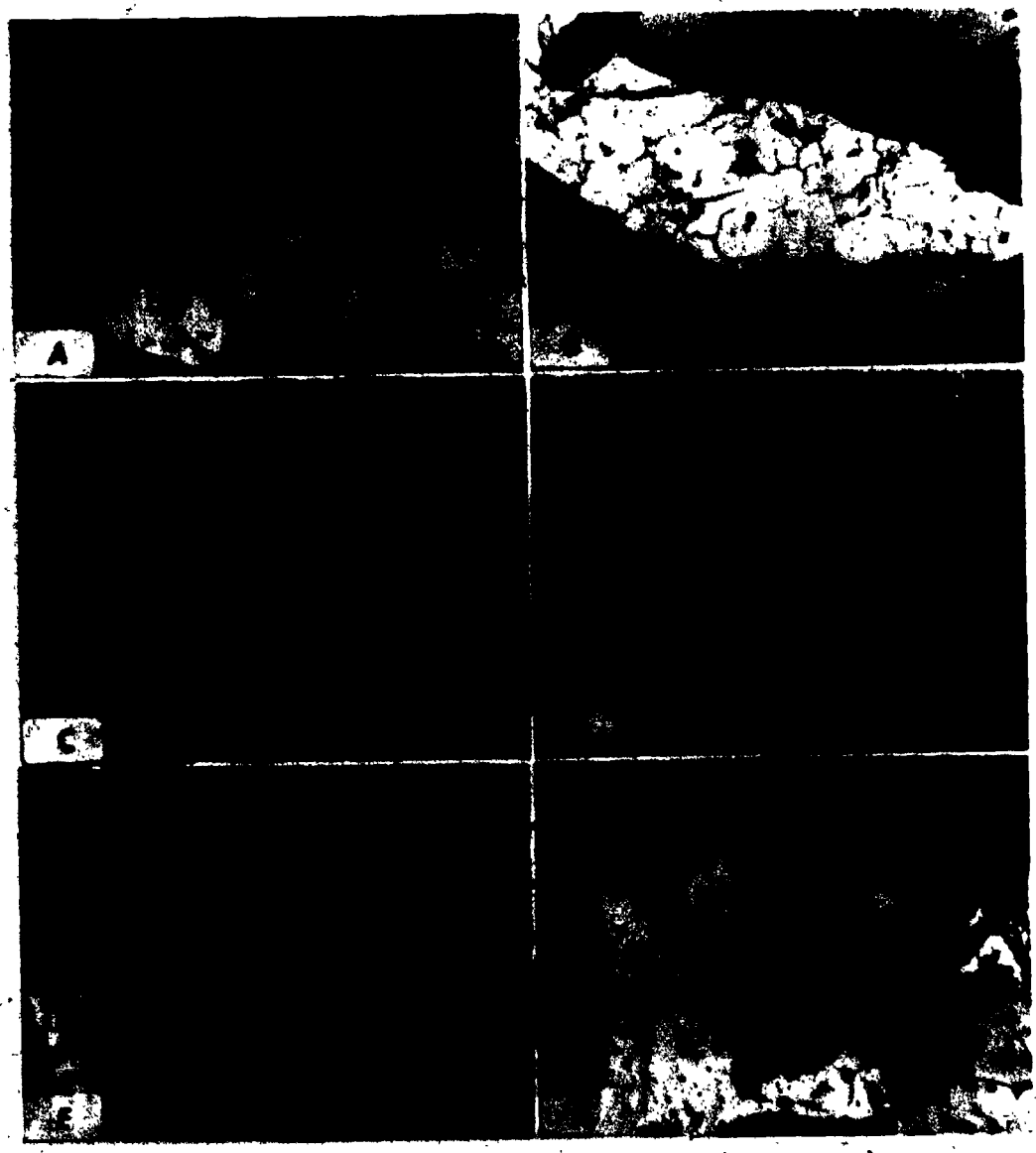
A
C
E

Plate 8, Textures in Violarite-bearing Ore

a) Fresh pentlandite occurs as pods and flames in pyrrhotite with minor smythite in breccia ore, 1cm=0.08mm, West Pit (Po)

b) Lamellar violarite developed along fractures in pyrrhotite with halo of smythite; breccia ore, 1cm=0.08, Th 9

c) Pentlandite altered to violarite and Ni-rich pyrite, and pyrrhotite altered to lamellar violarite, 1cm=0.08mm , Th 10

d) Violarite after pentlandite (top half of photo) and lamellar violarite after pyrrhotite (lower half of photo), 1cm=0.04mm , Th 10

e) Violarite after pentlandite showing remnant octahedral cleavage from breccia ore, 1cm=0.08mm , Th 9

f) Nickel-rich pyrite in violarite with octahedral shrinkage fracture (breccia ore), 1cm=0.04mm , Th 9

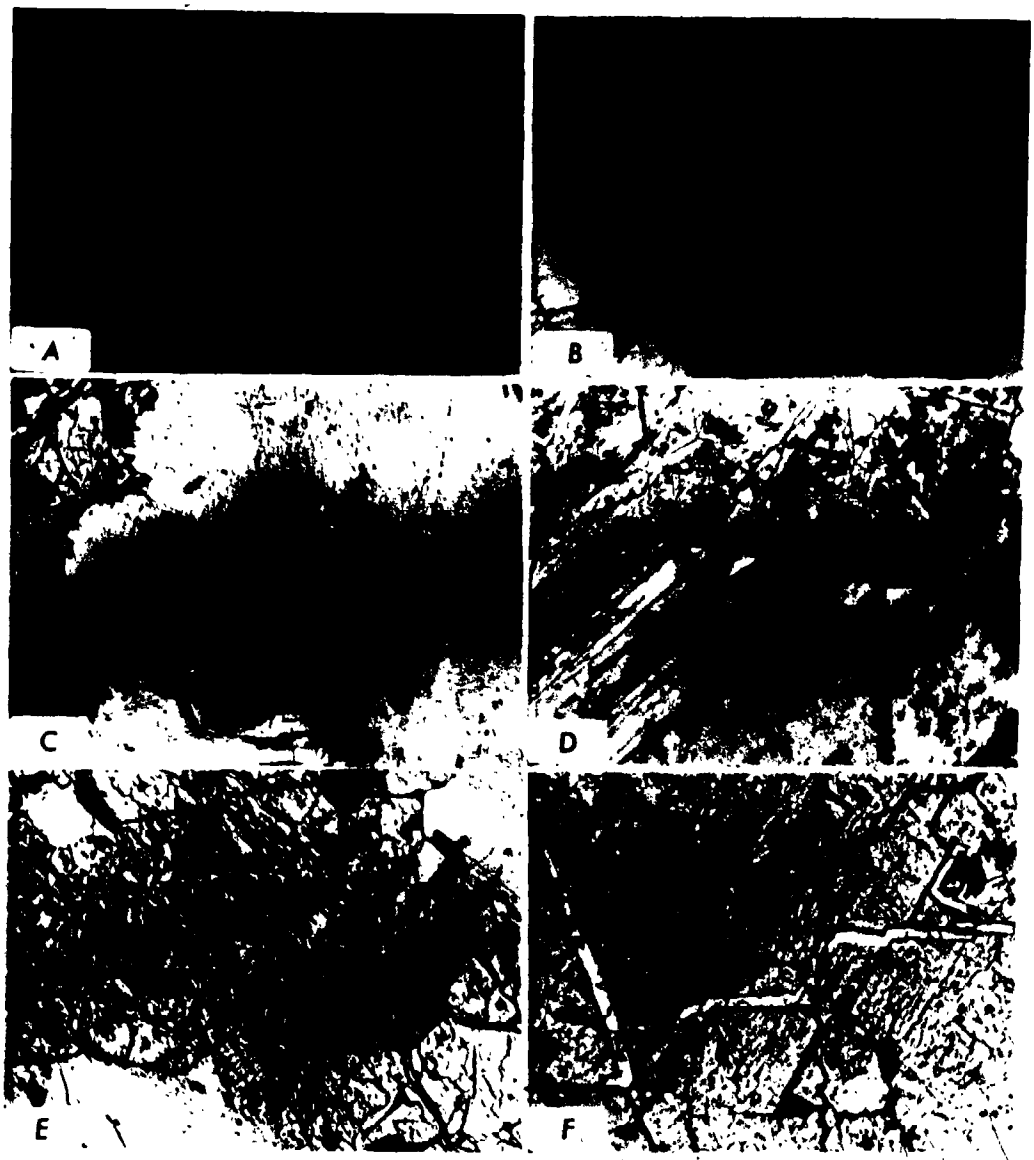
A
B
C
D
E
F

Plate 9, Breccia and Chlorite-Biotite Schist Ores

a) Fragment of mafic metagabbro containing hematite with a rim of pyrrhotite-pentlandite-magnetite in a matrix of chalcopyrite, 1cm=2cm, 600 cross-cut

b) Deformed fragments of mafic metagabbro in a matrix of chalcopyrite 1cm=3cm, 600 cross-cut

c) Deformed fragments of mafic metagabbro with sulfides (chalcopyrite and pyrrhotite) in fractures and joints 1cm=1.5cm, West Pit, 2nd Bench

d) Mylonitized um-m rock with highly folded and deformed fragments of mafic metagabbro. Sulfide occurs as fine dissemination stretched parallel to the foliation 1cm=1.5cm, West Pit, 2nd Bench

e) Mylonitized um-m rock with interference patterns defined by folded layers with varying chlorite to biotite ratios; sulfides occur as disseminations stretched parallel to foliation and minor stringers cutting the foliation, 1cm=1.5cm, West Pit, 2nd Bench

f) Contact between a diorite dyke (right, with a chilled margin) with mafic metagabbro. Biotite developed in the mafic metagabbro and decreases away from the contact, 1cm=2cm, K1:1, K329-158

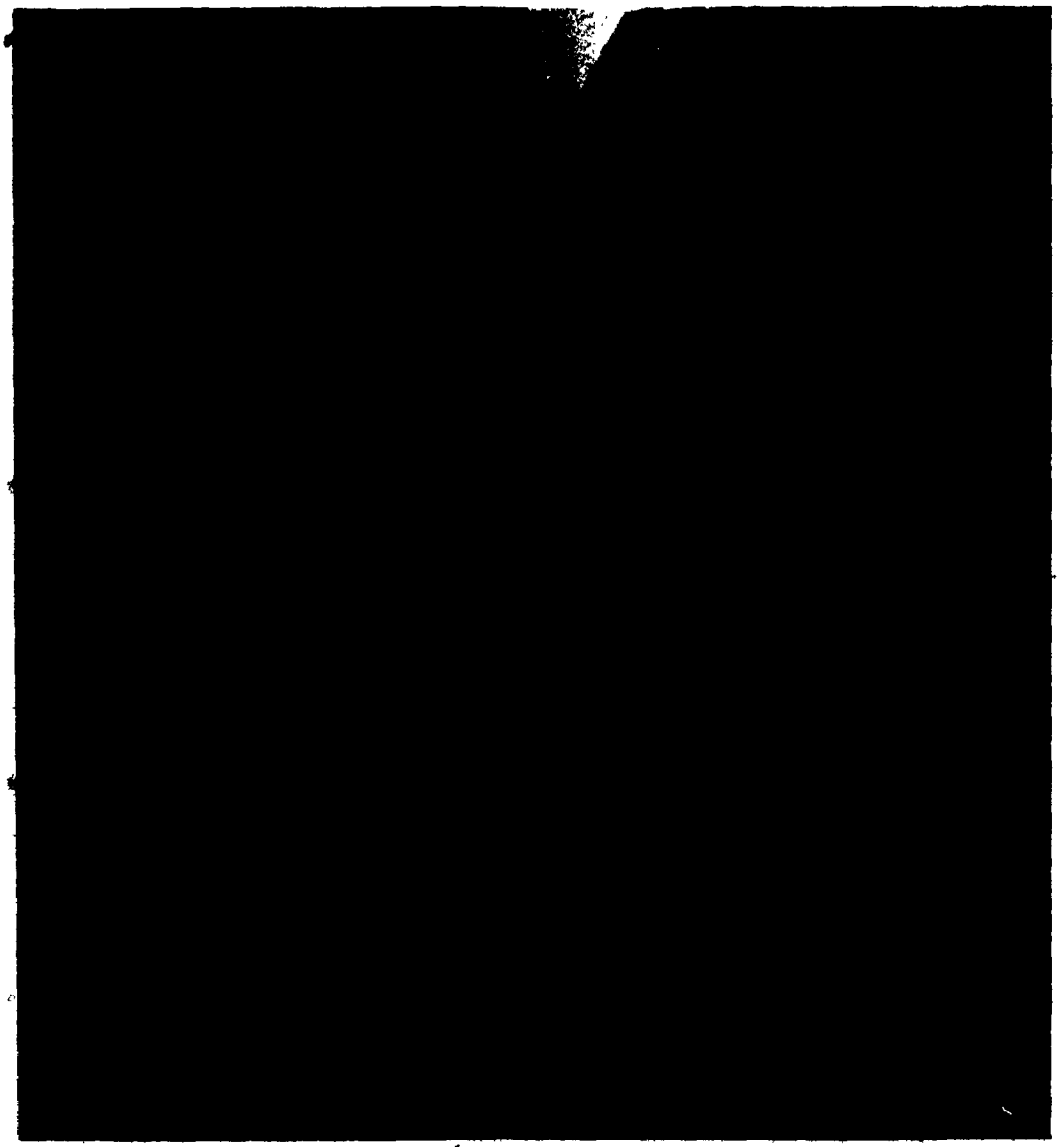

Plate 10, Platinum-group Minerals from the Thierry Mine

a) Moncheite (white) in chalcopyrite (dark grey) with associated pyrrhotite (light grey) and exsolved pentlandite, 1cm=.04mm, breccia ore, 600 level, cross-cut.

b) Moncheite grain with fine exsolution of dark grey stuetzite in chalcopyrite (left), breccia ore, 600 level, cross-cut, 1cm-0,01mm

c) Moncheite (white) with fine exsolution and blebs of dark-grey stuetzite in violarite after pentlandite, 600 level, cross-cut, breccia ore, 1cm=0.01mm

d) Merenskyite (white) with exsolved stuetzite (light grey) and Ag_3BiTe_2 (dark grey), breccia ore, 1cm=0.01mm, 600 level, cross-cut

e) Merenskyite (white) in pyrrhotite with flames of pentlandite, breccia ore, 2nd bench, west pit 1cm=0.01mm

f) Moncheite (white) with inclusions of silicates in breccia ore, 1cm=0.01mm, 600 level cross cut

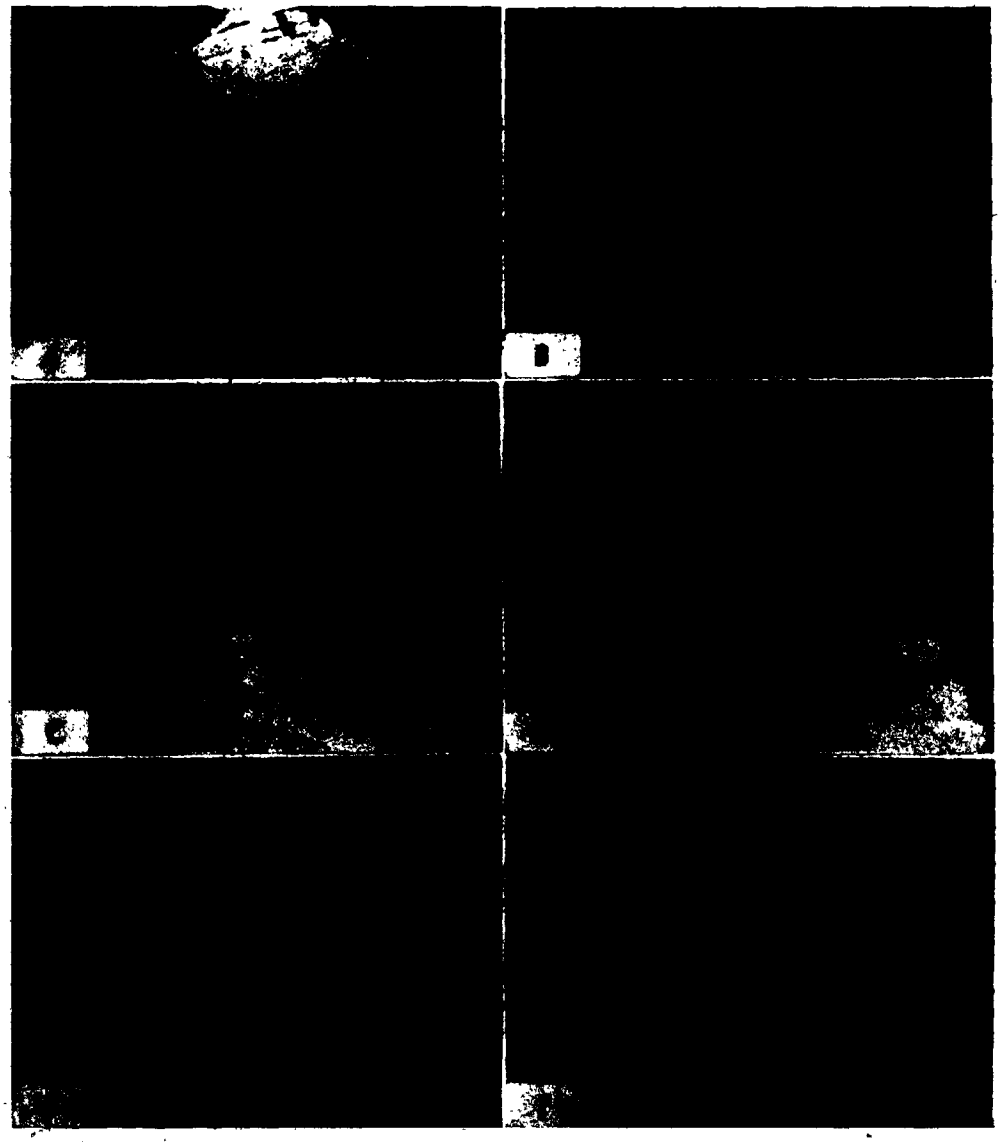

10.0 References

Arnold, R.G., and Malik, O.P. (1975): The NiS-S System above 980°C, A Revision. Econ. Geol. Vol. 70, pp176-182

Arndt, N.T. (1975): Ultramafic Lavas in Munro Township, Economic and Tectonic Implications Metallogeny and Plate Tectonics; Ed. by D.F. Strong, Geological Association of Canada, Special Paper 14, pp617-658

———— (1977): Thick, Layered Peridotite-Gabbro Lava Flows in Munro Township, Ontario. Can. Jour. of Earth Science, Vol. 14, No 11, p2620-2637

Atherton, M.P. (1968): The Variations in Garnet, Biotite and Chlorite Composition in Medium Grade Rocks from the Dalradian, Scotland with Particular Reference to the Zonation in Garnet, Contr. Min. and Pet. V. 18, p347-371

Barrett, F.M., Binns, R.A., Groves, D.I., Marston, R.J., and McQueen, K.G. (1977): Structural History and Metamorphic Modifications of Archean Volcanic-Type Nickel Deposits, Yilgarn Block, Western Australia. Econ. Geol. V. 72, P1195-1123

Barton, P.B. Jr and Toulmin P. III, (1966): Phase Relations Involving Sphalerite in the Fe-Zn-S System. Econ. Geol, V. 61, p815-849

Bowdidge C. (1970): Petrography of the Kapkichi Lake, Copper-Nickel Deposits and Associated Rocks, Pickle Lake Area, North-West Ontario. T0196 UMEX Internal Report, 23pp

Brett, P.R. (1964): Experimental Data from the System Cu-Fe-S and their Bearing on Exsolution Textures in Ores, Econ. Geol. V. 59, p1241-1269

Buddington, A.F. and Lindsley, D.H. (1964): Iron-Titanium Oxide Minerals and Synthetic Equivalents. Jour. of Pet. Vol 5, p310-348

Cabri, L.J. and Pickwick, K.M., (1974): A Complex Bismuthian Palladium Telluride Intergrowth from Stillwater Complex, Montana. Jour. of Pet. Vol. 69, pp263-274

Chamberlain, J.A. (1967): Sulfides in the Muskox Intrusion. Can. Jour. of Earth Science Vol. 4, p105-153

Cousins, C.S. and Vermaak, C.F. (1976): The Contribution of Southern African Ore Deposits to the Geochemistry of the Platinium Group Metals. Econ. Geol. Vol. 71, p. 287-305

Craig, J.R. (1973): Pyrite-Pentlandite and other Low-Temperature Relations in Fe-Ni-S System. Amer. Jour. of Science, Vol. 273A, p496-510

_____ and Higgins, J.B. (1975): Cobalt-and-Iron-Rich Violarites from Virginia.. Amer.Min., Vol. 60, No. 1-2, p35-38

_____ and Kullerud, G. (1969): Phase Relations in the Cu-Fe-Ni-S System and their Application to Magmatic Ore Deposits: in H.D.B. Wilson Ed., Magmatic Ore Deposits: Econ. Geol. Mono. 4, pp344-358

_____ and Scott, S.D. (1974): Sulfide Phase Equilbria, in Sulfide Mineralogy, ed Ribbe, P.H.: Mineralogic Society of America, Short Course Notes, VI, PCS 1 to CS 110

Desborough, G.A. and Czamanske, G.K. (1973): Sulfides in Eclogite Nodules from a Kimberlite Pipe, South Africa with Comments on Violarite Stoichiometry; Amer. Min. Vol. 58, p195-202

Eckstrand, O.R. (1975): The Dumont Serpentinite a Model for Control of Nickeliferous Opaque Mineral Assemblages by Alteration Reactions in Ultramafic Rocks, Econ. Geol. Vol. 70, p183-201

Erd, R.C., Evans, H.T., and Richter, D.H., (1957): Smythite, A New Iron Sulfide and Associated Pyrrhotite from Indiana: Amer. Min. Vol. 42, p309-333

Ernst, W.G. (1968): Amphiboles, Crystal Chemistry, Phase Relations and Occurrence, Springer-Velag, New York pp132

Evans, B.W., and Trommsdorff, V. (1970): Regional Metamorphism of Ultramafic Rocks in the Central Alps, Parageneses in the System CaO-MgO-SiO_2-H_2O, Schweiz Mineral Petrogr. Mitt. 50, p480-492

_____ (1974): Stability of Enstatite Plus Talc and Co_2 Metasomatism of Metaperidotite Val D'Efra, Leponţine Alps, Amer. Jour. Sci. Vol. 274, p274-296

Ewers, W.E., and Hudson, R.D. (1972): An Interpretive Study of a Nickel-Iron Sulfide Ore Intersection Lunnon Shoot, Kambalda, Western Australia: Econ. Geol, V. 69, p1075-1092

Ewert, W.D. (1977): Metamorphism of Siliceous Carbonate Rocks in the Grenville Province of Southeastern Ontario. Carleton University, PhD Thesis

Ferguson, S.A. (1966): Geology of Pickle Crow Gold Mines Limited and Central Patricia Gold Mines Limited, No. 2 Operation. Misc. Paper MP-4, Nov. 1966, Ontario Dept. of Mines

Froese, E. and Gunter, A.E. (1976): A note on the Pyrrhotite-Sulfur Vapour Equilibrium. Vol. 72, p1589-1594

Goldman, D.S. and Albee, A.L. (1976): Correlation of Mg/Fe Partitioning between Garnet and Biotite with O^{18}/O^{16} Partitioning between Quartz and Magnetite: Amer. Min. (Prepub. Copy)

Goldsmith, J.R., Graf, D.L., and Joensuu, O.I. (1955): The Occurrence of Magnesian Calcites in Nature; Geochem. et Cosmochim Acta, Vol. 7, pp212-230

_____ and Heard, H.C., (1961): Subsolidus Phase Relations in the System $CaCO_3$-$MgCO_3$; Jahrb. Geol., Vol. 69, pp45-74

Goodwin, A.M. (1976): Lithologic and Major Element Compositions Superior Geotraverse: in Proceedings of the 1976 Geotraverse Conference

Gorbatschev, A. (1968): Distribution of Elements between Cordierite, Biotite and Garnet: Neues Jahrb. Mineralogie. Vol. 110, p.57-80.

Graf, D.L. and Goldsmith, J.R. (1955): Dolomite-Magnesian Calcite Relations at Elevated Temperatures and CO_2 Pressures; Geochem. et Cosmochim Acta, Vol. 7, pp109-128

_____ (1958): The Solid Solubility of $MgCO_3$ in $CaCO_3$: a revision; Geochim. et Cosmochm. Acta, Vol. 13, pp218-219

Graterol, M. and Naldrett, A.J. (1971): Mineralogy of the Marbridge No. 3 and No. 4 Nickel-Iron Sulfide Deposits, Econ. Geol., Vol. 66, pp886-900

Green, J.C. and Schulz, K.J. (1977): Iron-Rich Basaltic Komatiites in the Early Precambrian Vermilion District, Minnesota, Can. Jour. Earth Sci., Vol. 14, No. 10

Ghent, E.E. (1977): Application of Activity-Composition Relations to Displacement of a Solid-Solid Equilbrium Grossular=Anorthite + Quartz; in MAC Short Course in Application of Thermodynamics to Petrology and Ore Deposits, ed. H.J. Greenwood

Groves, D.I., Hudson, D.R. and Hack, T.B.C. (1974): Modification of Iron-Nickel Sulfides during Serpentinization and Talc-Carbonate Alteration at Black Swan, Western Australia. Econ Geol., Vol. 69, p1265-1281

Harker, R.I., and Tuttle, O.F. (1955): Studies in the System CaO-MgO-CO_2. Part 2. Limits of Solid Solutions along the Binary Join $CaCO_3$-$MgCO_3$. Amer. Jour. Sci. Vol. 253, p274-282

Helgeson, H.C., Delany J.M., Nesbitt, H.W. and Bird, D.K (1978): Summary and Critique of Thermodynamic Properties of Rock-Forming Mineral. Amer. Jour. Sci. Vol. 278A, 229p

Hurst, M.E. (1930): Pickle Lake-Crow River Area, District of Kenora (Patricia Portion); Accompanied by Map 39a ODM. Vol. XXXIX, pt 2, p1-35

Hutcheon, I, (1977): The Metamorphism of Sulfide-Bearing Pelitic Rocks from Snow Lake, Manitoba. PhD Thesis Carleton University.

Hyndman, D.W. (1972): Petrology of Igneous and Metamorphic Rocks, McGraw-Hill Book Company, New York.

Irvine, T.N. and Baragar, W.R.A. (1971): A Guide to the Chemical Classification of the Common Volcanic Rocks. Can. Jour. Earth Sci. Vol. 8, p523-547.

Johannes, W. (1969): An Experimental Investigation of the System $MgO-SiO_2-H_2O-CO_2$ Amer. Jour. Sci. Vol. 267, p1083-1104

Keays, R.R., and Crocket, J.H. (1970): A Study of Precious Metals in the Sudbury Nickel Irruptive Ore: Econ. Geol. Vol. 65, p438-450

Keele R.A. and Nickel, E.H. (1974): The Geology of a Primary Millerite-Bearing Sulfide Assemblages and Supergene Altération at the Otter Shoot, Kambalda, Western Australia. Econ. Geol., Vol. 69, p1102-1117

Kelly, W.C., and Clarke, B.R. (1975): Sulfide Deformation Studies III Experimental Deformation of Chalcopyrite to 2000 bars and 500°C. Econ Geol. Vol. 70, p431-453

Kennedy P. (1978): Personnal Communication Umex Mine Geologist, Thierry Mine

Kerrich, R., Fyfe W.S., Gorman, B.E. and Allison I, (1977): Local Modification of Rock Chemistry by Deformation Contrib. Min. Petrol, Vol. 65, p183-190

Kingston, G.A. (1966): The Occurrence of Platinoid Bismutho-Tellurides in the Merensky Reef at Rustenburg Platinium Mine in the Western Bushveld: Min. Mag. Vol. 35, p815-834

Kullerud, G., (1969): Cubic Hexagonal Inversions in some M_3S_4- Type Compounds. Carnegie Inst. Wash. Year Book, Vol. 67, p179-182

_____ Yund, R.A. and Moh, G.H. (1969): Phase Relations in the Cu-Fe-S, Cu-Ni-S and Fe-Ni-S System in H.D.B. Wilson, Ed., Magmatic Ore Deposits Econ. Geo. Mono. 4, p323-343.

Leatherbarrow, B. (1977): Personnal Communication

Lefebvre, J. (1977): Personnal Communication, Research Geologist UMEX

(1977b): Preliminary Research on Localization of Precious Metals in the Ore of the Thierry Mine, UMEX Memo TOR/INTER 129

Lyons, J.B. and Morse, S.A., (1970): Mg/Fe Partioning in Garnet and Biotite from some Granitic, Pelitic and Calcic Rocks. Amer, Min. Vol. 55, p231-245

McCallum, M.E., Loucks, R.R., Carlson, R.R., Cooley, E.F., and Doerge, T.A. (1976): Platinum Metals Associated with Hydrothermal Copper Ores of the New Rambler Mine, Medicine Bow Mountains, Wyoming. Econ. Geol. Vol. 71, p1429-1450

McInnes, W. (1912): Report of the North-West Territories of Canada Drained by the Winisk and Attawapiskat Rivers Accompanied by Map of the District of Patricia, Province of Ontario. Ontario Bur. Mines, VXXI, pt. 2, p108-130

Mihalik, P., Jacobsen, J.B.E. and Hiemstra, S.A. (1974): Platinium-Group Minerals from a Hydrothermal Environment: Econ. Geol., Vol. 69, p257-262

Misra, K.C. (1973): The Chemical Compositions of Synthetic and Natural Pentlandite Assemblages. Econ. Geol. Vol. 68, p518-539
and Fleet, M.E. (1974): Chemical Composition and Stability of Violarite. Econ. Geol. Vol. 69, p391-403

Miyashiro, A. (1961): Evolution of Metamorphic Belts. Jour. Pet. Vol. 2, p277-311
(1973): Metamorphism and Metamorphic Belts. George Allen and Unwin Ltd., London, pp492

Moore, R.L., (1976): Metamorphic Petrology of the Area between Mattawa, North Bay and Temiscaming, Ontario. PhD Thesis, Carleton University.

Morton, P. (1978): Personnal Communication
and Watkinson, D. (1974): Ore Mineralogy of the Thierry Mine, Preliminary Report UMEX

Naldrett, A.J. and Cabri, L.J. (1976): Ultramafic and Related Mafic Rocks: Their Classification and Genesis with Special Reference to the Concentration of Nickel Sulfides and Platinium-Group Elements. Econ. Geo. Vol. 71, p1131-1158

Nickel, E.H. (1972): Nickeliferous Smythite from some Canadian Occurrences, Can. Min. VII, p514-519

Nickel, E.H., Ross, J.R. and Thornber, M.,R. (1974): The Supergene Alteration of Pyrrhotite-Pentlandite Ore at Kambalda, Western Australia. Econ. Geol. Vol. 69, pp83-107

Patterson, G.C. (1974): Distribution of Chlorine in Ultrabasic Rocks, MSc Thesis, University of Toronto

Pshenichnii, G.N. (1961): Mode of Occurrence and Distribution Pattern of Tellurium in Sulfide Ores, Geochemistry, No. 8, p751-762

Ragan, D.M. (1973): Structural Geology, An Introduction to Geometrical Techniques, 2nd Edition, pub. John Wiley and Sons, New York, pp207

Richardson, S.W., Gilbert, M.C. and Bell, P.M. (1969): Experimental Determination of Kyanite-Andalusite and Andalusite-Sillimanite Equilibria; The Aluminum Silicate Triple Point. Amer. Jour. Sci. 267, p259-272

Robie, R.A. and Waldbaum, D.R. (1968): Thermodynamic Properties of Minerals and Related Substances at 298.15°C, 25°C and one atmosphere, 1.013 bars Pressure and at Higher Temperatures. U.S. Geol. Survey Bull 1259, p256

Ross, J.R. and Hopkins, G.M. (1975): The Nickel Sulphide Deposits of Kambalda, Western Australia, in Knight C.L. ed., Economic Geology of Australia and Papua-New Guinea I. Metals: Melbourne, Australasian Inst. Mining Metallurgy, p100-121

Sage, R.D. and Breaks, F.W. (1976): Open File Report 5180, Operation Pickle Lake Districts of Kenora, Patricia Portion, Thunder Bay, O.D.M.

Saxena, S.K., (1969): Silicate Solid Solutions and Geothermometry 3. Distribution of Fe and Mg between Coexisting Garnet and Biotite. Contr. Min. and Petr. Vol. 22, p259-267

Scott, S.D. (1973): Experimental Calibration of the Sphalerite Geobarometer. Econ. Geol. Vol. 68, pp466-474

Scott, S.D. and Barnes, H.L. (1971): Sphalerite Geothermometry and Geobarometry. Econ. Geol. 66, p653-669

Skinner, B.J., Luce, F.D., Dill, J.A., Ellis, D.E., Hagan, H.A., Lewis, D.M., Odell, D.A., Sverjensky, D.A., and Williams, N.: Phase Relations in Ternary Portions of the System Pt-Pd-Fe-As-S, Econ. Geol., pp1469-1475 (1976)

Shido, F. (1958): Plutonic and Metamorphic Rocks of the Nakoso and Iritono Districts in the Central Abukuma Plateau, Tokyo Univ. Fac. Sci. Jour., Sec. 2, Vol. 11, p131-217

Stanton, R.L. (1972): Ore Petrology, pub. McGraw-Hill Book Company, New York, pp713

Storre, B. and Nitsch K.H (1972): The Reaction: 2 ZOISITE + $1CO_2$ = 3 ANORTHITE + 1 CALCITE + $1H_2O$ Contr. Min. and Petr, Vol. 35, p1-10, (ENG. Abstract)

Taylor, L.A. and Williams, K.L. (1972): Smythite, $(Fe,Ni)_9S_{11}$, A Redefinition, Amer. Min. Vol. 57, p1571-1577

Thompson, A.B. (1976): Mineral Reactions in Pelitic Rocks II. Calculation of some P-T- X (Fe-Mg) Phase Relations. Amer. Jour. of Sci., Vol. 276, No. 4, p425-454

Thomson, J.E. (1938): The Crow River Area; Accompanied by map 47b; ODM Vol. XLVIII, pt 3, p1-65

Thurston, P.C. and Breaks, F.W. (1978): Metamorphism and Tectonic Evolution of the Uchi-English River Subprovince, in Metamorphism in the Canadian Shield, ED. Fraser, J.A. Geo. Survey Paper 78-10, p49-62

Turner, F.J., and Hutton, C.O. (1936): Metamorphic Zones in North-West Otago. Trans. Roy. Soc. New Zealand, Vol. 65, p405-451

_____ and Verhoogen, J. (1960): Igneous and Metamorphic Petrogy. pub. McGraw-Hill, New York, 694pp

Verbeek, T: Dehenne R., and Bowdidge, C. (1972): Geophysical Case-History: The Thierry Copper-Nickel Deposit in Northwestern Ontario, Canada. 24th IGC, Section 9, p135-151

Viljoen, R.P. and Viljoen, M.J. (1969): The Geological and Geochemical Significance of the Upper Formation of the Onverwacht Group. Geol. Soc. of S.A., Spec. Pub. 2, pp113-151

Vokes, F.M., (1967): Linnaeite from the Precambrian Raipas Group of Finnmark, Norway; Min. Dep. V. 2, p11-25

Wager, L.R. and Brown, G.M. (1968): Layered Igneous Rocks, pub. Oliver and Boyd, London, 588pp

Watmuff, I.G., (1974): Supergene Alteration of the Mt. Windarra Nickel Sulphide Ore Deposit, Western Australia. Mineral Deposita, Vol. 9, p199-221

Wells, G., Grant A. Pearce, T.H. and Roeder P.L. (1977): Archean Pillow Lavas from the Pickle Crow and Noranda Areas. in Proceedings of the 1977 Geotraverse Conference.

Wilson, H.D.B., and Anderson, D.T. (1959): The Composition of Canadian Sulfides Ore Deposits: Can. Inst. Min. Met. Trans., Vol. 62, p327-339

Winkler, H.G.F. (1976): Petrogenesis of Metamorphic Rocks. 4th edition, pub. Springer-Verlag, New York pp334

Yoder, H.S. Jr. (1968): Hydrous Systems. Carnegie Institution, Annual Report (1968) of the Director Geophysical Lab.

11.0 Appendices, Table of Contents

Appendix A. Modal Composition of rocks from the Kapkichi Lake Area 216-243

11.1 Amphibolite Descriptions 217-220

11.2 Metasediments Descriptions 221-222

11.3 Table 1. Modes of Rocks from the Thierry Mine Area 223-225

Table 2. Modes of Rocks from the J+I and G um-m body 226-228

Table 3. Modes of Rocks from the K1:1 um-m body 229-230

11.4 Geothermometer and Geobarometer 231-243

11.4.1. Garnet-Biotite Geothermometer 231-234

11.4.2. Calcite-Dolomite Geothermometer 235-236

11.4.3. Magnetite-ilmenite Geothermometer 237-239

11.4.4. Garnet-Plagioclase Geobarometer 240-241

11.4.5. Sphalerite-Pyrite-Pyrrhotite Geobarometer 242-243

Appendix B. Modes of Polished Sections 244-257

Table 1. Abbreviations used in descriptions of polished sections 245

Table 2a Modes of polished sections, K1:1 um-m body 246

Table 2b Modes of polished sections, G um-m body 247

Table 2c Modes of polished sections, J+I um-m body 248-252

Table 2d Modes of polished sections, Thierry Mine, um-m body 253-257

Appendix C. Electron Microprobe Analyses of Sulfides 258-275

11.5 Methods used and detection limits 259

Table 1. Electron Microprobe analyses of sulfides in C.B.S. ore. 260-262

Table 2. Electron Microprobe analyses of sulfides in Breccia ore 263-267

Table 3. Electron Microprobe analyses of sulfides in Bornite ore 268-269

Table 4. Electron Microprobe analyses of sulfides in Altered Breccia Ore 270-271

Table 5. Electron Microprobe analyses of sulfides in Primary Disseminated sulfides 272-273

Table 6. Electron Microprobe analyses of Ag-Pd-Pt minerals 274-275

Appendix D. Electron Microprobe Analyses of Silicates and Oxides 276-288
Table 1. Electron Microprobe Analyses of clinopyroxene, Thierry Mine 277
Table 2. Electron Microprobe Analyses of metamorphic olivine, Thierry Mine 278
Table 3. Electron Microprobe Analyses of igneous olivine remnants, Thierry Mine 279
Table 4. Electron Microprobe Analyses of hornblende, Thierry Mine 280-282
Table 5. Electron Microprobe Analyses of plagioclase in pelites 283
Table 6. Electron Microprobe Analyses of garnets in pelites 284
Table 7. Electron Microprobe Analyses of biotites in pelites 285
Table 8. Electron Microprobe Analyses of green spinels from K31-1005, G um-m body 286
Table 9. Electron Microprobe Analyses of magnetites from K31-1005, G um-m body 287
Table 10 Electron Microprobe Analyses of ilmenites from K31-1005, G um-m body 288

Appendix E. Whole Rock Chemistry 289-307
11.6 Methods used 290
Table 1 Chemical Labs and Analytical procedure
Table 2a Whole Rock Analyses Thierry Mine, C.B.S. 291
Table 2b Whole Rock Analyses Thierry Mine, ultramafic and mafic metagabbro 292-293
Table 2c Whole Rock Analyses, Thierry Mine, Amphibolite schist 294
Table 3a Whole Rock Analyses from K1:1 ultramafic body, ultramafic rocks with blackwall alteration 295-296
Table 3b Whole Rock Analyses from K1:1 ultramafic body metagabbro and mafic metagabbro 297-299
Table 4 Whole Rock Analyses from J+I um-m body 300
Table 5 Whole Rock Analyses from G um-m body 301

Table 6a Trace element analyses from the Thierry Mine 302-304
Table 6b Trace element analyses from K1:1 um-m body 305
Table 6c Trace element analyses from J+I-um-m body 306
Table 6d Trace element analyses from G um-m body 307

Appendix F Mine Sections 308-331

Table 1 Key to drill hole numbers 309
Table 2 Drill holes used to construct geologic sections 310-314
Table 3 Drill holes logged by author 315-317

Location of Sections
Geologic Interpretation of section 90E, 0-2000 level 319
Geologic Interpretation of section 95E, 0-2000 level 320
Geologic Interpretation of section 98E, 0-800 level 321
Geologic Interpretation of section 98E, 0-2200 level 322
Geologic Interpretation of section 101E 0-800 level 323
Geologic Interpretation of section 101E 0-2200 level 324
Geologic Interpretation of section 103E 0-800 level 325
Geologic Interpretation of section 103E 0-2200 level 326
Geologic Interpretation of section 105E 0-800 level 327
Geologic Interpretation of section 105E 0-2200 level 328
Geologic Interpretation of section 110E 0-2000 level 329
Geologic Interpretation of section 115E 0-2000 level 330
Geologic Interpretation of section 120E 0-2000 level 331

Appendix A Modal Composition of Rocks from Kapkichi Lake Area.

11:1, Amphibolite Descriptions

1) Banded Amphibolite Schist

Banded amphibolite schist is the most common type of amphibolite in the region, making up 80% of the mafic volcanic rocks. In drill core, it grades into epidote amphibolite schist and porphyroblastic amphibolite. The banded amphibolite is dark grey-green and weathers grey in outcrop. It is medium-to fine-grained, strongly foliated and commonly lineated. It consists of 50% to 60% prismatic hornblende crystals and 40 to 50% plagioclase. Banding is due to 1mm to 1cm layers rich in either hornblende or plagioclase. Individual layers can be traced up to three metres in outcrop. Rare round red garnets up to 5mm in diameter occur at the cores of elongated feldspathic patches.

In thin section, the amphibolite shows a nematoblastic to granoblastic fabric. The hornblende (X: pale yellow, Y: pale green, Z: blue-green; $Z \wedge c = 18^{\circ}$, $2V_x = 80^{\circ}$) in the felsic layers forms prismatic crystals defining a strong foliation. In the mafic layers, the hornblende forms subequant, subhedral crystals with a much weaker preferred orientation than those in the felsic layers. The hornblende in mafic layers is typically poikiloblastic containing inclusions of plagioclase and smaller hornblende crystals (Plate 3C).

The plagioclase has recrystallized to polygonal aggregates with the individual grains showing strong oscillatory zoning. They are An_{30} at the core and having alternating zones of An_{20}. Garnet is rimmed by plagioclase, quartz and rarely biotite. Most speciments contain minor quartz, potassic feldspar and accessory apatite, sphene, magnetite and ilmenite. Plagioclase is partially altered to sericite and epidote, and hornblende to chlorite and epidote. Biotite and chlorite are common near shears and contacts with dykes.

ii) Massive Amphibolite

The massive amphibolite occurs as narrow bands within the banded amphibolite schist. The contacts between the two are parallel to or sharply cross-cut the foliation. In handspecimen, the massive amphibolite is dark green, fine-grained, composed of 50% hornblende and 50% plagioclase. In thin section some samples contain up to 10% sphene as small round masses. The plagioclase is An_{30} in sphene-poor samples and An_{60} in sphene-rich samples. These amphibolites are interpreted as mafic dykes and sills.

iii) Porphyroblastic Amphibolite

Porphyroblastic amphibolite makes up 2% of the mafic volcanics in the area. It is interbanded with felsic volcanics as layers up to 12 metres thick. In handspecimen the rock is green, medium-grained, massive to moderately well foliated and composed of 50 to 60% hornblende and 40 to 50% plagioclase. Hornblende occurs as groups of crystals whose maximum length is 3mm elongated parallel to the foliation.

In thin section, the larger crystals of hornblende are commonly zoned with rims less intensely coloured than cores. The hornblende often contains very fine exsolved colourless amphibole, probably tremolite. The plagioclase is polygonally recrystallized and zoned as in the banded amphibolite. Plagioclase is increasingly calcic with the amount of accessory epidote and attains the composition An_{40} in epidote-rich samples. Accessory minerals are sphene, magnetite and ilmenite.

iv) Epidote-Amphibolite Schist

The epidote-amphibolite schist makes up about 10% of the amphibolites in the area and is associated with sediments and tuff. It is well foliated, fine-to medium-grained, light green, with layers 1 to 10mm wide. The layers are composed of 50% epidote, 25% hornblende, 25% plagioclase; and 50% hornblende, 50% plagioclase. Diopside occurs as a minor mineral in the epidote-rich layers.

In thin section the epidote is porphyroblastic including plagioclase; commonly with an hour-glass structure and concentric zoning. Minor accessory minerals are sphene, apatite and biotite.

v) Epidote-Carbonate Amphibolite Schist

The epidote-carbonate amphibolite schist occurs near contacts with granites, fault and shear zones. A wide zone of epidote-carbonate schist is associated with the hornblende-chlorite-biotite schist in the Thierry Mine. The epidote occurs as pods and lenses with carbonate (calcite and dolomite) in banded amphibolite. In outcrop the epidote lenses are zoned, with epidote-carbonate at the core rimmed by plagioclase. The lenses are up to 4 metres by 10cm and elongated parallel to foliation. The plagioclase is polygonally recrystallized and shows oscilatory zoning. Plagioclase in the epidote lenses is An_{60}, those in the hornblende-rich section are An_{20} to An_{30}.

11:2, Metasediments

i) Biotite-Garnet-Sillmanite-Staurolite Schist

The biotite-garnet-sillmanite-staurolite schist is interpreted as a pelite. The pelite is associated with a tuffaceous unit to the west of the mine. In handspecimen it is grey, fine-grained, well foliated, with layers rich in garnets. In thin section the garnet-rich layers contain sillimanite and staurolite. The garnets have felsic coronas of quartz and feldspar and contain inclusions of quartz and sillmanite (Plate 3A). Minor K-feldspar occurs in the biotite-rich layers. Staurolite occurs as irregular porphyroblasts with quartz inclusions. The rock is composed of 30% biotite, 30% plagioclase, 10% quartz, 20% garnet, 10% sillmanite and 1% staurolite. Accessory minerals are magnetite as coarse porphyroblasts, zircon and sphene.

ii) Calc-silicate Gneiss

The calc-silicate rocks (Plate 3B) commonly contain garnet (as porphyroblasts up to 2cm in diameter), epidote, biotite, actinolite, hornblende, plagioclase, quartz, carbonate (calcite and dolomite) and rarely lizardite plus talc pseudomorphic after diopside. The calc-silicate gneiss is commonly banded with layers rich in plagioclase plus quartz, epidote plus carbonate and garnet plus carbonate. The layers are sharply defined from 2cm to 1 metre in thickness. The garnet contains inclusions of carbonate and epidote.

The carbonate commonly forms a mosaic with actinolite in the triple junctions. Staining with alizarin red shows a fine exsolution of dolomite in calcite. The epidote forms irregular porphyroblasts with compositional zoning (hourglass structure) and inclusions of carbonate. Plagioclase has a composition of An_{30}.

iii) Graphitic Schist

The graphitic schist occurs as conformable bands associated with other metasediments, 750 metres south of K1:1 and as a 300m thick lens near the western margin of the belt. Both occurrences have 20 to 50% pyrite and pyrrhotite as rounded pods elongated parallel to foliation and massive layers up to 10cm in thickness containing 25-45% graphite, 15-20% quartz, 10-20% plagioclase and 10-20% hornblende. In handspecimen the graphitic schist is black and well foliated.

Table 1, Modes of Rocks from the Thierry Mine Area.

olivine	augite	tremolite	hornblende	cummingtonite	talc	chlorite	Mg-chlorite	lizardite	biotite	plagioclase	K-feldspar	carbonate	sphene	quartz	epidote	thin section number	rock type
			60						tr	30				10		Th-1	amphibolite schist
			70	1					15	5						Th-2	amphibolite schist
			60			30			1	10				tr		Th-3	mafic rock
			95			5				tr		tr				Th-4	mafic rock
			40						20	40			tr			Th-5	metagabbro
			50							50			tr		tr	Th-6	metagabbro
			15			5			5							Th-7	massive sulfides
			~~60~~							45			tr	5	tr	Th-8	metagabbro
			20	10					30					35		Th-9	chlorite-biotite sch.
			10			40			20			tr		30	2	Th-10	chlorite-biotite sch.
			60							40					tr	Th-11	metagabbro
			60	tr					10	30						Th-12	metagabbro
			50	tr		tr			30	20				10		Th-13	metagabbro
					80	tr						10				Th-14	talc-carbonate sch.
			15			80										Th-15	chlorite-biotite sch.
			70	tr						10		tr		tr	20	Th-16	metagabbro
			70							30			tr			Th-17	metagabbro
			30							50			tr		tr	Th-18	metagabbro
		15			60	25						tr				Th-19	talc-chlorite schist
			60							35				5	tr	Th-20	amphibolite schist
			70			15				10					tr	Th-21	mafic rock
			35	15	tr	tr			40	5	2					Th-22	metagabbro
			18			60				tr				20		Th-23	chlorite-biotite sch.
			35						tr	40			tr			Th-24	diorite
30					40	10		tr								Th-25	ultramafic rock
	10		75	tr								tr		tr		Th-26	mafic rock
			40			20			40				tr			Th-27	chlorite-biotite sch.
			20			50								20		Th-28	chlorite-biotite sch.
			40	10					40	10			tr			Th-29	chlorite-biotite sch.
			60							30		tr		10	tr	Th-30	amphibolite schist
			35	5					35	tr				20		Th-31	chlorite-biotite sch
			30	5					40					1		Th-32	chlorite-biotite sch.
									95							Th-33	mafic rock
		99														Th-34	mafic rock
		70				20										Th-35	mafic rock
			70							25	2			tr	tr	Th-36	metagabbro
			70			tr	30							tr		Th-37	sheared mafic
			64							30		1	tr	tr	5	Th-38	m. amphibolite
			85	13		2			tr		tr					Th-39	sheared mafic rock
			60							20				20		Th-40	amphibolite schist

Table 1 (continued). Modes of Rocks from the Thierry Mine Area

olivine	augite	tremolite	hornblende	cummingtonite	talc	chlorite	Mg-chlorite	lizardite	biotite	plagioclase	K-feldspar	carbonate	sphene	quartz	epidote	thin section number	rock type
			35	tr					20	30				15		Th-41	metagabbro
			97						tr	2				tr		Th-42	mafic rock
		5	60						20	10				5		Th-43	mafic rock
			60							30			2	8		Th-44	massive amphibolite
		1	2							90				8		Th-45	diorite
			20			30				tr				50		Th-46	chlorite-biotite schist
			99			tr			tr	tr			tr		1	Th-47	mafic rock
			98							tr		tr	tr	tr	tr	Th-48	mafic rock
			45			tr				15				10	30	Th-49	epidote-plag. vein
			95			3			tr	2			tr			Th-50	mafic rock
			25	30		40			5	1				1		Th-51	sheared ultramafic rock
			70						tr	30					tr	Th-52	ultramafic rock
			65	tr						18				2	20	Th-53	massive amphibolite
			90	tr		9				tr				tr	tr	Th-54	mafic rock
			98			1				1				tr		Th-55	mafic rock
			10	30		40				10					tr	Th-56	sheared mafic rock
			40			tr				20		tr		tr	40	Th-57	amphibolite schist
			60							39					1	Th-58	amphibolite schist
			30	38		30			2	tr				tr		Th-59	sheared mafic rock
			60							38				tr	2	Th-60	amphibolite schist
			60						tr	40						Th-61	metagabbro
			40							50		tr		10	tr	Th-62	metagabbro
									3	75	10		tr	15	2	Th-63	aplite
			60							35		tr	tr	5	tr	Th-64	amphibolite schist
			50						5	40			tr	tr	tr	Th-65	diorite
			5							30				tr	tr	Th-66	massive sulfides
			70							30			tr	tr		Th-67	metagabbro
			39							30	10		tr	25	1	Th-68	granite
			50			20						tr			20	Th-69	epidote-chlorite schist
			68							30			1	1		Th-71	P.amphibolite
			70							20		2		5	3	Th-72	amphibolite schist
																Th-73	mafic rock
	15	55				tr		20									
			40							5		tr		15	40	377	amphibolite schist
			40							50			5	5	tr	376	amphibolite schist
			40							55			tr	tr	tr	375a	metagabbro
			30							10	30	tr,	tr	30		375b	amphibolite schist
			75		2	3				tr				15		374	mafic rock
			50							50			tr		tr	373	amphibolite schist
			20	10		55										372	chlorite-biotite schist

Table 1 (continued), Modes of Rocks from the Thierry Mine Area.

olivine	augite	tremolite	hornblende	cummingtonite	talc	chlorite	Mg-chlorite	lizardite	biotite	plagioclase	K-feldspar	carbonate	sphene	quartz	epidote	thin section number	rock type
			5	20		25			25	tr				tr		371	chlorite-biotite schist
			85			12				tr				tr		370	sheared mafic rock
			40	tr		45				5				10		369	chlorite-biotite schist
			40		tr	tr				20		tr	tr	tr	40	368	epidote amphibolite
			5	80		15										367a	sheared mafic rock
			tr	70		20				tr						367b	sheared mafic rock
				25		10								5		366	breccia sulfides
			30			40			tr					10		365	chlorite-biotite schist
			10	25		25			25							364	chlorite-biotite schist
			50	35		tr				5						363	breccia sulfides
			65	5		20				5						361a	breccia sulfides
			40	10		15				10				tr		361b	breccia sulfides
			85	tr		12								tr	tr	360	sheared mafic rock
			60							20					20	359	amphibolite schist
			45							30			tr		5	358	metagabbro
			15						tr	60	15	tr		5	tr	357	diorite
			96						tr			tr		1	3	356	mafic rock
			30							tr		5		5	10	355	massive sulfides
			90						8				tr		tr	354	mafic rock
			99						1							353	mafic rock
			65							10	tr	20		tr	tr	352	mafic rock
			75									2				350	mafic rock
			75			25								tr	tr	349	sheared mafic rock
			5	30		25			5							348	breccia sulfides
			30	tr		tr			tr	tr				tr		347	sheared mafic rock
			60							40						336	metagabbro
			5			9 5										327	chlorite schist

Table 2. Modes of Rocks from the J-I and G ultramafic Area.

olivine	augite	hypersthene	tremolite	anthophyllite	hornblende	cummingtonite	talc	chlorite	Mg-chlorite	Ilmenite	biotite	plagioclase	K-feldspar	carbonate	sphene	quartz	epidote	thin section number	rock type
					5						5	20	50		tr	20	tr	59	granite mylonite
			50					20	30					tr				60	ultramafic rock
			1	50					48									61	ultramafic rock
40		10	20	10				20		5								62	ultramafic rock
									70		30							63	biotite-chlorite sch.
70		10		5					5		10			tr				64	ultramafic rock
25				25					48		tr			1				65	ultramafic rock
			60		10			25	5			tr						66	ultramafic rock
			50					2	48									67	ultramafic rock
5			45						45	2				3				68	ultramafic rock
					50							30			2		15	69	metagabbro
					tr						10	55	25		tr	5	5	79	biotite schist
					40							15			tr	5	40	80	ep. amphibolite
					25							15			tr	10	50	81	ep. amphibolite
					28							20		2	tr	10	45	82	ep. amphibolite
					60							40						83	amphibolite
					55							30					tr	84	amphibolite schist
1									90	5				4				86	ultramafic rock
			20	10			5		50					15				87	ultramafic rock
30		tr		35					30					tr				88	ultramafic rock
5			45						30	15								89	ultramafic rock
						2						50	30	tr	tr	18	tr	91	granodiorite
	15		68									15						92	metagabbro
50	24		15					tr	10		tr	1						93	ultramafic rock
					2			tr				80	18	tr		2	tr	94	monzodiorite
			20					40			40	tr						95	ultramafic rock
					60							40					tr	96	metagabbro
			50					25	25									97	ultramafic rock
			40				2		43									98	ultramafic rock
			50						10			30						99	metagabbro
			30						5		25			tr				100	ultramafic rock
	35				55							10						101	metagabbro
					15				tr		10	65		tr		10		102	diorite
			25					30	25					tr				103	ultramafic rock
30			5	30			tr		30	tr								104	ultramafic rock
												85	5			10		105	diorite
					60				30									106	mafic rock
					60							30			tr	10	tr	107	amphibolite schist
					30							20			tr	10	40	108	ep. amphibolite
	35				65									tr	tr		tr	109	mafic rock
			15					80			5			tr				110	ultramafic rock
					85			15										111	mafic rock
			60					35						2				296	ultramafic rock
			55					10	30					tr				297	ultramafic rock
60	5		10						10	15				tr				298	ultramafic rock
30			30					5	10	20								299	ultramafic rock

Table 2 (continued), Modes of Rocks from the J-I and G Ultramafic Area

olivine	augite	hyperstene	tremolite	anthophyllite	hornblende	cummingtonite	talc	chlorite	Mg-chlorite	lizardite	biotite	plagioclase	K-feldspar	carbonate	K-spar	carbonate	sphene	quartz	epidote	thin section number	rock type
					70			20			tr		tr							300	mafic rock
			20		40			40												301	mafic rock
3	15	2	tr		50		12					20								302	metagabbro
5			30		40					20				tr						303	mafic rock
20	tr		30				10	10	20	tr		10		tr						304	metagabbro
35								tr	5	40				tr						305	ultramafic rock
15		5	75				5													306	ultramafic rock
tr			50						45											308	ultramafic rock
20	tr		40	20				20	tr											309	ultramafic rock
5			65					tr		30										310	ultramafic rock
5			14	60						tr		20								311	metagabbro
30								tr	10	35		20								312	ultramafic rock
2			50				15		30	tr										313	ultramafic rock
10	tr		30				27		30											314	ultramafic rock
			60		10			30												315	mafic rock
					85			tr			5	10								316	mafic rock
					10	50		5			35									317	sheared mafic rock
			50		10				tr	20		20								318	mafic rock
					5							40	40				tr	10		319A	monzonite
					1							40	45							319B	syenite
					40						40	15						5		320	amphibolite schist
			20		tr			20	60											321A	ultramafic rock
			20		tr			20	60											321B	ultramafic rock
15			50				tr	3	30				tr							322	ultramafic rock
			40				8	10	40											323	ultramafic rock
			35					20	30		tr									325	ultramafic rock
			35			60										tr			tr	324	metagabbro
			40					40								15				325a	mafic rock
					45			2				50								326	mafic rock
					5			95												328	chlorite schist
			54					40	5											329	mafic rock
					90			10			tr										330	mafic rock
					35							60								331	metagabbro
					80							15					tr	2	tr	332	metagabbro
					60							35						3		333	metagabbro
					tr			40			20	35					tr			334	metagabbro
					40						10	30	5					10		335	amphibolite schist
					70			25				5								337	mafic rock
			50					45		tr				tr						338	ultramafic rock
			60					30												339	ultramafic rock

Table 2 (continued), Modes of Rocks from the J-I and G Ultramafic Area.

olivine	augite	hypersthene	tremolite	anthophyllite	hornblende	cummingtonite	talc	chlorite	Mg-chlorite	lizardite	biotite	plagioclase	K-feldspar	carbonate	sphene	quartz	epidote	thin section number	rock type
20			30				tr	15	10	15								340	ultramafic rock
			40		8			10	40									341	ultramafic rock
	50				20							30						342	mafic rock
40			20					20	15	5								343	ultramafic rock
60							2	15	10	2								344	ultramafic rock
3			50					25	20					tr				345	ultramafic rock
			40					10			45							346	biotite schist

Table 3, Modes of Rocks from Kitl Ultramafic Area.

augite	hypersthene	tremolite	hornblende	Mg-chlorite	lizardite	biotite	plagioclase	K-feldspar	carbonate	sphene	quartz	epidote	thin section number	rock type
			30				40					20	K327-246	massive amphibolite
			70			20	5						K328-68	mafic rock
			5				80			tr	10		K328-80	diorite
		20				70				tr			K328-131	biotite schist
		85		tr		10							K328-148	mafic rock
tr			80				20						K328-160	metagabbro
		30		5		60							K328 168	mafic rock
			50			40	10						K328-258	mafic rock
			70			30		tr					K328-303	mafic rock
			60			40	tr						K328-313	mafic rock
35			60						tr	tr		tr	K328-480	mafic rock
			50				50					tr	K328-530	metagabbro
			30		tr	65							K328-569	biotite schist
			40				45					15	K329-41	amphibolite schist
		70		10		20							K329-249	mafic rock
			20				40		tr			40	K329-233	metagabbro
			40				40					20	K329-225	metagabbro
			60	tr		40							K329-471	mafic rock
		35		tr		60							K330-157	mafic rock
			60			20	20						K330-216	amphibolite schist
			40			20	40						K330-264	amphibolite schist
			70			20	10						K330-273	mafic rock
		35		20		40							K330-418	ultramafic rock
		45		45									K330-429	ultramafic rock

Abbreviations

Fo	Olivine
Anth	Anthophyllite
En	Enstatite
Dol	Dolomite
Mag	Magnesite
Cc	Calcite
Ta	Talc
Chl	Chlorite
Sta	Staurolite
Mus	Muscovite
Gar	Garnet
Als	Aluminum Silicate
Bio	Biotite
Trem	Tremolite

11:4 Geothermometers and Geobarometers

11:4:1 Garnet-Biotite Geothermometry

As the temperature increases both garnet and biotite become more iron-rich. The amount of modal biotite and aluminium silicate increases above muscovite breakdown.

(sta + mus = bio + gar + als) Thompson (1976)

An exchange reaction between garnet and biotite may be written $KFe_3Si_3AlO_{10}(OH)_2 + Mg_3Al_2Si_3O_{12} = KMg_3Si_3AlO_{10}(OH)_2 + Fe_3Al_2Si_3O_{12}$ 1

$$K_D = \frac{a^{BIO}_{Mg} \; a^{GAR}_{Fe}}{a^{BIO}_{Fe} \; a^{GAR}_{Mg}} \qquad 2$$

assuming ideal ionic solution, the activities can be written as

$$a^{BIO}_{Mg} = Mg^{BIO} = \left(\frac{Mg}{Mg+Fe}\right)^3 \qquad 3$$

then $$K_D = \frac{BIO\left(\frac{Mg}{Mg+Fe}\right)^3 \; GAR\left(\frac{Fe}{Fe+Mg}\right)^3}{BIO\left(\frac{Fe}{Fe+Mg}\right)^3 \; GAR\left(\frac{Mg}{Mg+Fe}\right)^3}$$

$$K_D = \frac{Fe^{GAR} \; Mg^{BIO}}{Fe^{BIO} \; Mg^{GAR}} \qquad 4$$

and $\Delta G^o = 3RT \ln K_D - \Delta V_s \; (P-1)$ 5

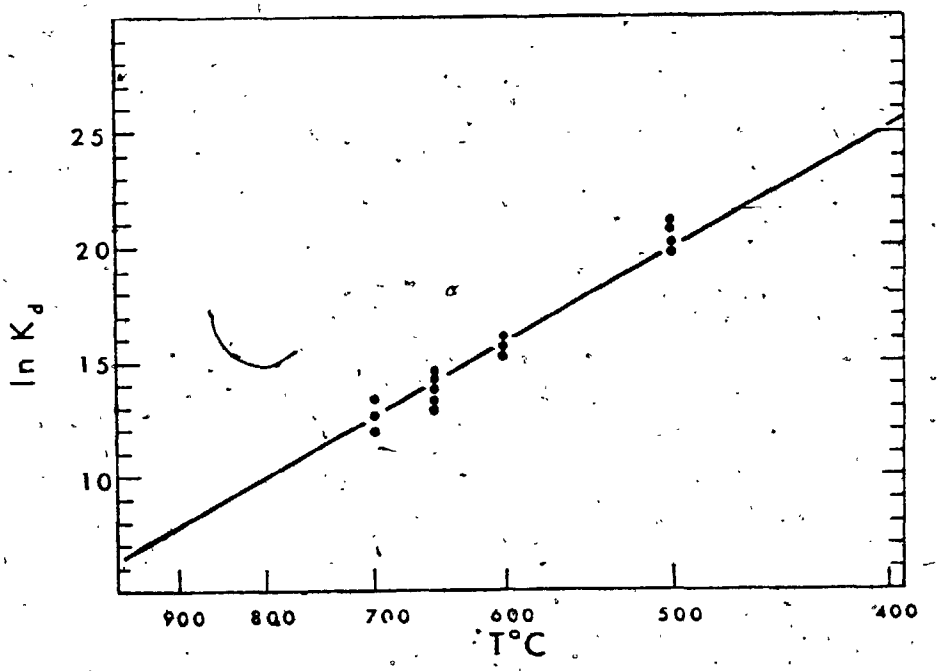

Fig.11:1, Plots of ln K_D vs T°C for iron-magnesium exchange reactions, for coexisting garnet-biotite (after Thompson, (1976)

The K_D values for garnet-biotite pairs at known temperatures have been obtained from Thompson (1976). The K_D plot used in this study (Thompson (1976)) is shown in Fig. 11:1. This allows G^o to be calculated as a function of temperature. The effect of pressure is very small since $\Delta V_{bio-gar} = -0.0465$ and the pressure term of equation 5 is small. Comparison of the temperatures resulting from various K_D vs T plots to other geothermometers such as the calcite-dolomite system has shown that the Thompson K_D values are the most consistent (Leatherbarrow (1978)). In using this method it is assumed that no other Mg-Fe exchange reaction was taking place; thus samples with hornblende, staurolite and iron oxides were omitted.

The compositions of four garnet-biotite pairs were determined on four samples of pelite occurring in diamond drill core K329 associated with pyrite tuff. The garnets were analyzed from core to rim and were found to be homogeneous the almandine component varying from 70.8 to 76.0 (Appendix D, Table 6). Biotites were in direct contact with the garnets analyzed. The average temperature using Thompson's values is 608°C.

Table 11.1 Temperatures from Garnet-Biotite Assemblages in Pelites

Thompson (1976)

Assemblage #1 607°C

Assemblage #2 612°C

Assemblage #3 606°C

Assemblage #4 604°C

11.3: Calcite-Dolomite Geothermometer

The magnesium content of calcite and geological factors that effect it were studied by Graf and Goldsmith (1955, 1958). Goldsmith, Graf and Joensuu (1955), Harker and Tuttle (1955) and Goldsmith and Heard (1961). They suggested that the magnesium content of calcite was dependent upon temperature but independent of pressure. Ewert (1977) used expressions developed by Goldsmith and Heard (1961) to produce an equation relating the molar % $MgCO_3$ in calcite at 5 kbars.

$$T = 474.96 + 82.24x - 5.11x^2 + 0.17x^3 - 0.0022x^4$$

Since pressure effects are minor, the 5 kilobar equation was used. Coexisting calcite and dolomite were analyzed using a defocussed beam (two to three times the focussed beam diameter). Approximately 20 points on each of 10 grains per section were analyzed. The temperature determined was based on the analyses giving the highest $MgCO_3$ content. Many factors can reduce the maximum amount of $MgCO_3$ such as the degree to which equilibrium was originally approached, the cooling rate, diffusion rates of magnesium and the amount of alteration.

Table 11:2, Composition of Coexisting Calcite and Dolomite

1. Range on 20 points of calcite on each of 10 grains, Slide #1

Weight Percent

FeO	0.15		0.12	
MgO	2.03		1.22	
CaO	53.0		54.3	
CO_2	42.9		42.9	
	98.08		98.54	

Atomic Ratio

Fe	0.0027	⎫	0.0021	⎫
Mg	0.0835	1.428	0.0502	1.407
Ca	1.3216	⎭	1.3548	⎭
CO_2	0.715		0.715	

2. Range on 20 points of calcite on each of 10 grains, Slide #2

Weight Percent

FeO	0.16		0.10	
MgO	2.18		1.13	
CaO	53.8		55.2	
CO_2	42.9		42.9	
	98.94		99.33	

Atomic Ratio

Fe	0.0029	⎫	0.0018	⎫
Mg	0.0897	1.4344	0.0465	1.4255
Ca	1.3418	⎭	1.3775	⎭
CO_2	0.715		0.715	

Table 11:2 shows the average $MgCO_3$ and maximum $MgCO_3$ content in calcite obtained in two sections containing calcite and dolomite from drill hole K328. The temperatures determined are 581 and 590°C. All samples contained minor iron whereas manganese was below detection.

11:4, Magnetite-Ilmenite Geothermometer

An oxide layer containing ilmenite and ilmeno-magnetite occurs in the G zone ultramafic. The magnetite and ilmenite are polygonally recrystallized with ilmenite occurring as isolated pods on the margins of the ilmenite-magnetite grains. (Plate 5b) In general the ilmenite forms a regular pattern near the core of the magnetite with the lamellae of ilmenite wider and more irregular near the margins. This texture leads to problems in applying the magnetite-ilmenite geothermometer.

The magnetite-ilmenite geothermometer is based on the solid solutions between ilmenite and hematite, and magnetite and ulvospinel. On an f_{O_2}-T diagram these solid solutions define unique curves for a given composition. The intersection of these curves for coexisting ilmenite-hematite, and magnetite and ulvospinel pairs define f_{O_2} and temperature (Fig. 11:2).

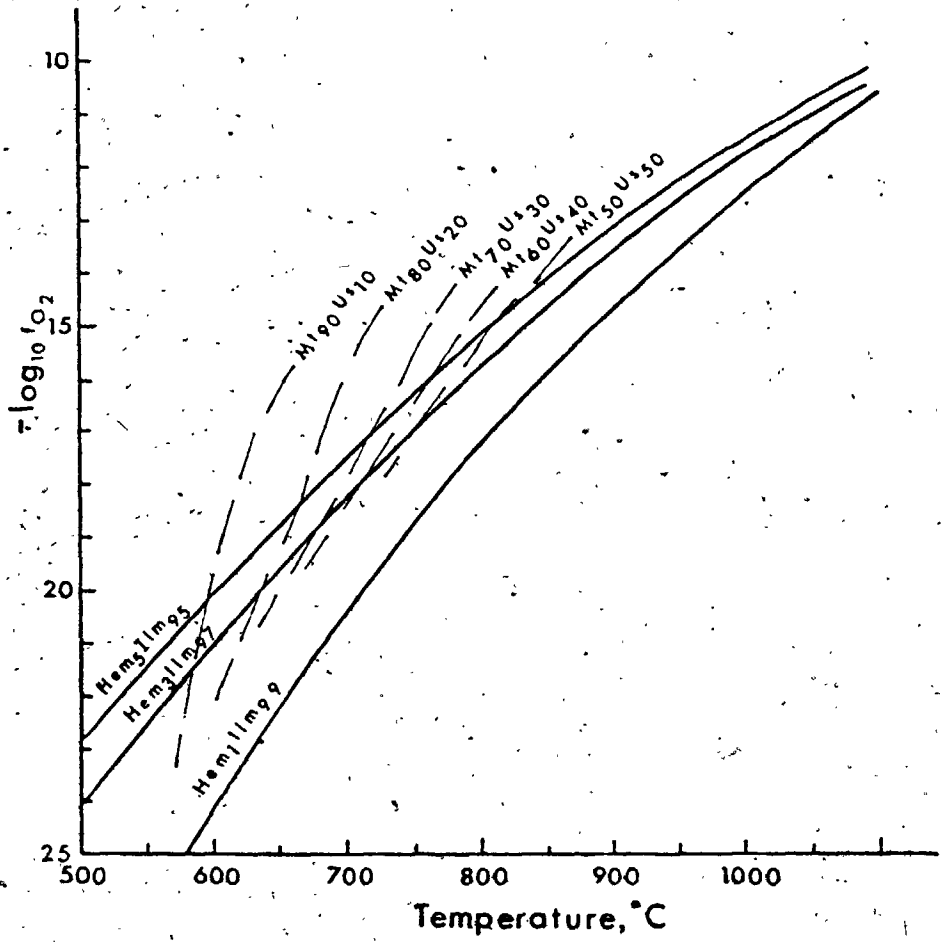

Fig. 14:2, $-\log_{10} f_{O_2}$ vs temperature diagram for hematite-ilmenite and magnetite-ulvospinel pairs. (after Buddington and Lindsley (1964))

The composition of ilmenites from rims, cores and isolated grains are essentially identical containing from 2.5 to 3.1% hematite in the ilmenite. The magnetite contains only minor amounts of TiO_2 implying that ulvospinel has oxidized to ilmenite from the magnetite. It is not certain whether the exsolution occurred during the original igneous stage or metamorphism. This uncertainty causes a wide range in the estimated composition of the magnetite (15 to 45%). The curve from Hem_3Ilm_{97} is relatively flat from 15-45% ulvospinel in magnetite giving a temperature range from 600° to 700°C. The estimated f_{O_2} range is very wide 10^{-22} to 10^{-18}.

4.11 Garnet-Plagioclase Geobarometer

Many pelites contain the assemblage plagioclase-garnet-quartz-sillimanite. Ghent (1977) has discussed the equilibrium.

$3CaAl_2Si_2O_8 = Ca_3Al_2Si_3O_{12} + 2Al_2SiO_5 + SiO_2$

anorthite grossular sillimanite quartz

Since $G^P_T = RT \log K_D = \Delta H^o_T - T\Delta S^o_T + (p-1)(\Delta V_S)$ and substituting values of ΔH^o_T, ΔS^o_T, ΔV_S from Robie & Waldbaum (1968) at equilibrium

$$o = -\frac{2551.4}{T} + 7.1711 - \frac{0.2842}{T}(P-1) + \log K_D$$

Assuming ideal solid solution

$$K_D = \frac{a^{Ga}_{Gr}}{a^{Pl}_{AN}{}^3} = \frac{X^{Ga}_{Gr}}{X^{Pl}_{AN}{}^3}$$

By determining the composition of plagioclase and garnet, K_D can be calculated. Using the temperatures obtained from the geothermometers described above, the pressure can be calculated.

Table 4:3 shows the pressures obtained from the temperature of various geothermometers. The pressures obtained using Helgeson's (1978) data give values higher than those using Robie & Walbaum's (1968) data.

Table 11:3, Pressures estimated by the Ghent (1977) geobarometer

	Temperature	R & W	Helgeson
garnet-biotite	608°C	5.67 kbars	7.06 kbars
cc-dol	593°C	5.32 kbars	6.84 kbars
mag-ilmenite	650°C	6.49 kbars	8.08 kbars

The compositions of the feldspar and garnets are shown in Appendix D, Table 5 and 6. R & W, Robie and Walbaum (1968)

4:6, Sphalerite-Pyrite-Pyrrhotite Geobarometer

A reaction can be written for co-existing sphalerite and pyrrhotite, $FeS_{po} = FeS_{sp}$ which is dependent on pressure. Barton and Toulmin (1966), Scott and Barnes (1971) and Scott (1973) have investigated the equilibrium between pyrite, hexagonal pyrrhotite and sphalerite at various pressures and temperatures. Scott (1973) has suggested that from 300 to 600°C and pressures up to 5kbars the activity of FeS in sphalerite is independent of temperature. Hutcheon (1977) used the data of Barton and Toulmin (1966) to calculate activity coefficients for FeS and ZnS in sphalerite applying a two-constant, Margules solution model. These activity coefficients were combined with molar volume and data for pyrite-pyrrhotite equilibrium (Toulmin and Barton, 1964; Froese and Gunter, 1976) to calculate a T-X projection for sphalerite. (Fig.11.3)

Three samples from Thierry Mine were found with coexisting sphalerite-pyrite-pyrrhotite and their compositions are tabulated in Appendix C, Tables 1, 2 & 3. They indicate a pressure of 5.0 - 6.0 kbars.

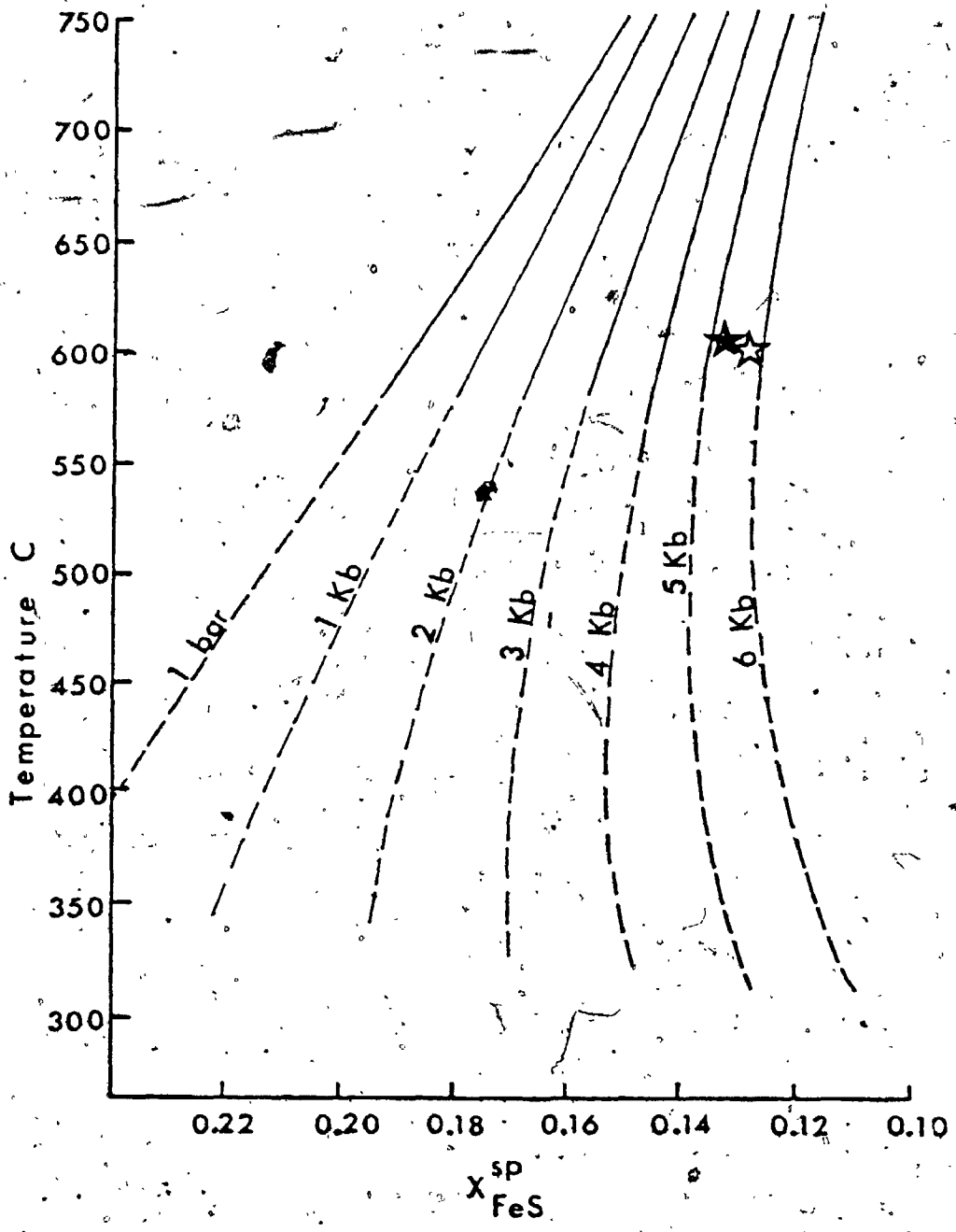

Fig.11:3, Plot of temperature vs X^{sp}_{FeS} for sphalerite coesisting with pyrrhotite and pyrite, open star, indicates sphalerite in hornblende-chlorite-biotite schist; filled star indicates sphalerite in breccia ore; (Hutcheon, 1977)

Appendix B Modes of Polished Sections

Table 1: Abbreviation for Terms Used in Table 2

A. Sulfide Type

P.D.	Primary Disseminated Ore
M.D.	Metamorphosed Disseminated Ore
M.B.	Metamorphic Dissemination in Blackwall Altered Rocks
Brec	Breccia Ore
C.B.S.	Chlorite Biotite Schist Ore
B.N.	Bornite Ore
Ox	Oxidized Ore
Str	Stringer Ore

B. Phases

Mpo	Monoclinic Pyrrhotite	Sph	Sphalerite
Py(Co)	Co Pyrite	Ilm	Ilmenite
Py(Ni)	Ni Pyrite	Mag	Magnetite
Py(Sk)	Skeletal Pyrite	Ag	Native Silver
Py(Re)	Resorbed Pyrite	St	Stuetzite
Smy	Smythite	Wi	Wittichenite
Vio	Violarite	Em	Emplectite
Pn	Pentlandite	Ac	Acanthite
Mill	Millerite	Linn	Linnaeite
Vaes	Vaesite		
Cpy	Chalcopyrite		
Bn	Bornite		
Mack	Mackinawite		

C. Texture

Po.Pn	Pyrrhotite exsolved in Pentlandite
Pn(Vio)	Pentlandite altering to Violarite

Table 2a, Modes of Polished Sections, K1:1 Ultramafic Body

Section No.	location	ore type	% sulfide	mpo	py (type)	stmu	vio	pn	mill	vaes	cpy	bn	mack	sph	mag	ilm	others	textures
K1	K1:1	M.B.	5	30	1(Co)			5			25				40			cpy+po.pn.+py(Co)+mag
K2	K1:1	M.D.	3	10	10(sk)			tr			80							cpy+po.pn.+mag+py(sk)
K3	K1:1	M.D.	2	5				tr			95				tr			cpy+po.pn.+mag
K4	K1:1	M.B.	2	25	tr(Co)			5			30				40			cpy+po.pn.+py(Co)+mag
K5	K1:1	M.B.	1	25	tr(Co)			5			55							cpy+po.pn.+py(Co)
K6	K1:1	M.B.	1	40	10(Co)						50				tr			cpy+po+py(Co)+mag
K7	K1:1	M.D.	1	10	tr(Co)			tr			90				tr			cpy+po.pn.+py(Co)+mag
K8	K1:1	M.D.	2	tr	10(Co)			tr			90				tr			cpy+po.pn+py(Co)+mag
K9	K1:1	Brec	80	80	5(Co)			10			5				tr			cpy+po.pn.+py(Co)
K10	K1:1	Brec	70	70	10(Co)			10			10				tr			cpy+po.pn.+py(Co)

Table 2b, Modes of Polished Sections, G Ultramafic Body

Section no.	location	ore type	% sulfide	mpo	py(type)	-	smu	vio	pn	mil	vaes	cpy	bn	mack	sph	mag	ilm	others	textures
K31-740	G	Ox	60		tr(Co)							tr	tr		tr	65	35	cub(tr)	cpy.bn.cub.+sph.cpy ilm.mag.+ilm
K30-446	G	Ox	75		1(sk)							tr			tr	95	4		cpy+py ilm.mag.+ilm
K29-268	G	M.D.	15	75	20(co)			tr	tr			5						tr(mar)	cpy+po.pn.(vio) +pu(Co)-(hem)
K28-122	G	Str	80		95(sk)							tr						5(mar)	cpy+py(sk)(mar,hem)
K28-119	G	Str	30		40(sk)			tr				60			tr			tr(mar)	cpy+py(sk)(mar)+pn(vio)
K29-300	G	M.D.	5		60(sk)			1				35						tr(mar)	cpy+py(sk)+viol
K29-600	G	M.D.	2		25(sk)							75				tr			cpy+py(sk)+mag
K29-400	G	M.D.	5	65				tr	1			35				tr	tr		cpy+po.pn.(vio)+mag.ilm.
K29-200	G	M.D.	1	85								15							cpy+po
K29-100	G	M.D.	5	20					tr			80			tr	tr			cpy+po.pn.+sph
K31-1085	G	P.D.	5	50					5			10				35			cpy+po.pn.+mag

Table 2c, Modes of Polished Sections, J+I Ultramafic Body

section no	location	ore type	% sulfide	mpo	py(type)	smu	vio	pn	mill	vaes	cpy	bn	mack	sph	mag	ilm	others	textures
K17 232	J+I	M.D.	5	75	20(Co)						5				tr			po+py+cpy+mag
K17 147	J+I	Ox	25	tr	50(Co)		tr	tr							tr		50(hem)	po.pn.(vio)+py(hem)+mag
K17 25	J+I	Ox	50		100(sk)						tr						Tr(hem)	py(hem)+cpy
K14 100	J+I	M.D.	1	5	50(skCo)						45				tr			cpy+po(py)+py(Co)+mag
K11 281	J+I	M.D.	10	30	10(Co)		tr	2			40			tr	18			po.pn.(vio)+py+mag
K11 220	J+I	M.D.*	tr								100				tr			cpy+mag granite*
K9 208	J+I	P.D.	5	70				tr			30				tr			cpy+po.pn.+mag
K9 113	J+I	M.D.	2		tr(Co)						90				10	tr		cpy+py+mag.ilm
K8 320	J+I	Brec	90	5							60			tr	5		30(cub)	cpy.cub.+po+sph.cpy.+mag
K1 266	J+I	Brec	80	tr	70(sk)		tr	tr			30				tr	tr	tr(mar)	po(py(mar,hem)).pn(vio).
K1 240	J+I	Brec	80	85				5			10				tr	tr		po.pn.+cpy+mag.ilm
K12 490	J+I	M.D.	2	60				tr			35				15			cpy+po.pn.+mag
K12 447	J+I	M.D.	2	50				tr			50			tr			tr(cub)	cpy.cub.+po.pn.+sph

Table 2c (continued)

section no	location	ore type	% sulfide	mpo	py(type)	smu	vio	pn	mil	vaes	cpy	bn	mack	sph	mag	ilm	others	textures
K12-357	J+I	P.D.	4	35				tr			5				60		tr(cub)	cpy.cub.+po.pn.+mag
K12-240	J+I	P.D.	5					5			20				20		tr(cub)	cpy.cub.+po.pn.+mag
K 9-338	J+I	Str.	50	55							25				1		15(cub); (mack)	cpy(mack).cub.+po+mag
K 9-382	J+I	P.D.	2	58				1			10				30		1(cub)	cpy.cub.+po.pn.+mag
K64-1100	J+I	M.D.	1	20							tr				80			cpy+po+mag
K64-1000	J+I	M.D.	5	25				tr			5				70		tr(cub)	cpy.cub.+po.pn.+mag
K64-900	J+I	P.D.	5	70	tr(Co)			tr			25				5			cpy+po.pn.+py+mag
K64-800	J+I	P.D.	5	20				tr			60				20			cpy+po.pn.+mag
K64-700	J+I	M.D.	5	70	tr(Co)			tr			30				tr			cpy+po.pn.+py(Co)+mag
K64-600	J+I	P.D.	3	40	tr(Co)			tr			20			tr	40		tr(mack)	cpy(mack)+po.pn.+py(Co) +mag
K64-500	J+I	P.D.	2	30				tr			40				30			cpy+po.pn.+mag
K64-400	J+I	M.D.	3	40	tr(Co)			10			20				30		tr(hem)	cpy+po.pn.+py(hem)+mag
K64-300	J+I	M.D.	3	30				10			10				50		**	cpy+po.pn.+mag

Table 2c (continued)

section no	location	ore type	% sulfide	mpo	py(type)	smu	vio	pn	mil	vaes	cpy	bn	mack	sph	mag	ilm	others	textures
K61-600	J+I	M.D.	1	30	10(Co)			tr			40				20		tr(hem)	cpy+po.pn.+py(hem)+mag
K61-500	J+I	M.D.	1	3							2				95	tr		cpy+po+mag.ilm
K61-400	J+I	M.D.	2	60							20				20	tr		cpy+po+mag.ilm.
K61-300	J+I	P.D.	3	40	10(reb)		tr	tr			30			tr	20	tr		cpy+po.(vio)+py(re) +mag.ilm
K61-200	J+I	M.D.	tr	50							50							cpy+po
K61-100	J+I	M.D.	5	10	80(sk)			tr			10				tr			cpy+po(py)+mag
K20-550	J+I	M.D.	3	tr	80(sk)						tr				tr		tr(hem)	cpy+po(py(hem))+mag
K20-400	J+I	M.D.	10	10	50(reb)	10					10				tr		tr(hem)	cpy+po.pn(vio).+py(hem)
K20-300	J+I	M.D.	15		30(sk)						50				tr		10(mar) 10(hem)	cpy+py(mar,hem)+mag
K16-400	J+I	P.D.	5	60				tr			5				35			cpy+po.pn.+mag.ilm
K16-150	J+I	M.D.	tr		40(Co)						40				20			cpy+py(Co)+mag
K14-400	J+I	M.D.	1	25	tr(Co)						60				5		10(hem)	cpy+po+py(hem)+mag
K14-500	J+I	M.D.	tr	40							50				10			cpy+po+mag

Table 2c (continued)

Section no	location	ore type	% sulfide	mpo	py(type)	smu	vio	pn	mil	vaes	cpy	bn	mack	sph	mag	ilm	others	textures
K14-300	J+I	M.D.	1	30	tr(Co)						30				40			cpy+po+py+mag
K14-200	J+I	M.D.	1	40							40				20			cpy+po+mag
K14-100	J+I	M.D.	3	40	20(sk)						40				tr		tr(hem)	cpy+po(hem)+py(hem)+mag
K11-300	J+I	Str	5		40(sk)		10				10				5		35(hem)	cpy+py(hem)+viol+mag
K11-200	J+I	M.D.	5	20	1 (reb)			tr			30				50		tr(hem)	cpy+po.pn.+py(hem)+mag
K11-100	J+I	M.D.	10		15(reb)		tr				5				80		tr(hem)	cpy+po+vio+py(hem)+mag
K10-600	J+I	P.D.	5	30				20			15				35			cpy+po.pn.+mag
K10-500	J+I	P.D.	1	50				10			10				30			cpy+po.pn.+mag
K10-400	J+I	M.D.	2	30				5			25				40			cpy+po.pn.+mag
K10-300	J+I	P.D.	4	30				15			15				40			cpy+po.pn.+mag
K10-200	J+I	M.D.	5	50				5			10				35			cpy+po.pn.+mag
K9 -600	J+I	P.D.	3	40	tr(Co)			1			40	tr			20			cpy.bn.+po.pn.+py+mag
K9 -500	J+I	P.D.	5	50				5			20				25			cpy+po.pn.+mag

Table 2c (continued

Section no.	location	ore type	% sulfide	mpo	py type	smu	vio	pn	mill	vaes	cpy	bn	mack	sph	mag	ilm	others	textures
K9 -400	J+I	P.D.	5	50				20			20			tr	10			cpy+po.pn.+sph.cpy +mag
K9 -300	J+I	M.D.	1	70							10				20			cpy+po+mag
K9 -200	J+I	P.D.	2	tr				tr			60				40			cpy+po.pn.+mag
K8 -600	J+I	M.D.	1	70	tr(Co)						20				10	tr	tr(hem)	cpy+po+py(hem)+mag
K8 -400	J+I	P.D.	2	10				10			50				30			cpy+po.pn.+mag
K8 -300	J+I	P.D.	5	50			tr	15			15				20	1	tr cub	cpy.cub.+po.pn.(vio) +mag.ilm
K8 -200	J+I	M.D.	1								2				98			cpy+mag
K8 -100	J+I	M.D.	2								tr				100			cpy+mag

Table 2d, Modes of Polished Sections, Thierry Mine, Ultramafic Body

section no.	location	ore type	%sulfide	mpo	py(type)	smy	vio	pn	mill	vaes	cpy	bn	mack	sph	mag	ilm	others	textures
600-1E-Hor	K2:1	M.D.	15		tr(Co)			tr			tr		99				hem(tr)	cpy+pn+py+mag(hem)
600-1E-Hor 173	K2:1	M.D.	10	1			tr	tr			35				60	5		cpy+po.pn(vio).+mag. ilm+ilm
600-1E-Hor 173B	K2:1	Brec	90	15	(re)tr			5			50				27	3		cpy+po.pn.+mag.ilm.
600-1E-Hor 169	K2:1	Brec	40	25			1	5			70				tr			cpy+po.pn(vio).+mag
600-1E-Hor 164	K2:1	M.D.	2	tr				tr			99				1			cpy+po.pn.+mag
600-1E-Hor 158	K2:1	Brec	50	15			1	5			80				tr		pt. minerals	cpy+po.pn(vio).+mag
600-1E-Hor 93	K2:1	Brec	65	30	tr(re)		1	5			64				1	tr		cpy+po.pn(vio).+py+mag
600-1E-Hor 65	K2:1	Oxid	10		5(sk)		tr				85				10			cpy+vio+py+mag
1600-1E-2 245	K2:1	Brec	10	15		1	tr	5			15				65			cpy+po(smy,vio). pn(vio).+mag
1600-1E-2 204	K2:1	M.D.	10	2				tr							90			cpy+po.pn.+mag
260/98/50	K2:1	Brec	80	10	tr(re)			1			90			1	1		cub(tr) mac(tr)	cpy(mac).cub.+po.pn. +py+mag
260/99/132	K2:1	C.B.S.	5		3(sk)						97				tr			cpy+py(sk)+mag
4-017-99	K2:1	M.D.	5	tr			tr	tr			1	1			tr	tr	mill(tr)	cpy.bn.+po.pn.+mill +mag

Table 2d (continued)

section no	location	ore type	% sulfide	mpo	py (type)	smy	vio	pn	mill	vaes	cpy	bn	mack	sph	mag	ilm	others	textures
4-032-153	K2:1	M.D.	25	15	3 (re)	tr		tr			80				tr		2(mar) hem	cpy+po(smy).pn+py (hem,mar)+mag
4-035-71	K2:1	C.B.S.	25	5	10(re)			tr			85				1		tr(mar)	cpy+po.pn.+py(re) (mar)+mag
4-038-68	K2:1	C.B.S.	35	5	5 (Co)			tr			90			tr	tr			cpy+po.pn+py(Co)+mag
5-001-6	K2:1	C.B.S.	30	tr	1 (re)		tr				98				tr			cpy+po(py)+vio+mag
6-024-167	K2:1	M.D.	2	15	tr(Ni)	tr	tr	tr			5				80			cpy+po(smy,vio). pn(vio,py)+mag
600-1E-Hor 247	K2:1	M.D.	1	5	25(sk)						20				20		40(hem)	cpy+py+po+mag(hem)
600-1E-Hor 218	K2:1	Brec	80	75	tr(Ni)		tr	10			5				5	tr		cpy+po.pn(vio,py)+mag
600-1E-Hor 199	K2:1	Bn	1								70	30			tr			cpy.bn.+mag
600-1E-Hor 185	K2:1	M.D.	3		tr(sk)						tr				30		70(hem)	cpy+py+mag(hem)
Bn West	K2:1	Bn	10						tr		70	30					lin,ag, wit	cpy+bn.+wit.emp. +mill
Bn West	K2:1	Bn	3						tr		60	30					ar,ar, hem,em, wit,ag	cpy.bn.+wit. emp.+mill
Bn East	K2:1	Bn	3								60	30					em,wit, ag	cpy.bn+wit. emp+mill
K78 441	K2:1	C.B.S.	20		30(Co)		1	tr			50				20			cpy+po.pn(vio) +py(Co)+mag

Table [redacted] (continued)

Section no.	location	ore type	% sulfide	mpo	py(type)	smu	vio	pn	mill	vaes	cpy	bn	mack	sph	mag	ilm	others	textures
K78 421	K2:1	M.D.	[redacted]		5(Co)						80		tr		12	tr		cpy(mack)+py(Co) +mag.ilm
K71 516	K2:1	Ox	35		10(Co)		tr				90				tr		1(mar)	cpy+vio+py(mar)+mag
K71 424	K2:1	C.B.S.	25	tr	5(Co)				tr		35			tr	60			cpy+po(py)+mill+mag
K71 415	K2:1	Ox	60								35				5		10(hem) 50(mar)	cpy+mar+hem(mag)
K75 870	K2:1	C.B.S.	25	3				tr			90				7	tr	tr(hem)	cpy+po.pn.+mag(hem)
K50 320	K2:1	C.B.S.	15	40	40(re)		tr	2			10				10			cpy+py+po.pn(vio).+mag
K50 315	K2:1	C.B.S.	10	50	25(re)		tr	2			8				10		5(mar)	cpy+py(mar)+po.pn(vio) +mag
K60 215	K2:1	C.B.S.	20	50	10(Ni)	tr	20				20		tr		tr			cpy+po(vio,amy) +vio+py(ni)+mag
K60 207	K2:1	Ox	10		15(Ni)		10				75							cpy+py(ni)+vio
K68 682	K2:1	M.D.	4		tr(sk)						20				80			cpy+py(sk)+mag
K68 632	K2:1	Brec	50		10(Co)						80				10			cpy+py(Co)+mag
K68 605	K2:1	M.D.	1		tr(Co)						5				95			cpy+py(Co)+mag
K68 471	K2:1	M.D.	3		tr(Co)						99				1			cpy+py(Co)+mag

Table 2d (continued)

Section no.	location	ore type	%sulfide	mpo	py (type)	smy	vio	pn	mill	vaes	cpy	bn	mack	sph	mag	ilm	others	textures
K68 347	K2:1	C.B.S.	35	tr	10(Co)			tr			80			tr	10	tr	pt minerals	cpy+po.pn.+py+mag
K68 290	K2:1	Ox	10		5(Co)		5			10	80	tr						cpy+vio+py(Co) vac
K68 280	K2:1	Ox	10				10		10		80							cpy+vio+mill
K68 155	K2:1	C.B.S.	30	60			5	5			20				10	tr	tr(hem)	cpy+po.pn(vio).+mag (hem)
K68 132	K2:1	Brec	50	70	tr(Ni)		20	tr			8			tr	2			cpy+po(vio).pn(vio,py) +mag
K68 115	K2:1	Brec	70	75		tr	15	tr			10			tr				cpy+po(vio,smy). pn(vio)+mag
West Pit (Ag)	K2:1	Brec	40	68	2(Co)	tr	tr	5			15			tr	10		pt minerals	cpy+po(vio,smy). pn(vio)+py(Co)+mag
West Pit (Po)	K2:1	Brec	30	60	2(Co)	tr	tr	8			20		tr		tr		pt minerals	cpy+po(vio,smy). pn(vio)+py(Co)+mag
Th1 - 1	K2:1	C.B.S.	15	55	20(Co, Ni)		tr	tr			20				5			cpy+po(vio.pn(vio,py) +py(Co)+mag
Th - 2	K2:1	Brec	30	10	tr(Co)		tr	tr			75			tr	15			cpy+po.pn(vio). +py(Co)+mag
Th -3	K2:1	C.B.S.	35	30	tr(Co)		tr	1			60				10			cpy+po.pn(vio) +py(Co)+mag
Th -4	K2:1	Bn	3						tr		20	40			40	tr		cpy.bn.+mill+mag.ilm
TH -5	K2:1	Bn	3				tr				20	40			40	tr	pt minerals	cpy.bn.+vio+mag.ilm

Table 2d (continued)

section no	location	type	% sulfide	mpo	py(type)	smy	vio	pn	mill	vaes	cpy	bn	mack	sph	mag	ilm	others	textures
Th-7	K2:1	Brec	90	30		tr	1	9			60		tr		1			cpy(mach)+po(vio,smy). pn(vio).+mag
Th-8	K2:1	Brec	80	20		tr	1	3			75		tr		1			cpy(mach)+po(vio,smy). pn(vio).+mag
Th-9	K2:1	Brec	70		1(Ni)	1	2	10			10				1		mar(1)	cpy+po(vio,smy).pn(vio) +py(mar)
Th10	K2:1	Brec	60	30		tr	9	10			60				1		cub(tr)	cpy.cub.+po(vio,smy). pn(vio)+mag
Th11	K2:1	Brec	40		1(Co)						98				1			cpy+py+mag
12-107-1 470	K2:1	C.B.S.	5	30	1(Co)		tr	1			60				10			cpy+po.pn(vio).+py+mag
12-108-0 26A	K2:1	C.B.S.	10	25	5(Co)			1			60				12			cpy+po.pn.+py(Co)+mag
12-108-0 26B	K2:1	C.B.S.	10	50	5(Co)			5			30				10			cpy+po.pn.+py(Co)+mag
12-111E-0 45	K2:1	C.B.S.	20	50	1(Co)			1			40				3			cpy+po.pn.+py(Co)+mag
12-112-0 26	K2:1	C.B.S.	50	20	1(Co)			1			75				5			cpy+po.pn.+py(Co)+mag
12-114-0 36	K2:1	C.B.S.	10	20	5(Co)			1			60			tr	25			cpy+po.pn.+py(Co)+mag
12-115E-47 47	K2:1	C.B.S.	10		5(Co)		tr	5			35				10			cpy+py(Co)+pn(vio)+mag
12-123E-0	K2:1	C.B.S.	10	25	5(Co)			tr			50				25			cpy+py(Co)+pn+mag

4 4

OF / DE

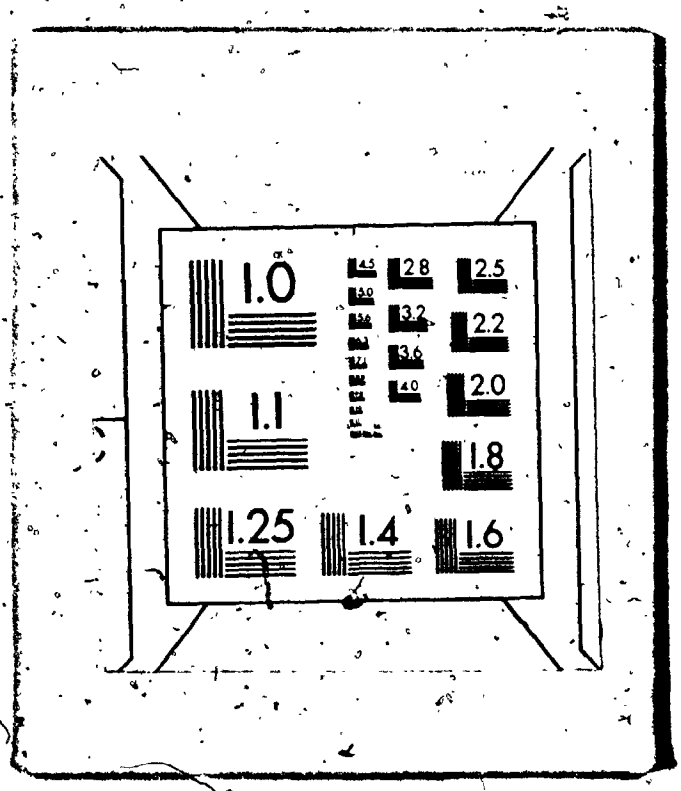

Appendix C \ Electrom Microprobe Analyses of Sulfides

11.5 Methods Used and Detection Limits

All samples were analysed on the Cambridge Microprobe at Carleton University. The data were processed using the Empadr V computer program. In general, counting time was 10 sec at 15KV on silicates and 20 KV on sulfides and tellurides. The detection limits are on the order of 0.1% for most elements at 95% confidence level with the exception of Ag, 0.14%; Pt, 0.21%; Pd, 0.22% for the standards used in this project (Morton, 1978).

Two problems in the reliability of the probe data were encountered. In general the PGM analysed had totals above 100% although the stoichiometry was correct. This was thought due to the use of standards with markedly different PGE contents, (Morton, 1978). The analysis of olivine was found to be very sensitive to the thickness of the carbon coating. Totals were usually above 100%.

Table 1, Electron Microprobe Analyses of Sulfides in CBS Ore

CHALCOPYRITE

	1	2	3	4	5	Average	Atomic Ratio	Std Dev
S	34.9	34.7	34.6	34.1	34.5	34.6	1.08	0.265
Fe	29.8	29.5	29.1	29.8	29.9	29.6	0.53	0.292
Co	tr	tr	tr	tr	tr	tr	--	
Cu	34.3	33.9	34.5	34.2	34.1	34.2	0.54	0.200
	99.0	98.1	98.2	98.1	98.5	98.4		

1-2 Th3
3-5 12-8E-0+26

PYRRHOTITE

	1	2	3	4	5	6	7
S	40.5	40.2	40.2	40.4	40.3	40.1	40.6
Fe	59.4	59.4	59.3	58.9	58.2	57.6	57.5
Ni	0.61	0.55	0.63	0.93	0.86	0.69	0.49
Co	0.10	tr	tr	tr	tr	0.11	0.16
	100.62	100.19	100.22	100.34	99.42	98.50	98.75

	8	9	10	11	12	13	14
S	39.6	40.1	40.6	41.2	40.23	40.7	40.2
Fe	56.5	60.0	59.9	57.5	59.5	58.6	59.4
Ni	1.17	0.55	0.71	1.16	0.67	0.68	0.57
Co	0.13	0.16	0.18	0.19	0.16	0.17	0.19
	97.40	100.81	101.39	100.05	100.56	100.15	100.36

	15	Average	Atomic Ratio	Std Dev
S	41.2	40.4	1.26	0.414
Fe	58.3	58.7	1.05	0.999
Ni	0.97	0.75	0.013	0.211
Co	0.16	0.12	0.002	
	100.63	99.97		

1-5 12-8E-0 26
6-15 Th-3

Table 1, Electron Microprobe Analyses of Sulfides in CBS Schist Ore

PYRITE (Ni)

	1	2	3	Average	Atomic Ratio
S	52.8	53.9	53.8	53.5	1.68
Fe	44.1	46.9	45.4	45.5	0.814
Co	0.15	0.13	0.13	0.14	0.002
Ni	3.24	0.48	2.19	1.97	0.034
	100.36	101.41	101.48	101.11	

1 Th-3
2 Th-3
3 12-8E-0 26

PYRITE (Co)

	1	2	3	4	5	6	7
S	52.8	53.4	54.0	53.2	54.6	53.5	54.24
Fe	42.7	44.0	45.7	42.8	46.3	44.6	45.1
Co	3.97	4.45	2.18	3.49	0.74	2.78	1.38
Ni	n.d.	n.d.	tr	.33	n.d.	n.d.	n.d.
	99.55	101.91	101.88	99.84	101.67	100.88	100.68

	Average	Atomic Ratio	Std Dev
S	53.7	1.68	0.577
Fe	44.5	0.797	1.277
Co	2.71	0.046	1.263
Ni	tr		
	100.91		

1-4 Th-3
5 12-115E-0-47
6-7 Pt350

Table 1. Electron Microprobe Analyses of Sulfides in C.B.S. Ore

PENTLANDITE

	1	2	3	Average	Atomic Ratio
S	37.3	36.5	37.0	36.9	1.15
Fe	26.0	27.8	26.0	26.6	0.476
Ni	34.8	34.3	33.7	34.3	0.584
Co	0.54	0.35	0.42	0.44	0.007
	98.69	98.95	97.08	98.24	

1-2 12-8E-0 26
3 12-113E-0 47

VIOLARITE IN PENTLANDITE

	1	2	3	4	5	Average	Atomic Ratio	Std Dev
S	40.0	40.5	40.7	39.1	38.2	39.9	1.246	0.932
Fe	24.7	27.9	28.1	29.2	26.0	27.2	0.487	1.611
Ni	29.0	25.6	25.4	24.2	31.7	27.2	0.463	2.767
Co	1.90	1.62	1.25	1.72	0.72	1.44	0.024	0.419
	96.73	95.64	95.04	94.14	96.62	95.74		

1 Th-3
2-5 12-8E-0 26

SPHALERITE With Py-Po

	1	2	Average	Atomic Ratio
S	31.4	31.8	31.6	0.99
Fe	7.57	7.55	7.56	0.13
Zn	60.6	60.3	60.4	0.92
Cu	tr	tr	tr	
	99.57	99.65	99.56	

1-2 12-8E-0 26

Table 2, Electron Microprobe Analyses of Sulfide in Breccia Ore

CHALCOPYRITE

	1	2	3	4	5	6
S	35.5	35.0	34.0	34.0	35.0	34.8
Fe	30.5	30.3	30.2	30.6	29.9	30.3
Cu	34.2	34.0	34.0	34.3	34.7	34.4
Co	tr	0.14	0.12	0.14	nd	tr
	100.2	99.44	98.32	99.04	99.60	98.8

	7	8	9	Average	Std Dev	Atomic Ratio	
S	35.8	34.0	35.3	34.8	0.644	1.09	
Fe	30.7	30.3	30.7	30.3	0.247	0.54	
Cu	34.1	34.1	33.8	34.2	0.248	0.54	1.08
Co	nd	tr	tr	tr			
	100.6	98.4	99.8	99.3			

1-5 Th 7 600-level cross-cut
6-7 Th 9 " "
8 Th 6 " "
9 Th 6 " "

PENTLANDITE

	1	2	3	4	5	6
S	34.1	34.0	33.1	32.8	33.2	34.5
Fe	26.2	26.6	26.8	27.1	26.2	25.7
Co	3.51	2.77	3.30	3.31	3.05	3.28
Ni	36.3	37.2	36.4	36.1	37.0	35.2
	100.14	100.52	99.56	99.26	99.51	99.01

	Average	Std Dev	Atomic Ratio	
S	33.6	0.615	1.049	
Fe	26.4	0.457	0.473	1.147
Co	3.20	0.235	0.054	
Ni	36.4	0.672	0.62	
	99.6			

1-6 Th7 600 level cross-cut

Table 2, Electron Microprobe Analyses of Sulfides in Breccia Ore

REABSORBED PYRITE

	1	2	3	4	5	6	Average	Atomic Ratio	Std Dev
S	53.0	52.6	53.0	52.7	53.2	53.1	52.9	1.65	0.213
Fe	45.4	39.3	40.1	46.0	45.5	46.0	43.7	0.782	2.859
Co	0.16	0.17	0.13	0.10	0.17	0.16	0.15	0.003	7.547
Ni	1.34	6.24	6.82	0.50	1.34	1.05	2.88	0.049	2.600
	99.90	98.31	100.06	99.29	100.22	100.31	99.63		

1 in Po Th9 600 level cross-cut
2 in Pn Th9 " " "
3 in Pn Th9 " " "
4 in cpy Th9 " " "
5 in Po Th7 " " "
6 in Po Th7 " " "

PYRITE (Co)

	1	2	3	4	Average	Atomic Ratio	Std Dev
S	54.1	54.1	53.5	53.1	53.7	1.677	0.424
Fe	44.5	43.1	44.6	44.2	44.1	0.790	0.596
Ni	0.12	tr	tr	tr	tr	--	
Co	1.41	3.38	2.78	2.91	2.62	0.044	0.733
	100.15	100.66	100.88	100.21	100.42		

1 Th9 600 level cross-cut
2 Th9 " " "
3 Po-9 2nd bench west pit.
4 Po-9 " " "

PYRITE (Ni)

	1	2	3	4	5	6	7
S	52.9	52.6	52.6	49.5	52.6	52.9	52.8
Fe	45.6	45.5	43.8	40.6	39.3	45.6	45.4
Co	0.16	0.17	0.20	0.93	0.16	0.16	0.17
Ni	0.85	0.65	3.62	8.38	6.32	0.85	0.66
	99.47	98.97	100.62	99.39	98.38	99.47	99.01

	8	9	10	11	Average	Atomic Ratio	Std Dev
S	53.0	53.8	52.3	51.8	52.4	1.636	1.039
Fe	40.1	45.6	45.1	45.4	43.8	0.784	2.404
Co	0.13	0.22	0.21	0.26	0.25	0.004	0.217
Ni	6.82	1.41	2.06	1.48	2.67	0.045	6.652
	100.07	101.03	99.58	98.93	99.12		

1-8 Th9 600 level cross-cut
9-11 Po-9 2nd bench west pit

Table 2, Electron Microprobe Analyses of Sulfides in Breccia Ore

SPHALERITE IN PYRRHOTITE

	1	2	3	4	5	Average	Atomic Ratio	Std Dev
Fe	5.79	6.33	6.51	6.18	5.67	6.22	0.11	0.319
Cu	n.d.	n.d.	1.90	0.73	0.52	1.05	0.017	
Zn	56.7	57.0	58.1	59.6	60.3	59.9	0.92	1.412
Co	n.a.	n.a.	0.12	0.10	0.14	0.12	0.002	
Ni	n.a.	n.a.	tr	tr	0.40	0.15	0.002	
S	36.8	36.9	36.1	32.9	31.9	32.2	1.00	2.10
	99.28	100.28	98.28	99.27	98.99	99.05		

1-5 Th-2 600 Level cross-cut

SPHALERITE WITH PYRRHOTITE AND PYRITE

	1	Atomic Ratio
Fe	7.71	0.138
Cu	tr	--
Zn	59.9	0.916
Co	n.a.	--
Ni	n.a.	--
S	32.6	1.02
	100.65	

1 Pl. 600 level cross-cut

SMYTHITE

	1	2	3	4	Average	Atomic Ratio	Std Dev
S	40.9	41.0	40.6	40.5	40.7	1.27	0.192
Fe	56.0	56.4	57.1	57.1	56.6	1.01	0.472
Co	0.21	0.15	0.12	0.12	0.16	0.003	5.667
Ni	2.00	1.65	1.36	1.65	1.66	0.03	0.227
	99.11	99.2	98.18	99.37	99.16		

1-4 Th9 600-level cross-cut

Table 2, Continued
LOW Ni SULFIDE (Th9 600-level cross-cut)

	1	2	3	4	5	6	7	8
S	41.0	40.9	40.9	41.3	41.0	42.2	42.7	42.3
Fe	56.6	56.1	56.5	56.4	56.5	55.2	55.9	56.5
Co	0.13	0.15	0.14	0.14	0.14	0.23	0.28	0.26
Ni	1.13	1.90	1.35	1.42	0.95	1.18	0.99	1.32
	99.86	99.05	98.89	99.19	98.59	98.81	99.87	100.32

	9	10	11	12	13	14	15	16
S	42.8	41.0	40.9	40.9	40.9	41.0	41.0	40.7
Fe	57.4	56.6	56.4	56.5	56.5	56.6	56.5	57.1
Co	0.28	0.13	0.15	0.14	0.14	0.15	0.15	0.14
Ni	0.68	1.13	1.90	1.35	1.42	1.57	0.95	1.09
	101.16	98.86	99.35	98.89	98.96	99.52	98.60	99.03

	Average	Std Dev	Atomic Ratio		
S	41.49	0.75	1.296		
Fe	56.49	0.58	1.011		$M_{8.8}S_{11}$
Co	0.19	0.06	0.001	1.033	
Ni	1.23	0.33	0.021		
	99.40				

Table 2, Continued

PYRRHOTITE $M_{6.9}S_8$

	1	2	3	4	5	6	7	8
S	40.2	39.3	40.0	39.8	39.5	39.1	39.1	39.1
Fe	59.2	59.2	59.1	58.9	59.1	58.9	59.4	59.3
Co	0.29	0.24	0.16	0.18	0.15	0.18	0.15	0.18
Ni	0.40	0.52	0.48	0.55	0.68	0.63	0.41	0.51
	100.39	99.26	99.74	99.41	99.43	98.81	99.06	99.09

	9	10	11	Average	Atomic Ratio	
S	39.0	39.0	39.0	39.4	1.230	
Fe	59.5	59.7	59.5	59.2	1.060	
Co	0.16	0.20	0.14	0.18	0.003	1.072
Ni	0.42	0.43	0.67	0.52	0.009	
	99.08	99.33	99.31	99.3		

1-5 Breccia ore Pt348
5-11 Pt351 with sph+py

Table 3, Electron Microprobe Analyses of Sulfides in Bornite Ore

VIOLARITE IN PYRRHOTITE $M_{3.12}S_4$

	1	2	3	4	5	6	7
S	40.21	40.4	40.8	40.7	40.6	40.9	39.9
Fe	28.0	27.8	27.7	29.3	28.0	27.7	23.6
Co	1.74	1.66	1.78	0.33	1.74	1.78	4.23
Ni	26.5	26.3	27.8	27.6	26.7	27.9	28.8
Cu	n.a.	n.a.	n.a.	n.a.	n.a.	n.a.	n.a.
	96.44	96.17	98.01	97.98	97.00	98.08	96.52

	8	9	Average	Std Dev	Atomic Ratio
S	41.0	42.4	40.8	0.665	1.27
Fe	31.0	28.5	28.0	1.841	0.501
Co	0.32	0.38	1.55	1.163	0.026
Ni	26.5	27.6	27.3	0.794	0.465
Cu	n.a.	n.a.	n.a.		n.a
	98.86	98.85	97.65		

1-9 Th2 600 cross-cut

VIOLARITE IN PENTLANDITE $M_{3.01}S_4$

	1	2	3	4	5	6	7
S	39.9	41.0	41.6	42.1	42.6	41.4	43.0
Fe	23.6	24.4	26.6	26.9	26.0	26.4	27.1
Ni	28.8	27.8	30.7	26.6	27.3	27.1	25.9
Co	4.23	4.68	0.29	1.65	1.82	1.86	2.12
	96.52	97.98	99.16	97.27	97.64	96.8	98.09

	Average	Std Dev	Atomic Ratio
S	41.7	0.962	1.30
Fe	25.9	1.237	0.464
Ni	27.7	1.472	0.472
Co	2.39	1.700	0.041
	97.69		

1-7 Th-2 600 cross-cut

Table 3, Electron Microprobe Analyses of Sulfides in Bornite Ore

BORNITE $Cu_{4.7}Fe_{.97}S_4$

	1	2	3	4	Average	Atomic Ratio	Std Dev
S	26.7	25.0	26.1	26.5	26.3	0.821	0.657
Ni	n.d.	tr	n.d.	n.d.	--	--	
Co	n.d.	n.d.	n.d.	n.d.			
Fe	11.9	10.8	11.3	10.6	11.5	0.200	0.502
Cu	60.1	61.8	61.4	61.4	61.2	0.963	0.612
	98.7	98.6	98.79	98.73	99.0		

1-4 Th-4 600 level cross-cut

CHALCOPYRITE $Cu_{1.02}Fe_{1.00}S_2$

	1	2	Average	Atomic Ratio
S	34.0	34.8	34.4	1.074
Ni	n.d.	n.d.	--	
Co	0.14	0.11	0.12	0.002
Fe	30.1	30.1	30.1	0.539
Cu	34.9	34.5	34.7	0.546
	99.10	99.50	99.32	

1-2 Th-4 600 level cross-cut

CARROLLITE $M_{3.06}S_4$

	1	2	3	4	Average	Atomic Ratio	Std Dev
S	41.3	41.3	41.9	38.5	40.8	1.27	1.320
Ni	11.0	11.7	11.2	13.6	11.9	0.202	1.028
Co	33.8	33.5	33.6	30.4	32.8	0.557	4.07
Fe	0.97	0.95	1.05	1.93	1.22	0.022	
Cu	10.9	11.1	10.6	16.3	12.2	0.192	1.404
	98.09	98.8	98.34	100.76	98.92		

1-4 Th-5 600 level cross-cut

MILLERITE $M_{1.02}S$

	1	2	3	4	Average	Atomic Ratio	Std Dev
S	34.3	34.8	34.7	35.0	34.7	1.08	0.255
Ni	58.2	57.9	57.8	58.3	58.4	0.99	0.552
Co	5.32	5.59	5.37	5.33	5.40	0.092	0.109
Fe	1.02	1.44	1.82	1.47	1.44	0.026	0.284
Cu	1.20	2.18	1.85	1.54	1.69	0.027	0.629
	101.22	101.92	101.52	101.65	101.51		

1-4 Th-5 600 level cross-cut

Table 4, Electron Microprobe Analyses of Sulfides in Altered Breccia Ore

PYRITE (Co)

	1	2	3	4	Average	Atomic Ratio	Std Dev
S	53.8	54.4	53.7	54.2	54.0	1.686	0.286
Cu	n.d.	n.d.	n.d.	0.13	tr		
Ni	n.d.	n.d.	n.d.	n.d.	n.d.	--	
Fe	44.8	44.8	44.0	45.2	44.7	0.900	0.436
Zn	n.d.	n.d.	n.d.	n.d.	n.d.	--	
Co	1.38	1.29	1.62	0.51	1.20	0.020	0.416
	99.98	99.49	99.32	100.04	99.9		

1-4 pt.350

POLYDYMITE

	1	2	3	4	Average 1-4	Atomic Ratio	Std Dev
S	42.4	41.9	41.7	41.4	41.8	1.305	0.364
Cu	n.d.	n.d.	0.24	n.d.	tr	--	
Ni	34.5	34.3	34.4	34.6	34.4	0.586	0.112
Fe	8.24	8.43	8.27	8.00	8.24	0.148	0.154
Zn	n.d.	n.d.	n.d.	n.d.	n.d.	--	
Co	13.3	12.1	12.3	13.5	12.7	0.217	0.608
	98.44	96.73	96.91	97.5	97.24		

	5	6	7	Average 5-7	Atomic Ratio
S	38.7	38.2	38.9	38.6	1.205
Cu	9.7	11.6	9.66	10.3	0.162
Ni	41.4	37.0	41.5	40.0	0.681
Fe	6.00	9.33	6.69	7.34	0.131
Zn	n.d.	n.d.	n.d.	n.d.	--
Co	0.67	0.94	1.13	0.91	0.015
	96.47	97.07	97.98	97.15	

1-4 Polydymite +Py+Vaesite Pt.350
5-7 Millerite +Polydymite pt.351

VAESITE

	1	2	Average	Atomic Ratio
S	51.3	51.1	51.2	1.599
Cu	n.d.	n.d.	n.d.	—
Ni	48.2	48.7	48.4	0.824
Fe	0.21	.11	0.16	0.003
Zn	n.d.	n.d.	n.d.	—
Co	0.58	0.46	.52	0.009
	100.29	100.37	100.28	

1-2 Pt.350

Table 4, Electron Microprobe Analyses of Sulfides in Altered Breccia Ore

MILLERITE

	1	2	3	Average	Atomic Ratio
S	35.0	35.0	34.9	35.0	1.09
Cu	.18	0.43	0.10	0.24	0.004
Ni	60.6	60.5	60.7	60.6	1.03
Fe	1.40	0.78	0.79	0.99	0.018
Zn	n.d.	n.d.	n.d.	n.d.	--
Co	0.59	0.72	0.75	0.69	0.012
	97.77	97.43	97.24	97.52	

1-3 Pt-351

BORNITE

	1	2	Average	Atomic Ratio
S	26.2	26.2	26.2	0.816
Cu	64.5	65.1	64.8	1.02
Ni	n.d.	n.d.	n.d.	--
Fe	6.35	6.45	6.40	0.114
Zn	n.d.	n.d.	n.d.	--
Co	n.d.	n.d.	n.d.	--
	97.24	97.75	97.4	

1-2 pt-351 Very Small Grains

CHALCOPYRITE

	1	2	Average	Atomic Ratio
S	34.9	33.7	34.3	1.09
Cu	36.2	36.1	35.0	0.0576
Ni	n.d.	n.d.	n.d.	--
Fe	29.2	30.0	29.6	0.54
Zn	n.d.	n.d.	n.d.	--
Co	tr	n.d.	n.d.	--
	100.3	99.8	99.9	

1-2 pt 351 with Bn.

Table 5, Electron Microprobe Analyses of Sulfides in Primary Disseminated Sulfides

CHALCOPYRITE

	1	2	Average	Atomic Ratio
S	34.0	35.2	34.6	1.081
Cu	34.1	33.7	33.9	.534
Co	tr	n.d.	--	--
Fe	30.3	30.8	30.6	0.548
	98.53	99.7	99.1	

1-2 4-013 113

BORNITE

	1	2	3	Average	Atomic Ratio
S	28.5	27.0	25.2	26.9	0.840
Cu	52.8	60.6	60.8	58.1	0.914
Co	n.d.	0.11	tr	tr	
Fe	17.8	11.5	15.1	14.8	0.265
Zn	0.14	.15	0.14	0.14	0.002
	98.94	99.36	101.24	99.94	

1-3 4-013 113

CUBANITE

	1	2	3	Average	Atomic Ratio
S	35.2	35.5	35.4	35.4	1.105
Cu	25.6	23.1	25.8	24.8	0.391
Co	n.d.	n.d.	n.d.	--	
Fe	39.4	40.4	40.6	40.1	0.719
Zn	n.d.	n.d.	n.d.	--	
	100.30	98.9	101.8	10013	

1-3 4-013 113

PYRRHOTITE

	1	2	3	Average	Atomic Ratio
S	36.8	36.7	36.3	36.6	1.143
Cu	n.d.	n.d.	n.d.	—	
Ni	n.d.	n.d.	n.d.	—	
Co	n.d.	n.d.	n.d.	—	
Fe	62.6	62.4	62.7	62.6	1.12
	99.4	99.1	99.0	99.2	

1-3 4-013 113

Table 5, Electron Microprobe Analyses of Disseminated Sulfides

PENTLANDITE

	1	2	3	Average	Atomic Ratio
S	33.5	32.0	32.4	32.6	1.019
Cu	0.86	1.25	2.54	1.55	0.024
Ni	27.4	30.9	31.0	29.8	0.507
Co	6.29	10.7	10.4	9.13	0.155
Fe	33.0	24.7	24.8	27.5	0.492
	101.05	99.55	101.14	100.21	

1-3 4-013 218

VIOLARITE

	4	Atomic Ratio
S	31.4	0.981
Cu	0.19	0.003
Ni	28.4	0.484
Co	5.92	0.100
Fe	31.6	0.566
	97.51	

4 4-013 218

Table 6, Electron Microprobe Analyses of Ag-Pd-Pt Minerals

STUETZITE

	1	2	3	4	5	Average	Atomic Ratio
Te	44.7	38.6	38.2	39.7	37.5	39.7	0.31
Bi	tr	0.5	n.d.	5.18	tr	--	--
Pd	4.10	0.53	n.d.	n.d.	n.a.	0.75	0.007
Pt	0.47	tr	n.d.	tr	n.a.	0.38	0.002
Fe	0.19	0.13	0.79	n.d.	n.a.	--	--
Ag	50.4	57.0	58.7	52.6	60.4	56.8	0.53
Ni	tr	n.d.	n.d.	1.02	n.a.	--	--
Co	n.d.	n.d.	n.d.	n.d.	n.a.	--	--
Au	4.12	2.15	n.d.	n.a.	1.41	1.54	0.008
	99.84	98.90	99.21	99.0	99.31	99.17	

1. Pt 348 Exsolved with Merenskyite
2. " " " "
3. " " " "
4. 600 Level cross-cut with Moncheite
5. BN Ore East Pit

UNKNOWN Ag_3BiTe_2

	1	2	Average	Atomic Ratio
Te	32.9	33.0	33.0	0.26
Bi	25.6	25.7	25.7	0.13
Pd	n.d.	n.d.	--	
Pt	n.d.	n.d.	--	
Fe	n.d.	n.d.	--	
Ni	0.98	0.16	0.57	0.01
Ag	40.0	40.1	40.1	0.37
Sb	tr	tr	tr	
	99.70	99.09	99.37	

1-2 600 Level cross-cut

Table 6, Electron Microprobe Analyses of Ag-Pd-Pt Minerals

MONCHEITE

	1	2	3	4	5	6	7	8
Te	56.3	56.2	54.5	53.1	55.0	55.5	56.4	56.5
Bi	7.24	6.73	7.38	7.27	7.47	7.77	7.36	7.44
Pd	11.6	12.0	11.8	11.3	11.8	11.1	11.7	11.8
Pt	21.9	22.4	23.2	24.4	22.6	23.0	22.1	21.9
Fe	0.17	0.13	0.13	0.21	0.45	0.15	0.11	0.20
Ni	0.84	0.87	0.82	0.88	0.95	1.04	0.97	1.02
	98.06	98.29	97.78	97.11	98.14	98.54	98.64	98.80

	9	10	11	Average	Std Dev	Atomic Ratio
Te	55.2	55.0	55.9	55.4	1.12	0.434
Bi	7.78	7.25	7.58	7.38	0.31	0.035
Pd	11.4	11.8	11.5	11.6	0.29	0.109
Pt	23.3	22.9	22.6	22.8	0.81	0.117
Fe	0.45	0.23	0.21	0.22	0.13	0.002
Ni	1.06	0.86	1.01	0.93	0.09	0.016
	99.03	98.04	98.77	98.33		

1-8. Th-8 600 Level cross-cut
9-11. Breccia " " "

MERENSKYITE

	1	2	3	Average	Atomic Ratio
Te	61.1	59.9	60.3	60.1	0.47
Bi	6.38	8.83	7.19	8.01	0.038
Pd	16.5	24.0	27.9	26.0	0.249
Pt	3.52	3.76	3.85	3.80	0.019
Fe	tr	n.d.	n.d.	n.d.	
Ag	9.53	2.23	2.01	2.12	0.02
Ni	n.d.	n.d.	n.d.	n.d.	
Co	0.41	n.d.	n.d.	n.d.	
Au	n.d.	n.a.	n.a.	n.a.	
	97.48	98.72	101.25	100.03	

KOTULSKITE

	4	Atomic Ratio
Te	53.5	0.42
Bi	1.80	0.009
Pd	44.2	0.41
Pt	2.31	0.012
Fe	n.d.	
Ag	n.d.	
Ni	n.d.	
Co	n.d.	
Au	n.a.	
	101.91	

1. Pt 348 Exsolved with Stuetzite
2. Pl Exsolved with Kotulskite
3. Pl Exsolved with Kotulskite
4. Pl Exsolved with Merenskyite

Appendix D. Electron Microprobe Analyses of Silicates and Oxides

Table 1 , Electron Microprobe Analyses of Silicate
Thierry Mine

Weight Percent

	1	2	3	4	5	6	Average
CaO	24.1	25.0	24.6	24.1	24.6	24.3	24.4
TiO_2	tr	tr	tr	tr	0.12	0.15	tr
MgO	12.0	13.1	13.4	14.4	14.0	14.8	13.6
FeO	8.65	7.32	6.85	7.24	7.47	7.31	7.47
NiO	tr	tr	n.d.	n.d.	n.d.	tr	tr
MnO	0.21	0.17	0.18	0.17	0.16	0.11	0.17
SiO_2	52.3	52.1	53.3	53.0	52.2	52.2	52.5
Al_2O_3	0.92	0.85	0.73	0.67	0.99	0.85	0.84
Total	98.3	98.6	99.1	99.6	99.5	99.8	99.0

Atomic Proportion

Ca	3.99	4.10	3.99	3.91	4.01	3.95	3.99
Ti	tr	tr	tr	tr	0.01	0.02	--
Mg	2.77	3.00	3.04	3.25	3.16	3.33	3.09
Fe	1.12	0.94	0.87	0.82	0.95	0.83	0.92
Mn	0.03	0.02	0.02	0.02	0.02	0.01	0.02
Ni	tr	tr	--	--	--	--	
Al	0.17	0.15	0.13	0.12	0.18	0.15	0.15
Si	7.92	7.84	7.93	7.85	7.79	7.76	7.85

1-6 Clinopyroxene Remnant in 4-013 In Mafic Metagabbro

Table 2 , Electron Microprobe Analyses of Silicates
Thierry Mine

	1	2	3	4	5	6	7
MgO	47.7	47.6	49.1	49.6	50.4	49.4	47.2
FeO	9.61	10.4	9.41	9.76	9.45	10.9	12.4
MnO	0.64	0.58	0.64	0.65	0.66	0.67	0.68
CaO	0.33	0.35	tr	tr	0.25	tr	tr
NiO	tr	0.10	tr	tr	tr	tr	tr
SiO_2	41.2	39.8	39.8	39.8	40.0	39.6	38.8
Total	99.5	98.8	99.0	99.9	100.7	100.7	99.1
Mg	10.5	10.6	10.9	10.9	11.0	10.8	10.6
Fe	1.19	1.30	1.17	1.21	1.16	1.35	1.56
Mn	0.08	0.08	0.08	0.08	0.08	0.08	0.09
Ca	0.05	0.06	--	--	0.04	0.01	--
Ni	--	--	--	--	--	--	--
Si	6.09	5.97	5.92	5.89	5.86	5.85	5.86
	Fo_{89}	Fo_{89}	Fo_{90}	Fo_{88}	Fo_{90}	Fo_{89}	Fo_{87}

	8	9	10	Average
MgO	47.8	48.6	48.2	48.6
FeO	11.9	11.8	11.2	10.7
MnO	0.66	0.60	0.63	0.64
CaO	tr	tr	tr	tr
NiO	tr	tr	tr	tr
SiO_2	39.4	39.3	39.7	39.7
Total	99.9	100.5	100.4	99.6
Mg	10.6	10.8	10.7	10.8
Fe	1.49	1.48	1.39	1.33
Mn	0.08	0.08	0.08	0.07
Ca	--	--	--	--
Ni	--	--	--	--
Si	5.88	5.84	5.89	5.91
	Fo_{88}	Fo_{88}	Fo_{88}	Fo_{89}

1-10 Metamorphic Olivine in 16-1E-2 an altered peridotite

Table 3, Electron Microprobe Analyses of Silicate
Thierry Mine

	1	2	3	4	5	6	7	Average
MgO	31.8	29.5	32.7	32.0	32.0	29.5	32.1	31.4
FeO	29.0	33.0	29.0	29.4	31.4	33.0	31.4	30.9
SiO_2	37.8	37.6	37.7	38.9	37.7	36.4	35.5	37.4
Total	98.6	100.1	99.5	100.3	101.0	98.9	100.3	99.7
Mg	7.72	7.18	7.88	7.63	7.66	7.32	7.91	7.61
Fe	3.96	4.52	3.92	3.93	4.28	4.59	4.34	4.22
Si	6.16	6.15	6.10	6.22	6.06	6.04	5.87	6.08
	Fo_{66}	Fo_{62}	Fo_{66}	Fo_{66}	Fo_{64}	Fo_{61}	Fo_{65}	Fo_{64}

1-7 Olivine remnants, 4-016, Al,Mn,Ca,Ni not detected in
Altered Dunite

table 4, Electron Microprobe Analyses of Silicates
Thierry Mine

	1	2	3	4	Average
K_2O	tr	0.18	tr	0.13	0.11
Na_2O	0.60	0.95	0.49	0.60	0.66
CaO	14.0	13.5	13.7	13.8	13.7
MgO	13.6	12.3	13.6	13.5	13.3
FeO	14.5	14.7	15.8	14.7	14.9
TiO_2	0.38	0.38	0.40	0.36	0.38
MnO	0.19	0.15	0.18	0.21	0.18
NiO	0.14	0.71	0.13	0.10	0.26
Al_2O_3	6.67	8.22	5.95	6.94	6.94
SiO_2	48.2	47.6	46.1	47.9	47.5
Total	98.4	98.7	96.4	98.2	97.9

K	--	0.04	--	0.03	0.02
Na	0.18	0.28	0.15	0.18	0.20
Ca	2.29	2.20	2.31	2.27	2.27
Mg	3.10	2.80	3.20	3.08	3.05
Fe	1.85	1.88	2.08	1.88	1.92
Ti	0.04	0.04	0.05	0.04	0.04
Mn	0.02	0.02	0.02	0.03	0.02
Ni	0.02	0.09	0.02	0.01	0.03
Al	1.20	1.48	1.10	1.25	1.26
Si	7.36	7.27	7.27	7.33	7.31

1-4 Hornblende from 4-013 in Mafic Metagabbro

Table 4b, Electron Microprobe Analysis of Silicates
Thierry Mine

	1	2	3	4	5	6	7	Average
K_2O	0.13	0.20	0.15	0.29	0.13	0.15	0.15	0.17
Na_2O	2.08	2.08	2.01	2.28	1.88	2.13	1.93	2.06
CaO	11.6	11.9	11.9	11.7	11.7	12.0	12.1	11.8
MgO	11.7	11.6	11.4	10.9	12.0	11.5	11.3	11.5
FeO	16.0	16.0	16.3	16.9	16.0	14.7	16.0	16.0
TiO_2	0.52	0.52	0.52	0.55	0.51	0.50	0.57	0.53
MnO	0.31	0.28	0.26	0.25	0.23	0.21	0.20	0.25
NiO	0.13	0.11	0.13	0.12	0.12	0.13	0.16	0.13
Al_2O_3	11.8	12.2	12.5	12.9	12.4	11.3	12.5	12.2
SiO_2	43.1	43.6	42.4	41.9	42.6	42.6	42.2	42.7
Total	97.3	98.5	97.5	97.7	97.7	96.8	97.2	97.3
K	0.03	0.04	0.03	0.06	0.03	0.03	0.03	0.03
Na	0.63	0.62	0.61	0.69	0.57	0.61	0.59	0.62
Ca	1.94	1.97	1.99	1.97	1.96	2.01	2.04	1.98
Mg	2.73	2.66	2.66	2.54	2.79	2.67	2.64	2.67
Fe	2.09	2.07	2.13	2.21	2.08	2.09	2.10	2.11
Ti	0.06	0.06	0.06	0.07	0.06	0.07	0.07	0.06
Mn	0.04	0.04	0.04	0.03	0.03	0.02	0.03	0.03
Ni	0.02	0.01	0.02	0.02	0.02	0.02	0.02	0.02
Al	2.18	2.22	2.31	2.39	2.28	2.28	2.31	2.28
Si	6.74	6.73	6.63	6.57	6.64	6.66	6.63	6.66

1-7 Hornblende from Amphibolite Schist 600 Level cross-cut

Table 4c , Electron Microprobe Analyses of Silicates
Thierry Mine

	1	2	3	4	5	Average
K_2O	0.15	0.23	0.14	0.14	0.15	0.16
Na_2O	1.98	1.86	1.78	1.95	1.84	1.88
CaO	12.0	11.7	12.3	12.0	12.2	12.0
MgO	12.1	11.8	11.8	11.6	11.5	11.8
FeO	16.0	16.0	15.6	15.7	16.0	15.9
TiO_2	0.65	0.51	0.49	0.53	0.58	0.55
MnO	0.23	0.19	0.22	0.24	0.19	0.21
NiO	0.11	0.13	0.14	0.14	0.16	0.14
Al_2O_3	12.0	12.7	12.2	12.5	12.3	12.4
SiO_2	42.7	41.6	42.6	42.6	42.5	42.3
Total	97.9	96.8	97.3	97.3	97.5	97.3
K	0.03	0.05	0.03	0.03	0.03	0.03
Na	0.60	0.57	0.54	0.59	0.56	0.57
Ca	2.00	1.98	2.07	2.00	2.05	2.02
Mg	2.81	2.78	2.76	2.69	2.69	2.75
Fe	2.08	2.12	2.04	2.05	2.10	2.08
Ti	0.08	0.06	0.06	0.06	0.07	0.06
Mn	0.03	0.03	0.03	0.03	0.02	0.03
Ni	0.01	0.02	0.02	0.02	0.02	0.02
Al	2.21	2.36	2.25	2.31	2.27	2.28
Si	6.64	6.55	6.66	6.66	6.64	6.63

1-5 Hornblende in Mafic Metagabbro 1600' cross-cut

Table 5, Electron Microprobe Analyses of Plagioclase from Pelites

	1		2		3		4	
CaO	7.62		7.96		7.97		7.84	
Na_2O	10.3		11.1		10.7		10.6	
K_2O	tr		n.d.		0.28		0.15	
Al_2O_3	22.3		21.8		22.4		22.2	
SiO_2	59.9		60.7		60.1		60.4	
Total	100.1		101.6		101.6		101.3	
Si	2.735	3.88	2.774	3.86	2.699	3.87	2.73	3.87
Al	1.178		1.075		1.173		1.14	
Ca	.336	1.26	.367	1.33	.377	1.33	.37	1.30
Na	.850		.945		.928		.93	
K	.000		.00		.002		--	
O	8.00		8.00		8.00		8.00	
Ab	70.8		71.6		71.0		70.5	
An	29.2		28.4		28.9		29.3	
Or	--		--		0.13		--	

1. Av 3 Points Core to Rim, in Contact with Garnet #1, Biotite #1
2. Av 2 Points Core to Rim, in Contact with Garnet #2, Biotite #2
3. Av 3 Points Core to Rim, in Contact with Garnet #3, Biotite #3
4. Av 8 Points Average

Table 6, Electron Microprobe Analyses of Garnets from Pelites

	1		2		3		4	
FeO	33.3		33.6		33.7		33.5	
MgO	3.67		3.76		3.39		3.62	
MnO	1.67		2.22		1.72		1.82	
Al_2O_3	19.2		19.3		19.5		19.3	
CaO	1.60		1.54		1.42		1.54	
SiO_2	38.1		37.9		38.0		38.0	
Total	97.5		98.4		97.9		98.0	
Fe	4.56		4.58		4.62		4.58	
Mg	0.90	5.96	0.91	6.07	0.81	5.92	0.88	5.98
Mn	0.23		0.31		0.23		0.25	
Ca	0.28		0.27		0.25		0.27	
Al	3.71		3.71		3.75		3.72	
Si	6.23		6.18		6.24		6.22	
O	24.0		24.0		24.0		24.0	
Alm	76.4		75.5		77.9		76.5	
Pyr.	15.0		15.0		13.9		14.7	
Sps.	3.9		5.1		4.0		4.2	
Grs.	4.7		4.4		4.2		4.5	

1. Av 4 Points Core to Rim in Contact with Plagioclase #1 and Biotite #1
2. Av 2 Points Core and Rim, in Contact with Plagioclase #2 and Biotite #2
3. Av 2 Points Core and Rim, in Contact with Plagioclase #3 and Biotite #3
4. Av 8 Points

Table 7, Electron Microprobe Analyses of Biotites from Pelites

	1		2		3		4	
FeO	17.1		18.5		17.4		17.5	
MgO	10.8		10.7		10.8		10.8	
K_2O	9.26		9.27		9.48		9.35	
SiO_2	36.2		35.6		36.3		36.0	
MnO	n.d.		.04		n.d.		tr	
Al_2O_3	20.3		20.1		20.3		20.2	
TiO_2	1.61		1.71		1.57		1.63	
Na_2O	.37		.29		.37		.34	
H_2O	4.01		3.98		4.03		4.00	
Total	99.7		100.2		100.2		100.0	
Si	5.42	8.0	5.32	8.0	5.401	8.0	5.374	8.0
Al	2.58		2.68		2.599		2.626	
Al	1.01		.87		.96		.93	
Ti	.18		.19		.18		.18	
Fe	2.04	5.70	2.32	5.82	2.17	5.69	2.21	5.72
Mn	nil		.05		nil		nil	
Mg	2.47		2.39		2.39		2.40	
Na	.11	1.82	.06	1.77	.11	1.91	.10	1.88
K	1.71		1.78		1.80		1.78	
H	4.0		4.0		4.0		4.0	
O	24.0		24.0		24.0		24.0	

1. Av3 Points, in Contact with Plagioclase #1 & Garnet # 1
2. Av3 Points, in Contact with Plagioclase #2 & Garnet #2
3. Av2 Points, in Contact with Plagioclase #3 & Garnet # 3
4. Av8 Points

Table 8. Electron Microprobe Analyses of Green Spinels from K31-1005, C Um-m Body

	1		2		3		4		5	
FeO	26.6		26.4		26.4		26.0		26.5	
Al_2O_3	54.7		55.1		55.3		56.2		56.6	
TiO_2	0.09		0.10		0.21		0.56		0.25	
MgO	12.4		11.7		11.8		11.9		11.8	
Cr_2O_3	0.16		0.15		0.19		0.17		0.16	
NiO	0.15		0.14		0.16		0.15		0.17	
ZnO	2.95		2.73		2.73		2.67		2.56	
MnO	0.24		0.20		0.19		0.19		0.20	
Total	97.2		96.5		96.9		97.8		98.2	
Recal	99.3		98.6		99.0		99.9		100.2	
Al_2O_3	11.0		11.2		11.1		11.2		11.2	
Cr_2O_3	0.02	12.27	0.02	12.42	0.03	12.44	0.02	12.45	0.02	12.48
TiO_2	0.01		0.01		0.03		0.07		0.03	
Fe_2O_3	1.24		1.19		1.28		1.26		1.23	
FeO	2.37		2.80		2.82		2.52		2.62	
MgO	3.13	6.13	3.00	6.21	3.01	6.22	2.99	6.23	2.95	6.24
NiO	0.20		0.02		0.02		0.02		0.02	
ZnO	0.37		0.36		0.34		0.33		0.32	
MnO	0.03		0.03		0.03		0.03		0.03	
$MgAl_2O_4$	52.0		49.0		49.2		48.6		48.2	
$ZnAl_2O_4$	6.16		5.65		5.63		5.41		5.19	
$FeAl_2O_4$	33.1		33.1		33.6		37.1		41.0	
$MnFe_2O_4$	0.60		0.65		0.67		0.60		0.60	
$FeFe_2O_4$	8.14		11.6		11.0		8.39		5.01	

Table 9, Electron Microprobe Analyses of Magnetites from Drill Hole K31-1005', G Um-m Body

	1		2		3		4	
FeO	87.8		87.4		87.8		87.6	
Al_2O_3	1.02		0.76		0.61		0.29	
TiO_2	0.67		0.83		0.71		0.73	
MgO	0.60		0.20		0.26		0.38	
Cr_2O_3	0.23		0.25		0.25		0.24	
NiO	tr		tr		tr		tr	
ZnO	tr		tr		tr		tr	
MnO	0.15		0.24		0.34		tr	
Total	90.5		89.8		90.0		89.4	
Recal.	99.3		98.9		99.1		98.6	
Al_2O_3	0.37		0.28		0.23		0.29	
Cr_2O_3	0.06	15.8	0.06	15.6	0.06	15.8	0.24	15.7
TiO_2	0.16		0.20		0.17		0.23	
Fe_2O_3	15.2		15.6		15.8		15.5	
FeO	7.59	7.92	7.82	7.82	7.90	7.91	7.64	7.82
MgO	0.28		0.09		0.12		0.18	
MnO	0.04		0.06		0.09			

Table 10, Electron Microprobe Analyses of Ilmenites
Drill Hole K31-1005, G Um-m Body

	1		2		3	
FeO	44.4		44.5		44.3	
Al_2O_3	tr		tr		n.d.	
TiO_2	51.8		50.6		50.7	
MgO	1.63		1.54		1.43	
Cr_2O_3	tr		tr		tr	
NiO	n.d.		n.d.		n.d.	
ZnO	n.d.		n.d.		0.16	
MnO	1.27		1.54		1.26	
Total	99.2		98.4		97.9	
CrO_2	7.88	8.06	7.80	8.0	7.84	8.08
Fe_2O_3	0.18		0.20		0.24	
FeO	7.35	8.02	7.30	8.0	7.40	8.08
MgO	0.49		0.47		0.44	
ZnO	--				0.02	
MnO	0.22		0.23		0.23	

1. Ilmenite Exsolution in Magnetite Rim
2. Ilmenite Exsolution in Magnetite Core
3. Ilmenite Isolated Grains

Appendix E Whole Rock Chemistry

11.1 Methods Used

The samples analysed for major and trace elements in this project were carried out at the following labs Durham England (samples with prefix D), Geological Survey of Canada, Ottawa, (samples with prefix GSC), X-Ray Assay Labs, Don Mills, (samples without prefix) and those carried out by UMEX Corp. Ltd. at an unknown lab, (samples with prefix KAP, K). Standard X-ray fluorescence, wet chemical, and emision spectroscopy are used by the first three labs. It was not possible to correlate the data from these labs.

One problem was noted in samples with high Cu, Ni or sulfur values due to difficulty in forming a fused sample for X-ray fluorescence. These samples have poor totals, (these are noted in tables).

Table 2a, Whole Rock Analyses Thierry Mine, Hornblende Chlorite Biotite Schist

	D1	D4	D6	D10	D14	2110	2960	3413	K_1-34	6029B
SiO_2	44.7	43.1	45.6	44.1	46.7	41.9	44.7	33.6	41.7	40.4
Al_2O_3	7.62	9.05	8.09	8.12	8.66	7.30	6.6	7.80	9.83	5.72
Fe_2O_3	4.74	4.85	4.31	4.07	4.76	12.5	11.9	16.3	20.7	27.6
FeO	13.9	13.91	12.3	12.4	13.4	5.83	1.37	5.36		
MgO	10.9	12.97	15.0	12.2	13.4	10.9	12.9	10.9	14.9	14.7
CaO	6.45	5.13	4.95	3.81	4.65	4.24	10.2	4.49	5.58	1.27
Na_2O	2.38	1.47	1.12	1.09	1.69	0.62	1.45	0.75	1.36	0.43
K_2O	0.25	2.48	2.85	2.85	1.86	2.90	0.07	0.97	0.50	0.45
TiO_2	0.38	0.53	0.40	0.44	0.42	0.60	0.60	0.80	0.30	0.31
P_2O_5	0.22	0.20	0.22	0.16	0.20	0.07	0.02	0.08	n.a.	n.a.
MnO	0.24	0.24	0.22	0.22	0.23	0.28	0.20	0.29	0.28	0.48
S	5.43	4.00	2.47	2.80	4.46	10.3	5.84	12.95	n.a.	n.a.
NiO	2.00	0.12	0.09	0.11	0.13	0.34	0.28	0.62	n.a.	n.a.
Cr_2O_3	n.d.	0.01	n.d.	n.d.	n.d.	0.01	0.06	.01	n.a.	n.a.
CO_2	3.11	1.46	0.99	7.36	n.d.	n.a.	n.a.	n.a.	n.a.	n.a.
H_2O	2.47	2.60	3.00	1.76	2.22	3.20	1.40	5.20	2.78	3.62
Total	104.77	102.14	101.65	100.83	102.84	101.08	100.18	100.74	97.93	94.98

D1 Hornblende Chlorite-Biotite Schist, 101E-10890N-312
D4 Hornblende Chlorite-Biotite Schist, 101E-11291N-1185
D6 Hornblende Chlorite-Biotite Schist, 312/98+75E/-17 150
D10 Hornblende Chlorite-Biotite Schist, 101E-11683N-1593
D14 Hornblende Chlorite-Biotite Schist, 101E-10841N-545
2110 Hornblende Chlorite-Biotite Schist, location unknown
2960 Hornblende Chlorite-Biotite Schist, location unknown
K-34 Hornblende Chlorite-Biotite Schist, location unknown
6029B Hornblende Chlorite-Biotite Schist, location unknown

Table 2b, Whole Rock Analyses Thierry Mine, Ultramafic Rocks and Mafic Metagabbro

	D3	D5	D17	D20	D21	D22	D23	KAP4	GSC13
SiO_2	41.9	39.8	45.7	49.0	42.0	48.8	45.0	49.1	38
Al_2O_3	9.64	8.50	3.77	4.06	11.1	4.47	7.67	5.00	2
Fe_2O_3	5.42	4.98	3.36	3.09	4.49	3.12	4.31	4.02	12
FeO	15.5	14.5	9.56	8.67	12.9	8.79	12.1	6.58	7.4
MgO	15.0	21.6	23.2	18.7	15.2	18.3	15.0	17.1	26
CaO	4.31	3.80	10.2	13.2	6.76	12.7	11.9	13.8	3
Na_2O	0.65	0.08	0.21	0.79	1.82	0.80	1.40	0.87	0.07
K_2O	2.18	0.01	0.01	0.07	0.76	0.23	0.04	0.18	0.10
TiO_2	0.64	0.21	0.30	0.47	0.38	0.44	0.51	0.40	0.18
P_2O_5	0.19	0.17	0.19	0.05	0.22	0.07	0.13	0.03	tr
MnO	0.31	0.31	0.20	0.21	0.30	0.20	0.22	0.20	0.18
S	0.23	0.80	0.88	0.24	0.13	0.06	0.08	0.47	0.52
NiO	0.03	0.07	0.10	0.05	0.05	0.06	0.03	0.08	0.19
Cr_2O_3	tr.	tr.	0.09	0.12	tr.	0.14	0.02	0.08	0.01
CO_2	1.23	0.67	0.33	n.d.	1.03	0.42	n.d.	n.a.	n.d.
H_2O	2.84	4.84	2.57	1.60	2.94	1.66	1.77	0.60	5.3
Total	100.13	100.48	100.64	100.31	100.12	100.23	100.10	98.51	95.48

D3 Biotite-Hornblende Schist, 105+50E, 10603N, 414
D5 Talc-Chlorite Schist, 101E, 11195N, 1197
D17 Talc Schist, 101E, 11215N, 1192
D20 Mafic Metagabbro, 101E, 11385N, 1593
D21 Mafic Metagabbro, 101E, 10970N, 539
D22 Mafic Metagabbro, 101E, 10650N, 312
D23 Mafic Metagabbro, 101E, 10867N, 544
KAP4 Mafic Metagabbro, Unknown Location
GSC13 Olivine-Tremolite Ultramafic, 101E, 16-1E-2-200
Approximate due to excess Sulfur & Copper

Table 2b, Whole Rock Analyses Thierry Mine, Metagabbro

	D9	D12	D15	D16	D24	D25	KAP6
SiO_2	48.6	53.43	44.9	49.8	43.8	48.0	46.0
Al_2O_3	13.9	15.19	12.1	5.60	9.73	10.8	12.1
Fe_2O_3	2.70	2.09	4.57	3.16	5.28	4.06	7.09
FeO	7.54	5.85	12.7	8.85	14.8	11.3	9.46
MgO	10.6	3.86	10.5	15.5	14.5	11.3	9.12
CaO	11.1	6.27	7.31	12.8	5.56	7.41	6.84
Na_2O	3.26	4.81	3.02	1.45	1.66	3.41	3.75
K_2O	0.23	2.86	1.75	0.18	1.31	1.15	2.10
TiO_2	0.54	0.80	0.87	0.60	0.81	0.59	0.80
P_2O_5	0.17	0.17	0.23	0.07	0.22	0.23	0.11
MnO	0.16	0.16	0.25	0.20	0.33	0.24	0.25
S	0.06	1.17	0.39	0.07	0.22	0.22	0.91
NiO	0.02	0.02	0.03	0.02	0.03	0.03	0.04
Cr_2O_3	0.06	n.d.	n.d.	n.d.	n.d.	n.d.	n.d.
CO_2	0.10	2.96	n.d.	n.d.	n.d.	n.d.	n.a.
H_2O	1.09	0.70	1.60	1.64	1.96	1.33	0.40
Total	101.72	100.30	100.23	100.04	100.1	100.07	98.93

D9	Metagabbro	101E-11625N-1593
D12	Biotite Metagabbro	101E-10525N-312
D15	Biotite Metagabbro	101E-10600N-312
D16	Metagabbro	101E-10622N-257
D24	Biotite Metagabbro	105+50-10559N-421
D25	Biotite Metagabbro	101E-10625N-312
KAP6	Metagabbro	Location Unknown

Table 2c, Whole Rock Analyses Thierry Mine, Amphibolite Schist

	D2	D7	D8	D13	D18	D19	KAP2	K_1-11	K_1-1
SiO_2	47.9	48.4	47.8	47.7	47.9	47.5	44.7	46.2	50.9
Al_2O_3	13.6	12.4	13.3	13.9	14.0	10.4	15.7	15.4	14.6
Fe_2O_3	3.11	3.51	3.10	3.19	3.62	4.25	2.87	12.5	10.3
FeO	8.74	9.96	8.72	8.92	10.1	11.9	5.34		
MgO	9.74	8.24	10.1	9.30	7.19	8.21	12.1	11.3	5.70
CaO	11.3	12.6	12.0	11.9	12.7	10.8	10.3	8.24	8.94
Na_2O	2.59	0.93	2.11	2.03	2.03	3.45	1.95	1.91	3.88
K_2O	0.22	0.07	0.13	0.34	0.08	0.21	0.96	0.47	0.57
TiO_2	0.68	0.82	0.70	0.73	0.92	1.42	0.30	0.74	1.24
P_2O_5	0.16	0.08	0.13	0.14	0.10	0.19	0.06	n.a.	n.a.
MnO	0.17	0.21	0.18	0.20	0.22	0.24	0.15	0.18	0.24
S	0.08	0.08	0.10	0.14	0.16	0.10	0.72	n.a.	n.a.
NiO	0.02	0.01	0.01	0.01	0.01	0.01	0.60	n.a.	n.a.
Ca_2O_3	0.04	0.02	0.04	0.05	0.02	0.02	0.05	n.a.	n.a.
CO_2	0.68	1.62	0.48	0.12	0.08	n.d.	n.a.	n.a.	n.a.
H_2O	1.08	1.14	1.28	1.45	1.02	1.48	2.20	2.04	1.08
Total	100.1	100.1	100.1	100.2	100.1	100.1	98.0	98.94	97.86

D2	Amphibolite Schist	101E-11615N-1593
D7	Amphibolite Schist	312-101E-10460N
D8	Amphibolite Schist	101E-11010N-536
D13	Amphibolite Schist	101E-10710N-312
D18	Amphibolite Schist	101E-111N-35-1196
D19	Massive Amphibolite	101E-10577N-262
KAP2	Amphibolite Schist	Unknown Location
K_1-11	Epidote Amphibolite Schist	Unknown Location
K_1-1	Amphibolite Schist	Unknown Location

Table 3a, Whole Rock Analyses K1:1 Ultramafic Body, Ultramafic Rocks with Blackwall Alteration

	1488	1498	1500	1434	1435	1442	1444	1446	1447	1448	1474	1475	1478	1479	1457	1460
SiO_2	42.8	58.3	35.7	45.6	57.7	43.2	44.3	42.4	40.7	41.9	54.2	42.2	46.4	47.3	33.6	34.4
Al_2O_3	17.6	11.9	12.0	8.15	13.5	5.51	9.29	14.3	12.2	8.34	11.9	17.4	6.57	6.63	14.2	14.2
FeO	10.4	5.07	15.8	14.1	5.39	17.0	17.0	16.3	15.4	16.2	6.08	11.4	9.51	6.91	17.1	17.1
MgO	9.59	8.59	20.5	18.2	7.63	18.7	17.5	11.02	14.2	16.0	10.8	9.26	20.7	20.9	16.6	18.7
CaO	7.27	4.94	5.49	8.99	4.34	7.83	8.68	9.07	7.09	8.10	5.86	7.66	6.93	6.95	4.59	0.14
Na_2O	3.73	5.85	0.67	1.18	6.77	0.56	1.51	2.90	1.81	1.11	4.50	2.79	0.24	0.32	0.80	0.28
K_2O	1.42	1.05	0.05	1.06	0.71	1.95	0.58	0.88	2.59	0.86	1.61	2.84	4.36	4.55	3.44	7.79
TiO_2	0.07	0.34	0.43	0.14	0.38	0.16	0.21	0.13	0.13	0.28	0.39	0.09	0.43	0.53	0.36	0.20
MnO	0.12	0.08	0.17	0.23	0.10	0.23	0.25	0.21	0.18	0.22	0.11	0.13	0.17	0.12	0.23	0.16
L.O.I.	2.35	1.06	6.18	2.71	1.38	2.80	2.85	1.29	1.92	3.34	1.05	2.15	2.09	1.93	3.58	3.35
Total	95.36	97.17	97.00	100.43	97.95	97.95	97.01	96.47	96.52	96.33	96.44	95.81	97.44	96.15	94.38	96.95

1488 K371 -124,
1498 K371 -310,
1500 K371 -327,
1434 K372 - 98,
1435 K372 - 99,
1442 K372 -182,
1444 K372 -190,
1446 K372 -192,
1447 K372 -197,
1448 K372 -206,
1474 K372 -325,
1475 K372 -345,
1478 K372 -385,
1479 K372 -388,
1457 K373 -164,
1460 K373 -170,

Table 3a, Whole Rock Analyses K1:1 Um-m Body with Blackwall Alteration

	1461	1462
SiO_2	23.1	43.9
Al_2O_3	12.5	2.30
Fe_2O_3		
FeO	26.3	19.0
MgO	24.6	18.7
CaO	0.04	8.30
Na_2O	n.d.	0.10
K_2O	n.d.	0.93
TiO_2	0.53	0.16
MnO	0.19	0.36
L.O.I.	9.59	2.35
Total	96.95	96.05

	GSC20	GSC21	GSC22	GSC23	GSC26	GSC28
SiO_2	41	44.5	43.5	44.4	46	48
Al_2O_3	8	8.0	10.3	12.1	8	13
Fe_2O_3	16	5.8	3.2	3.4	16	2
FeO		9.4	10.8	9.6		7
MgO	16	17.6	17.2	13.9	14	9
CaO	9	6.01	5.29	6.80	7	10
Na_2O	1.04	1.3	1.6	2.4	1.01	3
K_2O	2	2.68	1.72	2.6	3.0	1
TiO_2	0.33	0.19	0.17	0.26	0.19	0.6
MnO	0.18	0.24	0.26	0.20	0.15	0.12
H_2O	2.5	2.8	3.8	2.6	2.6	1.6
CO_2	n.d.	n.d.	n.d.	n.d.	n.d.	n.d.
S	1.1	0.25	0.22	0.02	1.8	0.25
P_2O_5	tr	0.05	0.04	0.16	tr	0.3
Total	97.52	99.0	98.1	98.7	100.23	96.05

1461	K373 178
1462	K373-178
GSC20	K208 770
GSC21	K208 685
GSC22	K208 545
GSC23	K208 470
GSC26	K329 491
GSC28	K329 56

Table 3b, Whole Rock Analyses K1:1 Ultramafic Body, Metagabbro and Mafic Metagabbro

	1491	1495	1496	1499	1503	1505	1432	1458	1459	1463	1465	1466
SiO_2	53.1	51.0	49.5	48.7	48.4	48.7	43.1	38.0	45.8	53.4	50.3	49.6
Al_2O_3	14.1	15.7	16.8	16.7	17.1	6.34	8.91	5.55	1.34	14.7	16.7	11.9
Fe_2O_3												
FeO	7.34	10.6	6.05	7.87	6.63	14.6	14.4	21.9	18.3	7.51	6.80	10.3
MgO	6.73	5.37	4.92	3.73	4.80	12.41	15.7	19.7	16.8	6.63	6.09	10.3
CaO	7.59	8.38	15.7	15.1	13.7	11.01	9.80	7.29	10.6	7.60	11.7	10.1
Na_2O	5.34	5.05	2.65	2.96	3.15	1.40	1.66	0.19	0.21	5.70	3.87	3.13
K_2O	0.20	0.37	0.17	0.12	0.22	0.24	0.13	0.04	0.05	0.49	0.31	0.48
TiO_2	0.50	0.79	0.36	0.66	0.48	0.21	0.19	0.37	0.18	0.55	0.23	0.28
MnO	0.14	0.14	0.11	0.21	0.13	0.24	0.22	0.29	0.26	0.13	0.13	0.17
L.O.I.	1.36	1.02	0.93	1.23	1.44	1.63	2.71	4.17	2.60	0.78	0.73	0.86
Total	96.41	98.37	97.17	97.33	96.10	96.71	96.79	97.46	96.12	97.52	96.88	97.09

1491	K371	200,
1495	K371	265,
1496	K371	284,
1499	K371	321,
1503	K371	353,
1505	K371	394,
1432	K372	94,
1458	K37	165,
1459	K373	169,
1463	K373	205,
1465	K373	214,
1466	K373	235.

Table 3b, Whole Rock Analyses K1:1 Ultramafic Body, Metagabbro amd Mafic Metagabbro

	1433	1436	1437	1438	1439	1440	1441	1443	1473	1477	1449	1451	1454	1455
SiO_2	42.4	41.8	48.1	43.5	42.3	53.4	56.9	42.1	36.9	47.9	49.0	49.1	48.7	58.6
Al_2O_3	6.13	11.6	9.1	16.0	11.5	16.0	16.8	5.99	2.11	15.9	15.6	14.4	16.4	13.3
Fe_2O_3														
FeO	18.0	14.6	8.31	11.7	15.0	7.13	4.98	19.8	28.0	8.68	6.30	7.48	5.76	5.01
MgO	17.8	13.8	7.66	9.55	12.6	6.62	2.85	19.6	22.2	4.32	6.65	7.43	6.32	6.77
CaO	8.32	9.74	10.9	7.64	10.8	8.56	5.62	8.28	1.05	15.5	16.2	14.4	15.1	5.76
Na_2O	0.67	1.75	3.84	3.31	2.12	5.25	7.03	0.48	n.d.	2.74	2.15	2.80	2.41	6.72
K_2O	0.06	1.25	0.39	1.72	0.45	0.27	0.18	0.03	n.d.	0.19	0.23	0.28	0.15	0.10
TiO_2	0.13	0.41	0.19	0.13	0.12	0.81	0.75	0.21	0.25	0.75	0.43	0.32	0.36	0.35
MnO	0.20	0.19	0.13	0.13	0.20	0.13	0.07	0.26	0.29	0.21	0.13	0.14	0.11	0.09
L.O.I.	4.12	2.17	1.03	1.86	1.78	1.02	1.75	3.43	6.55	1.17	1.13	1.32	0.65	1.18
Total	97.80	97.19	99.62	95.53	96.82	99.12	95.78	100.25	97.26	97.25	97.91	96.25	96.25	97.90

1433	K372	96,
1436	K372	104,
1437	K372	107,
1438	K372	112,
1439	K372	116,
1440	K372	151,
1441	K372	180,
1443	K372	185,
1473	K372	312,
1477	K372	345,
1449	K373	56,
1451	K373	71,
1454	K373	133,
1455	K373	148,

Table 3b, Whole Rock Analyses K1:1 Um-m Body

	METAGABBRO				AMPHIBOLITE	
	GSC19	GSC18	GSC25	GSC29	GSC24	GSC30
SiO_2	48.3	42	47	46.9	47.0	48.5
Al_2O_3	11.5	16	9.0	14.5	14.0	14.8
Fe_2O_3	7.8	4	11.9	2.7	2.8	2.8
FeO	3.2	7.5	[illegible]0	8.2	9.5	9.1
MgO	11.7	10	12	9.61	9.44	7.73
CaO	12.9	11	14	11.2	11.9	12.1
Na_2O	1.6	2	1.08	2.6	1.9	2.3
K_2O	0.43	0.5	0.4	0.38	0.44	0.33
TiO_2	0.56	0.08	0.6	0.37	0.80	1.01
MnO	0.18	0.11	0.15	0.17	0.18	0.22
H_2O	1.9	1.6	1.6	1.7	1.9	1.3
CO_2	0.1	0.1	n.d.	n.d.	n.d.	n.d.
S	0.06	1.10	0.25	0.06	0.07	0.06
P_2O_5	0.02	tr	n.d.	0.01	0.02	0.07
Total	100.5	96.37	97.19	98.15	100.1	100.6

GSC19	K208	880
GSC18	K208	995
GSC25	K329	56
GSC29	K329	31
GSC24	K208	425
GSC30	K234	21

Approximate due to Excess S
" " " " "

Table 4, Whole Rock Analyses J. Um-m Body

	ULTRAMAFIC ROCKS					METAGABBRO			AMPHIBOLITE
	GSC7	GSC8	GSC9	GSC10	KAP3	GSC5	GSC6	KAP5	KAP1
SiO_2	40.5	38.3	42.8	41.0	35.0	48.4	48.6	46.2	46.9
Al_2O_3	11.9	6.6	8.9	3	5.10	9.6	13.8	12.9	10.9
Fe_2O_3	16.7	20.5	3.5	16	13.7	2.8	14.9	3.00	4.41
FeO			12.8		20.7	9.4		12.7	10.4
MgO	13.0	20.7	19.1	26	14.4	10.5	6.0	7.15	7.24
CaO	7.6	3.72	4.47	2	2.61	11.5	9.0	7.37	10.7
Na_2O	2.0	n.d.	0.5	0.12	0.80	1.4	2.8	3.70	1.78
K_2O	0.34	n.d.	0.05	tr	0.46	0.64	0.40	0.81	0.22
TiO_2	0.36	0.32	0.23	0.13	2.50	0.86	1.68	1.10	1.70
MnO	0.22	0.32	0.28	0.17	0.40	0.22	0.20	0.25	0.24
H_2O	3.9	5.5	6.1	4.9	0.80	2.0	1.40	0.60	0.30
CO_2	0.1	1.40	0.1	3.4	n.a.	0.1	n.d.	n.a.	n.a.
S	1.9	1.40	0.37	1.8	0.45	0.28	1.0	0.75	0.90
P_2O_5	0.08	0.06	0.09	tr	0.10	0.07	0.10	0.09	0.10
Total	98.6	98.7	99.4	98.63	97.12	98.1	100.0	96.63	95.81

GSC 7 K61 270
GSC 8 K61 450
GSC 9 K61 650
GSC10 K61 760 - Approximate due to Excess S
KAP 3 Unknown Location
GSC 5 K61 95
GSC 6 K61 150
KAP 5 Unknown Location
KAP 1 Unknown Location

Table 5, Whole Rock Analyses G Um-m Body

	ULTRAMAFIC ROCKS				AMPHIBOLITE	
	GSC1	GSC2	GSC3	GSC4	GSC11	GSC12
SiO_2	38	39	31	35.5	48.6	49.5
Al_2O_3	1.29	5	3	2.7	14.6	14.5
Fe_2O_3	23	5	36	24.8	4.1	2.1
FeO		11.8			5.0	10.6
MgO	19	17	17	25.2	4.51	7.42
CaO	5	5	2	2.24	15.5	9.67
Na_2O	0.17	0.87	0.50	n.d.	2.5	2.1
K_1O	0.20	2	0.2	0.02	0.34	0.34
TiO_2	0.33	0.11	2	0.26	1.39	1.18
P_2O_5	tr	tr	tr	0.08	0.13	0.12
MnO	0.24	0.23	0.29	0.38	0.28	0.20
S	2.6	0.77	1.3	2.1	0.28	0.09
CO_2	0.3	n.d.	0.10	0.2	0.9	n.d.
H_2O	3.3	3.7	2.9	5.3	1.1	1.80
Total	98.57	90.58	96.47	98.8	99.1	99.8

GSC1 K31 435 Approximate due to Excess S
GSC2 K31 710 " " "
GSC3 K31 930 " " "
GSC4 K31 1085 " " "
GSC11 Epidote Amphibolite Schist, K228 254
GSC12 Massive Amphibolite K228 378

Table 6a, Trace Element Analyses, Thierry Mine

	D2	D7	D8	D13	D18	D19	KAP2
Ba	19	37	7060	80	56	206	86
Nb	3	1	1	5	3	8	n.a.
Zr	42	48	39	43	55	96	36
Y	19	21	19	19	25	24	n.a.
Sr	110	104	122	128	119	615	139
Rb	3	2	3	9	3	4	60
Zn	86	88	85	82	94	135	85
Cu	115	46	113	169	611	307	47
Ni	159	129	138	147	126	119	272
Cr	391	227	416	450	247	250	549
Ce	12	19	14	14	16	35	n.a.
La	5	8	7	8	8	20	n.a.
Ag	2	2	2	2	2	2	n.a.
Th	1	1	1	1	1	1	n.a.
Pb	2	3	7	5	2	2	n.a.
V	n.a.	n.a.	n.a.	n.a.	n.a.	n.a.	39

D2 Amphibolite Schist, 101E-11615N-1593
D7 " " 312-101E-10460N
D8 " " 101E-11010N-536
D13 " " 101E-10710N-312
D18 " " 101E-111N-35 1196
D19 Massive Amphibolite 101E-10577N-262
KAP2 Amphibolite Schist, Location Unknown

Table 6a, Trace Element Analyses, Thierry Mine

	ULTRAMAFIC AND MAFIC METAGABBRO								METAGABBRO						
	D23	D22	D21	D20	D17	D5	D3	KAP6	D25	D24	D16	D15	D12	D9	KAP6
Ba	39	49	150	60	35	34	165	86	278	162	91	363	917	47	252
Nb	2	4	3	4	1	3	4	n.a.	4	7	5	5	8	1	n.a.
Zr	27	35	32	38	29	22	46	36	55	58	55	43	184	26	77
Y	14	12	9	11	10	9	9	n.a.	13	14	14	10	21	16	n.a.
Sr	146	150	182	131	74	62	50	139	504	231	216	316	1342	181	315
Rb	3	2	29	1	1	4	95	60	43	51	4	59	98	8	85
Zn	112	81	158	74	131	152	175	85	133	174	92	147	113	79	120
Cu	207	120	145	829	3844	445	195	47	333	155	151	308	37	112	172
Ni	312	629	478	562	997	716	355	272	345	373	479	256	11	209	222
Cr	225	1413	11	1240	895	19	29	549	18	8	798	18	7	374	37
Ce	16	19	15	20	12	13	14	n.a.	17	25	31	17	83	15	n.a.
La	4	9	5	11	7	4	2	n.a.	6	5	11	8	40	4	n.a.
Ag	2	2	2	2	5	3	2	n.a.	2	2	2	2	2	2	n.a.
Th	1	1	1	1	1	1	4	n.a.	1	54	1	1	1	1	n.a.
Pb	8	1	5	1	3	1	8	n.a.	2	4	3	1	10	6	n.a.
V	n.a.	n.a.	n.a.	n.a.	n.a.	n.a.	n.a.	39	n.a.	n.a.	n.a.	n.a.	n.a.	n.a.	2

D23	Mafic Metagabbro	101E-10867N-544
D22	" "	101E-10650N-312
D21	" "	101E-10970N-539
D20	" "	101E-11385N-1593
D17	Talc Schist	101E-11215N-1192
D5	Talc-Chlorite Schist	101E-11195N-1197
D3	Biotite-Hornblende Schist	105+50E-10603N-414
KAP4	Mafic Metagabbro, Unknown Location	
D25	Biotite Metagabbro	101E-10625N-312
D24	" "	105+50E-10559N-421
D16	Metagabbro	101E-10622N-257
D15	Biotite Metagabbro	101E-10600N-312
D12	" "	101E-10525N-312
D9	Metagabbro	101E-11625N-1593
KAP6	" Unknown Location	

Table 6a, Trace Element Analyses, Thierry Mine, Chlorite-Biotite Schist.

	D14	D10	D6	D4	D1	2110	2960	3413	GSC14	GSC15	GSC16	GSC17
Ba	206	148	149	220	58	115	n.d.	n.d.	135	20	230	35
Nb	3	4	5	4	3	n.a.	n.a.	n.a.	n.a.	n.a.	n.a.	n.a.
Zr	30	32	32	43	32	44	49	36	193	195	190	194
Y	9	4	9	9	10	n.a.	n.a.	n.a.	57	53	69	58
Sr	233	169	146	201	171	150	175	150	82	20	99	51
Rb	181	339	311	221	10	98	12	40	n.a.	n.a.	n.a.	n.a.
Zn	96	120	247	111	26	120	93	104	n.a.	n.a.	n.a.	n.a.
Cu	6350	21900	13700	16100	29800	16600	13700	14600	42900	84300	27600	25400
Ni	1307	1081	887	1169	1632	2200	1800	4000	2700	2900	2020	1530
Cr	70	53	170	144	94	103	611	147	50	200	57	180
Ce	5	22	12	21	8	n.a.	n.a.	n.a.	n.a.	n.a.	n.a.	n.a.
La	2	2	2	2	5	n.a.	n.a.	n.a.	n.a.	n.a.	n.a.	n.a.
Ag	20	6	12	13	25	n.a.	n.a.	n.a.	14	42	n.d.	n.d
Th	2	2	3	4	1	n.a.	n.a.	n.a.	n.a.	n.a.	n.a.	n.a.
Pb	8	7	13	4	8	n.a.	n.a.	n.a.	n.a.	n.a.	n.a.	n.a.
V	n.a.	n.a.	n.a.	n.a.	n.a.	67	50	75	36	28	52	83

D14 101E-10841N-545
D10 101E-11683N-1593
D6 312-98+75E-17 150
D1 101E-10890N-312
2110 Location Unknown
2960 Location Unknown
3413 Location Unknown
GSC14 12-9E-0 45
GSC15 12-8W-0 145
GSC16 12-23E-0 200
GSC17 12-14W-25 300

Table 6b, Trace Element Analyses, K1:1 Ultramafic Body

	ULTRAMAFIC ROCKS WITH BLACKWALL ALTERATION				METAGABBRO					AMPHIBOLITE		
	GSC20	GSC21	GSC22	GSC23	GSC26	GSC28	GSC19	GSC18	GSC25	GSC29	GSC24	GSC30
Ba	330	1330	460	902	2100	790	110	160	480	160	250	58
Co	130	120	110	89	100	39	59	100	64	51	51	35
Cr	120	23	17	49	55	280	98	19	185	230	230	150
Cu	2700	470	660	79	4200	1330	250	1800	1400	370	250	110
Ni	950	820	640	500	510	260	300	810	460	200	180	120
Sr	79	71	110	990	120	400	210	380	200	200	170	68
V	66	27	27	52	52	140	160	72	200	150	290	250
Y	46	44	n.d.	46	n.d.	n.d.	n.d.	n.d.	44	n.d.	46	50
Zr	79	60	58	81	83	98	57	77	64	38	49	63

GSC20	K208-770
GSC21	K208-685
GSC22	K208-545
GSC23	K208-470
GSC26	K329-491
GSC28	K329- 56
GSC19	K208-880
GSC18	K208-995
GSC25	K329-557
GSC[illegible]	K329-31
GSC[illegible]	K208-425
GSC30	K234-21

Table 6c, Trace Element Analyses, J+I Um-m Body

	ULTRAMAFIC ROCKS					METAGABBRO		AMPHIBOLITE	
	GSC7	GSC8	GSC9	GSC10	KAP3	GSC5	GSC6	KAP5	KAP1
B	204	n.d.	n.d.	n.d.	n.a.	n.d.	n.d.	n.a.	n.a.
Ba	74	n.d.	n.d.	9	n.d.	181	130	94	69
Co	171	212	160	200	n.a.	68	84	n.a.	n.a.
Cr	9	4	13	17	356	310	14	39	189
Cu	8630	3900	1200	2500	134	1900	3800	216	211
Ni	1260	1120	880	1120	308	400	690	172	160
Sr	280	67	28	90	168	230	350	409	93
V	36	42	n.d.	n.d.	144	180	320	72	78
Y	44	57	54	44	n.a.	58	47	n.a.	n.a.
Zn	n.d.	n.d.	n.d.	n.d.	138	n.d.	n.d.	110	112
Zr	11	100	62	78	54	110	130	92	86
Rb	n.a.	n.a.	n.a.	n.a.	22	n.a.	n.a.	28	10

GSC7	K61-270
GSC8	K61-450
GSC9	K61-650
GSC10	K61-760
KAP3	Unknown Location
GSC5	K61-95
GSC6	K61-150
KAP5	Unknown Location
KAP1	Unknown Location

Table 6d, Trace Element Analyses G Um-m Body

	ULTRAMAFIC ROCKS				AMPHIBOLITE	
	GSC1	GSC2	GSC3	GSC4	GSC11	GSC12
Ba	25	240	34	n.d.	130	54
Co	320	180	350	323	45	43
Cr	160	79	720	32	154	170
Cu	2700	1100	2250	4000	160	250
Ni	1200	710	1070	1010	130	140
Sr	61	160	43	56	280	160
V	36	46	66	n.d.	350	310
Y	60	49	78	65	51	57
Zr	110	61	95	106	80	91

GSC1 K31-435
GSC2 K31-710
GSC3 K31-930
GSC4 K31-1085
GSC11 Epidote-Amphibolite Schist, K228-254
GSC12 Massive Amphibolite, K228-378

Appendix F Mine Sections

Table 1, Key to Drill Hole Numbers

Co-Ordinates of Drill Holes used in Sections

Holes Outside Mine : Collars are located by co-ordinates of cut and chained lines, dips were determined with acid test approximately every 100'

Holes in Thierry Mine : Collars are located by survey, dips were determined with acid tests every 100' and azimuth by a tro-pari at the end of the hole, all holes projected on to section

Drill Hole Numbers

K Surface Hole

OP. Open Pit

260-101E + 5NW Direction Drilled
+ Up
- Down 5 Degrees

Section 101E

Level of Collar 1E

All Co-ordinates are in reference to head Frame, bench mark

10000E, 10000N, 00Z

Table 2, Drill Holes used to Construct Geologic Sections

SECTION THIERRY DEPOSIT

SECTION 90E

Hole Number	X	Y	Z
600-90E-0°SE	8999E	-11164N	-588'
600-90E-30°SE	8999E	-11165N	-591'
1200-10W-HOR.NW	9000E	-11064N	-1188
1200-10W-35°NW	9000E	-11064N	-1192
1600-80E°SE	9000E	-11847.0	-1586

SECTION 95E

K264, OP.5W-45°SE	9500E	-10480.	+2.6
K273, OP.5W-45°SE	9488E	-10580	+2.7
K239	9500E	-10650	+7
K94	9625E	-10847	+13 NOTE DRILLED OFF SECTION
600-95E-0°SE	9500E	-11208	-588
600-95E-45°SE	9500E	-11210	-592
600-95E-75°SE	9500E	-11214	-593
1200-95E-HOR NW	9501E	-11191	-1104
1200-95E-35°NW	9501E	-11194	-1105

SECTION 98E

OP.2W-45°SE	9800E	-10632	+7
OP.2W-45°SE K266	9795E	-10698	+9
OP.2W-45°SE K258	9804E	-10806	+14
K216	9800E	-10900	+18
K334 OP98E-60°SE	9800E	-11100	+1
260-98E+35°NW	9803E	-10521.N	-263
260-98E-5°NW	9803E	-10522N	-266
260-98E-20NW	9803.0E	-10522N	-269
260-98E-35°NW	9803.0	-10522N	-269
600-98E+23°SE	9800	-10692	-594
600-98E+2°SE	9800	-10692	-594
600-98E-33°SE	9800	-10692	-594
600-98E+74NW	9798	-10699	-594
600-98E+42NW	9798	-10705	-594
600-98E+20NW	9798	-10705	-594
600-98E+ONW	9798	-10702	-594
600-98E-20°NW	9798	-10702	-594
600-2W-HOR SW	9797	-11250	-591

Table 2, Drill Holes used to Construct Geologic Sections

Hole Number	X	Y	Z
600-103-170NW	10300E	-10691N	-596
600-3E-HOR SE	10299E	-1275N	-591
600-3E-35°SE	10299E	-1275N	-595
600-3E-75°SE	10302E	-1284N	-595
1200-3E+45NE	10300E	-11105	-1190
1200-3E+35NE	10300E	-11105	-1190
1200-3E-HOR NE	10300E	-1156N	-1190
1200-3E-30°NW	10299E	-1156N	-1191
1600-3E-HOR SE	10303E	-1938N	-1588
1600-3E-45°SE	10303E	-1937N	-1592
1600-3E-VERT SE	10303E	-1946N	-1592
SECTION 105E			
OP5E-45°SE K251	10506E	-10408N	+4
OP5E-45°SE K261	10498E	-10683N	-1
OP105E-53°SE K316	10500E	-10882N	+1
400-105E+78°NW	10503E	-10557N	-404
400-105E+38°NW	10501E	-10557N	-410
400-105E-0°	10501E	-10559N	-410
600-105E+72NW	10503E	-10664N	-588
600-105E+27°NW	10502	-10667	-591
600-105E+5°NW	10502	-10667	-590
600-105E-19°NW	10503	-10667N	-595
600-5E-HOR SE	10499	-1276N	-591
600-5E-35SE	10499E	-1276N	-594
600-5E-75°SE	10499E	-1276N	-594
1200-5E-HOR NW	10501E	-1132N	-1192
1200-5E-35°NW	10501E	-1133N	-1195
1600-5E-HOR SE	10498E	-1931N	-1589
1600-SE-45°SE	10498E	-1930N	-1592
1600-SE-VERT SE	10499E	-1947N	-1592
SECTION 110E			
OP.10E-45° 535°E	11002E	-10294N	-4
OP.110E-45°SE K295	10983E	-10394N	0
OP 10E-45° K245	11002E	-10601N	+2
600-110E-HOR SE	11000E	-11272N	-589
600-110E-25°SE	11000E	-11272N	-592

Table 2, Drill Holes used to Construct Geologic Sections

Hole Number	X	Y	Z
1200-10E+75NW	11000E	-11074N	-1194
1200-10E-HOR NW	11000E	-11077N	-1190
1200-10E-35°NW	11100E	-11077N	-1193
1600-10E-HOR SE	10995E	-11876N	-1586
1600-10E-35°SE	10996E	-11876N	-1590
SECTION 115E			
K311 OP.115E-45°SE	11498E	-10218N	+0
K307 OP.115E-45°SE	11501E	-10310N	-14
K362	11498E	-10639N	-13
600-115E-0°SE	11499E	-11269N	-584
600-115E-45°SE	11499E	-11260N	-590
600-115E-75°SE	11499E	-11275N	-590
1200-115E-HOR NW	11501E	-11048N	-1186
1200-115E-35°NW	11502E	-11048N	-1191
1200-115E-45°SE	11502E	-11035N	-1191
1600-115E+20°SE	11498E	-11820N	-1583
1600-115E-0°SE	11498E	-11820N	-1584
1600-115E-45°SE	11499E	-11819N	-1587
1600-115E-90°SE	11499E	-11825N	-1588
SECTION 120E			
K308 OP120E-45°SE	11999E	-10207N	-7
K191	12019E	-10263N	+0
K304 OP120E-45°SE	12000E	-10363N	-11
K200	12000E	-10450N	-5
K58	12004E	-105210N	-9
600-120E-0°SE	11999E	-11166N	-585
600-120E-36°SE	11999E	-11168N	-587
1200-120E+90NE	12000E	-10907N	-1181
1200-120E+50°NE	12000E	-10907N	-1181
1200-120E-HOR NW	12000E	-10910N	-1185
1200-120E-35°NW	12000E	-10903N	-1187

Table 2, Drill Holes used to Construct Geologic Sections

Hole Number	X	Y	Z
600-98E-50°SE	9796E	-11253	-595
1200-98E-HOR NW	9800E	-11192	-1126
1200-98E-35°NW	9799E	-11195	-1192
1600-2W-HOR SE	9798E	-11902	-1589
1600-2W-35SE	9798E	-19100	-1592
SECTION 101E			
K255	10100E	-10610N	+20
K235	10100E	-10660N	+28
K285	10100E	-10801N	+20
K286	10100E	-10890N	+18
260-101E+5NW	10100E	-10552N	-259
312-101E-0NW	10100E	-10603N	-310
312-101E-30°NW	10100E	-10602N	-311
400-101E+50NW	10132E	-10674N	-424
400-101E+16°NW	10138E	-10690N	-420
400-101E+2°NW	10138E	-10690N	-428
600-101E-45°SE	10100E	-11280N	-595
600-101E-70°SE	10100E	-11282N	-595
1200-1E-HOR NW	10100E	-11102N	-1202
1200-1E-30NW	10100E	-11102N	-1204
1200-1E+60NW	10100E	-11098N	-1200
1600-1E-HOR SE	10100E	-11952N	-1604
1600-1E-90	10100E	-11952N	-1608
SECTION 103E			
K253 OP.3E-45°SE	10300E	-10439N	+1
K116	10321E	-10473N	+14
K112	10356E	-10524N	+20
K284 OP.3E-45°SE	10300E	-10601N	+6
K263 OP.3E-45°SE	10297E	-10795N	+4
400-103E+75°NW	10302E	-10635	-410
400-103E+43°NW	10303E	-10636	-412
400-103E+11°NW	10303E	-10638	-413
400-103E-12°NW	10303E	-10638	-418
600-103E+45°NW	10300E	-10690	-590
600-103E+20°NW	10300E	-10692	-592
600-103E+5°NW	10300E	-10692	-593

Table 2, Drill Holes used to Construct Geologic Sections.

Hole Number	X	Y	
SECTION 160E		K1:1	
K175		160E-124N+20	
K111		160E-126N	
K156		160E-131N	
K190		160E-136N	
SECTION 180E		K1:1	
K373		180E-121N	
K373		180E-123N+50	
K136		180E-126N	
SECTION 46N		ZONE J	
K22		66E- 46N	
K14		72E- 46N	
K 9		76E- 46N	
K16		80E- 46N	45WEST
K15		80E- 46N	VERTICAL
SECTION 76E		ZONE J	
K55		76E-29N+50	
K89		76E-35N	
K11		76E-38 +50N	
K62		76E-42N	
K 9		76E-46N	
K10		76E-50N	
K13		76E-51 +50N	
SECTION ON		ZONE G	
K40		4W+25	-ON
K23		2W	-ON
K52		1E	-ON
K37		4E	-ON
SECTION OW		ZONE G	
K41		OW	59+50
K29 (Projected)		2W	ON
K31		OW	4N
K35		OW	8N

Table 3, Drill Holes Logged by Author

SURFACE

K185, K188, K235, K255, K285, K286, K342, K343
K344, K345, K348, K349, K358A, K358B, K358C, K376
K377, K378, K379, K380, K381, K382, K383, K384
K385, K386, K387

260 LEVEL

260-97E+45NW
260-97E+50E+70NW
260-97E+50E+20NW
260-97E+50E-30°NW
260-98+50E+70°NW
260-98+75E+55NW
260-98+75E-35°NW
260-99+50°+65NW
260-100+25E+45°NW
260-100+75E+15°NW
260-101E+5°NW
260-102E+30NW
260-97E+15NW
260-97E+50E+45°NW
260-97E+50E-10°NW
260-98E+25E-0°NW
260-98+50E+47NW
260-98+75E+20°NW
260-99E+32°NW
260-99+50E+40°NW
260-100+75E+47°NW
260-100+75E-20°NW
260-101+50E+50°NW
260-102E-51°SE

312 LEVEL

312-98+75E-17°NW

400 LEVEL

400-99+50E+53°NW
400-99+50E-30°NW
400-100E+50E+43°NW
400-100E+50E-8°NW
400-100E+75-75SE
400-101E+30NW
400-101E+10NW
400-101E-0°SE
400-101E+50-10SE
400-102E+50E+44°NW
400-102E+50E-11NW
400-103+50E+30°NW
400-100E+35°NW
400-100E-0°NW
400-100E+50E+15NW
400-100E+75°NW
400-101E+50NW
400-101E+16NW
400-101E+2NW
400-101E-52°SE
400-102E+50NW
400-102E+50E+12NW
400-103+50E+60°NW
400-103+50E+5°NW

Table 3, Drill Holes Logged by Author

400-103+50E-20°NW
400-104+50E40NW
400-104+50E-20°NW
400-105+50E+43°NW
600-105+50E-18°NW
400-10E+58°NW
400-104+50E+5°NW
400-105E+78°NW
400-105+50E+10°NW

550 LEVEL

550-101E+20°NW

600 LEVEL

600-96+50E-18°NW
600-97E+60°NW
600-97E+30°NW
600-97E+28°SE
600-98E+20°NW
600-98E-20°NW
600-98E+63°NW
600-99E-45°SE
600-100E+33°SE
600-100E+11°
600-100+50E-11°NW
600-101-HOR NW
600-101-43°SE
600-101-70°SE
600-103E-17°NW
600-103E-75°SE
600-104E+21°NW
600-104E-0°SE
600-105E-19°NW
600-97E+85°NW
600-97E+29°NW
600-97E-18°NW
600-98E+42°NW
600-98E-0°NW
600-98E+50E-11°NW
600-99E+34°NW
600-100E+60°SE
600-100E+13°
600-100E+23°
600-100+50E-11°NW
600-103E+45°NW
600-103E+20°NW
600-103E+30°NW
600-103E-35°SE
600-104E+74°NW
600-104E+12°NW
600-105E+72°NW

1200 LEVEL

1200-101EHOR
1200-101E-30°
1200-104E-35°NW
1200-105E-35°NW
1200-107E-0°NW
1200-108E-35°NW
1200-97E-0°NW
1200-98E-0°NW
1200-101E+31
1200-104E-0°NW
1200-105E-HOR NW
1200-106E-35°NW
1200-107E-33°NW
1200-103E-35°NW
1200-97E-35°NW

Table 3, Drill Holes Logged by Author

1600 LEVEL

1600-4E-35°	1600-1W-HOR SE
1600-1W-45°SE	1600-0-HOR NW
1600-1E-45°SE	1600-1E-90°
1600-2E-HOR SE	1600-3E-HOR SE
1600-3E-45SE	

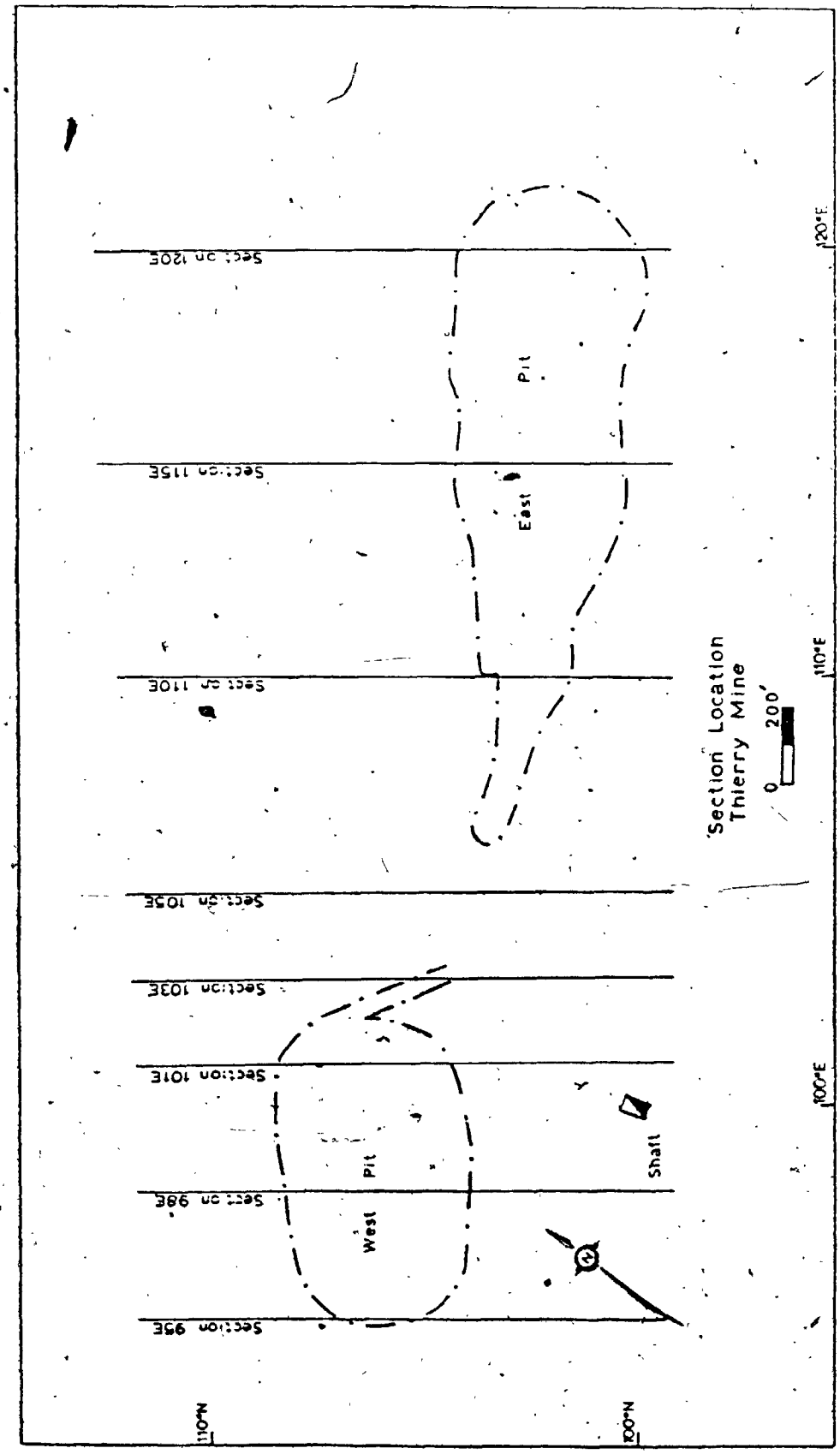
Section Location
Thierry Mine
0
200'
Section 120E
Section 115E
Section 110E
Section 105E
Section 103E
Section 101E
Section 98E
Section 95E
Pit
East
Pit
West
Shaft
110°N
100°N
120°E
110°E
100°E

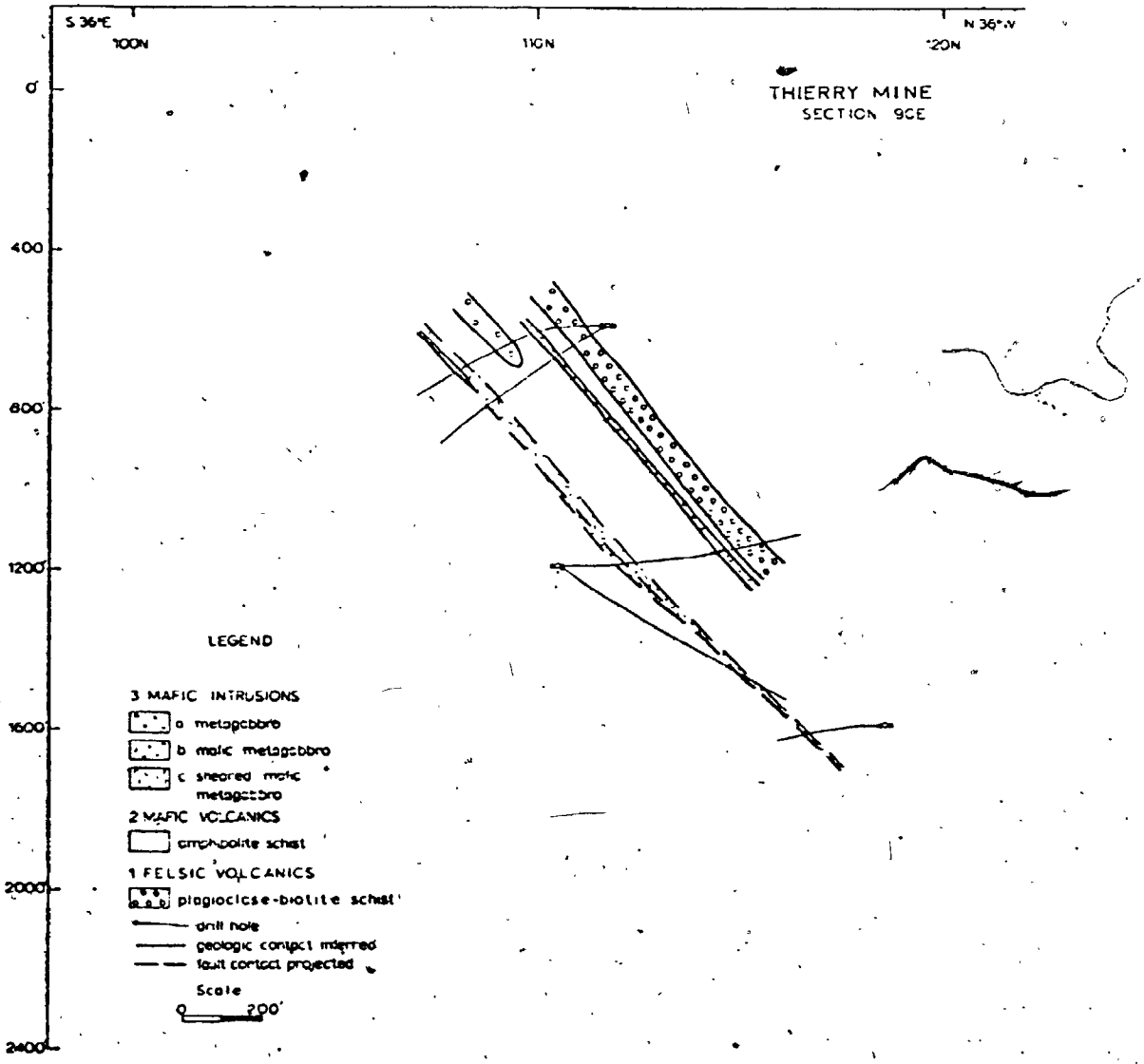
S 36°E
100N
110N
120N
N 36°W
0'
400'
800'
1200'
1600'
2000'
2400'
THIERRY MINE
SECTION 90E
LEGEND
3 MAFIC INTRUSIONS
a metagabbro
b mafic metagabbro
c sheared mafic metagabbro
2 MAFIC VOLCANICS
amphibolite schist
1 FELSIC VOLCANICS
plagioclase-biotite schist
drill hole
geologic contact inferred
fault contact projected
Scale
0
200'

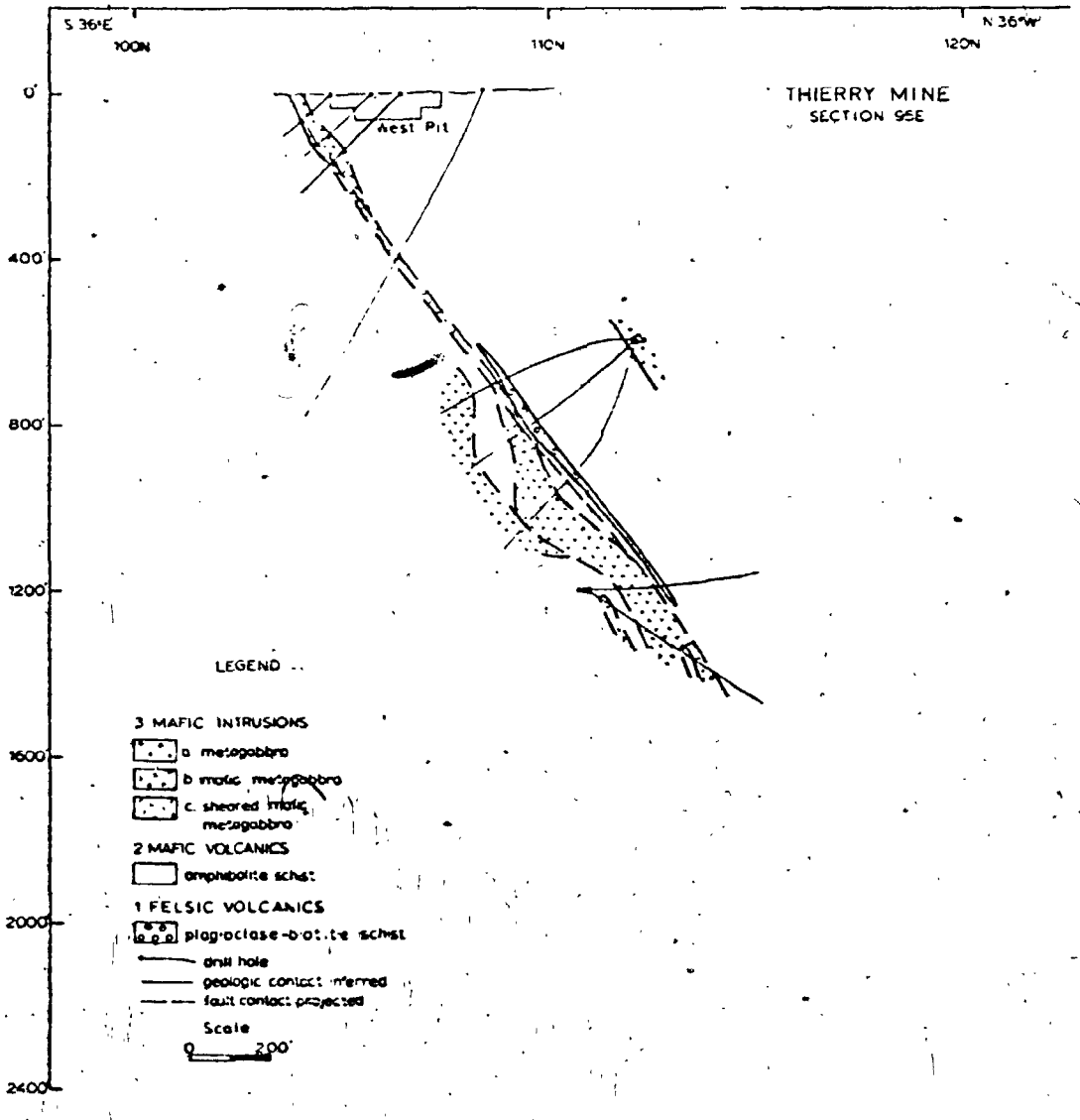
S 36°E
100N
110N
120N
N 36°W
0'
400'
800'
1200'
1600'
2000'
2400'
West Pit
THIERRY MINE
SECTION 95E
LEGEND
3 MAFIC INTRUSIONS
a metagabbro
b mafic metagabbro
c. sheared mafic metagabbro
2 MAFIC VOLCANICS
amphibolite schist
1 FELSIC VOLCANICS
plagioclase-biotite schist
drill hole
geologic contact inferred
fault contact projected
Scale
0
200'

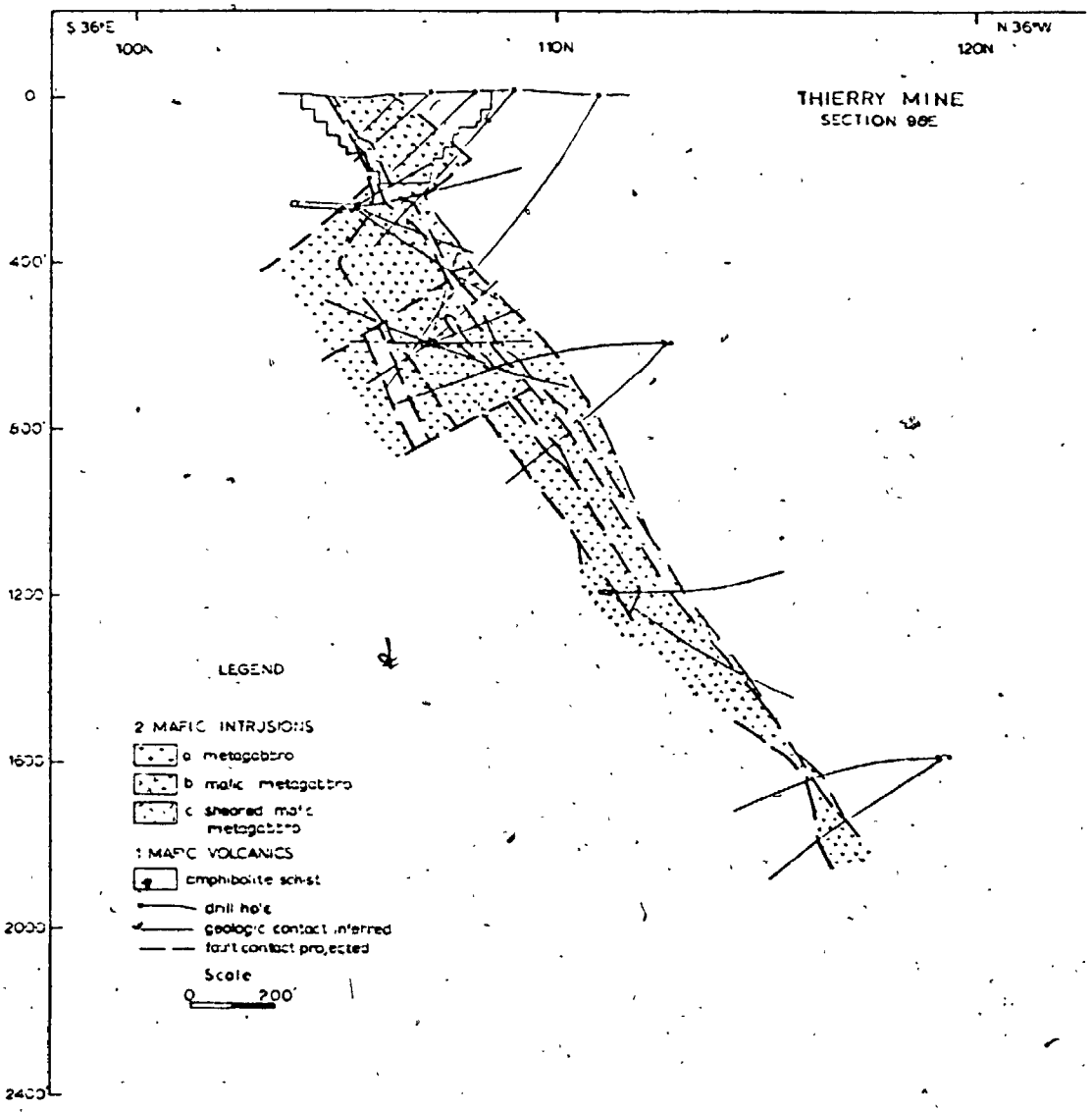
S 36°E
100N
110N
120N
N 36°W
0
400'
800'
1200
1600
2000
2400
THIERRY MINE
SECTION 98E
LEGEND
2 MAFIC INTRUSIONS
a metagabbro
b mafic metagabbro
c sheared mafic metagabbro
1 MAFIC VOLCANICS
amphibolite schist
drill hole
geologic contact inferred
fault contact projected
Scale
0 200'

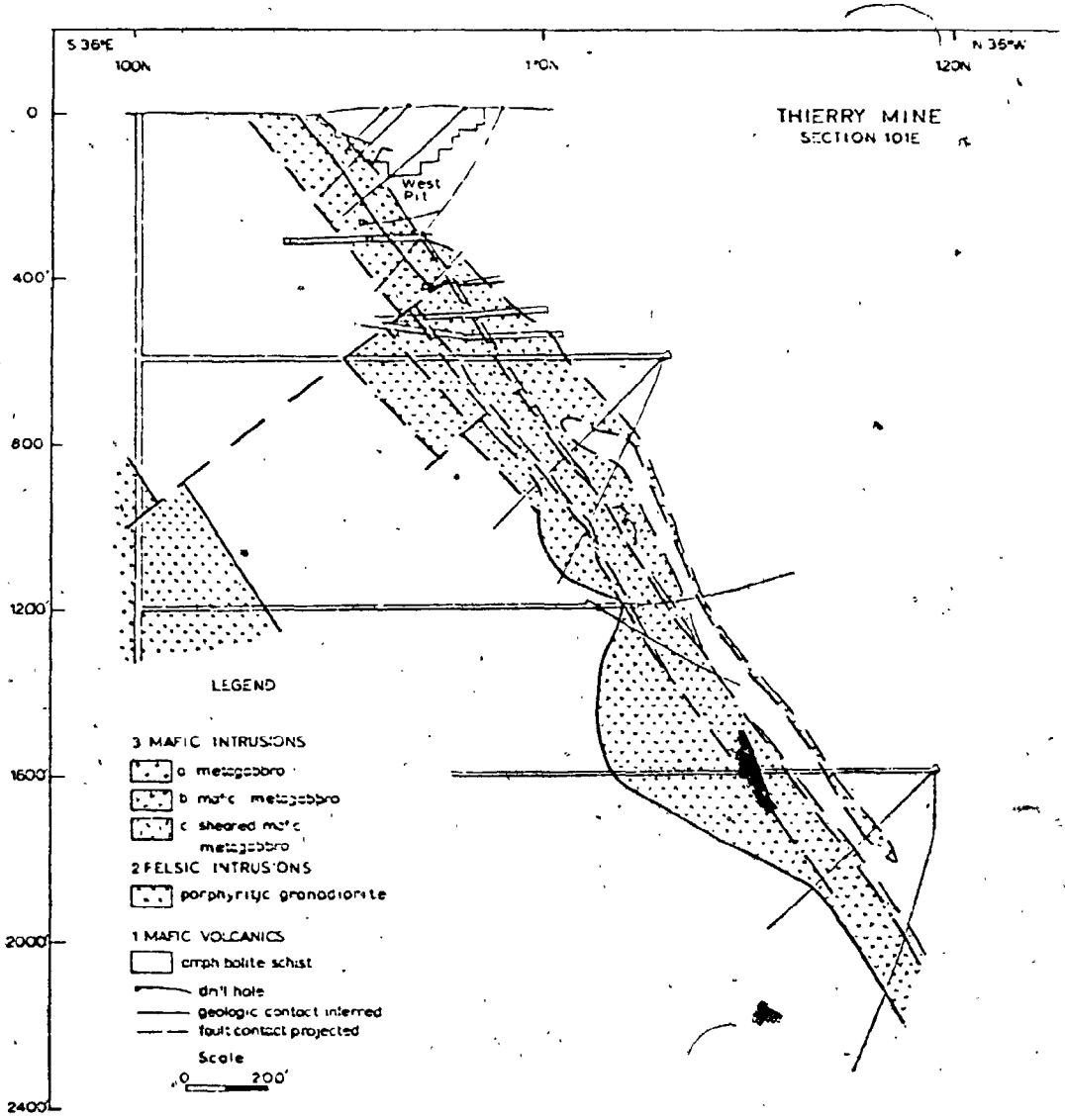
S 36°E
100N
1°0N
120N
N 35°W
0
400'
800
1200'
1600'
2000'
2400'
THIERRY MINE
SECTION 101E
West Pit
LEGEND
3 MAFIC INTRUSIONS
a metagabbro
b mafic metagabbro
c sheared mafic metagabbro
2 FELSIC INTRUSIONS
porphyritic granodiorite
1 MAFIC VOLCANICS
amph bolite schist
drill hole
geologic contact inferred
fault contact projected
Scale
0 200'

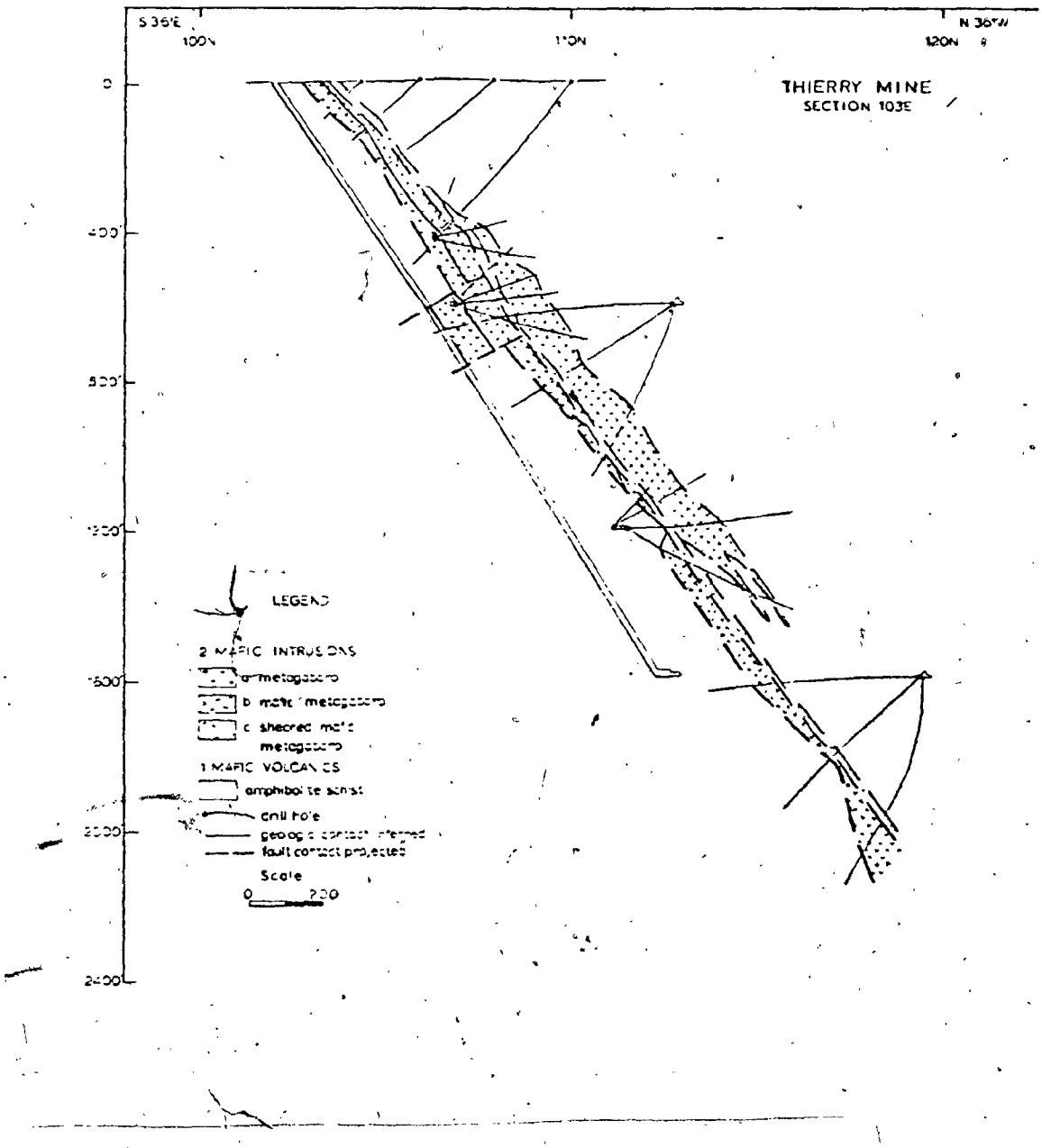
S 36°E
100N
N 36°W
120N
THIERRY MINE
SECTION 103E
0
400'
800'
1200'
1600'
2000'
2400'
LEGEND
2 MAFIC INTRUSIONS
a metagabbro
b mafic metagabbro
c sheared mafic metagabbro
1 MAFIC VOLCANICS
amphibolite schist
drill hole
geological contact inferred
fault contact projected
Scale
0
200

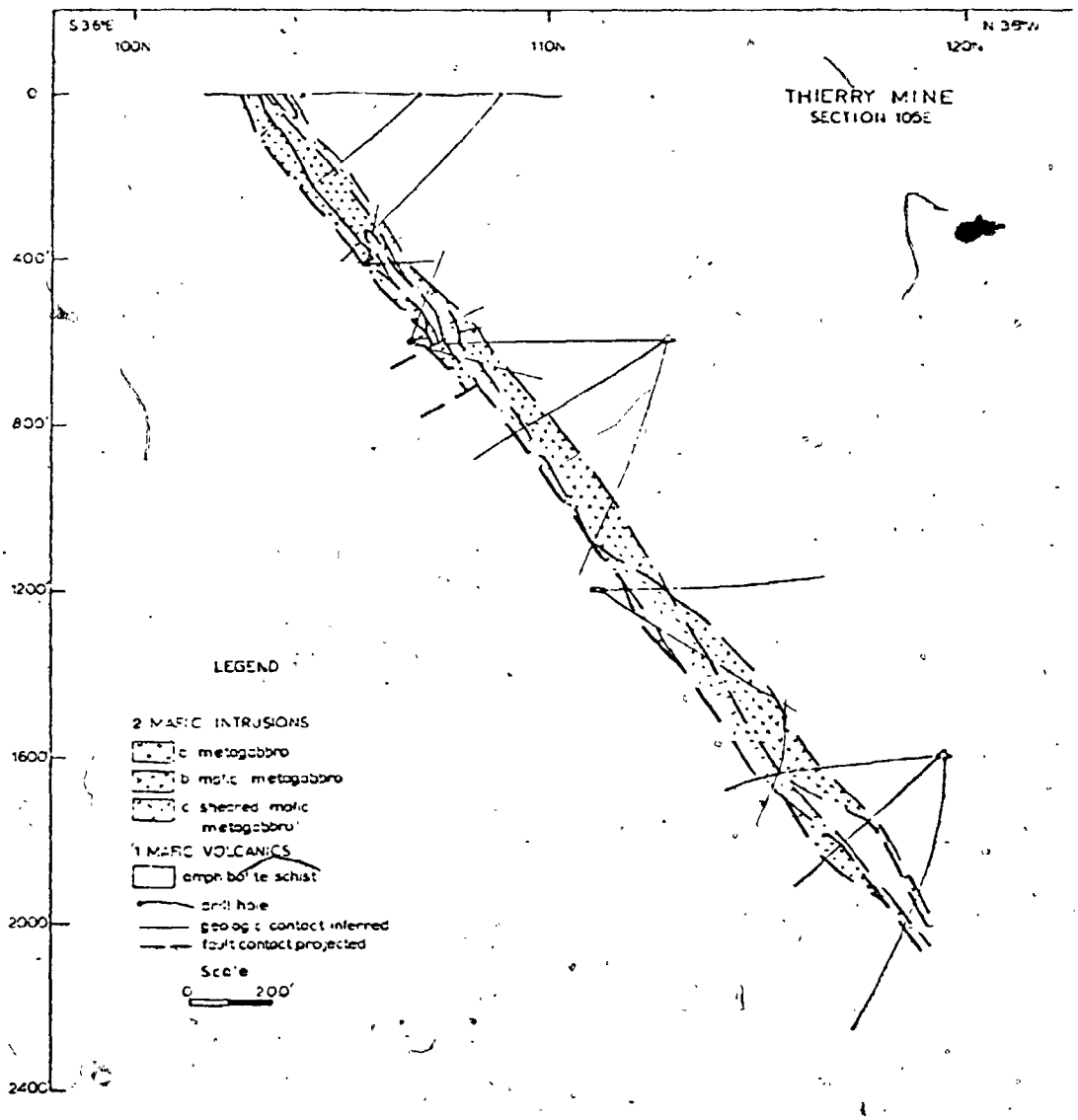
S 36°E
100N
110N
120N
N 36°W
0
400'
800'
1200'
1600'
2000'
2400'
THIERRY MINE
SECTION 105E
LEGEND
2 MAFIC INTRUSIONS
c metagabbro
b mafic metagabbro
c sheared mafic metagabbro
1 MAFIC VOLCANICS
amphibolite schist
drill hole
geologic contact inferred
fault contact projected
Scale
0 200'

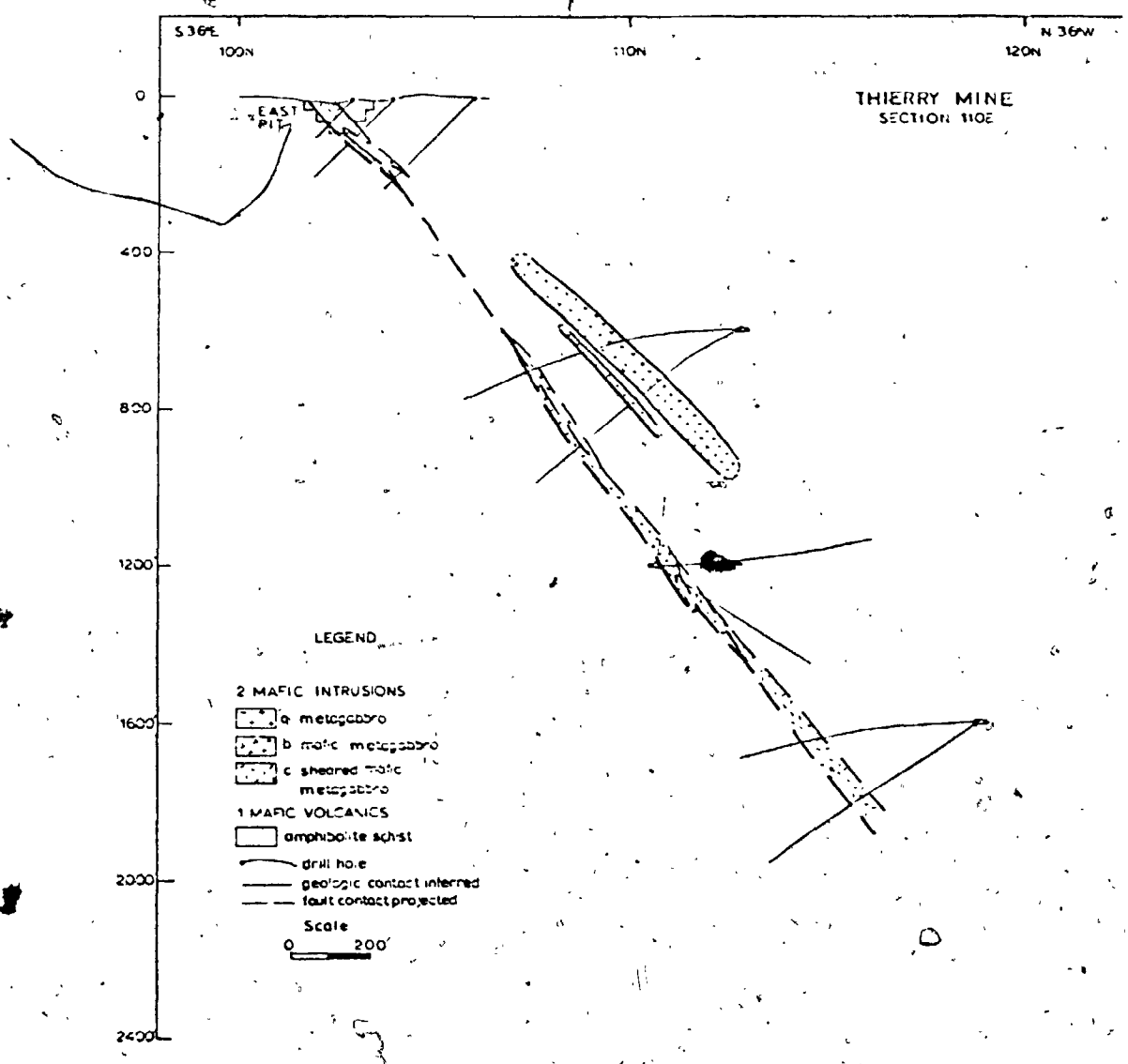
S 36E
100N
110N
120N
N 36W
0
400
800
1200
1600
2000
2400
EAST PIT
THIERRY MINE
SECTION 110E
LEGEND
2 MAFIC INTRUSIONS
a metagabbro
b mafic metagabbro
c sheared mafic metagabbro
1 MAFIC VOLCANICS
amphibolite schist
drill hole
geologic contact inferred
fault contact projected
Scale
0 200'

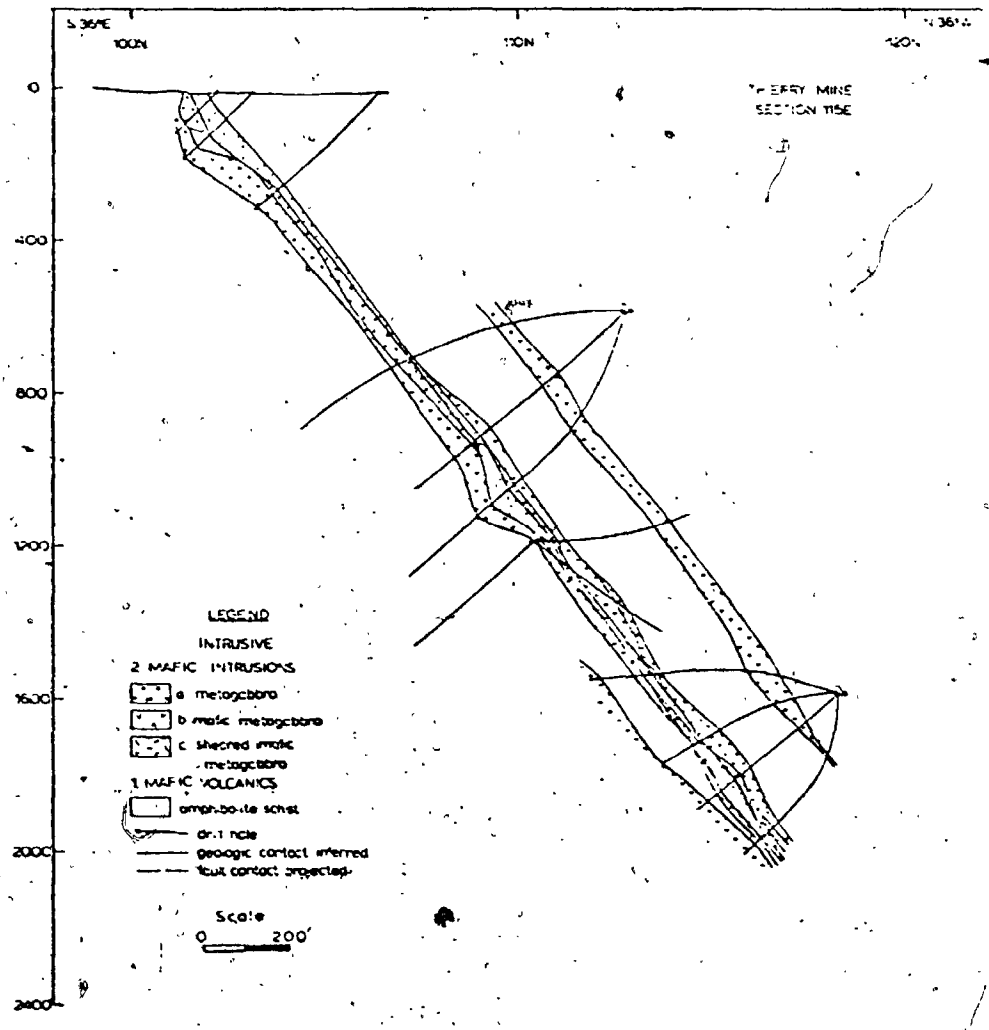
5,365E
100N
110N
120N
0
400
800
1200
1600
2000
2400
LEGEND
INTRUSIVE
2 MAFIC INTRUSIONS
a metagabbro
b mafic metagabbro
c sheared mafic metagabbro
1 MAFIC VOLCANICS
amphibolite schist
drill hole
geologic contact inferred
fault contact projected
Scale
0 200'

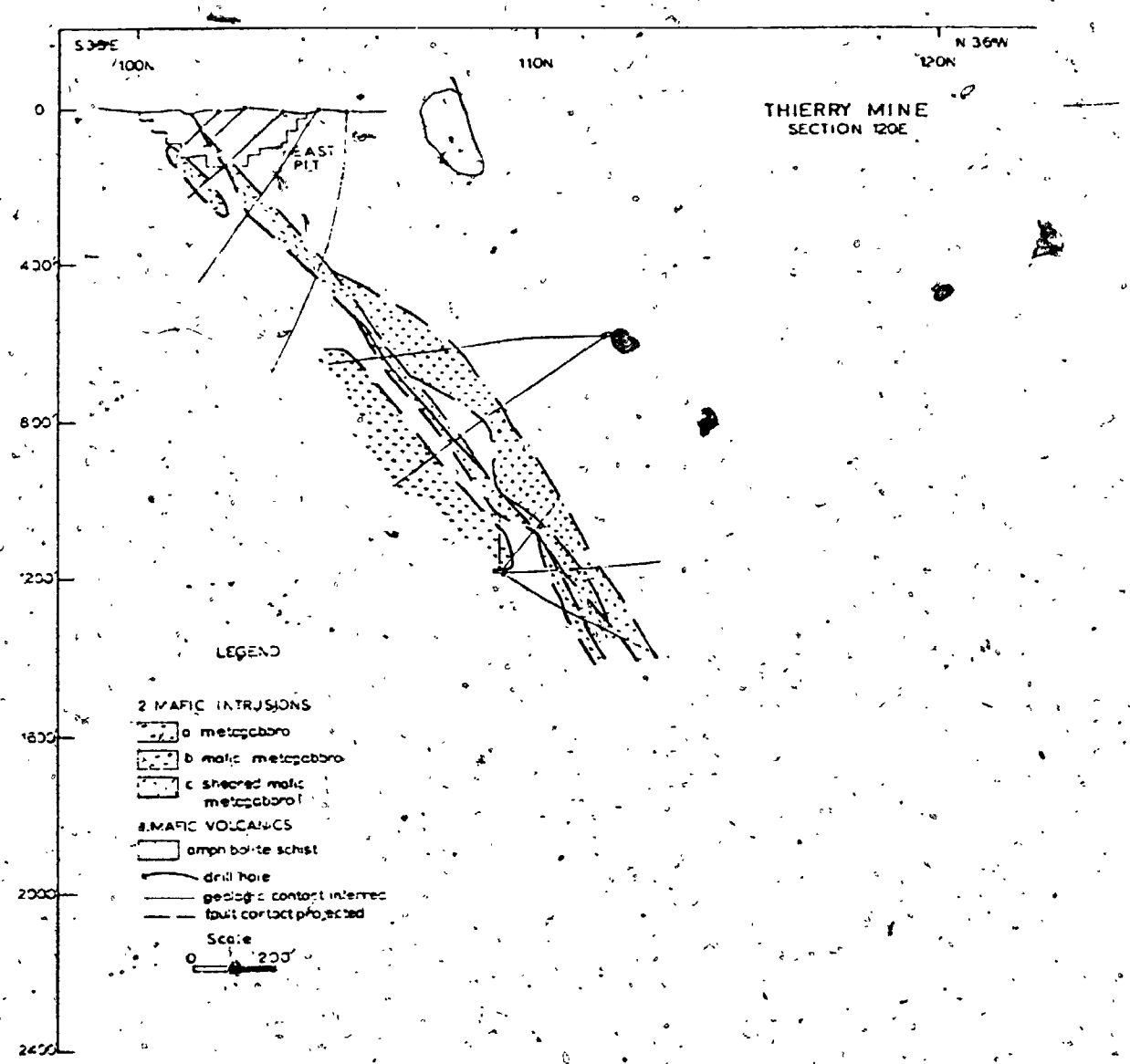
S 36E
100N
110N
120N
N 36W
0
400
800
1200
1600
2000
2400
EAST PIT
THIERRY MINE
SECTION 120E
LEGEND
2 MAFIC INTRUSIONS
a metagabbro
b mafic metagabbro
c sheared mafic metagabbro
1 MAFIC VOLCANICS
amphibolite schist
drill hole
geologic contact inferred
fault contact projected
Scale
0
200'

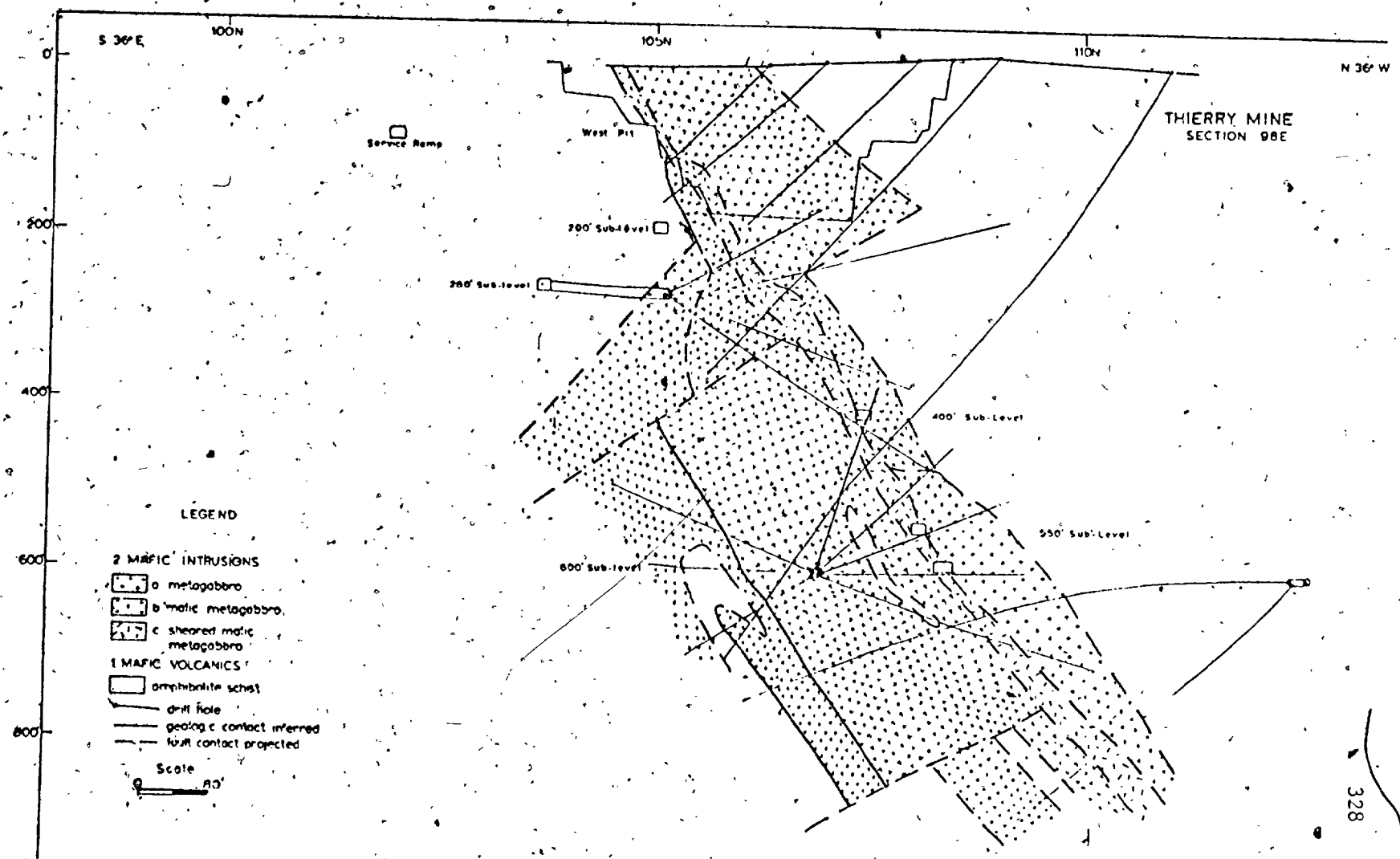
S 36° E
100N
105N
110N
N 36° W
0'
200'
400'
600'
800'
Service Ramp
West Pit
200' Sub-level
300' Sub-level
400' Sub-Level
550' Sub-Level
600' Sub-level
THIERRY MINE
SECTION 98E
LEGEND
2 MAFIC INTRUSIONS
a metagabbro
b mafic metagabbro
c sheared mafic metagabbro
1 MAFIC VOLCANICS
amphibolite schist
drill hole
geological contact inferred
fault contact projected
Scale
0
80'

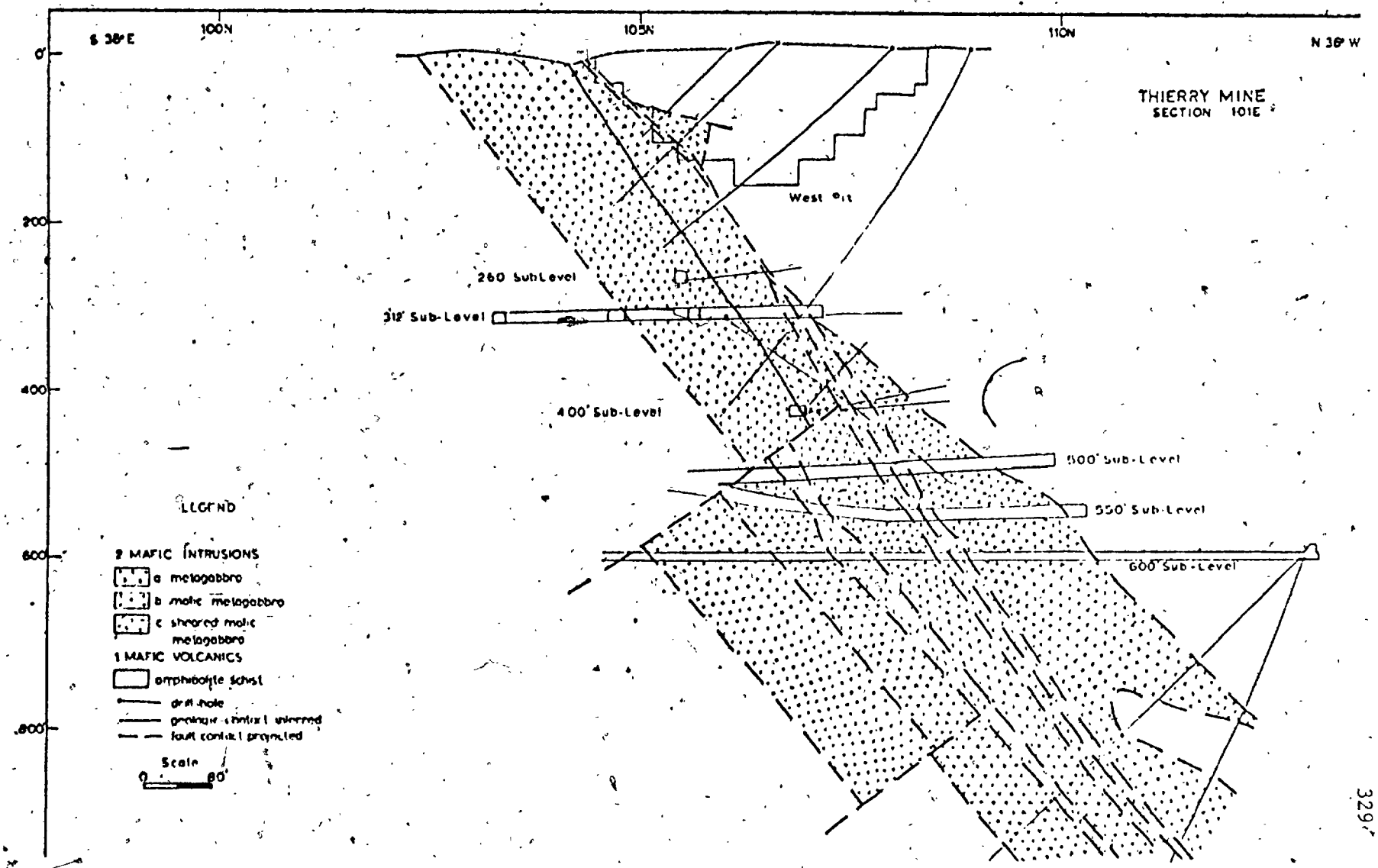
S 36° E
100N
105N
110N
N 36° W
0'
200
400
600
800
THIERRY MINE
SECTION 101E
West Pit
260 Sub Level
312' Sub-Level
400' Sub-Level
500' Sub-Level
550' Sub-Level
600' Sub-Level
LEGEND
2 MAFIC INTRUSIONS
a metagabbro
b mafic metagabbro
c sheared mafic metagabbro
1 MAFIC VOLCANICS
amphibolite schist
drill hole
geologic contact inferred
fault contact projected
Scale
0
80'

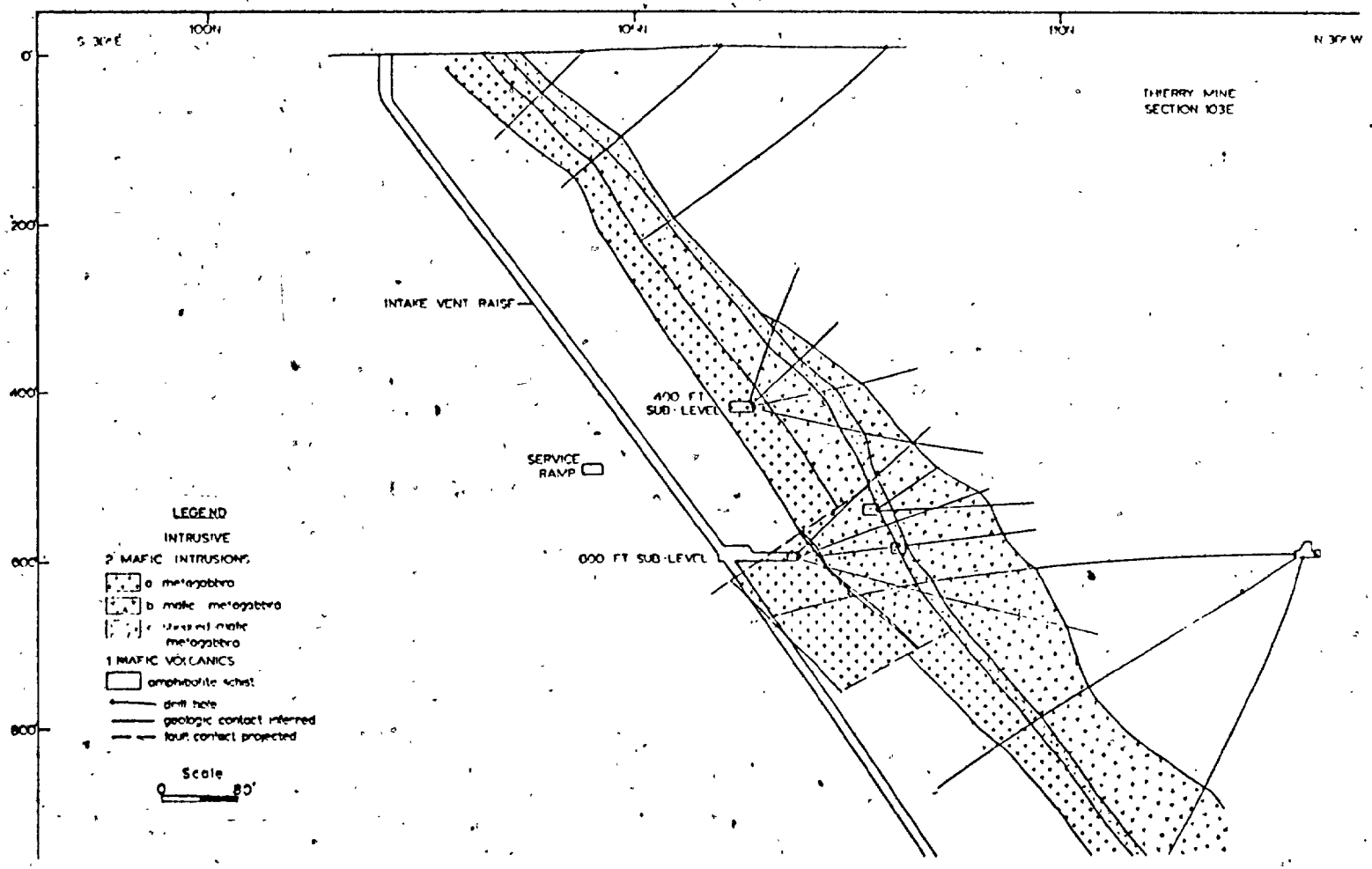
S 30°E
100N
N 30°W
0'
200'
400'
600'
800'
THERRY MINE
SECTION 103E
INTAKE VENT RAISE
400 FT
SUB-LEVEL
SERVICE
RAMP
000 FT SUB-LEVEL
LEGEND
INTRUSIVE
2 MAFIC INTRUSIONS
a metagabbro
b mafic metagabbro
1 MAFIC VOLCANICS
amphibolite schist
drill hole
geologic contact inferred
fault contact projected
Scale
0
80'

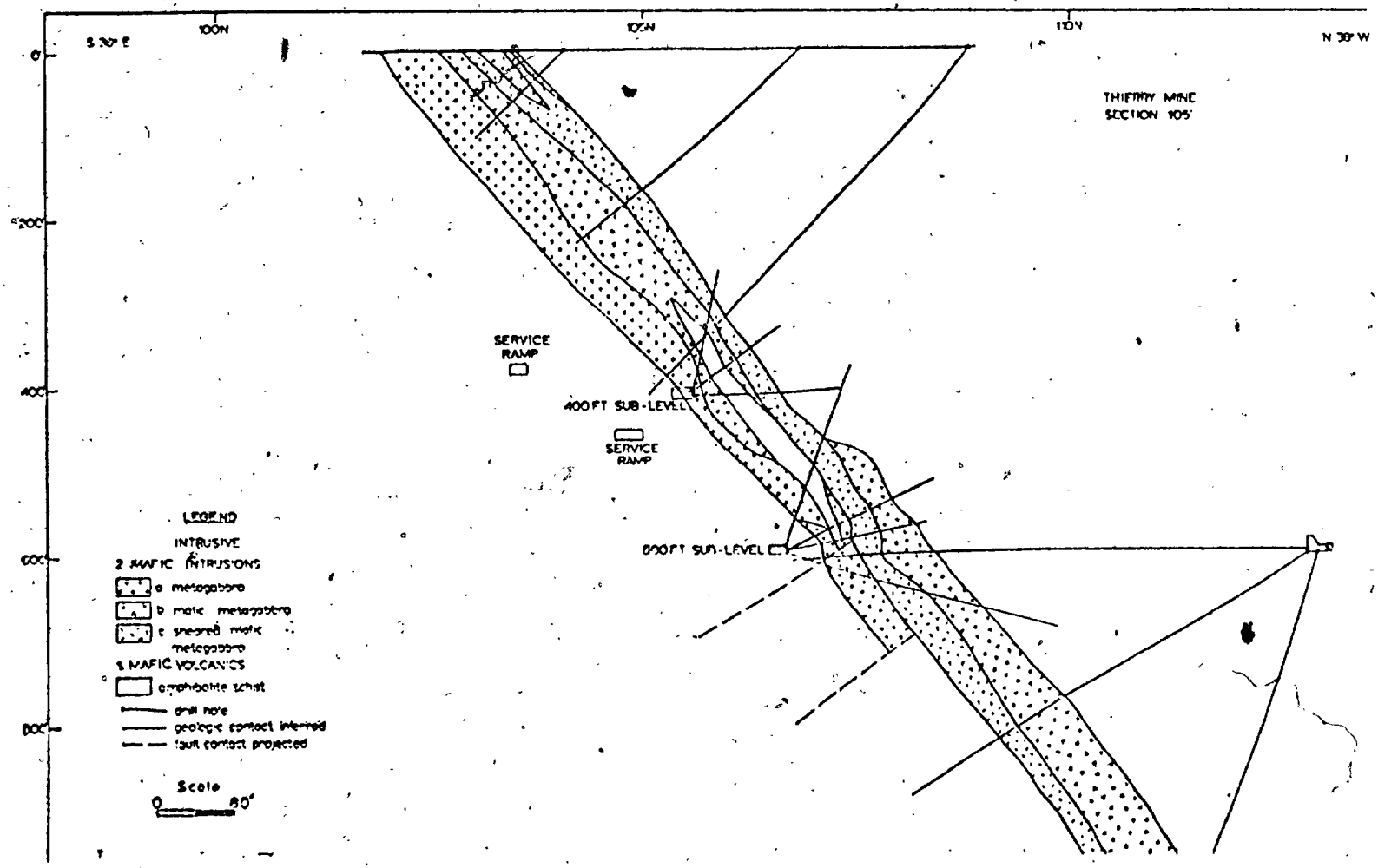
100N
105N
110N
S 30° E
N 30° W
0
200
400
600
800
THIRTY MINE
SECTION 105'
SERVICE
RAMP
400 FT SUB-LEVEL
SERVICE
RAMP
800FT SUB-LEVEL
LEGEND
INTRUSIVE
2 MAFIC INTRUSIONS
a metagabbro
b mafic metagabbro
c sheared mafic metagabbro
1 MAFIC VOLCANICS
amphibolite schist
drill hole
geologic contact inferred
fault contact projected
Scale
0
80'

END

22 12 81

FIN